Novel Approaches Towards The Discovery of Tumor-Selective Histone Deacetylase Inhibitors

A Dissertation

Presented to

The Academic Faculty

By

Idris Raji

In Partial Fulfilment of the Requirements for the Degree

Doctor of Philosophy in Chemistry

School of Chemistry and Biochemistry

Georgia Institute of Technology, Atlanta GA 30332

December 2016

Novel Approaches Towards The Discovery of Tumor-Selective Histone Deacetylase Inhibitors

Committee members:

Dr. Adegboyega K. Oyelere, Advisor
School of Chemistry and Biochemistry
Georgia Institute of Technology

Dr. M. G. Finn
School of Chemistry and Biochemistry
Georgia Institute of Technology

Dr. Stefan France
School of Chemistry and Biochemistry
Georgia Institute of Technology

Dr. Andreas Bommarius
School of Chemical and Biomolecular Engineering
Georgia Institute of Technology

Dr. Ravi Bellamkonda
Pratt's school of Engineering
Duke University

Date Approved: November 4th, 2016

To my mother, Mrs. Jolade Raji

AKNOWLEDGEMENTS

I have been very fortunate to have met and interact with people who have positively influenced my life since arriving at Georgia Tech for graduate studies. I will be forever grateful to my advisor, Dr. Adegboyega K. Oyelere, for giving me the opportunity to learn in his lab. I joined his lab with minimal research experience, but he has helped to tremendously enrich my knowledge base and instill a level of confidence in me that was previously nonexistent. I am very grateful for his patience, guidance, availability to discuss research progress and the countless recommendation letters he wrote on my behalf.

I am greatly indebted to my thesis committee members Dr. M G Finn, Dr. Stefan France, Dr. Ravi Bellamkonda, and Dr. Andreas Bommarius, for their time and invaluable discussions towards completing this thesis. I am particularly grateful to Dr. M G Finn and Dr. France for the innumerable recommendation letters they wrote on my behalf while applying for postdoctoral positions.

A lot of my success in the lab would not have been possible without the contributions from my colleagues in the lab. For this I am grateful to all current Oyelere lab members: Subhasish, Verjine, Nathanael and Bocheng. And also to previous lab members who helped me out when I was learning the ropes: Josh, Will, Berkley, Quaovi, Arren, and Shaghayegh.

It is very easy to overlook the contributions of undergraduate students towards the successful completion of a project. I would like to acknowledge the contributions of the following undergraduate students who worked with me at different times on various projects: Emily Janeira (REU from UNC Chapel Hill), Fatima Yadudu (Georgia Tech), Alex George (Georgia Tech), Kabir Ahluwalia (Georgia Tech) and Radhika Sharma (Georgia Tech).

My family played very important roles in facilitating my coming to the US for graduate studies. To all my brothers: Wasiu, Abidemi, Babatunde (Papy), Saheed, and Azeez; and sister Zainab, I am very grateful to you all. Despite being thousands of miles away, they provided the necessary emotional support. I am very grateful to my mother, Mrs. Jolade Raji, for her support and words of encouragement. No words can best capture how grateful I am to you.

To all my new friends here at Georgia Tech, I am very grateful to you all for the support and good memories!

TABLE OF CONTENTS

LIST OF TABLES

LIST OF FIGURES

LIST OF ABBREVIATIONS

A375	Homo sapiens skin malignant melanoma cell line
AR	Androgen receptor
A549	Non-small cell lung cancer
B16F10	Mouse skin melanoma cell line
BRCA1	Breast cancer type 1 susceptibility protein
^{13}C	Carbon 13
CD_3OD	Deuterated methanol
CO_2	Carbon dioxide
CoA	Coenzyme A
COX	Cyclooxygenase
CpG	5’-cytosine-phosphate-guanine-3’
Cu	Copper
d	Doublet
DCM	Dichloromethane
DDS	Drug delivery system
DIPEA	Diisopropyl ethyl amine
DMEM	Dulbecco’s modified eagle medium

DMSO	Dimethyl sulfoxide
DNA	Deoxyribonucleic acid
DOXIL	Liposomal Doxorubicin
DSPE	1,2-distearoyl-sn-glycero-3-phosphoethanolamine
DSPC	1,2-distearoyl-sn-glycero-3-phosphocholine
DU-145	Androgen independent prostate cancer cell line
EDCI	1-Ethyl-3-(3-dimethylaminopropyl) carbodiimide
EE	Encapsulation efficiency
EPR	Enhanced permeability and retention
ER	Estrogen receptor
Et_2O	Diethyl ether
EtOAc	Ethyl acetate
FDA	Food and Drug Administration
FBS	Fetal Bovine Serum
^1H	Proton
H_2O	Water
H4	Histone H4
HATs	Histone acetyl transferase

HDAC	Histone deacetylase
HDACi	Histone deacetylase inhibitor
HOBT	Hydroxybenzotriazole
HRMS	High resolution mass spectrometry
Hz	Hertz
IL	Interleukin
LNCaP	Androgen-dependent prostate cancer cell line
m	Multiplet
MCF-7	Estrogen-receptor positive breast cancer cell line
MHz	Mega Hertz
mL	Milliliters
MeOH	Methanol
mmol	Milimole
MTS	(3-carboxymethoxyphenyl)-2-(4-sulfophenyl)-2H-tetrazolium
m/z	Mass to charge ratio
Na_2SO_4	Sodium sulfate
$NaHCO_3$	Sodium bicarbonate
Nf-kB	Nuclear factor kappa B

NI	No inhibition
NMR	Nuclear magnetic resonance
NT	Not tested
NTHi	Nontypeable *Haemophilus influenza*
NAD^+	Nicotinamide adenine dinucleotide
NSAIDs	Non-steroidal anti-inflammatory drugs
^{31}P	Phosphorus-31
P16	Cyclin-dependent kinase inhibitor 2A
P21	Cyclin-dependent kinase inhibitor 1
P53	Tumor suppressor protein
PBS	Phosphate buffered saline
PCR	Polymerase chain reaction
PDB	Protein data bank
PEG	Polyethylene glycol
PGE_2	Prostaglandin E2
PI	Propidium iodide
PPh_3	Triphenyl phosphine
ppm	parts per million

Prep TLC	Preparatory thin layer chromatography
RAW 264.7	Murine macrophage cell line
RPMI	Roswell park memorial institute medium
s	Singlet
SAHA	Suberoylanilide hydroxamic acid
SAMDI	Self-assembled monolayers for matrix-assisted laser desorption ionization
SAR	Structure activity relationship
t	Triplet
TEA	Triethylamine
TFA	Trifluoroacetic acid
THF	Tetrahydrofuran
TIPS	Triisopropylsilane
TSTU	[dimethylamino-(2,5-dioxopyrrolidin-1-yl)oxymethylidene]-dimethylazanium;tetrafluoroborate
Zn^{2+}	Zinc (II) ion
ZBG	Zinc binding group

SUMMARY

As we continue to gain more insights into HDAC structures and the roles played by individual HDAC isoforms in tumor progression, the prospect of discovering safer HDACi therapy is looking brighter. An evolving strategy in the clinical application of HDACi as therapeutics for solid tumors involves combining HDACi with other therapeutics, with the goal of potentiating either of the two drugs being combined. However, dose optimization, toxicities from individual drugs, and possibility of drug-to-drug interactions associated with combination therapies are some of the bottlenecks that need to be surmounted. One way to mitigate these challenges is to make a single compound (referred to as "bifunctional compound" in this thesis) that can engage the two or more targets of interest in combination therapy. Another strategy gaining prominence in HDACi drug discovery field is to incorporate a targeting moiety, with affinity for receptors highly expressed in tumors, into the design of HDACi. Such targeted HDACi will have a higher propensity to accumulate in tumors relative to healthy tissues, and may also be able to access and localize in solid tumors easily. We explored the two approaches in my thesis projects, in addition to carrying out preliminary studies on drug delivery using either clarithromycin- or tamoxifen-functionalized liposomes.

Attempts to improve on the challenges faced by combination therapy led me to making bifunctional compounds capable of interacting with cyclooxygenase and HDACs. Two COX inhibitors, celecoxib and indomethacin, were used as structural templates on which the bifunctional compounds were developed. In one of the series based on celecoxib, we obtained compounds with low nanomolar activity towards class I and class IIB HDACs, in addition to COX-2 selectivity that is comparable to that of celecoxib. Likewise, one of the series of compounds

based on the indomethacin template showed potent activity towards class I and class IIB HDACs, in addition to selectivity towards COX-2 (a property lacking in indomethacin). A remarkable observation with some of the lead compounds is their enhanced cytotoxicity towards androgen dependent prostate cancer cell line (LNCaP) relative to androgen independent prostate cancer cell line (DU-145). Target validation in LNCaP, cell cycle analysis and inhibition of NF-kB activation showed that our lead compounds have unique mechanism of action in cells. Compared to vorinostat, these lead compounds displayed tumor-selective cytotoxicity as they have low anti-proliferative activity towards healthy cells (VERO); an attribute that makes them attractive candidates for drug development.

In chapter two, clarithromycin was incorporated into the head group of hydroxamate- and amino biaryl-based HDACi. Clarithromycin belongs to a class of compounds called macrolides, known for their preferential accumulation in the lung tissues. Hence, the goal of this project is to make HDACi that can localize in lung tissues with potential application in lung cancer treatment. Lead compounds from the hydroxamate-based series potently inhibited all the three HDAC isoforms they were profiled against, and showed cytotoxic effects in lung and breast cancer cell lines that surpass US FDA approved vorinostat. More importantly, the lead compounds were less cytotoxic towards the healthy cell line (Vero) compared to vorinostat. While hydroxamate-based compounds are known to have activity across all HDAC classes, amino biaryl-based compounds only show activity against HDAC 1 and HDAC 2, (class I HDACs). So, a sub-goal in this chapter is to make clarithromycin- amino biaryl-based HDACi that only inhibit HDAC 1 and HDAC 2, and also localize in lung tissues. Consistent with their selectivity for class I HDACs, all the amino biaryl-based compounds showed strong inhibitory profiles against HDAC 1 and HDAC 2.

However, their potent enzyme inhibitory activities did not translate into strong growth inhibition of lung- and breast cancer cell lines.

In continuation of our efforts towards making targeted HDACi, we incorporated a benzamide template, with high affinity for melanin, into the design of HDACi with the goal of selective delivery of the HDACi to melanoma cells. This effort resulted in a new series of compounds with high potency towards HDAC 1 and HDAC 6. Against HDAC 1, lead compound obtained is about ten-fold more potent than SAHA, though with the same level of potency towards HDAC 6. Surprisingly, all the compounds were only modestly cytotoxic activity towards melanoma cell lines, B16F10 and A375. We further explored a prodrug approach, whereby we made a compound bearing the benzamide template linked by a labile bond to a hydroxamate-based HDACi. While cytotoxicity was not significantly improved, the pro-drug compound showed some promise and warrants further study.

Lastly, preliminary studies were carried out, wherein we evaluated the suitability of clarithromycin and tamoxifen as targeting ligands on liposomes encapsulating propidium iodide. Liposomes formed with a phospholipid derivatized with clarithromycin showed some promise in enhancing propidium iodide uptake by macrophages (RAW 264.7). Similarly, phospholipid derivatized with tamoxifen helped facilitate substantial uptake of liposome made from it. Further studies are needed to validate the observations from the two uptake studies, and optimize the liposome formulation process to improve on encapsulation efficiency.

CHAPTER 1

INTRODUCTION

1.1. Epigenetic regulation of gene expression and cancer

Epigenetics, a term used to describe transfer of heritable traits that are independent of changes in the DNA sequence,[1] play a significant role in regulation of gene expression. As such, homeostatic regulation of gene expression is an important factor that determines the normal functioning of the cells. Consequently, there is a strict requirement for an efficient cellular epigenetic regulation of expression to keep the cells healthy. Diseases such as cancer, neuropsychiatric disorder, and inflammation have been associated with a dysfunctional epigenetic machinery.[2] This, necessitates having a thorough understanding of things/events that causes aberrant epigenetic regulation. The dynamics of the epigenetic regulation process involves a concerted regulation of events such as DNA methylation, histone modification, and chromatic remodeling -all epigenetic processes[3-4]. Among these epigenetic events, DNA methylation and histone modification are the most studied.

In cancer, hypermethylation of CpG islands of promoter regions of tumor suppressor genes is a frequent event that often results in silencing of the associated genes.[5] Suppression and/or mutation of genes such as $P16^{INK4A}$ (encodes cyclin dependent kinase inhibitor) and *BRCA1* are often due to hypermethylation of the CpG islands of their promoters.[5] One consequence of this is development of a dysregulated cell cycle, which enables cancer cells to evade natural cell death. Hypomethylating agents, such as azacitidine and decitabine, have been recognized to be of

therapeutic values in cancer, and have since been approved by the US Food and Drug Administration (FDA) for treating myelodysplastic syndromes.[6]

Likewise, histone hypoacetylation, due to upregulation of histone deacetylase activity, is a common occurrence in tumors which also leads to downregulation of tumor suppressor genes. The sections below are devoted to discussing histone acetylation/deacetylation and their associated enzymes.

1.2. Histone deacetylases (HDACs)

Histone deacetylases (HDACs), commonly referred to as "erazers" because of their mode of action, are a family of enzymes that facilitate the removal of the acetyl group on the lysine of histones to influence the dynamics of the chromatin[7]. While their substrate appears to be just histone, there have been reports of some HDAC isoforms catalyzing the deacetylation of other proteins[8]. A good example of this is the cytoplasmic localized HDAC6 that also deacetylates tubulin and HSP90[9]. In conjunction with histone acetyl transferases (HATs), HDACs control the accessibility of transcription factors to the promoter regions on the chromatin (Figure 1.1). Therefore, a balance in histone acetylation and deacetylation activities is required for maintaining a stable epigenome.[10] As will be discussed copiously in Chapters 2-5, one of the survival tricks employed by cancer is to ensure an imbalance in the acetylation and deacetylation activities which ultimately leads to silencing of tumor suppressor genes. This is achieved by maintaining a high expression level of HDACs relative to HATs.[11-13]

There are currently eighteen known isoforms of HDACs, grouped into four classes based on phylogenetic analysis, sequence homology and cellular localization.[11-12, 14] Among these four, class III HDACs, consisting of seven HDAC isoforms, are non-zinc dependent but rely on NAD^+ for their catalytic activity.[11] Classes I, II and IV make up the Zn dependent HDAC isoforms. While Class I comprises HDACs 1, 2, 3 and 8; class II is further subdivided into class IIA (comprising HDACs 4, 5, 7 and 9) and class IIB (comprising HDACs 6 and 10), with class IV having HDAC 11 as the only member of the class.

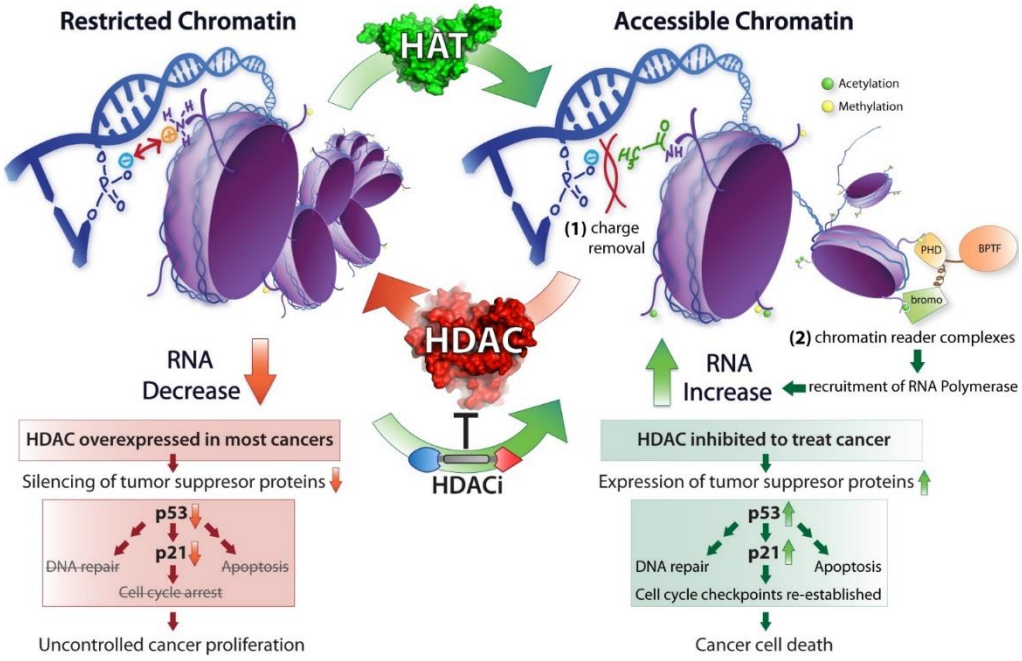

Figure 1.1: Cartoon representation of HDAC and HAT function. Image courtesy of Dr. Berkeley Gryder (an abridged version is published in ref. 11).

In terms of cellular localization, class I HDACs are located mainly in the nucleus, with class IIA HDACs located either in the nucleus or cytoplasm, and class IIB located predominantly

in the cytoplasm. Lastly, class IV HDACs could be found either in the nucleus or cytoplasm (Table 1.1).

Each HDAC isoform plays different roles in driving tumorigenesis. In most cancer cases, elevated levels of various HDAC isoforms have been reported as shown in Table 1.2 below.

Mechanistically, all Zn-dependent HDACs use a similar mechanism to facilitate the hydrolysis of acetyl groups on histone's lysine. Acetylated lysine residue traverses the

Table 1.1: Cellular localization of HDAC isoforms[11-12]

Class	Isoform	Cellular localization
I	HDACs 1,2,3, and 8	Nucleus
IIA	HDACs 4, 5, 7, and 9	Nucleus/cytoplasmic
IIB	HDACs 6 and 10	Cytoplasmic
IV	HDAC 11	Nucleus/cytoplasmic

hydrophobic pocket of the enzyme's active site until it gets to an optimum distance for chelation to the Zn^{2+}. Upon chelation, hydrolysis is thereafter facilitated by a sequence of events comprising

Table 1.2: HDAC isoform overexpressed in various cancer types[14-15]

Cancer Type	HDAC isoform overexpressed
Cutaneous T-cell lymphoma	HDAC1, HDAC2 and HDAC6
Colorectal	HDAC1, HDAC2 and HDAC3
Prostate	HDAC1, HDAC2 and HDAC3
Lung	HDAC1, HDACs4-6, and HDAC10
Breast	HDAC1, HDAC6
Gastric	HDAC1, HDAC2 and HDAC3
Liver	HDAC6

nucleophilic attack on the acetamide, by a water molecule activated by surrounding histidine residues, to form an oxyanion transition state, which then collapses to give acetate and free lysine as shown in Figure 1.2.

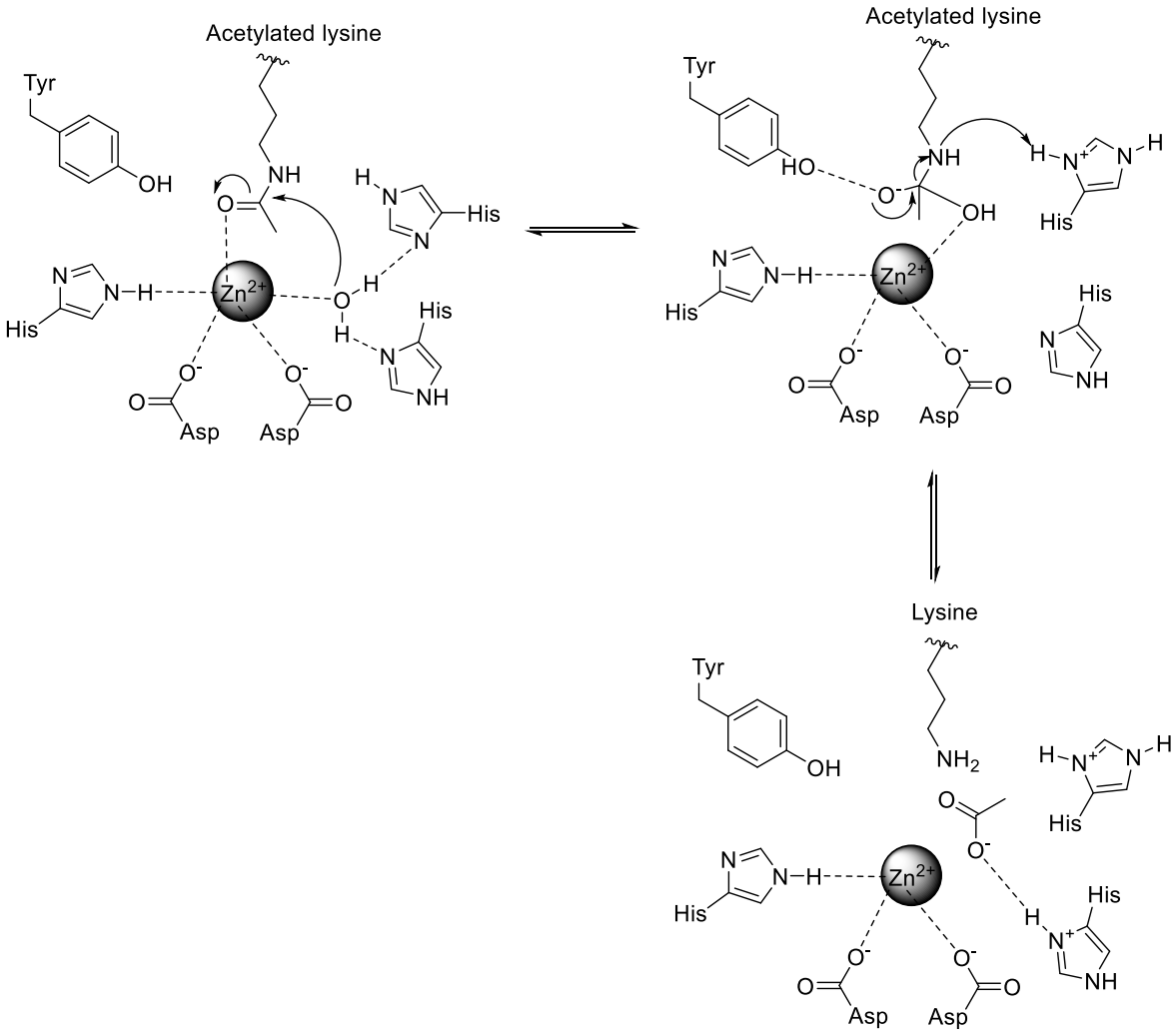

Figure 1.2: Proposed mechanism for histone deacetylation by HDAC enzymes[13]

1.3. Histone acetyl transferases (HATs)

HATs, often referred to as "writers" due to their mode of action, add acetyl group to the lysine on histone tail to disrupt the electrostatic interactions holding the DNA to histones. In conjunction with HDACs, HATs control access of transcription factors to promoter regions on the chromatin as shown in Figure 1.1 above. They are mostly found in complex with one another or

with other proteins. In contrast to HDACs, HATs utilize acetyl CoA in carrying out their catalytic activity.[16-17] Although it is widely believed that the consequence of lysine acetylation is the disruption of electrostatic interaction keeping the chromatin compact, covalent modification of histones could also serve as an epigenetic marker for gene expression.[16, 18] In addition to their acetylation function, HATs also have other functions, such as DNA damage repair and maintaining genome stability, as dictated by the protein complexes to which they are bound.[19] As with HDACs, HATs also have non-histone proteins as substrates, specifically P53 and several other mitochondrial proteins.[8]

The roles of HATs in the development and progression of certain malignancies have been a subject of recent studies.[20] Increased HATs activity on genes that drive tumorigenesis has been observed in some cancer types,[21] and this has sparked interest in developing HATs inhibitors for possible intervention in such types of cancer.[22-24]

1.4. Histone deacetylase inhibitors: pan inhibitors vs class-selective inhibitors

Since the observation that reversal of the balance in equilibrium dynamics of HDACs and HATs facilitates upregulation of tumor suppresor genes, hitherto silenced in cancer, efforts have been devoted to making small molecule inhibitors of commonly over expressed HDACs. These efforts paid off in 2006 with the US FDA approval of the first HDAC inhibitor, Vorinostat (also known as SAHA). The approval of SAHA paved the way for other HDACi (Figure 1.3A) to gain approval, resulting in a total of five HDACi in the clinic. Out of this five, only four (including SAHA) HDACi are approved for use in the US market. In addition to this, several HDACi are at different stages in various clinical trials worldwide for different malignancies. These compounds

have also stimulated interests in treatment of other disease characterized by aberrent gene expression[25].

A closer look at the structures of all clinically approved HDACi reveals a common structural feature, that could be divided into zinc binding group (ZBG), linker and surface recognition group (also known as cap) (Figure 1.3B). All these three components are amenable to structural modifications to generate a library of HDACi the could either be active across all HDAC isoforms (pan inhibitors) or selective towards a particular class of HDAC (isoform selctive). With the exception of a few (e.g tubacin and tubastatin A,[26] both selective HDAC6 inhibitors), compounds having hydroxamic acid as their ZBG always end up as pan inhibitors. On the other hand, compounds with benzamides as ZBGs have selective inhibitory activity towards class I HDAC.[27-29] While other less common ZBGs, such as ethyl carbamate (seen in santacruzamate A[30]), 3-hydroxypyridine-2-thione,[31] also confer isoform-selective inhibitory activities.

Though *in vitro* studies suggest that class I HDAC inhibition is essential in the anticancer activity of HDAC inhibitors,[32] it is yet to be seen if there is an advantage to having class-selective inhibitors over pan inhibitors in the clinic. Among the four US FDA approved HDACi, only romidepsin could be considered as being class-selective in its inhibitory activity, with low nanomolar IC_{50} against class I HDACs.[33] Despite this, romidepsin shows off-target toxicities typical of pan inhibitors.[34] Perhaps one could argue that hydroxamates (pan inhibitors) may not be the best due to their susceptibility to hydrolysis and glucuronidation,[35-36] which adversely affect the pharmacokinetic profile.

While HDACi have enjoyed tremendous successes in the clinic, off-target toxicity, poor bioavailability, and poor activity towards solid tumors as a single agent continue to be major

challenges.[11] Overall, the projects described in this thesis capture ways of mitigating the undesirable attributes of clinically approved HDACi. Chapters 2 and 3 cover targeted approaches towards discovery of novel HDACi, while Chapter 4 introduces the concept of bifunctional compounds active against HDAC and COX-2. With the eventual goal of achieving selectively delivery of HDACi, work described in Chapter 5 focuses on preliminary studies towards using targeted lipid nanoparticles for delivery of chemotherapeutic agents.

A.

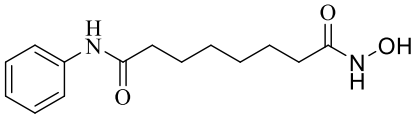

Vorinostat (or SAHA)

(for cutaneous T-Cell lymphoma)

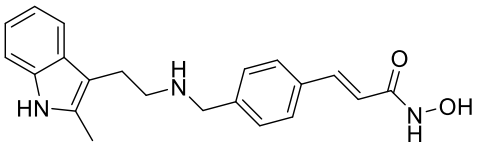

Panobinostat

(for multiple myeloma)

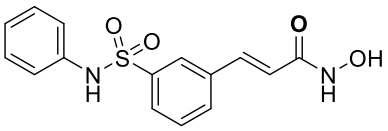

Belinostat

(for peripheral T-Cell lymphoma)

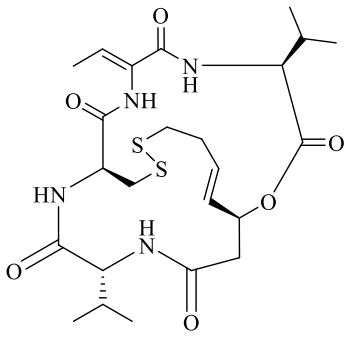

Romidepsin

(for cutaneous T-Cell lymphoma & peripheral T-Cell lymphoma)

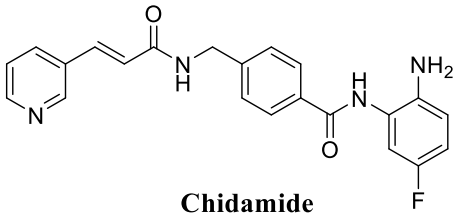

Chidamide

(for peripheral T-Cell lymphoma)

B)

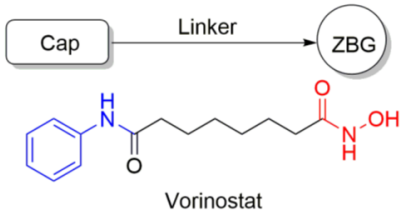

Figure 1.3: A) Structures of clinically approved HDAC inhibitors; B) HDACi pharmacophoric model.

1.5. Macrolide-derived HDACi

Macrolides are a class of antibiotics recommended as first line treatment for antimicrobial infections of soft tissues, especially lung tissues. Structurally, most macrolides possess either a 14- or 15-membered macrocyclic ring structure, with two sugar moieties attached (Figure 1.4). Their complex ring structures make them an excellent template to generate non-peptide macrocyclic HDACi. In addition to this, macrolides are known to show substantial localization in lung tissues,[37-39] making them ideal candidates to generate targeted chemotherapeutic agents specific for lung cancer tissues. Previous work in our lab has identified clarithromycin, azithromycin and TE-802 as excellent mimetics for the cap group of macrocyclic HDACi,[40-41] though SAR studies were restricted to modifications at the desosamine sugar, and linker lengths were varied from six to eight methylenes separating the cap group from the ZBG.

As a follow up, Chapter 2 of this thesis focuses on expanding the SAR studies to include modifications at the cladinose sugar of clarithromycin to generate a new series of HDACi with higher potency than previously reported.[40-41] Furthermore, the desosamine-modified series

described previously[40-41] was also expanded to generate compounds with shorter linker lengths to study the effect of short linkers on HDAC inhibitory activities and on anti-proliferation activity. Also, lead compounds generated were evaluated for their ability to downregulate NF-Kb mediated inflammatory activity. Lastly, considering the need for class I HDAC isoforms inhibition for the anticancer activity of HDACi, a bi-aryl ZBG known to confer selective inhibition of HDAC 1 and HDAC 2 on HDACi,[42-43] was adopted as ZBG to further generate a library of clarithromycin-based isoform selective HDACi.

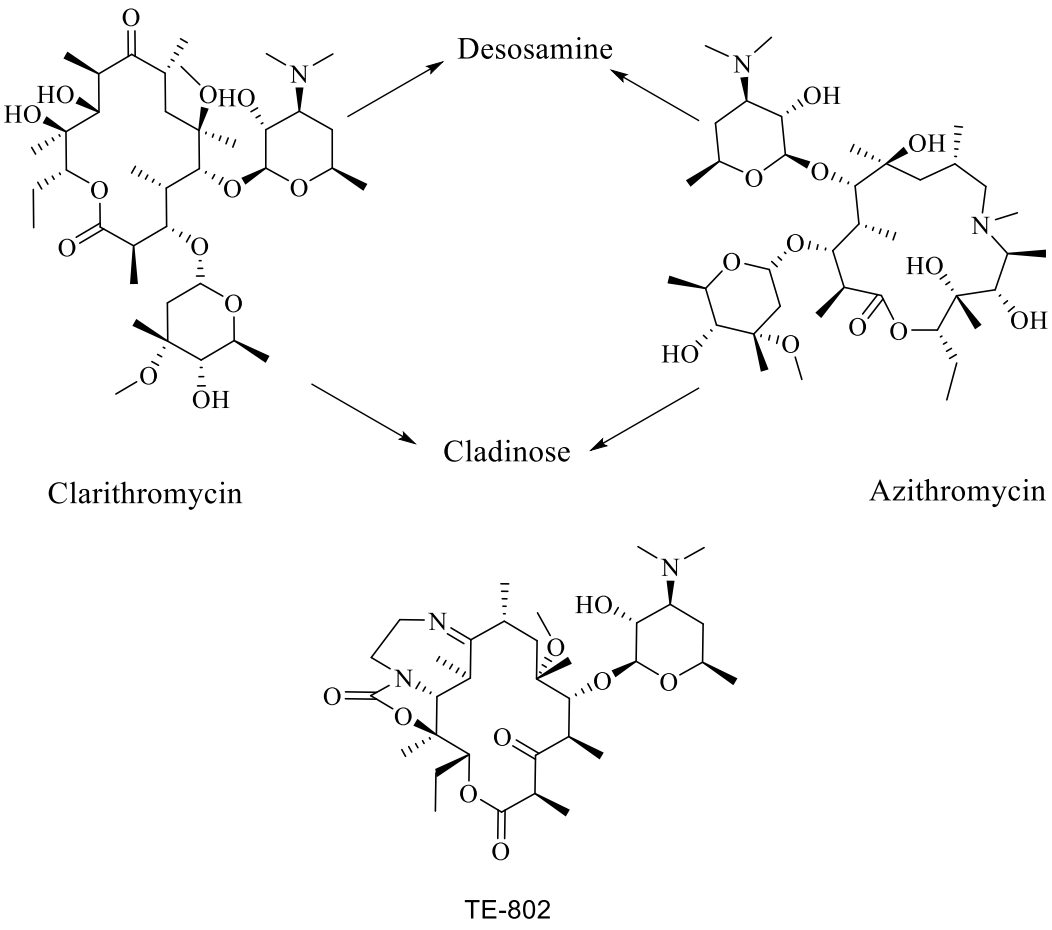

Figure 1.4: Structures of selected examples of macrolides

1.6. HDACi for melanoma

Melanoma of the skin ranks as the fifth most prevalent among estimated new cases of cancer in 2015.[44] At the advanced stage, melanoma becomes very aggressive and resistant to chemotherapy. A large subset (about 60 percent) of advanced melanoma cases is believed to carry $BRAF^{V600E}$ mutation, which drive signaling in the Mitogen-Activated Protein Kinase (MAPK) pathway, independent of upstream signaling by RAS.[45-46] Currently, the inhibitor of the hyperactivated BRAF, Vemurafenib,[46] is the most successful drug used to treat advanced melanomas having $BRAF^{V600E}$ mutation.

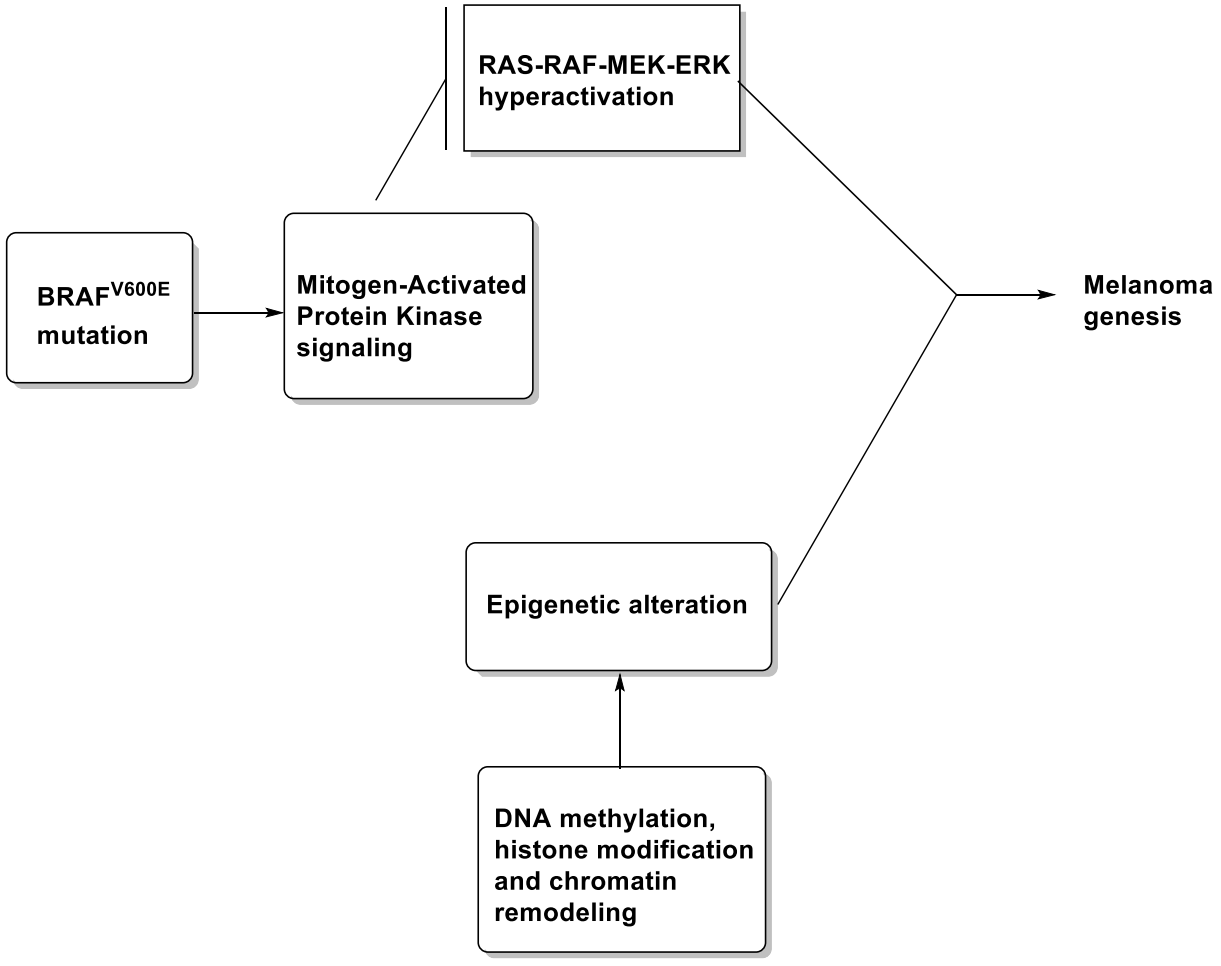

Figure 1.5: Possible mechanisms that drive melanoma[47]

To expand the treatment options available for melanoma, there has been tremendous effort towards understanding other pathways believed to be involved in melanoma development and progression. A critical understanding of such pathways will aid our effort towards developing better diagnosis and therapeutics for melanoma. One of such pathways is epigenetic regulation of genes that drive signaling pathways in melanoma. While about ten percent of all melanoma incidence is linked to genetic inheritance,[48] aberrant regulation of epigenetic events such as chromatin remodeling, DNA methylation and histone modification are believed to play significant roles in melanoma development.[47-49] For instance, histone hypo-acetylation, a consequence of overexpression of HDAC, leading to downregulation of tumor suppressor genes (P21 and P53) is a common occurrence that has been characterized in melanoma cells *in vitro*.[50] Recently, HDAC isoforms- 5 and 6 were shown to be the dominant HDAC isoforms expressed in melanoma.[51] Hence, inhibition of HDACs, with small molecules, could provide an alternative approach towards melanoma treatment.

Previous attempt to study the role of HDAC 6 selective inhibitors in inhibiting the growth of B16F10 melanoma cell line has shown some promise, as the lead compounds tested showed high micromolar IC_{50}.[32] Interestingly, a Phase 2 clinical trial study of vorinostat (SAHA) in metastatic uveal melanoma (ClinicalTrials.gov identifier: NCT01587352) is about to begin and is currently recruiting participants.

To further evaluate the effects of HDACi in melanoma, the project described in Chapter 3 of this thesis focuses on developing HDACi targeted towards melanoma. In doing this, a targeting moiety was incorporated into the surface recognition group of an hydroxamate-based HDACi template. The choice of targeting moiety for this project was inspired by a class of compounds

called benzamides. These compounds are unique for their ability to bind melanin, and are currently being developed as diagnostic agents for melanoma.[52-53] Two classes of HDACi were made in this study: one based on benzyl, and another based on pyridyl templates. These compounds showed potent inhibitory activity in HDAC assay against HDAC1 and HDAC6, though with only modest potency against melanoma cell lines. A prodrug approach was also employed to further exploit the utility of the benzamide template as a targeting group, and improve on potency in cell growth inhibition assay.

1.7. Designed-multiple ligand approach in the design of HDACi

Despite the clinical successes of HDACi towards different types of lymphomas, HDACi are currently being evaluated in combination with other chemotherapeutic agents to derive maximum therapeutic benefits in solid tumors. The rationale behind combining HDACi with other drugs could be attributed to HDAC inhibition acting in synergy with the pathways targeted by other drugs, to make cancer cells more susceptible to cell death.[54] Although this approach is quite appealing, patients, in most cases, have to deal with the individual toxicities associated with the combined drugs.[55] Likewise, dose optimization as well as differences in the pharmacokinetic profiles of the combined agents could be a bottle-neck in deriving maximum benefits from combining two different drugs.[56] In addition to this, patients' compliance to dose regimens and the economic implication of buying multiple drugs further complicates combination therapy. An emerging approach being proposed as an alternative to combination therapy in the drug discovery field is the designed-multiple ligand approach.[57-60] This approach involves making a single molecule that is capable of interacting with two or more different targets.

The designed-multiple ligand approach could become beneficial in cancer and other diseases in which: i) Concurrent inhibition of two or more pathways relevant for the sustained progression of such diseases is crucial; ii) Inhibition of one pathway leads to activation of a different pathway that drives such diseases-hence the chances of resistance to chemotherapy becomes reduced; and iii) Inhibition of two pathways elicit a synergistic effect.

With regards to HDACi drug design, the designed-multiple ligand approach has enjoyed a considerable amount of attention.[56] Incorporation of estrogen receptor modulators,[61-63] androgen receptor antagonist,[64] topoisomerase inhibitors,[65] tubulin depolymerization inhibitor,[43] and kinase inhibitors[66] unto the cap group of SAHA-like molecules all demonstrated advantages over using the individual components and/or physically combining the individual components *in vitro* (and *in vivo* in some cases).

Given the important roles played by inflammation in driving tumorigenesis, and the fact that HDAC inhibition perturb most pathways relevant in inflammation induction and progression,[66] it is reasonable to explore the benefits of combining drugs that block any of the inflammation development pathways and an HDACi.

Cyclooxygenase (COX) is an enzyme that facilitates the conversion of arachidonic acid (obtained from distressed cell membrane through phospholipase A2 activity) to prostaglandins and other signaling molecules in the body[68] (Figure 1.6). One of COX isoforms, COX-2, is ubiquitously expressed in most cancer types where it promotes inflammation development and progression.[69] As a result, several studies are currently targeted towards repurposing COX inhibitors, also known as NSAIDs (Figure 1.7), as chemotherapeutic agents.[70-71] Previously, it was

shown that simultaneous blockade of COX-2 and HDAC activities results in enhanced antiangiogenic effects in lung cancer cells.[72]

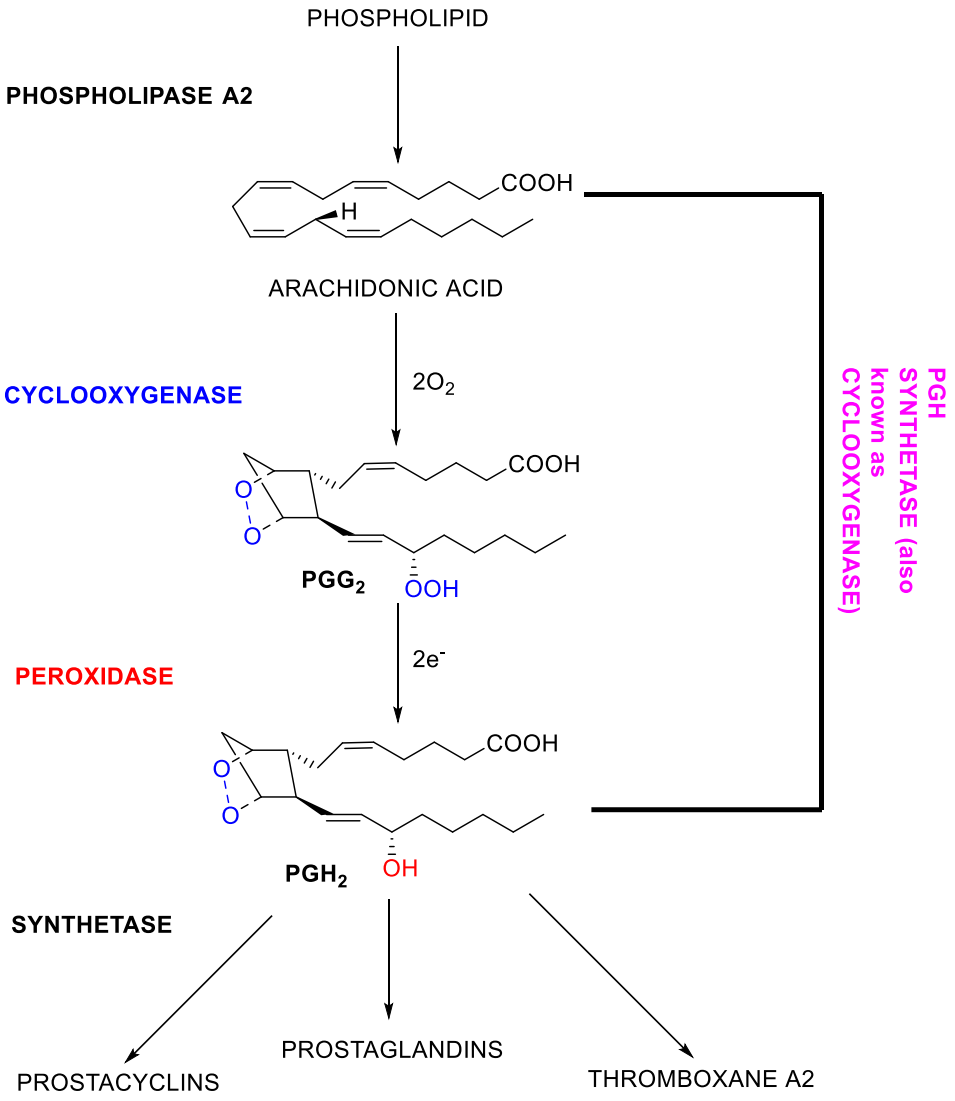

Figure 1.6: COX-mediated synthesis of prostaglandins from arachidonic acid[73]

To further explore the benefits of simultaneous inhibition of COX-2 and HDAC in tumors, Chapter 4 of this thesis is focused on making bifunctional molecules, based celecoxib and indomethacin templates, having both COX and HDAC inhibitory activities. Lead compounds generated from this project showed superior therapeutic index compared to SAHA, and showed

preferentially cytotoxicity towards androgen-dependent prostate cancer. Some of the compounds made were able to downregulate activation of Nf-kB induced inflammation, making them potential candidates for regulation of inflammation.

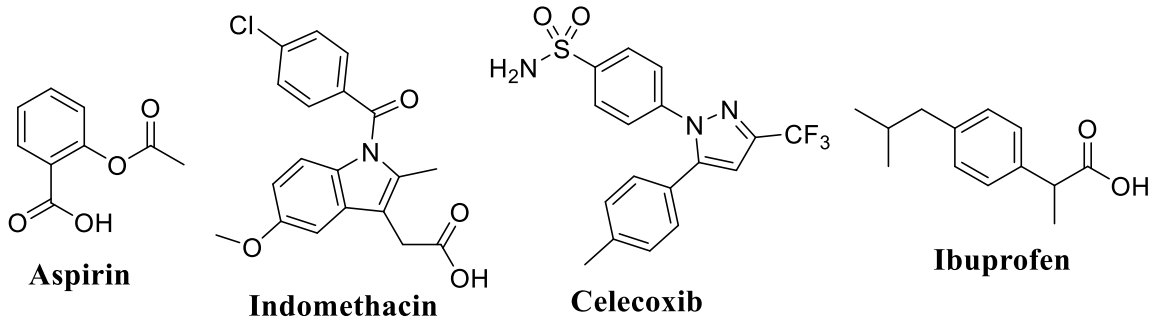

Figure 1.7: Structures of selected US FDA approved NSAIDs

1.8. Lipid nanoparticle-based drug delivery system

Lipid nanoparticle-based drug delivery systems are attractive for drug delivery purposes because of their ability to traverse the cellular membrane easily, due to their amphiphilic nature. Their composition, mainly phospholipids, imparts membrane-like properties on them, making the nanoparticles suitable for delivery of drugs with poor pharmacokinetic profile. More importantly, lipid nanoparticles are biodegradable,[74] and could be used to mask the off-target toxicities associated with encapsulated drugs, if drug release can be controlled. The two most studied lipid nanoparticle drug delivery systems are micelles and liposomes. While micelles are composed of a single monolayer of phospholipid, liposomes comprise one or more phospholipid bilayers having both hydrophilic and hydrophobic compartments (Figure 1.8).[74]

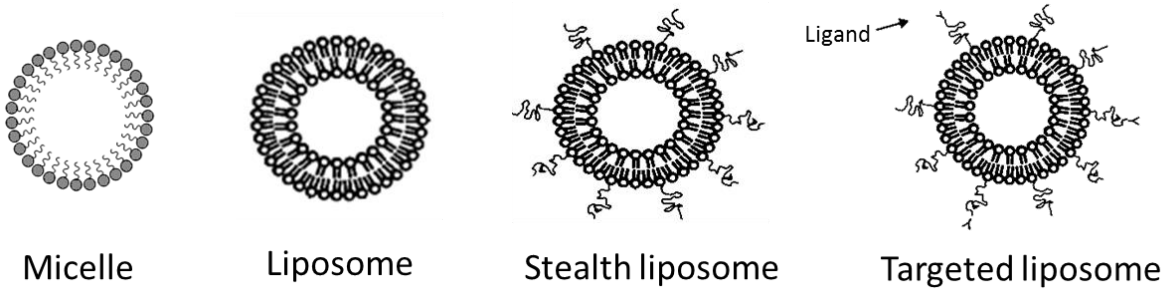

Figure 1.8: Structural annotations of micelle and liposomes[75]

Liposome formulation for drug delivery purposes is explored in chapter 5 of this thesis. Liposomes could be used to package hydrophilic and hydrophobic agents in their hydrophilic and hydrophobic compartments respectively.[75] During the early stages of development, one of the challenges faced by liposomes in systemic circulation is rapid uptake by the mononuclear phagocyte system (MPS).[76] To circumvent this, stealth liposomes (Figure 1.9), having PEG coating on the surface of the liposomes, were developed. Stealth liposomes have longer circulation times due to their ability to evade uptake by the MPS. This makes them highly desirable for drug delivery. In recognition of their impressive drug delivery capabilities, the first US FDA approved liposomal formulation, DOXIL (or Caelyx),[77] was based on the stealth liposome design.

1.8.1. Passive targeting of liposomes

One very attractive property of liposomes as drug delivery systems for cancer therapy is their ability to explore the defect inherent in most cancer types to selectively accumulate in tumors. Cancer blood vessels have a leaky vasculature compared to those in normal tissues. This leaky vasculature (a defect) enables a circulating nanoparticle of the right size to percolate into tumors

and get trapped. This process by which nanoparticle get into tumors is known as the Enhanced Permeability and Retention effect (EPR),[78-79] Figure 1.10. Passively targeted liposomes (e.g stealth liposome) get to tumors by the EPR effect.

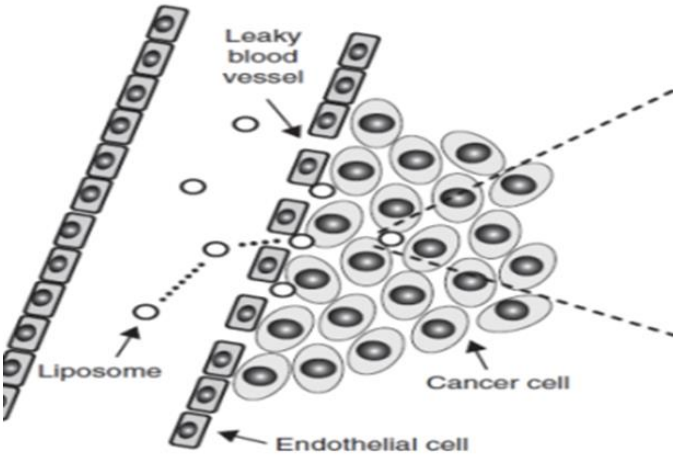

Figure 1.9: Liposomes getting to tumor via EPR effect[80]

1.8.2. Active targeting of liposome

In addition to the EPR effect, tumor accessibility to liposomes could be enhanced by having ligands with affinity for receptors, preferentially expressed in tumors, attached to the surface of the liposome (Figure 1.8). Due to the targeting ligands' specificity for receptors expressed in tumors, it is anticipated that actively targeted liposomes will show superior therapeutic index compared to passively targeted ones. It is noteworthy to point out that despite DOXIL (a passively targeted liposome) being successful at alleviating the cardiotoxic effects associated with doxorubicin, off target effects such as palmar-plantar erythrodysesthesia (also known as hand and foot syndrome) and other skin conditions are still noticeable in patients using it.[81]

As promising as active targeting sounds, no actively targeted nanoparticle has received the approval of US FDA for clinical use, while several stealth liposomes carrying various chemotherapeutic drugs are in use.[75]

A critical look at the literature for factors that influence choice of ligands for targeted liposome applications reveal that the nature of tumor microenvironment (e.g acidity) and high expression of cell surface receptors in tumors relative to healthy tissues play prominent roles.[82] Several small molecules and macromolecules have been studied for their suitability as targeting ligands on liposomes. Among the small molecules studied, folate, targeting folate receptor, is probably the most studied.[83] Other macromolecules that have been studied include proteins and peptides (e.g. transferrin[84] and glutathione[85]), antibodies,[86] DNA aptamers,[87] etc.

Previously, macrolide-functionalized gold nanoparticles were demonstrated to show substantial accumulation in macrophage cells (RAW 264.7), consistent with the accumulation of the parent macrolides in macrophages.[88-89] To further explore the suitability of macrolides as targeting ligands on lipid nanoparticles, liposomes were formulated with phospholipids having clarithromycin attached. These liposomes were used to encapsulate propidium iodide and thereafter used to study uptake of propidium iodide in RAW 264.7 cells. Preliminary results from this study are described in Chapter 5. Likewise, tamoxifen, a US FDA approved drug for treatment of estrogen receptor positive (ER+) breast cancer, was also appended on phospholipids. Liposomes formed with the tamoxifen-functionalized phospholipids were used for uptake experiments in ER+ breast cancer (MCF-7). The suitability of tamoxifen as a targeting ligand on gold nanoparticles has been previously demonstrated.[90]

1.9. Summary

Off-target toxicity ranks very high among the challenges faced by HDACi in the clinic. Though none of the clinically approved HDACi were designed to address this, it is believed that making HDACi more isoform-selective and incorporating a targeting group into the design of these compounds may mitigate some of the off- target effects observed in patients. By incorporating groups like clarithromycin, benzamide and NSAIDs into the design of HDACi *ab initio*, we obtained new sets of HDACi with very promising *in vitro* therapeutic index suggesting that they may be safer therapeutics to the compared to the clinically approved HDACi.

Another approach that could potentially lessen the toxic effects associated with the use of HDACi is to package them in an appropriate drug delivery system. we explored the suitability of ligand-functionalized liposomes for this purpose, by first carrying out preliminary evaluation of clarithromycin- and tamoxifen- functionalized liposome for their ability to facilitate selective delivery of cargoes (in this case propidium iodide) to tumors. These two ligands showed some promise and warrants further investigation.

1.10. References

1. Yoo, C. B.; Jones, P. A., Epigenetic therapy of cancer: past, present and future. *Nat Rev Drug Discov* **2006,** *5* (1), 37-50.

2. Arrowsmith, C. H.; Bountra, C.; Fish, P. V.; Lee, K.; Schapira, M., Epigenetic protein families: a new frontier for drug discovery. *Nat Rev Drug Discov* **2012,** *11* (5), 384-400.

3. Ning, B.; Li, W.; Zhao, W.; Wang, R., Targeting epigenetic regulations in cancer. *Acta Biochim et Biophys Sin* **2016,** *48* (1), 97-109.

4. You, J. S.; Han, J. H., Targeting components of epigenome by small molecules. *Arch. Pharm. Res.* **2014,** *37* (11), 1367-1374.

5. Baylin, S. B.; Herman, J. G., DNA hypermethylation in tumorigenesis: epigenetics joins genetics. *Trends Genet.* **2000,** *16* (4), 168-174.

6. Dawson, Mark A.; Kouzarides, T., Cancer Epigenetics: From Mechanism to Therapy. *Cell* **2012,** *150* (1), 12-27.

7. Scholz, C.; Weinert, B. T.; Wagner, S. A.; Beli, P.; Miyake, Y.; Qi, J.; Jensen, L. J.; Streicher, W.; McCarthy, A. R.; Westwood, N. J.; Lain, S.; Cox, J.; Matthias, P.; Mann, M.; Bradner, J. E.; Choudhary, C., Acetylation site specificities of lysine deacetylase inhibitors in human cells. *Nat Biotech* **2015,** 33(4): 415-423.

8. Choudhary, C.; Kumar, C.; Gnad, F.; Nielsen, M. L.; Rehman, M.; Walther, T. C.; Olsen, J. V.; Mann, M., Lysine Acetylation Targets Protein Complexes and Co-Regulates Major Cellular Functions. *Science* **2009,** *325* (5942), 834-840.

9. Minucci, S.; Pelicci, P. G., Histone deacetylase inhibitors and the promise of epigenetic (and more) treatments for cancer. *Nat. Rev. Cancer* **2006,** *6* (1), 38-51.

10. Bowman, G. D.; Poirier, M. G., Post-Translational Modifications of Histones That Influence Nucleosome Dynamics. *Chem. Rev.* **2015,** 115(6), 2274-2295.

11. Gryder, B. E.; Sodji, Q. H.; Oyelere, A. K., Targeted cancer therapy: giving histone deacetylase inhibitors all they need to succeed. *Future Med. Chem.* **2012,** *4* (4), 505-524.

12. Micelli, C.; Rastelli, G., Histone deacetylases: structural determinants of inhibitor selectivity. *Drug Discovery Today* **2015,** *20* (6), 718-735.

13. Mohammed, M.; Chandrasekar, M. J. N.; Jeyapal, G. P.; Nanjan, M. J., Inhibitors of histone deacetylase as antitumor agents: A critical review. *Bioorg. Chem.* **2016,** 67, 18-42.

14. West, A. C.; Johnstone, R. W., New and emerging HDAC inhibitors for cancer treatment. *J. Clin Invest.* **2014,** *124* (1), 30-39.

15. Weichert, W., HDAC expression and clinical prognosis in human malignancies. *Cancer Lett.* **2009,** *280* (2), 168-176.

16. Carrozza, M. J.; Utley, R. T.; Workman, J. L.; Côté, J., The diverse functions of histone acetyltransferase complexes. *Trends Genet.* **2003,** *19* (6), 321-329.

17. Gallinari, P.; Di Marco, S.; Jones, P.; Pallaoro, M.; Steinkuehler, C., HDACs, histone deacetylation and gene transcription: from molecular biology to cancer therapeutics. *Cell Res.* **2007,** *17* (3), 195-211.

18. Strahl, B. D.; Allis, C. D., The language of covalent histone modifications. *Nature* **2000,** *403* (6765), 41-45.

19. Lee, K. K.; Workman, J. L., Histone acetyltransferase complexes: one size doesn't fit all. *Nat. Rev. Mol. Cell Biol.* **2007,** *8* (4), 284-295.

20. Di Cerbo, V.; Schneider, R., Cancers with wrong HATs: the impact of acetylation. *Briefings in Functional Genomics* **2013,** *12* (3), 231-243.

21. Xie, N.; Elangwe, E. N.; Asher, S.; Zheng, Y. G., A Dual-Mode Fluorescence Strategy for Screening HAT Modulators. *Bioconjug. Chem.* **2009,** *20* (2), 360-366.

22. Gajer, J. M.; Furdas, S. D.; Grunder, A.; Gothwal, M.; Heinicke, U.; Keller, K.; Colland, F.; Fulda, S.; Pahl, H. L.; Fichtner, I.; Sippl, W.; Jung, M., Histone acetyltransferase inhibitors block neuroblastoma cell growth in vivo. *Oncogenesis* **2015,** *4*, e137.

23. Yang, C.; Ngo, L.; Zheng, Y. G., Rational Design of Substrate-Based Multivalent Inhibitors of the Histone Acetyltransferase Tip60. *ChemMedChem* **2014,** *9* (3), 537-541.

24. Furdas, S. D.; Shekfeh, S.; Bissinger, E.-M.; Wagner, J. M.; Schlimme, S.; Valkov, V.; Hendzel, M.; Jung, M.; Sippl, W., Synthesis and biological testing of novel pyridoisothiazolones as histone acetyltransferase inhibitors. *Bioorg. Med. Chem.* **2011,** *19* (12), 3678-3689.

25. Sharma, S.; Taliyan, R., Transcriptional dysregulation in Huntington's disease: The role of histone deacetylases. *Pharmacol. Res.* **2015,** *100,* 157-169.

26. Butler, K. V.; Kalin, J.; Brochier, C.; Vistoli, G.; Langley, B.; Kozikowski, A. P., Rational Design and Simple Chemistry Yield a Superior, Neuroprotective HDAC6 Inhibitor, Tubastatin A. *J. Am. Chem. Soc.* **2010,** *132* (31), 10842-10846.

27. Marson, C. M.; Matthews, C. J.; Atkinson, S. J.; Lamadema, N.; Thomas, N. S. B., Potent and Selective Inhibitors of Histone Deacetylase-3 Containing Chiral Oxazoline Capping Groups and a N-(2-Aminophenyl)-benzamide Binding Unit. *J. Med. Chem.* **2015,** *58* (17), 6803-6818.

28. Schroeder, F. A.; Lewis, M. C.; Fass, D. M.; Wagner, F. F.; Zhang, Y.-L.; Hennig, K. M.; Gale, J.; Zhao, W.-N.; Reis, S.; Barker, D. D.; Berry-Scott, E.; Kim, S. W.; Clore, E. L.; Hooker, J. M.; Holson, E. B.; Haggarty, S. J.; Petryshen, T. L., A Selective HDAC 1/2 Inhibitor Modulates Chromatin and Gene Expression in Brain and Alters Mouse Behavior in Two Mood-Related Tests. *PLoS One* **2013,** *8* (8), e71323.

29. Roche, J.; Bertrand, P., Inside HDACs with more selective HDAC inhibitors. *Eur. J. Med. Chem.* **2016,** 121, 451-483.

30. Pavlik, C. M.; Wong, C. Y. B.; Ononye, S.; Lopez, D. D.; Engene, N.; McPhail, K. L.; Gerwick, W. H.; Balunas, M. J., Santacruzamate A, a Potent and Selective Histone Deacetylase

Inhibitor from the Panamanian Marine Cyanobacterium cf. Symploca sp. *J. Nat. Prod.* **2013,** *76* (11), 2026-2033.

31. Patil, V.; Sodji, Q. H.; Kornacki, J. R.; Mrksich, M.; Oyelere, A. K., 3-Hydroxypyridin-2-thione as Novel Zinc Binding Group for Selective Histone Deacetylase Inhibition. *J. Med. Chem.* **2013,** *56* (9), 3492-3506.

32. Bergman, J. A.; Woan, K.; Perez-Villarroel, P.; Villagra, A.; Sotomayor, E. M.; Kozikowski, A. P., Selective Histone Deacetylase 6 Inhibitors Bearing Substituted Urea Linkers Inhibit Melanoma Cell Growth. *J. Med. Chem.* **2012,** *55* (22), 9891-9899.

33. Furumai, R.; Matsuyama, A.; Kobashi, N.; Lee, K.-H.; Nishiyama, M.; Nakajima, H.; Tanaka, A.; Komatsu, Y.; Nishino, N.; Yoshida, M.; Horinouchi, S., FK228 (Depsipeptide) as a Natural Prodrug That Inhibits Class I Histone Deacetylases. *Cancer Res.* **2002,** *62* (17), 4916-4921.

34. Shah, M. H.; Binkley, P.; Chan, K.; Xiao, J.; Arbogast, D.; Collamore, M.; Farra, Y.; Young, D.; Grever, M., Cardiotoxicity of Histone Deacetylase Inhibitor Depsipeptide in Patients with Metastatic Neuroendocrine Tumors. *Clin. Cancer Res.* **2006,** *12* (13), 3997-4003.

35. Daniel, K. B.; Sullivan, E. D.; Chen, Y.; Chan, J. C.; Jennings, P. A.; Fierke, C. A.; Cohen, S. M., Dual-Mode HDAC Prodrug for Covalent Modification and Subsequent Inhibitor Release. *J. Med. Chem.* **2015,** *58* (11), 4812-4821.

36. Shen, S.; Kozikowski, A. P., Why Hydroxamates May Not Be the Best Histone Deacetylase Inhibitors—What Some May Have Forgotten or Would Rather Forget? *ChemMedChem* **2015**, 11(1), 15-21.

37. Rodvold, K. A.; Gotfried, M. H.; Danziger, L. H.; Servi, R. J., Intrapulmonary steady-state concentrations of clarithromycin and azithromycin in healthy adult volunteers. *Antimicrob. Agents Chemother.* **1997,** *41* (6), 1399-402.

38. Patel, K. B.; Xuan, D.; Tessier, P. R.; Russomanno, J. H.; Quintiliani, R.; Nightingale, C. H., Comparison of bronchopulmonary pharmacokinetics of clarithromycin and azithromycin. *Antimicrob. Agents Chemother.* **1996,** *40* (10), 2375-9.

39. Gladue, R. P.; Bright, G. M.; Isaacson, R. E.; Newborg, M. F., In vitro and in vivo uptake of azithromycin (CP-62,993) by phagocytic cells: possible mechanism of delivery and release at sites of infection. *Antimicrob. Agents Chemother.* **1989,** *33* (3), 277-282.

40. Mwakwari, S. C.; Guerrant, W.; Patil, V.; Khan, S. I.; Tekwani, B. L.; Gurard-Levin, Z. A.; Mrksich, M.; Oyelere, A. K., Non-Peptide Macrocyclic Histone Deacetylase Inhibitors Derived from Tricyclic Ketolide Skeleton. *J. Med. Chem.* **2010,** *53* (16), 6100-6111.

41. Oyelere, A. K.; Chen, P. C.; Guerrant, W.; Mwakwari, S. C.; Hood, R.; Zhang, Y.; Fan, Y., Non-Peptide Macrocyclic Histone Deacetylase Inhibitors. *J. Med. Chem.* **2008,** *52* (2), 456-468.

42. Sodji, Q. H.; Kornacki, J. R.; McDonald, J. F.; Mrksich, M.; Oyelere, A. K., Design and structure activity relationship of tumor-homing histone deacetylase inhibitors conjugated to folic and pteroic acids. *Eur. J. Med. Chem.* **2015,** *96* (0), 340-359.

43. Zhang, X.; Kong, Y.; Zhang, J.; Su, M.; Zhou, Y.; Zang, Y.; Li, J.; Chen, Y.; Fang, Y.; Zhang, X.; Lu, W., Design, synthesis and biological evaluation of colchicine derivatives as novel tubulin and histone deacetylase dual inhibitors. *Eur. J. Med. Chem.* **2015,** *95* (0), 127-135.

44. Siegel, R. L.; Miller, K. D.; Jemal, A., Cancer statistics, 2015. *CA Cancer J. Clin.* **2015,** *65* (1), 5-29.

45. Mehnert, J. M.; Kluger, H. M., Driver Mutations in Melanoma: Lessons Learned From Bench-to-Bedside Studies. *Curr. Oncol. Rep.* **2012,** *14* (5), 449-457.

46. Korman, J. B.; Fisher, D. E., Developing melanoma therapeutics: overview and update. *Wiley Interdiscip. Rev. Syst. Biol. Med.* **2013,** *5* (3), 257-271.

47. Besaratinia, A.; Tommasi, S., Epigenetics of human melanoma: promises and challenges. *J. Mol. Cell. Biol.* **2014,** *6* (5), 356-367.

48. Sarkar, D.; Leung, E. Y.; Baguley, B. C.; Finlay, G. J.; Askarian-Amiri, M. E., Epigenetic regulation in human melanoma: past and future. *Epigenetics* **2015,** *10* (2), 103-121.

49. Sigalotti, L.; Covre, A.; Fratta, E.; Parisi, G.; Colizzi, F.; Rizzo, A.; Danielli, R.; Nicolay, H. J.; Coral, S.; Maio, M., Epigenetics of human cutaneous melanoma: setting the stage for new therapeutic strategies. *J. Transl. Med.* **2010,** *8* (1), 1-22.

50. Peltonen, K.; Kiviharju, T. M.; Järvinen, P. M.; Ra, R.; Laiho, M., Melanoma cell lines are susceptible to histone deacetylase inhibitor TSA provoked cell cycle arrest and apoptosis. *Pigment Cell Res.* **2005,** *18* (3), 196-202.

51. Liu, J.; Gu, J.; Feng, Z.; Yang, Y.; Zhu, N.; Lu, W.; Qi, F., Both HDAC5 and HDAC6 are required for the proliferation and metastasis of melanoma cells. *J. Transl. Med.* **2016,** *14* (1), 1-13.

52. Michelot, J. M.; Moreau, M. F. C.; Veyre, A. J.; Bonafous, J. F.; Bacin, F. J.; Madelmont, J. C.; Bussiere, F.; Souteyrand, P. A.; Mauclaire, L. P.; Chossat, F. M.; Papon, J. M.; Labarre, P. G.; Kauffmann, P.; Plagne, R. J., Phase II Scintigraphic Clinical Trial of Malignant Melanoma and Metastases with Iodine-123-N-(2-Diethylaminoethyl 4-Iodobenzamide). *J. Nucl. Med.* **1993,** *34* (8), 1260-1266.

53. Liu, H.; Liu, S.; Miao, Z.; Jiang, H.; Deng, Z.; Hong, X.; Cheng, Z., A Novel Aliphatic 18F-Labeled Probe for PET Imaging of Melanoma. *Mol. Pharm.* **2013,** *10* (9), 3384-3391.

54. Carew, J. S.; Giles, F. J.; Nawrocki, S. T., Histone deacetylase inhibitors: mechanisms of cell death and promise in combination cancer therapy. *Cancer Lett.* **2008,** *269* (1), 7-17.

55. Hutson, T. E.; Vukelja, S.; Atienza, D.; Awasthi, S.; Delaune, R.; Deutsch, M.; Dien, P. Y.; Gregory, T. F.; Kolodziej, M. J.; Muscato, J. J.; Raju, R. N.; Ruxer, R. L.; Mull, S.; Ilegbodu, D.; Hood, K.; Nicol, S.; Berry, W., Phase I study of a 3-drug regimen of gemcitabine/cisplatin/pemetrexed in patients with metastatic transitional cell carcinoma of the urothelium. *Invest. New Drugs* **2008,** *26* (2), 151-158.

56. Musso, L.; Dallavalle, S.; Zunino, F., Perspectives in the development of hybrid bifunctional antitumour agents. *Biochem. Pharmacol.* **2015,** *96* (4), 297-305.

57. Morphy, R.; Rankovic, Z., Designed Multiple Ligands. An Emerging Drug Discovery Paradigm. *J. Med. Chem.* **2005,** *48* (21), 6523-6543.

58 Costantino, L.; Barlocco, D., Designed multiple ligands: basic research vs clinical outcomes. *Curr. Med. Chem.* **2012,** *19* (20), 3353-87.

59 Van, d. S. C. J.; Geldenhuys, W. J., Multimodal drugs and their future for Alzheimer's and Parkinson's disease. *Int. Rev. Neurobiol.* **2011,** *100*, 107-25.

60 Zhan, P.; Liu, X., Designed multiple ligands: an emerging anti-HIV drug discovery paradigm. *Curr. Pharm. Des.* **2009,** *15* (16), 1893-917.

61. Gryder, B. E.; Rood, M. K.; Johnson, K. A.; Patil, V.; Raftery, E. D.; Yao, L.-P. D.; Rice, M.; Azizi, B.; Doyle, D. F.; Oyelere, A. K., Histone Deacetylase Inhibitors Equipped with Estrogen Receptor Modulation Activity. *J. Med. Chem.* **2013,** *56* (14), 5782-5796.

62. Patel, H. K.; Siklos, M. I.; Abdelkarim, H.; Mendonca, E. L.; Vaidya, A.; Petukhov, P. A.; Thatcher, G. R. J., A Chimeric SERM–Histone Deacetylase Inhibitor Approach to Breast Cancer Therapy. *ChemMedChem* **2014**, 9(3), 602-13.

63. Tang, C.; Li, C.; Zhang, S.; Hu, Z.; Wu, J.; Dong, C.; Huang, J.; Zhou, H.-B., Novel Bioactive Hybrid Compounds Dual Targeting Estrogen Receptor and Histone Deacetylase for Treatment of Breast Cancer. *J. Med. Chem.* **2015,** 58(11), 4550-72.

64. Gryder, B. E.; Akbashev, M. J.; Rood, M. K.; Raftery, E. D.; Meyers, W. M.; Dillard, P.; Khan, S.; Oyelere, A. K., Selectively targeting prostate cancer with antiandrogen equipped histone deacetylase inhibitors. *ACS Chem. Biol.* **2013,** *8* (11), 2550-60.

65. Guerrant, W.; Patil, V.; Canzoneri, J. C.; Oyelere, A. K., Dual Targeting of Histone Deacetylase and Topoisomerase II with Novel Bifunctional Inhibitors. *J. Med. Chem.* **2012,** *55* (4), 1465-1477.

66. Ko, K. S.; Steffey, M. E.; Brandvold, K. R.; Soellner, M. B., Development of a Chimeric c-Src Kinase and HDAC Inhibitor. *ACS Med. Chem. Lett.* **2013,** 4(8), 779-783.

67. Adcock, I. M., HDAC inhibitors as anti-inflammatory agents. *Br. J. Pharmacol.* **2007,** *150* (7), 829-831.

68. Smith, W. L.; DeWitt, D. L.; Garavito, R. M., CYCLOOXYGENASES: Structural, Cellular, and Molecular Biology. *Annu. Rev. Biochem.* **2000,** *69* (1), 145-182.

69. Tucker, O. N.; Dannenberg, A. J.; Yang, E. K.; Zhang, F.; Teng, L.; Daly, J. M.; Soslow, R. A.; Masferrer, J. L.; Woerner, B. M.; Koki, A. T.; Fahey, T. J., Cyclooxygenase-2 Expression Is Up-Regulated in Human Pancreatic Cancer. *Cancer Res.* **1999,** *59* (5), 987-990.

70. Steinbach, G.; Lynch, P. M.; Phillips, R. K. S.; Wallace, M. H.; Hawk, E.; Gordon, G. B.; Wakabayashi, N.; Saunders, B.; Shen, Y.; Fujimura, T.; Su, L.-K.; Levin, B.; Godio, L.; Patterson,

S.; Rodriguez-Bigas, M. A.; Jester, S. L.; King, K. L.; Schumacher, M.; Abbruzzese, J.; DuBois, R. N.; Hittelman, W. N.; Zimmerman, S.; Sherman, J. W.; Kelloff, G., The Effect of Celecoxib, a Cyclooxygenase-2 Inhibitor, in Familial Adenomatous Polyposis. *N. Engl. J. Med.* **2000,** *342* (26), 1946-1952.

71. Tsioulias, G.; Go, M.; Rigas, B., NSAIDs and Colorectal Cancer Control: Promise and Challenges. *Curr Pharmacol Rep* **2015**, 1-7.

72. Wang, X.; Li, G.; Wang, A.; Zhang, Z.; Merchan, J. R.; Halmos, B., Combined histone deacetylase and cyclooxygenase inhibition achieves enhanced antiangiogenic effects in lung cancer cells. *Mol. Carcinog.* **2013,** *52* (3), 218-228.

73. Smith, W. L.; Garavito, R. M.; DeWitt, D. L., Prostaglandin Endoperoxide H Synthases (Cyclooxygenases)-1 and −2. *J. Biol. Chem.* **1996,** *271* (52), 33157-33160.

74. Lopes, S. C. d. A.; Giuberti, C. d. S.; Rocha, T. G. R.; Ferreira, D. d. S.; Leite, E. A.; Oliveira, M. C., *Liposomes as Carriers of Anticancer Drugs, Cancer Treatment - Conventional and Innovative Approaches*, Prof. Letícia Rangel (Ed.), 2013. InTech, DOI: 10.5772/55290.

75. Torchilin, V. P., Recent advances with liposomes as pharmaceutical carriers. *Nat Rev Drug Discov* **2005,** *4* (2), 145-160.

76. Ishida, T.; Harada, M.; Wang, X. Y.; Ichihara, M.; Irimura, K.; Kiwada, H., Accelerated blood clearance of PEGylated liposomes following preceding liposome injection: Effects of lipid dose and PEG surface-density and chain length of the first-dose liposomes. *J. Control. Release* **2005,** *105* (3), 305-317.

77. Ranson, M. R.; Cheeseman, S.; White, S.; Margison, J., Caelyx (stealth liposomal doxorubicin) in the treatment of advanced breast cancer. *Crit. Rev. Oncol. Hematol.* **2001,** *37* (2), 115-120.

78. Theek, B.; Gremse, F.; Kunjachan, S.; Fokong, S.; Pola, R.; Pechar, M.; Deckers, R.; Storm, G.; Ehling, J.; Kiessling, F.; Lammers, T., Characterizing EPR-mediated passive drug targeting using contrast-enhanced functional ultrasound imaging. *J. Control. Release* **2014,** *182* (0), 83-89.

79. Nichols, J. W.; Bae, Y. H., EPR: Evidence and fallacy. *J. Control. Release* **2014,** *190* (0), 451-64.

80. Kaasgaard, T.; Andresen, T. L., Liposomal cancer therapy: exploiting tumor characteristics. *Exp Opinion Drug Del.* **2010,** *7* (2), 225-243.

81. Rakowski, J. A.; Ahmad, S.; Holloway, R. W., Use of pegylated liposomal doxorubicin in the management of platinum-sensitive recurrent ovarian cancer: current concepts. *Expert Rev. Anticancer Ther.* **2012,** *12* (1), 31-40.

82. Byrne, J. D.; Betancourt, T.; Brannon-Peppas, L., Active targeting schemes for nanoparticle systems in cancer therapeutics. *Adv. Drug Del. Rev.* **2008,** *60* (15), 1615-1626.

83. Kue, C. S.; Kamkaew, A.; Burgess, K.; Kiew, L. V.; Chung, L. Y.; Lee, H. B., Small Molecules for Active Targeting in Cancer. *Med. Res. Rev.* **2016**, 36(3) 494-575.

84. Mendonça, L. S.; Firmino, F.; Moreira, J. N.; Pedroso de Lima, M. C.; Simões, S., Transferrin Receptor-Targeted Liposomes Encapsulating anti-BCR-ABL siRNA or asODN for Chronic Myeloid Leukemia Treatment. *Bioconjug. Chem.* **2010,** *21* (1), 157-168.

85. Rotman, M.; Welling, M. M.; Nabuurs, R. J. A.; van, B. M. A.; Bunschoten, A.; de, B. M. E.; Rip, J.; Gaillard, P. J.; van, d. M. S. M.; van, d. W. L., Enhanced glutathione PEGylated liposomal brain delivery of an anti-amyloid single domain antibody fragment in a mouse model for Alzheimer's disease. *J. Control. Release* **2015,** *203*, 40-50.

86. Shmeeda, H.; Tzemach, D.; Mak, L.; Gabizon, A., Her2-targeted pegylated liposomal doxorubicin: Retention of target-specific binding and cytotoxicity after in vivo passage. *J. Control. Release* **2009,** *136* (2), 155-160.

87. Xing, H.; Tang, L.; Yang, X.; Hwang, K.; Wang, W.; Yin, Q.; Wong, N. Y.; Dobrucki, L. W.; Yasui, N.; Katzenellenbogen, J.; Helferich, W.; Cheng, J.; Lu, Y., Selective Delivery of an Anticancer Drug with Aptamer-Functionalized Liposomes to Breast Cancer Cells in Vitro and in Vivo. *J. Materials Chem. B* **2013**.

88. Dreaden, E. C.; Raji, I. O.; Austin, L. A.; Fathi, S.; Mwakwari, S. C.; Humphries, W. H.; Kang, B.; Oyelere, A. K.; El-Sayed, M. A., P-Glycoprotein-Dependent Trafficking of Nanoparticle-Drug Conjugates. *Small* **2014,** *10* (9), 1719-1723.

89. Dreaden, E. C.; Mwakwari, S. C.; Austin, L. A.; Kieffer, M. J.; Oyelere, A. K.; El-Sayed, M. A., Small Molecule–Gold Nanorod Conjugates Selectively Target and Induce Macrophage Cytotoxicity towards Breast Cancer Cells. *Small* **2012,** *8* (18), 2819-2822.

90. Dreaden, E. C.; Mwakwari, S. C.; Sodji, Q. H.; Oyelere, A. K.; El-Sayed, M. A., Tamoxifen−Poly(ethylene glycol)−Thiol Gold Nanoparticle Conjugates: Enhanced Potency and Selective Delivery for Breast Cancer Treatment. *Bioconjug. Chem.* **2009,** *20* (12), 2247-2253.

CHAPTER 2

SYNTHESIS, ANTI-CANCER ACTIVITY EVALUATION AND ANTI-INFLAMMATORY STUDY OF CLARITHROMYCIN-BASED HDACI

Some of the work described in this chapter have been published in:

Bioorganic and Medicinal Chemistry, 2015, 23 (24), 7543-7564

2.1. Introduction

Histone deacetylases (HDACs) are emerging therapeutic targets for cancer and other diseases such as malaria and leishmania.[1,2] In conjuction with histone acetyltransferases (HATs), they regulate the chromatin dynamics by controlling the acetylation state of histone proteins as well as non-histone proteins such as tubulin, ERα, p53, HSP90, and GATA-1.[3] Histone deacetylase inhibitors (HDACi) have been shown to cause growth arrest, differentiation, and apoptosis in a variety of cancer cell lines.[4] To date, several classes of small molecule HDACi exist conforming to a three-motif pharmacophoric model, namely, a zinc binding group (ZBG), a hydrophobic linker, and a recognition cap group.[5] Moreover, five HDACi have been clinically approved for hematological malignancies (Figure 2.1a). The clinically approved HDACi include: suberoylanilide hydroxamic acid (SAHA)[6,7] and FK228[8], approved for the treatment of cutaneous T-cell lymphoma; Panobinostat and Chidamide, approved for multiple myeloma;[9,10] and Belinostat granted approval for peripheral T cell lymphoma[11]. Among all HDACi, macrocyclic HDACi (Figure 2.1b) have the most complex cap group moieties capable of interacting optimally with amino acid residues at the surface of the HDAC active site, an attribute that is essential for the modulation of the biological activities of these agents. Although they possess potent HDAC

inhibition activity (nanomolar range), synthetic challenges posed by their complex structural features, as well as the disadvantages resulting from their peptide group (s) make the clinical development of macrocylic HDACi almost impossible.[12]

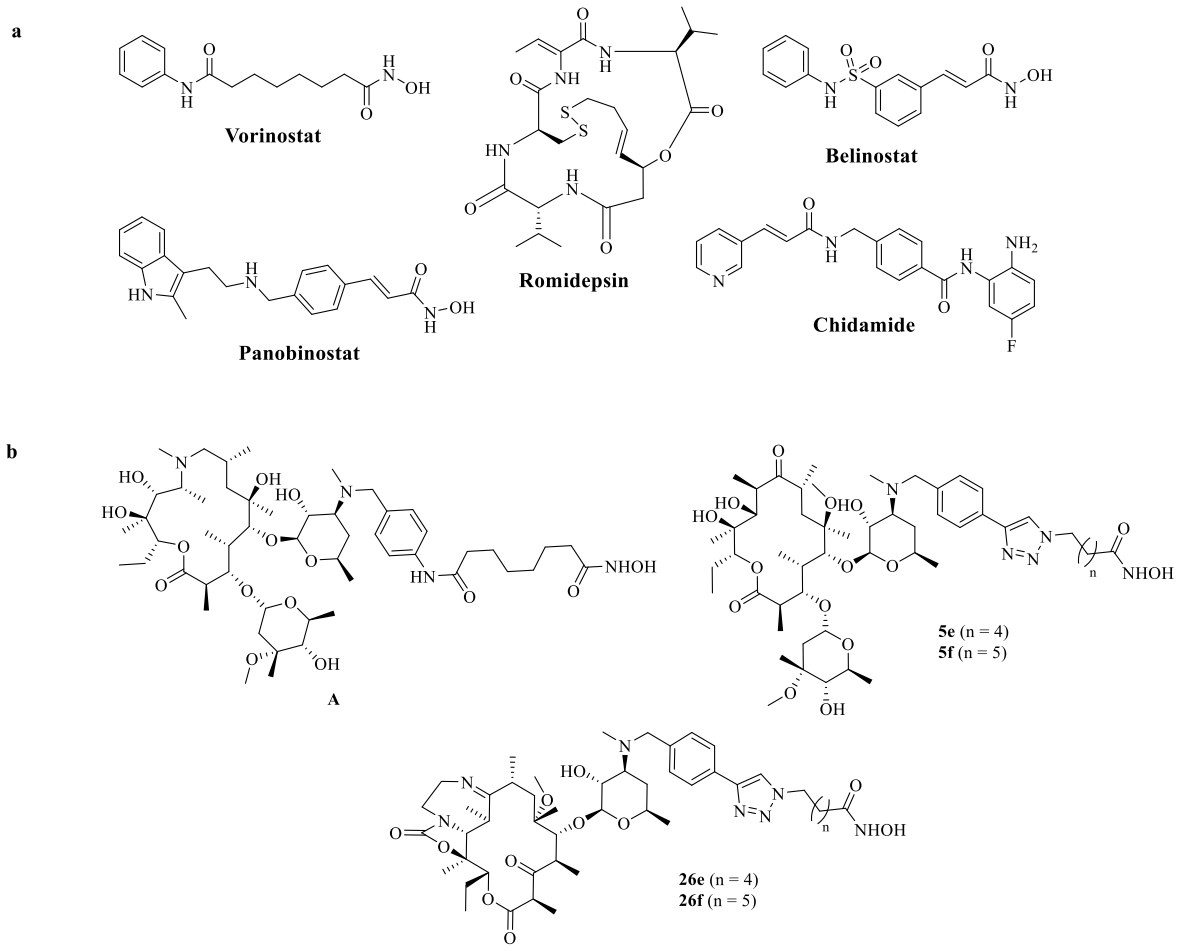

Figure 2.1. Structures of representative HDACi: (a) Clinically approved HDACi, (b) Selected examples of non-peptide (**5e-f**, **26e-f**) macrocyclic HDACi.

Previously, we showed that macrocycles derived from two 14-membered macrolide rings – clarithromycin (**5e** and **5f**) and TE-802 (**26e** and **26f**), are excellent mimetics for the peptide backbone of macrocyclic HDACi.[13,14,15] The replacement of the amide moiety, by its bioisostere, the triazole unit, increased the HDAC inhibitory potency of matched compounds by almost 8-

fold.[14] Drawing inspiration from the naturally occurring HDACi such as TSA (trichostatin A) we have hitherto studied the *para*-substitution pattern of the aryl-triazole cap group of these non-peptide macrocyclic HDACi.[14,15]

To gain further insight into the depth of the SAR of the class of HDAC inhibitors based on the 14-membered macrolide ring, clarithromycin, we investigated and disclosed herein the consequence of: (i) varied methylene linker lengths; (ii) point of attachment of aryl-triazole cap group; and (iii) having biaryl zinc binding group (ZBG), on their biological activities. We observed that the new compounds reported here possess anti-HDAC, anti-proliferative and anti-inflammatory activities that are highly dependent on the point of attachment of the HDAC inhibition group and the methylene linker lengths.

2.2. Chemistry

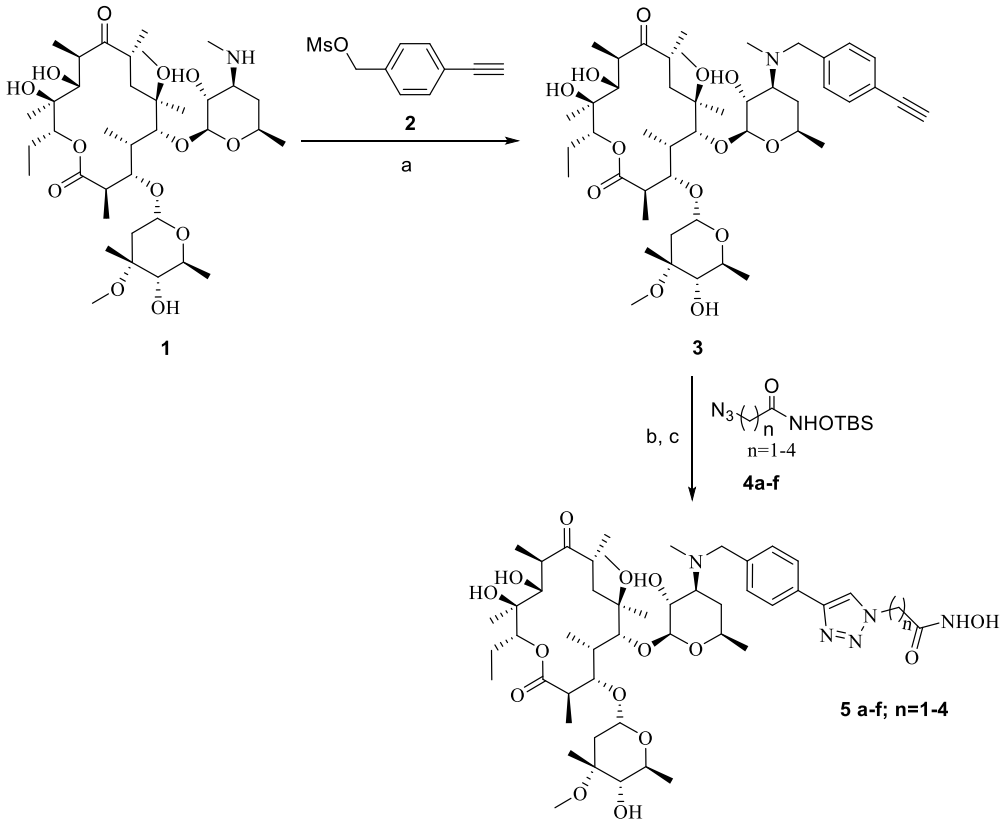

Scheme 2.1. (a) Hünig's base, DMSO, 85 °C, 3 h; 63 % (b) CuI (15 mol%), Hünig's base, THF, rt, 12 h; (c) CsF, MeOH, rt, 30 min, 30-40 %.

The syntheses of the target compounds were achieved following the reaction routes shown in Schemes 2.1-2.3. The crucial ethynylbenzyl moiety was installed at the desosamine sugar of clarithromycin to furnish the requisite alkynyl-clarithromycin **3**, following the literature procedure.[14,15,16,17] Copper (I)-catalyzed azide-alkyne-cycloaddition (CuAAC)[18] reaction between TBS-protected azidohydroxamates **4a-f** and compound **3**, followed by removal of TBS-group[19] afforded the desired compounds **5a-f** (Scheme 2.1).

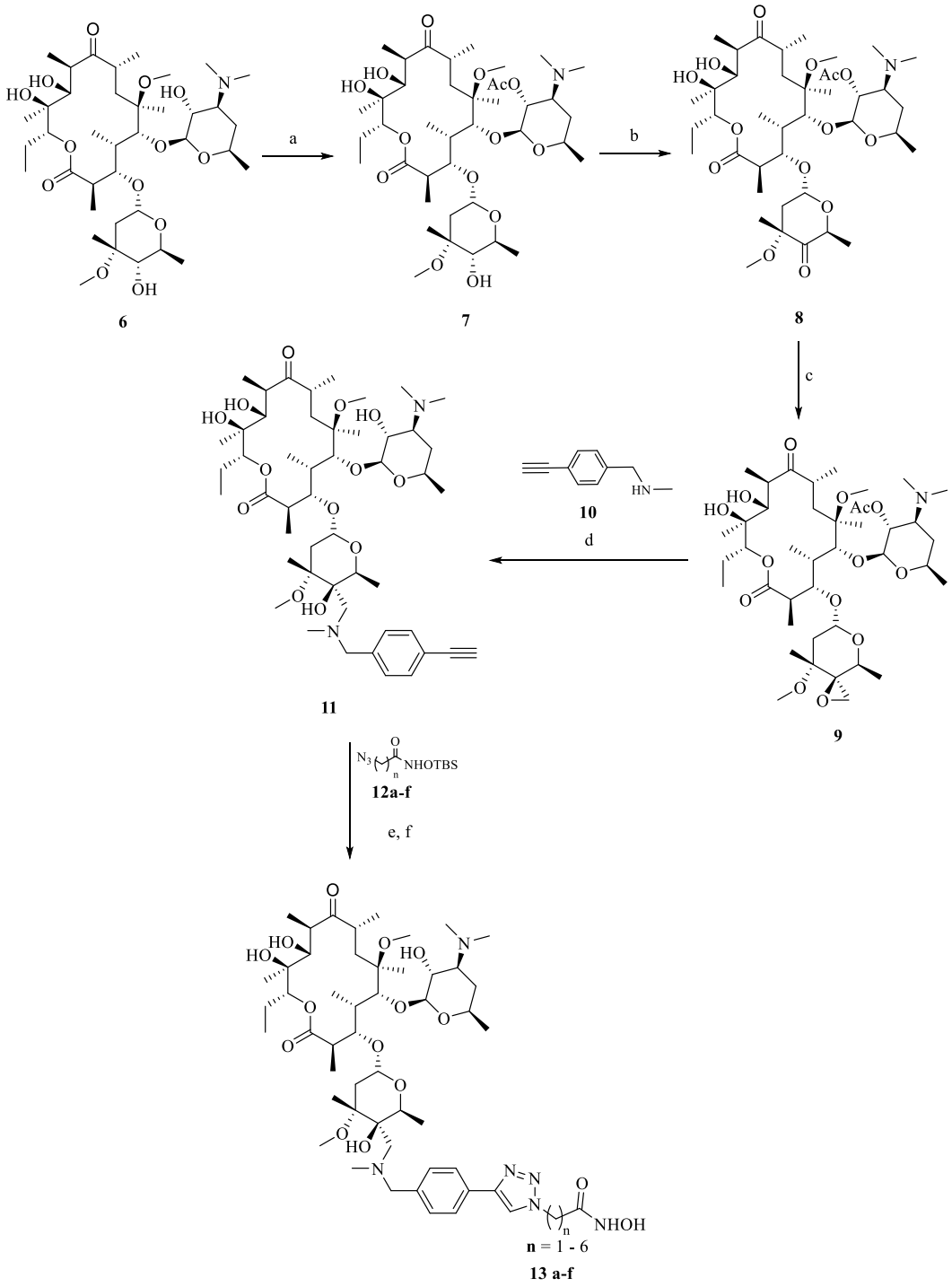

Scheme 2.2. (a) CH_2Cl_2, Ac_2O, rt, 3 h, 100 %; (b) NCS, DMS, TEA, CH_2Cl_2, -15 °C, 4.5 h, 100 %; (c) $(CH_3)_3SO^+I^-$, NaH, DMSO, THF, rt, 4 h, 38 %; (d) KI, MeOH, 60 °C, 6 h, 73 %; (e) CuI (15 mol%), Hünig's base, THF, rt, 12 h; (f) CsF, MeOH, rt, 2 h, 30-40 %.

Introduction of the ethynylbenzyl moiety to cladinose sugar of clarithromycin **6** was achieved in four steps (Scheme 2.2).[20b] Reaction of clarithromycin **6** with acetic anhydride in dichloromethane gave selective 2′-*O*-acetylclarithromycin **7**. Corey-Kim oxidation of **7** and subsequent Corey-Chaykovsky epoxidation of intermediate 4″-oxo-2′-*O*-acetylclarithromycin **8** yielded the epoxide **9**. Diastereoselective opening of epoxide **9** with 4-ethynylbenzyl-*N*-methyamine **10** in methanol, followed by a concomitant acetyl group deprotection, gave the vital intermediate **11**. The alkynyl intermediate **11** was subjected to CuAAC reaction with the requisite TBS-protected azido hydroxamates **12a-f** followed by TBS protection removal to furnish the target molecules **13a-f** in decent yields.

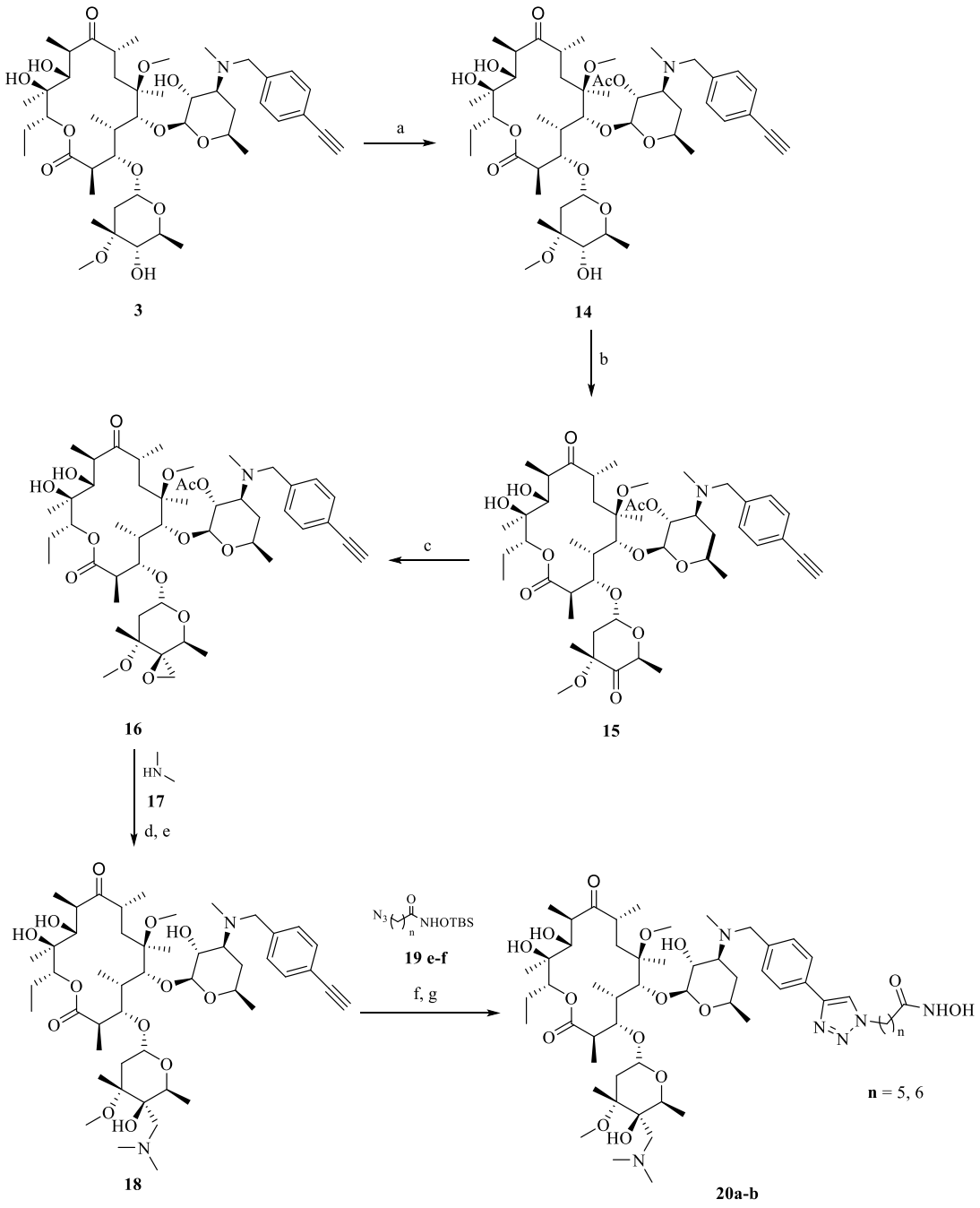

Scheme 2.3. (a) acetic anhydride, CH_2Cl_2, rt, 3 h, 95 %; (b) NCS, DMS, TEA, CH_2Cl_2, -15 °C, 6 h, 45 %; (c) $(CH_3)_3SO^+I^-$, NaH, DMSO, THF, rt, 4 h, 77%; (d) KI, MeOH, 60 °C, 6 h, 96 %; (e) MeOH, 90 °C, 3 days; (f) CuI (15 mol%), Hünig's base, THF, rt, 12 h; (g) CsF, MeOH, rt, 2 h, 30-44 %.

We thereafter synthesized clarithromycin-triazolyl-hydroxamic acids with dimethylamino methylene group placed in the *C*4" position of cladinose sugar (Scheme 2.3). We propose that this substitution should introduce extra acid-stability to the cladinose sugar glycosidic bond.[20c] In addition to this, we wanted to see if this small change will influence the HDAC inhibitory and growth inhibition activity profile of these compounds. The target compounds **20a-b** were made from intermediate **3** following a similar synthetic route as described for compounds **13a-f**. The previously synthesized compound **5f** was included here as a control.

2.3. Results and discussion

To evaluate the HDAC inhibitory activity of the newly synthesized compounds, we tested them against class I (HDAC1 and HDAC8) and class IIb (HDAC6) HDAC enzymes. Two previously synthesized compounds (**5e** and **5f**)[14,15] were added as controls. HDAC inhibition was measured using the label-free mass spectrometry-based SAMDI assay.[21] In agreement with previous observations, most of tested compounds were less active towards HDAC8 except for compounds **5f** (IC_{50} 713 nM, Table 2.1).

A closer look at the HDACs 1 and 6 inhibitory profiles of these compounds revealed an interesting trend that is largely dependent on the length of the methylene spacer-group separating the triazolyl group from the hydroxamate moiety. We observed that an increase in the length of the methylene spacer resulted in gradual increase in HDAC1 and HDAC6 inhibitory activities. In most cases, optimum potency was obtained with compounds having six methylene spacers. In general, compounds having five or six methylene spacers showed low to mid nanomolar HDAC1 (**5e-f**, **13e-f**, **20a-b**) and HDAC6 (**5e-f**, **13e-f**, **20a-b**) inhibitory potency (Table 2.1). Conversely,

compounds having one to four methylene spacers were either inactive or very poorly active (**5a-d**, **13a-d**).

Table 2.1. HDAC 1, HDAC 6, and HDAC 8 Inhibition Activities (IC_{50} in nM) of clarithromycin derived hydroxamic acid compounds

Compound	n	HDAC 1	HDAC 6	HDAC 8
5a	1	> 10000	> 10000	> 10000
5b	2	> 10000	919 ± 45	2450 ± 600
5c	3	9910 ± 3000	70.9 ± 12.6	986 ± 81
5d	4	4870 ± 500	120 ± 19	877 ± 125
5e	5	533 ± 123	3.61 ± 1.01	1180 ± 310
5f	6	207 ± 84	6.67 ± 1.23	713 ± 748
13a	1	> 10000	5350 ± 190	7120 ± 2130
13b	2	> 10000	3560 ± 370	10200 ± 1600
13c	3	> 10000	361 ± 67	2530 ± 880
13d	4	3690 ± 860	269 ± 100	1820 ± 400
13e	5	652 ± 130	5.89 ± 2.73	985 ± 325
13f	6	23.9 ± 3.3	2.85 ± 1.07	1840 ± 460
20a	5	201 ± 17	32.9 ± 2.4	3200 ± 820
20b	6	33.3 ± 8.1	31.4 ± 5.5	2210 ± 300

Introduction of the dimethylamino methyl group at cladinose sugar C4 position had a modest effect on HDAC1 inhibitory activities of compounds **20a-b** when compared to their

analogs **5e-f**. However, HDAC6 inhibition was affected substantially in all the compounds, with a 5 to 10 fold drop in potency (**20a**: IC_{50} 32.9 nM; **20b**: IC_{50} 31.4 nM compared to **5e**: IC_{50} 3.61 nM, **5f**: IC_{50} 6.67 nM). Attachment of the aryl-triazolyl cap group to cladinose sugar (**13a-f**) also influenced HDAC1 and HDAC6 inhibitory activities. Among all the compounds, compound **13c**, in which the hydroxamic acid moiety was separated from aryl-triazole cap by three methylene groups, showed a five-fold decrease in HDAC6 (IC_{50} 361 nM) inhibitory potency compared to the analogous desosamine modified compound **5c** (IC_{50} 70.9 nM) and was completely inactive against HDAC1 (27% at 10μM for **13c** vs 9.91 μM IC_{50} value for **5c**). Interestingly for **13f**, in which the hydroxamic acid moiety was separated from the aryl-triazole cap by six methylene groups, the HDAC6 inhibitory activity increased by two fold compared to control compound **5f** (IC_{50} 2.85 nM vs 6.67 nM, respectively). Moreover, the HDAC1 inhibitory activity of **13f** was eight-fold higher than that of **5f** (IC_{50} 23.9 nM vs IC_{50} 207 nM, respectively).

Table 2.2. Anti-proliferative activity of selected HDACi (IC_{50} values in μM)[a]

Compound	A549	MCF-7	Vero
5f	2.29 ± 0.73	2.86 ± 0.10	4.90 ± 0.34
13f	0.99 ± 0.08	0.69 ± 0.05	1.55 ± 0.12
20b	3.58 ± 0.79	1.43 ± 0.17	2.08 ± 0.14
SAHA	5.00 ± 0.24	3.27 ± 0.05	1.03 ± 0.09

[a] Each value is obtained from a duplicate of three simultaneous experiments. NI=No inhibition, NT=not tested

2.4. Cell growth inhibition study

To verify if the potent HDAC inhibitory profiles of these clarithromycin-derived HDACi translate to growth inhibitory effects in cells, we tested representative members of each group against lung (A549) and breast (MCF-7) cancers cell lines– and normal cell line (Vero - monkey kidney epithelial cell). Our rationale for selecting a representative compound from each series is that the ideal compound should have robust activity against HDACs 1 and 6- two isoforms implicated in a lot of cancer cases. SAHA and the previously disclosed control compound **5f** are both cytotoxic to the two cancer cell lines (Table 2.2). Compounds **13f** and **20b,** with strong HDAC inhibitory activities, possess varying degree of anti-proliferative activities against A549 and MCF-7 cell lines. For analogous compounds (i.e. having same methylene-linker length), the points of attachment of HDACi moiety to clarithromycin is a strong determinant of potency. However, installing *N, N*-dimethylamine at the cladinose sugar slightly enhanced the cytotoxicity of compound **20b** compared to compound **5f** in MCF-7. In fact, the cladinose ring is the optimum point of attachment of the HDAC inhibiting moiety to the clarithromycin template, as the resulting HDACi **13f** is the most potent among the compounds tested for anti-proliferative activity.

To assess tumor cell selectivity of these series of compounds, we tested them against the non-transformed Vero cell line. The control compound SAHA is equipotent towards healthy and transformed cells, as it is about 3-5 fold more cytotoxic to the Vero cell compared to the two tumor cell lines. In contrast, the clarithromycin-derived compounds are either significantly less cytotoxic or equally cytotoxic to the transformed and normal cells tested.

2.5. Anti-inflammatory Activity Study

Inflammation is a salient factor in cancer, particularly lung cancer and many other chronic lung diseases. [22,23,24] HDACs have been implicated in the regulation of inflammation and HDACi[25] such as SAHA,[26] trichostatin A (TSA),[27] butyrates,[28] and MS-275,[29] attenuate cellular inflammation processes through inhibition of NF-κB activation and or blockage of pro-inflammatory cytokine release.[30] In addition to its antibiotic activities, the macrolide template, clarithromycin, incorporated into the design of HDACi described herein has intrinsic anti-inflammatory and immunostimulatory activities.

To test if the clarithromycin-derived HDACi preserve these useful properties and additively or synergistically enhance the latent anti-inflammatory activity of HDACi, we evaluated their anti-inflammatory activities in BEAS-2B cell infected with nontypeable *Haemophilus influenza (*NTHi) using NF-κB luciferase assay.[31] NTHi is a Gram-negative bacterium which causes infection in the human respiratory tract.[32,33] Upon infection by NTHi, transcriptional regulator, NF-*κ*B, in human epithelial cell is strongly activated by translocating from cytoplasm to nucleus and consequently up-regulating certain pro-inflammatory cytokines such as IL-1*β*, IL-6, and TNF-*α*. To pre-screen these compounds for their effect on NF-*κ*B activity, we treated NTHi infected BEAS-2B cells with the compounds at 1 μM. We observed the compounds lacking or those with weak anti-HDAC activities did not suppress NF-*κ*B activation while those compounds with potent anti-HDAC activities suppressed NF-*κ*B activation to varying degrees which closely correlate with their HDAC inhibition potency.

We then determined the IC_{50} values of selected compounds which suppressed NF-*κ*B activation in the pre-screening and we used SAHA as a positive control. We observed that these

compounds suppressed the NTHi-induced NF-κB activation with IC_{50} ranging from low to high nanomolar. Compounds **5f**, **13f** and **20b** have slightly lower I_{max} value compared to SAHA (Table 2.3), implying that at maximum concentration of 1 μM, these compounds suppressed NF-κB activity SAHA. Interestingly, the starting clarithromycin did not exhibit any anti-inflammatory activity in this assay as their relative percentage luciferase activity was indistinguishable from no drug treatment in presence of NTHi (100%).

Table 2.3. Anti-inflammatory activity (NF-κB inhibition) of selected HDACi

Compound	**IC_{50} (nM)**	***I_{max}%**
5e	785	45.1
5f	243	35.9
13e	785	50.7
13f	197	35.6
20b	260	33.4
SAHA	88	37.4

*Imax (%) at 1 μM

To further confirm the mechanism of anti-inflammatory activities of this class of macrolide HDACi, we performed Q-PCR analysis to determine the effect of these HDACi on the expression levels of mRNAs of inflammatory cytokines known to be NTHi-inducible.[35,36] We observed that compound **13f** more significantly suppressed NTHi-induced TNF-α, IL-1α, IL-1β mRNA expression relative to SAHA in BEAS-2B cells (Figure 2.2). Collectively, these data further

suggest that the suppression of NF-κB activation induced by these compounds is derived from their HDAC inhibition activities.

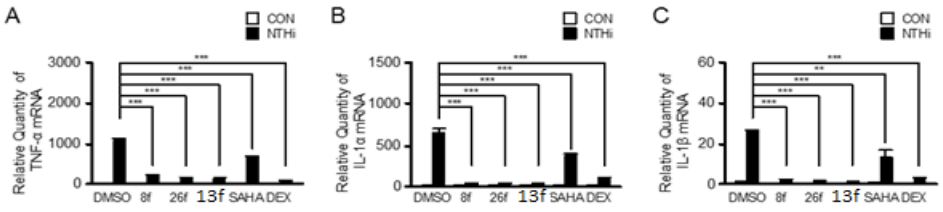

Figure 2.2. HDACi suppress NTHi-induced expression of Cytokines. BEAS-2B cells were pretreated with HDACi (**26f**, 1**3f**; 1 μM) or SAHA (1 μM) or DEX (0.1 μM) for 2 h followed by 1.5 h stimulation with NTHi, and cytokines mRNA (TNF-α, IL-1 α and IL-1β) expressions were analyzed. Data are mean ± std (*n=3*); **p<0.01, ***p<0.005. Data are representative of three independent experiments. CON = BEAS-2B cells treated with PBS control; NTHi = BEAS-2B cells treated with NTHi.

2.6. Targeted and isoform-selective HDACi

In furtherance of our quest to making safer small molecule HDACi, we extended our SAR studies to the ZBG of clarithromycin-based HDACi, with the goal of achieving class 1 selective HDACi. High expression levels of class 1 HDACs is a common feature in many tumors,[37-38] hence class 1-selective inhibitors could be beneficial as safer therapeutics to mitigate some of the adverse effects seen with pan-HDACi.[39]

Structurally, both HDAC 1 and HDAC 2 possess an internal cavity (about 14 Å), adjacent to the Zn ion in the active site (Figure 2.3), that is believed to serve as an exit route for acetate

upon hydrolysis from acetylated lysine substrate.[40] Miller *et. al.* carried out extensive SAR studies on the ZBG portion of the HDAC pharmacophoric model, and came up with compounds having biaryl groups as ZBG[41] (Figure 2.4). In their study, compounds having thiophene attached at the *para* anilinic position gave optimal inhibition and selectivity towards HDAC 1 and HDAC 2.

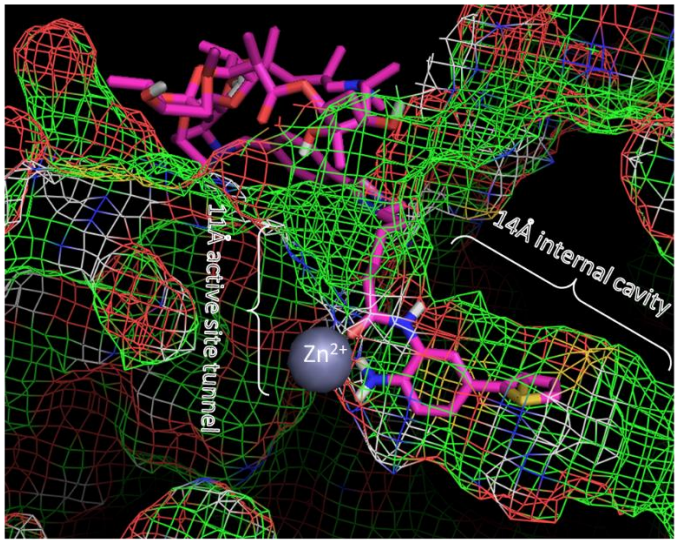

Figure 2.3: Docked structure of macrolide-based HDACi with benzamide ZBG in HDAC1 active site.

The rationale behind having biaryl ZBG is to achieve tighter chelation to Zn^{2+}, and occupy the 14Å internal cavity using the bulky thiophene attached at the *para* anilinic position.

In our approach, we adopted 2-amino-5-(thiophene phenyl) as ZBG in the design of a new series of clarithromycin-based HDACi. We propose that these series of compounds will be capable of selective localization in lung tissues, and show selectivity towards HDAC 1 and HDAC 2 in their HDAC isoforms inhibitory activity. Hypothetically, this approach should result in HDACi with minimal off-target effects.

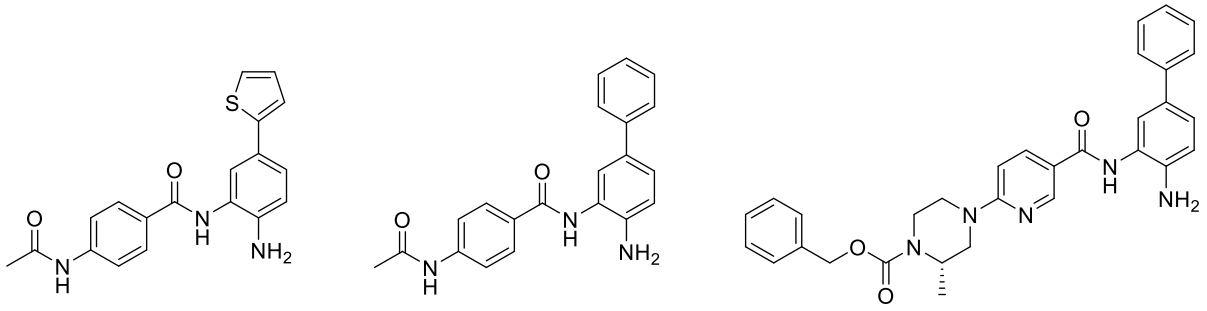

Figure 2.4: HDACi having a benzamide ZBG as reported by Miller *et al*[41]

2.6.1. Chemistry

Linkers used in this study were made as previously described.[42] Previous SAR studies in our lab identified compounds having six methylenes separating the cap group from the ZBG to give the optimum enzyme inhibitory effects.[43-44] Hence, linkers used in this study were restricted to those having five, six and seven methylenes separating the azido end from the ZBG. Using Cu (I)-catalyzed cycloaddition reaction between azido compounds (**21a-c**) and compound **3**, the desired compounds (**22a-c**) were made.

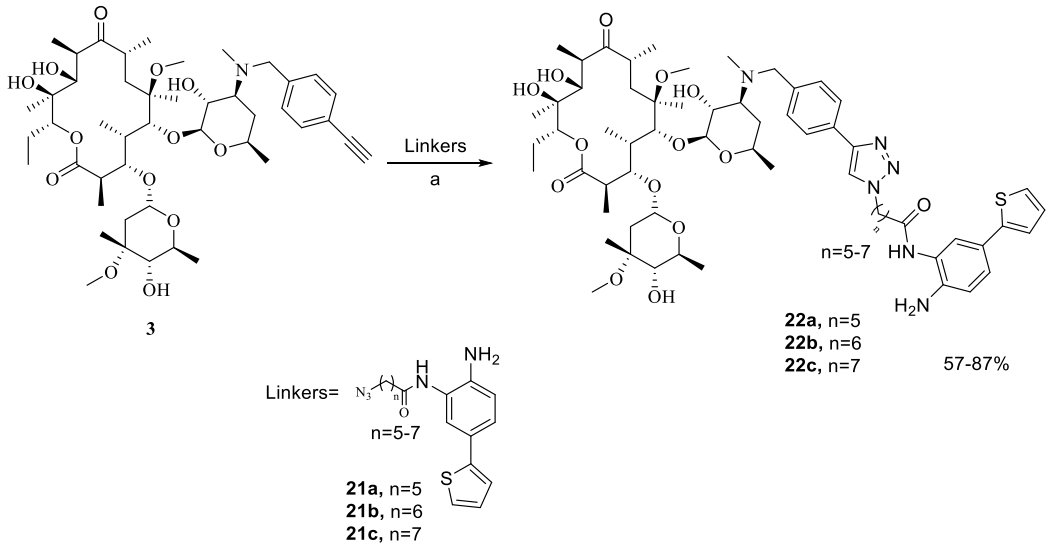

Scheme 2.4: (a) CuI (15 mol%), Hünig's base, THF, rt, 12 h.

2.6.2. HDAC inhibition study

We then profiled compounds **22a-c** against all class I (HDAC 1, HDAC 2, HDAC 3 and HDAC 8) and class IIB (HDAC 6) HDAC isoforms. These isoforms were chosen to evaluate the extent of selective inhibition within the class I HDACs, as well as across other HDAC classes. Consistent with literature observation for compounds having 2-amino-5-(thiophene phenyl) as ZBG[45-46], all the three compounds showed preferential inhibitory effects towards HDAC 1 and HDAC 2, with no activity towards HDAC 3, HDAC 6 and HDAC 8. Hence, they not only show sub-class selectivity, they also showed selectivity across HDAC classes.

Compounds **22a** and **22b** are equipotent towards HDAC 1 and HDAC 2, and there is no obvious selectivity towards either isoform. This is not surprising, as HDAC 1 and HDAC 2 have structural similarities that make it difficult for small molecules to distinguish between the two.[47] The same pattern is seen with compound **22c** against HDAC 1 and HDAC 2, although it is less potent towards the two HDAC isoforms compared to compounds **22a** and **22b**.

Table 2.4. HDAC inhibitory activity of 2-amino-5-(thiophene phenyl)-based HDACi

Compound	HDAC 1	HDAC 2	HDAC 3	HDAC 6	HDAC 8
22a	118 ± 24	101 ± 9	NI	NI	NI
22b	112 ± 20	146 ± 73	NI	NI	NI
22c	428 ± 111	279 ± 54	NI	NI	NI
SAHA	38 ± 2	NT	NT	144 ± 23	232± 19

2.6.3. Antiproliferation study and target validation

Impressed by the anti-HDAC activity of the newly synthesized compounds, we then tested compounds **22a-c** in A549 and MCF-7 cancer cell lines. To our surprise, none of the three compounds showed any growth inhibitory effect against the two cancer cell lines (Table 2.5). While we do not have a clear explanation for the observed lack of activity, we thought it may be due to lack of cell penetration by these compounds. To justify this, we tested a similar compound (compound **23**), based on the azithromycin template, made by a colleague in our lab (Shaghayegh Fathi). Compound **23** showed potent growth inhibitory activity in A549 and MCF-7 cancer cell lines, and is about six-fold less toxic towards healthy cells Vero. This suggests that the observed lack of activity may be peculiar to the clarithromycin-based compounds, and is not due to lack of cell penetration.

Table 2.5: Growth inhibitory activity of 2-amino-5-(thiophene phenyl)-based HDACi in cell lines

Compound	A549	MCF-7	Vero
22a	NI	NI	NT
22b	NI	NI	NT
22c	NI	NI	NT
23	1.72 ± 0.09	0.83 ± 0.07	6.46 ± 1.15
SAHA	5.00 ± 0.24	3.27 ± 0.05	1.03 ± 0.97

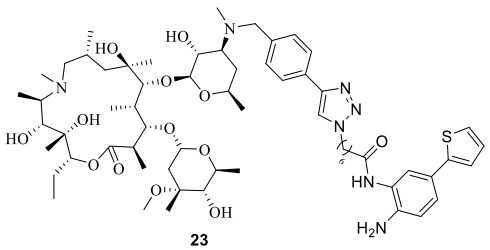

23

To unravel the reason behind the observed lack of cellular activity seen with compounds **22a-c** as compared with the robust activity of the azithromycin analogue, **23**, we used western blot to verify target engagement intracellularly. Class **I** HDAC inhibition in the cells results in accumulation of acetylated histones in the cells.[9] We treated MCF-7 cells with compounds **22b** and **23** at varying concentrations, using SAHA as a positive control. We observed substantial accumulation of acetyl H4 as expected for SAHA. To our surprise, we did not observe significant level of accumulation of acetyl H4 at the maximum tested concentration (5 μM) for the potent compound **23**. The same effect was seen for compounds **22b**, suggesting that there may be an alternative pathway perturbed by compound **23**, or that the test concentrations used in this study were too low to elicit significant accumulation of acetyl H4.

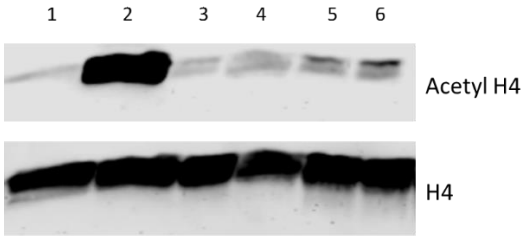

Figure 2.5: Western blot analysis of accumulation of acetylated H4. Lanes: 1= DMSO; 2= SAHA (5 μM); 3= **23** (0.8 μM); 4= **23** (5 μM); 5= **22b** (5 μM); 6= **22b** (10 μM).

2.7. Conclusion

We have synthesized diverse series of non-peptide macrocyclic hydroxamic acid- and benzamide- based HDACi derived from clarithromycin to further explore the SAR of this class of HDACi. Several of the hydroxamic acid-based compounds exhibited nanomolar anti-HDAC

activity against recombinant HDAC1 and HDAC6 enzymes. The benzamide- based compounds also showed nanomolar activity, in addition to their selectivity towards HDAC1 and HDAC2. Among the lead compounds tested for antiproliferation activity, compounds **13f** potently inhibited the growth of lung cancer cell line (A549) and breast cell line (MCF-7). Unlike SAHA which is much more toxic to healthy Vero cells, these clarithromycin-derived compounds are either significantly less cytotoxic to the Vero cells or equally cytotoxic to the transformed and normal cells tested. Also, some of these compounds exhibited anti-inflammatory activity in NTHi infected BSAS-2B cells.

2.8. Experimental

2.8.1. Materials and methods

All commercially available starting materials were used without further purification. Clarithromycin was purchased from Greenfield Chemicals. 2-Ethynylbenzyl alcohol, 3-bromobenzaldehyde, and 4-ethynylbenzyl alcohol were purchased from Sigma-Aldrich. Reaction solvents were either high performance liquid chromatography (HPLC) grade or American Chemical Society (ACS) grade and used without further purification. Analtech silica gel plates (60 F_{254}) were used for analytical TLC, and Analtech preparative TLC plates (UV 254, 2000 μm) were used for purification. UV light and anisaldehyde/iodine stain were used to visualize the spots. 200-400 Mesh silica gel was used in column chromatography. Nuclear magnetic resonance (NMR) spectra were recorded on a Varian-Gemini 400 MHz or Bruker 500 MHz magnetic resonance spectrometer. ^{1}H NMR Spectra were recorded in parts per million (ppm) relative to the residual peaks of $CHCl_3$ (7.24 ppm) in $CDCl_3$ or CHD_2OD (4.78 ppm) in CD_3OD or DMSO-d_5

(2.49 ppm) in DMSO-d_6. ^{13}C spectra were recorded relative to the central peak of the $CDCl_3$ triplet (77.0 ppm) or CD_3OD septet (49.3 ppm) or DMSO-d_6 septet (39.7 ppm) and were recorded with complete hetero-decoupling. Original 'fid' files were processed using MestReNova LITE (version 5.2.5-5780) program. High-resolution mass spectra were recorded at the Georgia Institute of Technology mass spectrometry facility in Atlanta. 3′-Desmethylclarithromycin (**1**), 4-ethynylbenzyl mathanesulfonate (**2**), 3′-*O*-acetylclarithromycin (**7**) were synthesized as we previously reported.[14,15,34]

(Clarithromycin-3′-(*N*-(4-triazolylbenzyl)))-*N*-hydroxyacetamide (**5a**)

3′-N-(Desmethyl)- 3′-*N*-(4-ethynylbenzyl) clarithromycin **3** (0.15 g, 0.18 mmol) and 2-azido-*N*-((*tert*-butyldimethylsilyl)oxy)acetamide **4a** (0.073 g, 0.318 mmol) are dissolved in anhydrous THF and purged with argon for 10 min. DIPEA (0.06ml, 0.35mmol) and CuI (0.017 g, 0.088 mmol) were then added to the mixture and purged further for another 20 minutes. The resulting suspension was stirred at room temperature for 12 h. Reaction was quenched with a solution of 4:1 satd. Aqueous NH_4Cl/NH_4OH and extracted with a mixture of 10% MeOH in DCM. Combined organic layer was dried over anhydrous Na_2SO_4 and concentrated *in vacuo*. The crude was subjected to next reaction without further purification.

The crude was dissolved in anhydrous methanol (2 mL) alongside caesium fluoride (0.04g, 0.27mmol) and left to stir under Ar until TLC showed complete conversion (1.5 h). Water was added to quench the reaction and the aqueous layer extracted with DCM. Combined organic layer was dried over Na_2SO_4 and concentrated *in vacuo*. Crude obtained was purified by preparative chromatography (Silica gel, 12:1:0.1 DCM-MeOH-NH_4OH) to give target compound **5a** as light yellow solid (0.068 g, 40%). ^1H NMR (400 MHz, CD_3OD) δ (ppm) 8.39 (s, 1H), 7.84 (d, J = 8.1

Hz, 2H), 7.50 (d, *J* = 8.2 Hz, 2H), 5.12 (d, *J* = 3.7 Hz, 2H), 4.53 (d, *J* = 7.2 Hz, 1H), 4.08 (dq, *J* = 12.6, 6.9 Hz, 3H), 3.80 – 3.68 (m, 5H), 3.42 (d, *J* = 7.5 Hz, 1H), 3.30 (dt, *J* = 3.3, 1.6 Hz, 4H), 3.17 (s, 3H), 3.15 – 3.07 (m, 2H), 3.04 (s, 1H), 3.01 (d, *J* = 9.5 Hz, 2H), 2.94 – 2.86 (m, 1H), 2.59 (d, *J* = 9.0 Hz, 1H), 2.44 (s, 3H), 2.38 (d, *J* = 15.2 Hz, 1H), 2.15 (s, 1H), 2.04 – 2.00 (m, 2H), 1.98 – 1.82 (m, 4H), 1.67 (d, *J* = 13.0 Hz, 1H), 1.52 (ddd, *J* = 18.2, 13.3, 6.1 Hz, 3H), 1.38 (d, *J* = 17.4 Hz, 4H), 1.24 (dq, *J* = 12.9, 8.0 Hz, 13H), 1.13 (dt, *J* = 12.5, 8.6 Hz, 16H), 0.85 (dd, *J* = 8.4, 6.3 Hz, 3H). ^{13}C NMR (126 MHz, $CDCl_3$) δ (ppm) 175.8, 147.2, 130.0, 125.8, 122.2, 102.5, 96.1, 81.2, 78.5, 78.3, 74.2, 72.7, 70.8, 69.1, 68.2, 65.7, 64.3, 57.7, 50.6, 49.4, 45.1, 39.2, 39.1, 37.3, 36.7, 34.9, 29.7, 22.7, 21.3, 21.0, 19.9, 18.7, 18.0, 16.0, 12.3, 10.6, 9.3. HRMS (ESI) *m/z* Calcd. for $C_{48}H_{78}N_5O_{15}$ [M+H$^+$]: 964.5494, found 964.5541.

(Clarithromycin-3′-(*N*-(4-triazolylbenzyl)))-*N*-hydroxypropanamide (**5b**)

Reaction of *3′-N*-(desmethyl)- 3′-*N*-(4-ethynylbenzyl) clarithromycin **3** (0.15 g, 0.18 mmol) with 3-azido-*N*-((*tert*-butyldimethylsilyl)oxy)propanamide **4b** (0.065 g, 0.265 mmol) followed by TBS deprotection with caesium fluoride as described for the synthesis of compound **5a,** gave **5b** as a light yellow solid (0.067 g, 39%). ^{1}H NMR (400 MHz, CD_3OD) δ (ppm) 8.25 (s, 1H), 7.78 (d, *J* = 8.1 Hz, 2H), 7.46 (d, *J* = 8.1 Hz, 2H), 5.13 (dd, *J* = 11.1, 2.1 Hz, 1H), 4.74 (t, *J* = 6.5 Hz, 2H), 4.51 (d, *J* = 7.2 Hz, 1H), 4.11 (dd, *J* = 9.4, 6.3 Hz, 1H), 3.93 (d, *J* = 13.2 Hz, 1H), 3.79 – 3.69 (m, 5H), 3.68 – 3.62 (m, 1H), 3.38 – 3.32 (m, 2H), 3.30 (dt, *J* = 3.3, 1.6 Hz, 3H), 3.18 (s, 3H), 3.11 (d, *J* = 7.8 Hz, 1H), 3.03 (d, *J* = 7.3 Hz, 4H), 3.01 (d, *J* = 9.5 Hz, 2H), 2.94 – 2.84 (m, 2H), 2.77 (t, *J* = 6.3 Hz, 2H), 2.64 – 2.53 (m, 1H), 2.40 (s, 1H), 2.34 (s, 4H), 1.96 – 1.78 (m, 5H), 1.67 (d, *J* = 13.0 Hz, 1H), 1.60 – 1.47 (m, 2H), 1.39 (d, *J* = 14.0 Hz, 4H), 1.25 (q, *J* = 7.8 Hz, 5H), 1.21 (d, *J* = 6.0 Hz, 7H), 1.18 – 1.08 (m, 17H), 0.85 (t, *J* = 7.4 Hz, 3H). ^{13}C NMR (126 MHz, $CDCl_3$) δ (ppm) 175.8, 167.1, 147.1, 129.7, 129.4, 127.3, 125.7, 121.3, 102.7, 96.0, 81.1, 78.4,

78.3, 77.8, 76.7, 74.3, 72.6, 70.8, 69.1, 69.0, 68.4, 65.7, 63.8, 57.6, 50.6, 49.4, 46.2, 45.2, 45.1, 39.3, 39.1, 37.3, 36.9, 34.8, 33.1, 29.9, 29.7, 21.4, 21.2, 21.0, 19.8, 18.6, 18.0, 16.0, 12.3, 10.6, 9.2. HRMS (ESI) m/z Calcd. for $C_{49}H_{79}N_5O_{15}Na$ [M+Na^+]: 1000.5454, found 1000.5479.

(Clarithromycin-3′-(*N*-(4-triazolylbenzyl)))-*N*-hydroxybutanamide (**5c**)

Reaction of *3′-N*-(desmethyl)-*3′-N*-(4-ethynylbenzyl) clarithromycin **3** (0.15g,0.18mmol) with 4-Azido-*N*-((*tert*-butyldimethylsilyl)oxy)butanamide **4c** (0.082 g, 0.318 mmol) followed by TBS deprotection with caesium fluoride as described for the synthesis of compound **5a,** gave **5c** as a light yellow solid (0.075 g, 43%). ^{1}H NMR (500 MHz, $CDCl_3$) δ (ppm) 7.85 (s, 1H), 7.74 (d, 2H), 7.34 (d, 2H), 5.03 (d, *J* = 11.2 Hz, 1H), 4.88 (d, *J* = 4.1 Hz, 1H), 4.41 (d, *J* = 6.9 Hz, 4H), 4.01 – 3.89 (m, 3H), 3.81 (d, *J* = 10.8 Hz, 1H), 3.77 – 3.69 (m, 4H), 3.67 – 3.55 (m, 3H), 3.46 (dd, *J* = 8.1, 5.3 Hz, 3H), 3.37 – 3.27 (m, 2H), 3.18 (d, *J* = 13.1 Hz, 1H), 3.15 (d, *J* = 16.9 Hz, 5H), 3.06 – 2.92 (m, 8H), 2.89 – 2.80 (m, 2H), 2.57 (dd, *J* = 11.0, 6.5 Hz, 3H), 2.35 – 2.13 (m, 11H), 1.90 (dd, *J* = 14.4, 7.3 Hz, 3H), 1.80 (dd, *J* = 26.9, 14.6 Hz, 3H), 1.68 (d, *J* = 13.9 Hz, 2H), 1.58 – 1.43 (m, 3H), 1.43 – 1.36 (m, 5H), 1.31 – 1.20 (m, 14H), 1.16 (d, *J* = 7.1 Hz, 5H), 1.14 – 0.99 (m, 23H), 0.96 – 0.85 (m, 1H), 0.87 – 0.77 (m, 5H). ^{13}C NMR (126 MHz, $CDCl_3$) δ (ppm) 176.0, 147.6, 129.8, 125.8, 120.3, 102.8, 96.0, 81.2, 78.4, 78.0, 74.4, 72.7, 70.9, 69.2, 68.7, 65.9, 64.0, 57.7, 50.8, 49.3, 45.4, 39.3, 37.4, 36.9, 35.1, 29.8, 29.7, 21.6, 21.0, 19.7, 18.9, 18.4, 16.0, 12.4, 10.7, 9.3. HRMS (ESI) *m/z* Calcd. for $C_{50}H_{83}N_5O_{15}$ [M+H^+]: 992.5807, found 992.5839.

(Clarithromycin-3′-(*N*-(4-triazolylbenzyl)))-*N*-hydroxypentanamide (**5d**)

Reaction of *3′-N*(desmethyl)- *3′-N*-(4-ethynylbenzyl) clarithromycin **3** (0.15 g, 0.18 mmol) with 5-Azido-*N*-((*tert*-butyldimethylsilyl)oxy)pentanamide **4d** (0.072g, 0.265mmol) followed by TBS deprotection with caesium fluoride as described for the synthesis of compound **5a,** gave **5d**

as a light yellow solid (0.068 g, 45%). ^{1}H NMR (500 MHz, $CDCl_3$) δ (ppm) 7.86 (s, 1H), 7.75 (s, 2H), 7.35 (s, 2H), 5.03 (dd, *J* = 11.1, 1.6 Hz, 1H), 4.87 (d, *J* = 3.7 Hz, 1H), 4.41 (t, *J* = 9.4 Hz, 1H), 4.35 (s, 2H), 3.99 – 3.89 (m, 2H), 3.83 (d, *J* = 10.5 Hz, 1H), 3.78 – 3.68 (m, 2H), 3.62 (d, *J* = 6.9 Hz, 1H), 3.54 – 3.41 (m, 2H), 3.38 – 3.29 (m, 1H), 3.17 (d, *J* = 20.3 Hz, 1H), 3.12 (s, 3H), 3.04 – 2.91 (m, 5H), 2.91 – 2.81 (m, 1H), 2.64 (s, 1H), 2.56 (dd, *J* = 10.3, 7.4 Hz, 1H), 2.24 (d, *J* = 40.5 Hz, 6H), 1.88 (dt, *J* = 26.6, 13.4 Hz, 4H), 1.85 – 1.73 (m, 2H), 1.71 – 1.56 (m, 3H), 1.56 – 1.41 (m, 2H), 1.42 – 1.33 (m, 3H), 1.33 – 1.27 (m, 2H), 1.30 – 1.18 (m, 8H), 1.16 (d, *J* = 7.0 Hz, 3H), 1.13 – 1.00 (m, 15H), 0.82 (t, *J* = 7.4 Hz, 3H). ^{13}C NMR (126 MHz, $CDCl_3$) δ (ppm) 175.8, 170.3, 147.3, 129.6, 125.7, 120.1, 102.6, 95.9, 80.9, 78.3, 74.2, 72.5, 70.7, 69.0, 68.4, 65.6, 63.8, 57.6, 50.5, 49.8, 49.3, 45.9, 45.1, 45.0, 39.2, 39.0, 37.2, 36.8, 34.7, 31.7, 29.8, 29.6, 29.3, 22.1, 21.4, 21.2, 20.9, 19.8, 18.6, 17.9, 15.9, 12.2, 10.5, 9.1, 8.5. HRMS (ESI) *m/z* Calcd for $C_{51}H_{83}N_5O_{15}Na$ [M+Na^+]: 1028.5783, found 1028.5795.

4″-Oxo-3′-*O*-acetylclarithromycin (**8**)

A solution of *N*-chlorosuccinimide (2.00 g, 14.97 mmol) in anhydrous DCM (30 mL) was stirred at -15 °C for 10 min. Dimethyl sulfide (1.10 mL, 14.97 mmol) was then added drop wise to the solution. After stirring for 20 minutes at the same temperature a DCM solution (10 mL) of acetylated clarithromycin **7** (5.91 g, 7.49 mmol) was added over a period of 30 min to the suspension and the resulting suspension was stirred at -15 ˚C for another 30 min, afterward TEA (2.09 mL, 14.97 mmol) was added. The resulting solution was stirred at -10 °C for another 2 h. The reaction was quenched by adding saturated aqueous $NaHCO_3$ solution (50 mL), the organic layer was separated. The aqueous layer was extracted with DCM (2 x 25 mL) and the combined organic layer was dried over anhydrous Na_2SO_4, filtered and concentrated *in vacuo*. The crude

compound **8** (6.35 g) was sufficiently pure to be used for the next step without further purification. ^{1}H NMR (400 MHz, $CDCl_3$) δ (ppm) 5.11 – 5.02 (m, 1H), 4.97 (d, *J* = 10.7 Hz, 1H), 4.75 (dd, *J* = 10.3, 7.6 Hz, 1H), 4.39 (t, *J* = 6.1 Hz, 1H), 4.29 (q, *J* = 6.7 Hz, 1H), 3.67 – 3.53 (m, 3H), 3.38 (td, *J* = 15.1, 5.0 Hz, 2H), 3.30 (d, *J* = 1.3 Hz, 4H), 3.15 (t, *J* = 9.1 Hz, 3H), 2.93 – 2.82 (m, 4H), 2.78 (dd, *J* = 16.9, 7.3 Hz, 1H), 2.68 (d, *J* = 1.3 Hz, 1H), 2.65 (d, *J* = 2.7 Hz, 1H), 2.60 (d, *J* = 1.2 Hz, 1H), 2.56 (d, *J* = 1.3 Hz, 1H), 2.49 – 2.37 (m, 8H), 2.29 – 2.14 (m, 3H), 2.07 – 2.02 (m, 2H), 1.97 (t, *J* = 8.3 Hz, 3H), 1.94 – 1.73 (m, 15H), 1.60 – 1.47 (m, 1H), 1.41 – 1.33 (m, 2H), 1.32 – 1.23 (m, 8H), 1.21 (d, *J* = 9.9 Hz, 3H), 1.12 (dd, *J* = 11.2, 6.4 Hz, 7H), 1.07 – 0.93 (m, 10H), 0.78 (t, *J* = 9.6 Hz, 3H), 0.70 (t, *J* = 7.2 Hz, 3H). ^{13}C NMR (101 MHz, $CDCl_3$) δ (ppm) 221.0, 210.6, 175.6, 170.4, 99.6, 96.4, 80.0, 78.7, 78.1, 78.0, 76.7, 76.0, 74.2, 72.9, 72.7, 69.8, 69.2, 67.5, 61.7, 51.2, 50.2, 49.9, 45.1, 44.4, 39.0, 38.4, 38.1, 37.9, 37.6, 37.2, 30.8, 30.4, 29.5, 28.3, 26.5, 21.3, 21.3, 20.9, 20.5, 20.4, 20.0, 19.5, 18.9, 17.8, 16.2, 16.1, 15.5, 14.7, 13.0, 12.2, 10.4, 8.9. HRMS (MALDI) *m/z* Calcd. for $C_{40}H_{70}NO_{14}$ [M+H$^+$]: 788.4791, found 788.4781.

4″-Epoxy-3′-*O*-acetylclarithromycin (**9**)

NaH (60% in mineral oil) (0.73 g, 17.7 mmol) was added to an oven dried three-neck round bottom flask and was washed with petroleum ether. The flask was immediately flushed with Ar and 5mL of anhydrous DMSO added through the septum. The mixture was stirred at room temperature under Ar and trimethyloxosulfonium iodide (3.90 g, 17.7 mmol) was added over a period of 5 min. When hydrogen evolution ceased and a clear solution obtained, a solution of compound **8** (6.35 g, 8.06 mmol) in anhydrous THF (10 mL) was added over a period of 10 min and left to stir for 2 h. Once TLC showed 100% conversion, THF was removed under vacuum and ethyl acetate was added to the remaining solution. The solution was washed severally with H_2O to remove DMSO. Organic layer was dried with $NaSO_4$ and concentrated *in vacuo*. The crude product

was purified by column chromatography using EtOAc: Acetone (5:1) to give compound **9** as a white solid (2.43g, 38%). ^{1}H NMR (400 MHz, $CDCl_3$) δ (ppm) 5.06 (dq, *J* = 6.2, 4.6 Hz, 2H), 4.77 – 4.59 (m, 4H), 3.95 (s, 1H), 3.76 – 3.66 (m, 3H), 3.55 (s, 1H), 3.45 (dd, *J* = 9.3, 6.0 Hz, 1H), 3.34 – 3.28 (m, 4H), 3.19 (s, 1H), 3.01 (d, *J* = 7.0 Hz, 1H), 3.01 – 2.95 (m, 4H), 2.94 – 2.90 (m, 1H), 2.86 (dd, *J* = 9.9, 7.1 Hz, 1H), 2.69 – 2.63 (m, 1H), 2.61 (dd, *J* = 9.8, 4.4 Hz, 2H), 2.53 (dd, *J* = 9.6, 7.1 Hz, 1H), 2.34 (s, 1H), 2.27 – 2.20 (m, 7H), 2.19 – 2.13 (m, 2H), 2.06 – 2.00 (m, 4H), 1.95 – 1.83 (m, 3H), 1.72 – 1.61 (m, 2H), 1.56 (d, *J* = 1.6 Hz, 1H), 1.53 (s, 1H), 1.49 – 1.36 (m, 1H), 1.33 (d, *J* = 7.2 Hz, 3H), 1.28 (s, 1H), 1.26 – 1.12 (m, 11H), 1.14 – 0.99 (m, 16H), 0.92 (t, *J* = 8.2 Hz, 3H), 0.81 (dd, *J* = 9.8, 4.9 Hz, 3H). ^{13}C NMR (101 MHz, $CDCL_3$) δ (ppm) 221.1, 175.3, 170.0, 100.1, 96.4, 96.3, 80.3, 78.9, 78.3, 78.2, 76.6, 76.1, 74.2, 73.7, 71.7, 69.1, 67.8, 64.3, 63.2, 60.4, 60.2, 50.4, 49.6, 46.6, 45.3, 44.8, 40.7, 38.6, 38.1, 37.2, 36.0, 30.8, 29.2, 21.6, 21.3, 21.0, 20.2, 19.7, 18.2, 18.0, 16.1, 15.9, 14.9, 14.2, 14.2, 12.4, 10.5, 9.1. HRMS (MALDI) *m/z* Calcd. for $C_{41}H_{77}NO_{14}$ [M+H^{+}]: 802.4947, found 802.4938.

(4″-(Methylamino)-*N*-(methyl)(4-ethynylbenzyl))clarithromycin (**11**)

1-(4-Ethynylphenyl)-*N*-methylmethanamine **10** (1.52 g, 10.47 mmol) was added to a solution of compound **9** (2.80 g, 3.49 mmol) in MeOH (20 mL). The solution was heated at 60 °C for 6 h. Excess MeOH was evaporated off and the crude was purified by column chromatography using Hexanes:EtOAc:MeOH:NH_4OH (2:1:0.6:0.1) to give compound **11** as a light yellow solid (2.41g, 73%). ^{1}H NMR (400 MHz, $CDCl_3$) δ (ppm) 7.33 (d, *J* = 8.1 Hz, 2H), 7.13 (d, *J* = 8.1 Hz, 2H), 4.98 – 4.86 (m, 2H), 4.35 – 4.28 (m, 1H), 4.06 (q, *J* = 5.9 Hz, 1H), 3.66 (d, *J* = 11.1 Hz, 2H), 3.57 (d, *J* = 7.0 Hz, 2H), 3.34 (s, 1H), 3.20 (s, 3H), 3.09 (dd, *J* = 10.0, 7.3 Hz, 2H), 3.02 (d, *J* = 10.1 Hz, 1H), 2.97 (d, *J* = 6.6 Hz, 1H), 2.94 (s, 2H), 2.91 – 2.85 (m, 2H), 2.81 – 2.72 (m, 1H), 2.47

(d, *J* = 7.4 Hz, 1H), 2.34 (dd, *J* = 15.6, 6.7 Hz, 1H), 2.24 (s, 1H), 2.20 (s, 6H), 2.10 (s, 3H), 2.04 (d, *J* = 3.6 Hz, 1H), 2.00 (s, 1H), 1.96 (s, 1H), 1.93 – 1.87 (m, 1H), 1.84 – 1.70 (m, 3H), 1.57 (dd, *J* = 19.0, 11.8 Hz, 2H), 1.41 – 1.31 (m, 1H), 1.30 (d, *J* = 11.1 Hz, 3H), 1.15 – 1.07 (m, 10H), 1.05 (s, 4H), 0.97 (dd, *J* = 17.3, 7.0 Hz, 10H), 0.71 (dd, *J* = 13.8, 6.6 Hz, 3H). ^{13}C NMR (101 MHz, $CDCl_3$) δ (ppm) 220.8, 175.7, 139.1, 132.1, 128.6, 121.2, 102.7, 96.4, 83.2, 80.9, 78.9, 78.0, 76.3, 76.1, 75.9, 74.2, 70.9, 70.6, 68.9, 68.2, 67.4, 65.4, 63.1, 56.9, 50.6, 49.5, 45.2, 44.8, 43.2, 40.2, 39.3, 38.8, 37.1, 31.3, 28.7, 21.7, 20.9, 20.2, 19.6, 19.1, 18.7, 18.0, 15.9, 15.3, 14.8, 14.6, 13.0, 12.2, 11.4, 10.6, 10.5, 9.3, 9.1. HRMS (ESI) *m/z* Calcd. for [$C_{49}H_{81}N_2O_{13}$ [M+H^+]: 905.5739, found 905.5693.

(Clarithromycin-(4″-(methylamino)-*N*(methyl)(4-benzyltriazolyl))-*N*-hydroxyacetamide (13a)

Reaction of (4″-(Methylamino)-*N*(methyl)(4-ethynylbenzyl)) clarithromycin **11** (0.15 g, 0.17 mmol) with 2-azido-*N*-((*tert*-butyldimethylsilyl)oxy)acetamide **12a** (0.057 g, 0.249 mmol) followed by TBS removal with caesium fluoride as described for the synthesis of compound **5a,** gave **13a** as a light yellow solid (0.057 g, 38%). ^{1}H NMR (400 MHz, CD_3OD) δ (ppm) 8.37 (d, *J* = 5.4 Hz, 1H), 7.82 (d, *J* = 8.1 Hz, 2H), 7.41 (d, *J* = 8.3 Hz, 2H), 5.50 (d, *J* = 5.4 Hz, 1H), 5.12 (d, *J* = 14.2 Hz, 2H), 5.00 – 4.95 (m, 1H), 4.43 (d, *J* = 7.3 Hz, 1H), 4.22 (d, *J* = 6.4 Hz, 1H), 3.85 – 3.65 (m, 5H), 3.61 (s, 1H), 3.50 (s, 1H), 3.32 – 3.25 (m, 5H), 3.13 – 3.00 (m, 5H), 2.96 – 2.85 (m, 1H), 2.76 (d, *J* = 10.3 Hz, 1H), 2.58 (s, 1H), 2.53 (s, 1H), 2.48 (s, 5H), 2.35 (s, 1H), 2.32 – 2.25 (m, 3H), 2.24 (s, 1H), 2.21 (s, 1H), 2.16 (d, *J* = 7.6 Hz, 1H), 2.14 (d, *J* = 5.4 Hz, 1H), 2.01 (s, 1H), 1.98 – 1.74 (m, 5H), 1.66 (d, *J* = 12.7 Hz, 1H), 1.57 – 1.44 (m, 1H), 1.40 (s, 3H), 1.31 – 1.15 (m, 17H), 1.12 (dt, *J* = 11.4, 4.9 Hz, 10H), 0.85 (t, *J* = 7.3 Hz, 3H). ^{13}C NMR (126 MHz, $CDCl_3$) δ (ppm) 176.0, 147.3, 129.4, 125.8, 122.3, 102.4, 96.5, 81.1, 78.3, 78.2, 74.3, 70.8, 69.1, 68.0, 67.5,

65.4, 62.9, 53.5, 50.7, 49.6, 45.2, 45.0, 43.4, 40.3, 39.1, 37.3, 31.5, 29.7, 21.5, 21.0, 19.8, 18.9, 18.0, 16.0, 15.4, 14.9, 14.8, 13.1, 12.3, 11.5, 10.7, 10.6, 9.3. HRMS (MALDI) *m/z* Calcd. for $C_{51}H_{86}N_6O_{15}$ [M+H$^+$]: 1021.6073, found 1021.6095.

(Clarithromycin-4″(methylamino)-*N*(methyl)(4-benzyltriazolyl))-*N*-hydroxypropanamide (13b)

Reaction of (4″-(methylamino)-*N*(methyl)(4-ethynylbenzyl)) clarithromycin **11** (0.15 g,0.17 mmol) with 3-azido-*N*-((*tert*-butyldimethylsilyl)oxy) propanamide **12b** (0.061 g, 0.249 mmol) followed by TBS removal with caesium fluoride as described for the synthesis of compound **5a,** gave **13b** as a light yellow solid (0.07g, 47%). ^{1}H NMR (400 MHz, CD_3OD) δ (ppm) 8.22 (s, 1H), 7.75 (d, *J* = 7.7 Hz, 2H), 7.36 (d, *J* = 7.9 Hz, 2H), 5.13 – 5.06 (m, 1H), 4.97 – 4.90 (m, 1H), 4.69 (d, *J* = 18.5 Hz, 2H), 4.40 (d, *J* = 7.0 Hz, 1H), 4.19 (d, *J* = 6.5 Hz, 1H), 3.81 – 3.64 (m, 5H), 3.47 (s, 1H), 3.30 – 3.20 (m, 5H), 3.09 – 3.03 (m, 2H), 3.00 (d, *J* = 8.3 Hz, 3H), 2.94 – 2.82 (m, 1H), 2.73 (t, *J* = 19.8 Hz, 3H), 2.56 (d, *J* = 7.6 Hz, 1H), 2.41 (s, 6H), 2.31 (s, 1H), 2.25 (d, *J* = 12.9 Hz, 4H), 2.18 (s, 1H), 2.16 – 2.12 (m, 1H), 2.14 – 2.09 (m, 7H), 1.95 – 1.80 (m, 4H), 1.76 (d, *J* = 12.9 Hz, 1H), 1.62 (d, *J* = 14.9 Hz, 1H), 1.53 – 1.41 (m, 1H), 1.36 (s, 3H), 1.27 – 1.13 (m, 16H), 1.09 (td, *J* = 13.0, 8.1 Hz, 11H), 0.83 (t, *J* = 12.0, 5.5 Hz, 3H). ^{13}C NMR (126 MHz, $CDCl_3$) δ (ppm) 175.7, 146.9, 137.8, 129.2, 125.5, 121.0, 102.2, 96.2, 80.9, 80.9, 78.7, 78.4, 78.1, 77.9, 76.4, 75.9, 75.4, 74.1, 71.2, 70.9, 70.5, 68.8, 67.8, 67.3, 65.1, 62.6, 56.3, 50.8, 50.5, 50.5, 49.4, 46.0, 45.0, 44.7, 44.6, 43.1, 40.2, 39.1, 38.8, 37.0, 31.2, 29.9, 29.5, 25.4, 21.3, 20.8, 20.1, 19.8, 19.5, 18.9, 18.6, 18.1, 17.8, 15.8, 15.2, 14.7, 14.5, 12.9, 12.1, 11.3, 10.4, 10.3, 10.3, 9.3, 9.2. HRMS (MALDI) *m/z* Calcd. for $C_{52}H_{87}N_6O_{15}$ [M+H$^+$]: 1035.6270, found 1035.6210.

(Clarithromycin-4″(methylamino)-*N*(methyl)(4-benzyltriazolyl))-*N*-hydroxybutanamide (13c)

Reaction of (4″-(methylamino)-*N*(methyl)(4-ethynylbenzyl)) clarithromycin **11** (0.15 g, 0.17 mmol) with 4-azido-*N*-((*tert*-butyldimethylsilyl)oxy)butanamide **12c** (0.064 g, 0.245 mmol) followed by TBS removal with caesium fluoride as described for the synthesis of compound **5a,** gave **13c** as a light yellow solid (0.060g, 40%). ^{1}H NMR (400 MHz, CD_3OD) δ (ppm) 8.32 (s, 1H), 7.77 (d, *J* = 7.7 Hz, 2H), 7.36 (d, *J* = 7.9 Hz, 2H), 5.09 (d, *J* = 9.2 Hz, 1H), 4.46 (s, 2H), 4.39 (d, *J* = 7.2 Hz, 1H), 4.19 (d, *J* = 6.4 Hz, 1H), 3.82 – 3.61 (m, 5H), 3.48 (s, 1H), 3.29 – 3.21 (m, 4H), 3.05 (t, *J* = 4.8 Hz, 2H), 3.00 (d, *J* = 9.9 Hz, 3H), 2.92 – 2.82 (m, 1H), 2.67 (s, 1H), 2.54 (s, 1H), 2.41 (s, 5H), 2.30 (s, 1H), 2.26 – 2.18 (m, 6H), 2.11 (t, *J* = 7.4 Hz, 3H), 1.95 – 1.79 (m, 4H), 1.75 (d, *J* = 13.0 Hz, 1H), 1.62 (d, *J* = 14.6 Hz, 1H), 1.52 – 1.40 (m, 1H), 1.36 (s, 3H), 1.18 (dt, *J* = 11.1, 7.0 Hz, 15H), 1.13 – 1.02 (m, 11H), 0.81 (t, *J* = 7.2 Hz, 3H). ^{13}C NMR (126 MHz, $CDCl_3$) δ (ppm) 176.1, 171.4, 147.5, 138.4, 129.8, 129.5, 125.9, 120.8, 102.7, 102.4, 96.9, 96.6, 81.2, 81.2, 80.3, 79.1, 78.8, 78.5, 78.2, 76.3, 76.2, 75.7, 74.4, 71.5, 71.1, 70.8, 70.1, 69.2, 68.3, 68.1, 67.9, 67.7, 65.6, 63.1, 60.6, 56.9, 53.6, 51.2, 50.8, 49.7, 49.5, 45.4, 45.1, 44.9, 43.4, 40.5, 39.4, 39.1, 37.4, 31.6, 29.8, 29.5, 26.2, 21.7, 21.2, 21.1, 20.4, 20.1, 19.9, 19.3, 19.0, 18.5, 18.2, 16.1, 15.6, 15.0, 14.9, 14.3, 13.2, 12.5, 11.7, 10.8, 9.6, 9.5. HRMS (MALDI) *m/z* Calcd. for $C_{53}H_{89}N_6O_{15}$ $[M+H^+]$1049.6386, found 1049.6376.

(Clarithromycin-4″-(methylamino)-*N*(methyl)(4-benzyltriazolyl))-*N*-hydroxypentanamide (13d)

Reaction of (4″-(methylamino)-*N*(methyl)(4-ethynylbenzyl)) clarithromycin **11** (0.15 g, 0.17 mmol) with 5-azido-*N*-((*tert*-butyldimethylsilyl)oxy)peantanamide **12d** (0.068 g, 0.249 mmol) followed by TBS removal with caesium fluoride as described for the synthesis of compound **5a,** gave **13d** as a light yellow solid (0.067g, 44%). ^{1}H NMR (400 MHz, CD_3OD) δ (ppm) 8.30 (s, 1H), 7.76 (d, J = 8.0 Hz, 2H), 7.36 (d, J = 8.1 Hz, 2H), 5.12 – 5.03 (m, 1H), 4.47 – 4.36 (m, 3H), 4.19 (d, J = 6.4 Hz, 1H), 3.81 – 3.59 (m, 5H), 3.48 (s, 1H), 3.29 – 3.18 (m, 4H), 3.04 (dd, J = 10.3, 4.5 Hz, 2H), 3.00 (d, J = 9.6 Hz, 4H), 2.92 – 2.82 (m, 1H), 2.66 (s, 1H), 2.55 (d, J = 7.3 Hz, 1H), 2.40 (s, 6H), 2.30 (s, 1H), 2.23 (s, 4H), 2.16 (d, J = 9.6 Hz, 1H), 2.15 – 2.06 (m, 4H), 1.86 (ddd, J = 20.9, 14.7, 7.6 Hz, 6H), 1.75 (d, J = 13.2 Hz, 1H), 1.62 (d, J = 12.2 Hz, 3H), 1.50 – 1.41 (m, 1H), 1.35 (s, 3H), 1.26 – 1.12 (m, 16H), 1.09 (td, J = 12.8, 7.9 Hz, 11H), 0.81 (t, J = 7.3 Hz, 3H). ^{13}C NMR (126 MHz, $CDCl_3$) δ (ppm) 176.5, 147.8, 138.7, 130.3, 129.9, 126.3, 121.0, 103.1, 97.0, 81.6, 79.5, 79.2, 78.9, 78.7, 76.7, 74.9, 71.5, 71.2, 69.6, 68.7, 68.1, 66.0, 63.6, 57.3, 51.6, 51.2, 50.4, 50.1, 45.8, 45.5, 43.8, 40.9, 39.9, 39.5, 37.8, 32.0, 30.2, 29.9, 22.7, 22.2, 21.5, 20.8, 20.3, 19.4, 18.9, 18.6, 16.5, 15.9, 15.4, 15.3, 13.6, 12.9, 12.1, 11.2, 11.1, 10.0, 9.9. HRMS (MALDI) *m/z* Calcd. for $C_{54}H_{91}N_6O_{15}$ [$M+H^+$]: 1063.6542, found 1063.6588.

(Clarithromycin-4″-(methylamino)-*N*(methyl)(4-benzyltriazolyl))-*N*-hydroxyhexanamide (13e)

Reaction of (4″-(methylamino)-*N*(methyl)(4-ethynylbenzyl)) clarithromycin **11** (0.135 g, 0.149 mmol) with 6-azido-*N*-((*tert*-butyldimethylsilyl)oxy)hexanamide **12e** (0.077 g, 0.268 mmol) followed by TBS removal with caesium fluoride as described for the synthesis of compound **5a,**

gave **13e** as a light yellow solid (0.053g, 35%). ^{1}H NMR (500 MHz, $CDCl_3$) δ (ppm) 7.86 (s, 1H), 7.77 (d, *J* = 7.4 Hz, 2H), 7.31 (d, *J* = 7.8 Hz, 2H), 5.06 – 4.95 (m, 2H), 4.43 – 4.30 (m, 2H), 4.19 – 4.11 (m, 1H), 3.81 – 3.71 (m, 2H), 3.65 (dd, *J* = 13.3, 6.4 Hz, 2H), 3.48 – 3.39 (m, 1H), 3.29 (s, 3H), 3.21 (dd, *J* = 12.4, 6.3 Hz, 3H), 3.06 (d, *J* = 6.5 Hz, 1H), 3.05 – 2.93 (m, 4H), 2.92 – 2.82 (m, 1H), 2.58 – 2.45 (m, 2H), 2.31 (dd, *J* = 28.6, 7.4 Hz, 6H), 2.20 (d, *J* = 14.3 Hz, 3H), 2.11 (dd, *J* = 35.3, 9.4 Hz, 5H), 2.00 – 1.83 (m, 5H), 1.75 – 1.57 (m, 6H), 1.57 – 1.49 (m, 2H), 1.41 – 1.27 (m, 7H), 1.28 – 1.11 (m, 16H), 1.13 – 1.01 (m, 11H), 0.90 – 0.85 (m, 1H), 0.85 – 0.74 (m, 3H). ^{13}C NMR (126 MHz, $CDCl_3$) δ (ppm) 176.0, 147.4, 138.4, 129.8, 129.4, 125.8, 120.1, 102.7, 96.6, 96.5, 81.1, 81.0, 78.4, 78.2, 77.3, 77.1, 76.8, 76.6, 76.2, 76.1, 76.0, 74.3, 71.1, 70.7, 69.1, 68.3, 67.6, 65.4, 63.1, 57.0, 51.2, 51.0, 50.7, 50.1, 49.6, 45.3, 45.0, 43.2, 40.3, 39.4, 39.0, 37.2, 31.5, 29.8, 29.7, 29.3, 28.5, 26.2, 25.6, 24.9, 24.5, 21.7, 21.0, 19.7, 18.9, 18.1, 16.0, 16.0, 15.4, 14.9, 14.8, 13.1, 12.3, 11.5, 10.6, 9.3. HRMS (MALDI) *m/z* Calcd. for $C_{55}H_{93}N_6O_{15}$ [M+H$^+$]: 1077.6699, found 1077.6692.

(Clarithromycin-4″-(methylamino)-*N*(methyl)-4-benzyltriazolyl))-*N*-hydroxyheptanamide (13f)

Reaction of (4″-(methylamino)-*N*(methyl)(4-ethynylbenzyl)) clarithromycin **11** (0.15 g, 0.17 mmol) with 7-azido-*N*-((*tert*-butyldimethylsilyl) oxy) heptanamide **12f** (0.075 g, 0.249 mmol) followed by TBS removal with caesium fluoride as described for the synthesis of compound **5a,** gave **13f** as a light yellow solid (0.060g, 40%). ^{1}H NMR (400 MHz, CD_3OD) δ (ppm) 8.34 (s, 1H), 7.81 (d, *J* = 8.2 Hz, 2H), 7.40 (d, *J* = 8.2 Hz, 2H), 5.16 – 5.08 (m, 1H), 4.96 (d, *J* = 5.2 Hz, 1H), 4.45 (t, *J* = 6.5 Hz, 3H), 4.22 (d, *J* = 6.4 Hz, 1H), 3.85 – 3.64 (m, 5H), 3.52 (s, 1H), 3.33 – 3.23 (m, 9H), 3.12 – 2.98 (m, 5H), 2.90 (dd, *J* = 19.0, 11.7 Hz, 1H), 2.77 (s, 1H), 2.58 (s, 1H), 2.49 (s,

6H), 2.35 (s, 1H), 2.31 – 2.23 (m, 4H), 2.21 (s, 1H), 2.18 – 2.12 (m, 3H), 2.12 – 2.04 (m, 4H), 1.99 – 1.85 (m, 6H), 1.83 (d, *J* = 13.2 Hz, 2H), 1.69 – 1.53 (m, 7H), 1.44 – 1.31 (m, 12H), 1.28 – 1.18 (m, 15H), 1.12 (dt, *J* = 11.4, 4.9 Hz, 12H), 0.90 (s, 1H), 0.85 (t, *J* = 7.3 Hz, 3H). ^{13}C NMR (126 MHz, $CDCl_3$) δ (ppm) 176.2, 147.6, 138.4, 130.1, 129.7, 126.1, 120.3, 102.8, 96.8, 81.4, 78.6, 78.4, 74.6, 71.3, 71.0, 69.3, 68.4, 67.9, 65.7, 63.3, 57.1, 51.6, 51.0, 50.4, 49.9, 45.5, 45.2, 43.5, 40.7, 39.6, 39.2, 37.5, 31.8, 30.1, 30.0, 28.9, 28.8, 28.2, 26.6, 26.0, 25.6, 25.3, 21.9, 21.3, 20.6, 20.0, 19.5, 19.1, 18.3, 16.3, 15.7, 15.2, 15.0, 12.6, 10.9, 9.7. HRMS (MALDI) *m/z* Calcd. for $C_{56}H_{95}N_6O_{15}$ [M+H$^+$]: 1091.6815, found 1091.6869.

((3′-*O*-Acetyl)-4′-*N*-(4-ethynylbenzyl)) clarithromycin (**14**)

(4′-Ethynylbenzyl) clarithromycin **3** (0.15 g, 0.177 mmol) was dissolved in anhydrous DCM (5 mL) and acetic anhydride (0.04 mL, 0.442 mmol) added to the solution. The mixture was left to stir at room temperature under Ar for 3 days after which TLC shows full consumption of the starting material. The reaction was washed with $NaHCO_3$, brine and H_2O, theorganic layer was dried with anhydrous Na_2SO_4 and concentrated *in vacuo* to give compound **14** (128 mg, 81%). ^{1}H NMR (400 MHz, $CDCl_3$) δ 7.38 (d, *J* = 8.2 Hz, 2H), 7.19 (d, *J* = 8.1 Hz, 2H), 5.01 (dd, *J* = 11.1, 2.2 Hz, 1H), 4.87 (d, *J* = 4.8 Hz, 1H), 4.74 (dd, *J* = 10.6, 7.4 Hz, 1H), 4.48 (d, *J* = 7.4 Hz, 1H), 3.94 (s, 1H), 3.86 (dt, *J* = 12.1, 6.1 Hz, 1H), 3.66 (t, *J* = 11.1 Hz, 2H), 3.63 (s, 1H), 3.52 (d, *J* = 6.5 Hz, 1H), 3.46 (s, 1H), 3.40 (dd, *J* = 11.3, 6.7 Hz, 1H), 3.18 (s, 1H), 3.07 (s, 3H), 3.02 (d, *J* = 6.2 Hz, 1H), 2.99 – 2.91 (m, 5H), 2.80 (dt, *J* = 14.2, 7.2 Hz, 1H), 2.73 (d, *J* = 4.5 Hz, 1H), 2.59 – 2.47 (m, 2H), 2.29 – 2.24 (m, 1H), 2.20 – 2.15 (m, 9H), 2.06 – 2.01 (m, 4H), 1.93 – 1.76 (m, 3H), 1.71 (t, *J* = 12.8 Hz, 1H), 1.62 (d, *J* = 11.6 Hz, 1H), 1.57 – 1.47 (m, 3H), 1.42 (ddd, *J* = 13.2, 8.3, 3.1 Hz, 1H), 1.37 (t, *J* = 5.2 Hz, 1H), 1.36 – 1.28 (m, 4H), 1.25 – 1.17 (m, 11H), 1.14 (t, *J* = 7.6

Hz, 3H), 1.08 (t, *J* = 6.0 Hz, 8H), 0.85 (t, *J* = 7.5 Hz, 3H), 0.79 (t, *J* = 7.4 Hz, 2H). HRMS (ESI) *m+z* Calcd. for $C_{48}H_{76}NO_{14}$ [M + H^+]: 890.5260, found 890.5256.

((4″-Oxo)-3′-*O*-acetyl)-4′-*N*-(4-ethynylbenzyl)) clarithromycin (**15**)

A solution of *N*-chlorosuccinimide (0.034 g, 0.23 mmol) in DCM (5 mL) was stirred at -15 °C for 10 min then dimethyl sulfide (0.020 mL, 0.26 mmol) was added drop wise to form a white turbid solution. After stirring for 20 min, a DCM (5 mL) solution of compound **14** (0.128 g, 0.144 mmol) was added over a period of 30 min and the resulting suspension was stirred at -15 ˚C for 30 min. Subsequently, TEA (0.030 mL, 0.23 mmol) was added and the suspension cleared up within a min. Stirring continued at -10 °C for 2 h and the reaction was quenched with saturated $NaHCO_3$ (10 mL). The organic layer extracted with DCM (50 mL), dried with anhydrous Na_2SO_4, filtered, and concentrated *in vacuo*. Residue was purified by preparative chromatography (Silica gel, Hexanes/EtOAc/MeOH (3:2:0.05) to give compound **15** as a yellow solid (0.055 g, 45%). ^{1}H NMR (400 MHz, CD_3OD) δ (ppm) 8.32 (s, 1H), 7.77 (d, *J* = 7.7 Hz, 2H), 7.36 (d, *J* = 7.9 Hz, 2H), 5.09 (d, *J* = 9.2 Hz, 1H), 4.96 – 4.91 (m, 1H), 4.46 (s, 2H), 4.39 (d, *J* = 7.2 Hz, 1H), 4.19 (d, *J* = 6.4 Hz, 1H), 3.81 – 3.60 (m, 5H), 3.48 (s, 1H), 3.28 – 3.19 (m, 4H), 3.10 – 2.95 (m, 5H), 2.92 – 2.82 (m, 1H), 2.67 (s, 1H), 2.54 (s, 1H), 2.41 (s, 6H), 2.30 (s, 1H), 2.27 – 2.16 (m, 7H), 2.13 (dd, *J* = 20.0, 10.6 Hz, 4H), 1.94 – 1.69 (m, 6H), 1.62 (d, *J* = 14.6 Hz, 1H), 1.50 – 1.41 (m, 1H), 1.42 – 1.31 (m, 4H), 1.26 – 1.13 (m, 16H), 1.13 – 1.01 (m, 12H), 0.86 – 0.76 (m, 3H). ^{13}C NMR (126 MHz, MeOD) δ (ppm) 212.0, 177.2, 172.2, 142.0, 133.0, 129.9, 122.5, 101.8, 97.9, 84.5, 81.5, 80.5, 79.8, 78.5, 78.2, 76.0, 74.2, 73.9, 73.1, 70.7, 69.9, 62.6, 59.1, 51.8, 51.1, 50.9, 46.6, 46.0, 39.8, 39.6, 39.2, 39.1, 39.1, 38.6, 37.4, 32.1, 22.3, 21.8, 21.7, 21.1, 20.9, 20.4, 19.4, 18.5, 17.3,

16.7, 16.3, 15.1, 13.7, 12.8, 11.1, 10.1, 9.9. HRMS (ESI) *m/z* Calcd. for $C_{48}H_{74}NO_{14}$ [M+H$^+$]: 888.5104, found 888.5113.

((4″-Epoxy)-3′-*O*-acetyl)-4′-*N*-(4-ethynylbenzyl))clarithromycin (**16**)

Compound **15** (0.40 g, 0.45 mmol) was reacted with NaH (60% dispersion in mineral oil) (0.040 g, 0.99 mmol) and trimethyloxosulfonium iodide (0.218 g, 0.99 mmol) as described for the synthesis of compound **9** to give compound **16** after purification by preparative chromatography (Silica gel, Hexanes/EtOAc/EtOH (4:1:0.5), as yellow solid (0.35 g, 77%). ^{1}H NMR (400 MHz, $CDCl_3$) δ (ppm) 7.40 (d, J = 8.1 Hz, 2H), 7.20 (d, J = 8.1 Hz, 2H), 4.88 (d, J = 3.5 Hz, 1H), 4.84 – 4.73 (m, 2H), 4.56 (d, J = 7.5 Hz, 1H), 3.98 – 3.91 (m, 1H), 3.69 (s, 1H), 3.67 – 3.61 (m, 2H), 3.49 (d, J = 14.0 Hz, 2H), 3.34 (s, 1H), 3.06 (s, 3H), 3.04 (s, 2H), 2.90 (d, J = 4.1 Hz, 1H), 2.81 – 2.67 (m, 3H), 2.64 (d, J = 4.1 Hz, 1H), 2.49 (dt, J = 21.9, 7.4 Hz, 1H), 2.38 (dt, J = 9.9, 4.9 Hz, 1H), 2.35 – 2.25 (m, 2H), 2.21 (s, 3H), 2.18 (s, 1H), 2.15 (s, 1H), 2.08 (s, 3H), 1.83 (d, J = 4.8 Hz, 1H), 1.81 – 1.71 (m, 2H), 1.43 – 1.32 (m, 3H), 1.30 – 1.22 (m, 9H), 1.19 (t, J = 5.8 Hz, 7H), 1.12 (t, J = 9.0 Hz, 4H), 1.04 – 0.97 (m, 10H), 0.92 (d, J = 6.5 Hz, 3H), 0.88 (dd, J = 10.4, 4.7 Hz, 2H). ^{13}C NMR (101 MHz, $CDCl_3$) δ (ppm) 216.1, 178.8, 171.3, 169.8, 140.7, 131.9, 128.4, 120.6, 99.7, 96.0, 83.7, 79.7, 78.7, 73.8, 71.5, 68.2, 63.1, 61.5, 60.4, 58.2, 50.3, 49.4, 46.7, 41.6, 41.1, 38.3, 37.0, 36.4, 35.7, 33.4, 31.3, 29.7, 24.6, 21.3, 21.1, 20.2, 19.2, 17.9, 14.3, 14.1, 10.9, 10.7, 7.8. HRMS (ESI) *m/z* Calcd. for $C_{49}H_{76}NO_{14}$ [M+H$^+$]: 902.5260, found 902.5260.

((4″-(*N*,*N*-Dimethylaminomethyl)-4′-*N*-(4-ethynylbenzyl))clarithromycin (**18**)

N,*N*-Dimethylmethylamine **17** (4.22 mL, 8.46 mmol, 2M in THF) was added to a solution of compound **16** (0.10 g, 0.11 mmol) in MeOH (20 mL). The solution was heated at 60 °C for 6 h. MeOH and residual methylamine was evaporated off to give light yellow solid which was again

dissolved in MeOH (10 mL) and heated at 90 °C for three days after which TLC showed complete conversion. Excess MeOH was evaporated off to give compound **18** as yellow solid (0.08 g, 83%). ^{1}H NMR (400 MHz, $CDCl_3$) δ (ppm) 7.43 (d, J = 8.2 Hz, 3H), 7.26 – 7.20 (m, 2H), 5.04 (dd, J = 11.0, 2.2 Hz, 1H), 4.98 (d, J = 5.0 Hz, 1H), 4.37 (d, J = 7.2 Hz, 1H), 4.07 – 4.00 (m, 1H), 3.94 (s, 1H), 3.79 (s, 1H), 3.75 (s, 2H), 3.73 – 3.69 (m, 2H), 3.66 (dd, J = 8.5, 5.8 Hz, 1H), 3.62 (dd, J = 6.6, 3.6 Hz, 1H), 3.61 – 3.57 (m, 1H), 3.50 – 3.42 (m, 2H), 3.39 (dd, J = 12.3, 7.7 Hz, 3H), 3.29 (dd, J = 10.2, 7.2 Hz, 1H), 3.21 (d, J = 3.9 Hz, 1H), 3.16 (d, J = 3.7 Hz, 2H), 3.09 (s, 3H), 3.06 (t, J = 4.5 Hz, 4H), 3.05 – 3.01 (m, 4H), 2.99 (d, J = 8.0 Hz, 1H), 2.91 – 2.80 (m, 1H), 2.66 (s, 1H), 2.62 (s, 1H), 2.52 (dd, J = 15.6, 7.6 Hz, 2H), 2.36 (s, 9H), 2.23 (d, J = 4.3 Hz, 4H), 2.18 – 2.15 (m, 1H), 2.07 (s, 1H), 2.03 (s, 2H), 1.99 (d, J = 6.8 Hz, 1H), 1.90 (dt, J = 30.0, 10.5 Hz, 6H), 1.64 – 1.52 (m, 2H), 1.49 – 1.42 (m, 1H), 1.41 – 1.33 (m, 6H), 1.31 – 1.22 (m, 10H), 1.22 – 1.17 (m, 5H), 1.15 – 1.01 (m, 25H), 0.91 (dt, J = 14.0, 5.6 Hz, 3H), 0.87 – 0.78 (m, 5H). ^{13}C NMR (126 MHz, $CDCl_3$) δ (ppm) 175.7, 169.9, 167.8, 132.3, 132.0, 130.9, 128.8, 128.5, 121.1, 102.8, 96.4, 83.4, 81.3, 78.3, 78.0, 76.5, 76.0, 74.3, 70.9, 70.3, 69.0, 68.3, 68.2, 67.6, 63.6, 58.0, 57.8, 50.8, 50.6, 49.4, 47.3, 45.3, 44.9, 39.3, 38.8, 38.7, 37.2, 36.9, 31.3, 30.4, 29.7, 28.9, 23.7, 23.0, 21.6, 21.0, 19.8, 18.5, 18.1, 16.0, 16.0, 15.1, 14.1, 12.4, 11.0, 10.6, 9.3. HRMS (ESI) *m+2/2z* Calcd. for $C_{49}H_{82}N_2O_{13}$ [M+2H$^+$]: 453.2903 found 453.2892.

(Clarithromycin-(4′-*N*-(4-benzyltriazolyl))-4′′-(*N*,*N*-dimethylaminomethyl))-*N*-hydroxyhexanamide (**20a**)

Reaction of compound **18** (0.05 g, 0.06 mmol) with 6-azido-*N*-((*tert*-butyldimethylsilyl)oxy)hexanamide **19e** (0.075 g, 0.249 mmol) followed by TBS removal with caesium fluoride as described for the synthesis of compound **5a,** gave **20a** as light yellow solid

(0.02 g, 44%).[1]H NMR (400 MHz, CD_3OD) δ (ppm) 8.36 (s, 1H), 7.81 (d, *J* = 8.2 Hz, 2H), 7.46 (d, *J* = 8.3 Hz, 2H), 5.12 (d, *J* = 10.8 Hz, 1H), 4.45 (t, *J* = 6.9 Hz, 3H), 4.31 (d, *J* = 7.2 Hz, 1H), 4.09 (d, *J* = 6.5 Hz, 1H), 3.90 (d, *J* = 13.4 Hz, 1H), 3.72 (d, *J* = 13.5 Hz, 2H), 3.59 (d, *J* = 12.8 Hz, 2H), 3.20 (dd, *J* = 19.5, 9.0 Hz, 3H), 3.11 (d, *J* = 15.2 Hz, 2H), 3.00 (d, *J* = 8.4 Hz, 6H), 2.89 (s, 1H), 2.65 (s, 1H), 2.59 (s, 3H), 2.42 (s, 6H), 2.34 (s, 4H), 2.28 (s, 1H), 2.21 (s, 1H), 2.10 (t, *J* = 7.4 Hz, 4H), 1.96 (dd, *J* = 15.3, 7.4 Hz, 5H), 1.82 (s, 7H), 1.73 – 1.60 (m, 5H), 1.44 – 1.33 (m, 9H), 1.27 (d, *J* = 10.6 Hz, 7H), 1.22 (dd, *J* = 12.4, 6.3 Hz, 7H), 1.21 – 1.16 (m, 6H), 1.17 – 1.09 (m, 17H), 1.06 (d, *J* = 7.5 Hz, 4H), 0.91 (d, *J* = 10.9 Hz, 5H), 0.84 (dd, *J* = 9.5, 5.1 Hz, 5H). [13]C NMR (101 MHz, $CDCl_3$) δ (ppm) 175.7, 147.5, 129.7, 125.8, 102.9, 96.8, 94.9, 78.3, 76.1, 74.3, 71.3, 70.9, 69.0, 68.3, 67.5, 51.3, 50.7, 50.7, 50.1, 50.5, 49.4, 47.2, 45.3, 45.3, 44.6, 39.4, 37.5, 36.8, 33.7, 31.9, 29.7, 28.6, 23.2, 22.7, 21.6, 21.3, 19.7, 18.1, 16.0, 15.9, 15.1, 14.1, 12.3, 10.6, 9.2, 7.8. HRMS (ESI) *m/z* Calcd. for $C_{55}H_{93}N_6O_{15}$ $[M+H^+]$1077.6693, found 1077.6692.

(Clarithromycin-(4′-*N*-(4-benzyltriazolyl))-4′′-(*N*,*N*-dimethylaminomethyl))-*N*-hydroxyheptanamide (**20b**)

Reaction of compound **18** (0.024 g, 0.022 mmol) with 7-Azido-*N*-((*tert*-butyldimethylsilyl)oxy)heptanamide **19f** (0.075 g, 0.249 mmol) followed by TBS removal with caesium fluoride as described for the synthesis of compound **5a,** gave **20b** as a light yellow solid (0.021 g, 83%).[1]H NMR (400 MHz, CD_3OD) δ 8.37 (s, 1H), 7.82 (d, *J* = 8.2 Hz, 2H), 7.46 (d, *J* = 8.2 Hz, 2H), 5.14 – 5.07 (m, 1H), 4.45 (t, *J* = 7.0 Hz, 2H), 4.30 (d, *J* = 7.2 Hz, 1H), 4.09 (d, *J* = 6.5 Hz, 1H), 3.92 (d, *J* = 13.0 Hz, 1H), 3.72 (d, *J* = 12.3 Hz, 2H), 3.64 – 3.57 (m, 2H), 3.34 (d, *J* = 2.4 Hz, 2H), 3.09 (s, 1H), 3.04 – 2.97 (m, 7H), 2.89 (s, 2H), 2.59 (s, 3H), 2.49 (s, 7H), 2.36 (s, 3H), 2.28 (s, 1H), 2.15 (s, 1H), 2.11 – 2.03 (m, 5H), 1.92 (dd, *J* = 13.5, 6.7 Hz, 6H), 1.83 (d, *J* = 10.2 Hz, 4H), 1.61 (d, *J* = 7.5 Hz, 6H), 1.42 – 1.33 (m, 12H), 1.28 (s, 6H), 1.23 (d, *J* = 6.0 Hz,

5H), 1.19 (d, *J* = 7.2 Hz, 4H), 1.17 – 1.08 (m, 16H), 1.05 (d, *J* = 7.5 Hz, 4H), 0.97 (s, 1H), 0.91 (d, *J* = 11.7 Hz, 4H), 0.84 (t, *J* = 7.4 Hz, 4H). ^{13}C NMR (101 MHz, cd_3od) δ 223.5, 179.1, 149.8, 132.2, 127.7, 123.6, 105.6, 99.1, 83.2, 80.8, 79.1, 77.0, 73.5, 71.6, 70.5, 69.7, 63.3, 60.6, 53.5, 52.2, 51.4, 48.7, 47.8, 47.4, 41.5, 38.1, 33.1, 32.2, 31.5, 30.9, 30.6, 28.2, 27.6, 23.1, 20.0, 19.8, 18.1, 17.7, 16.9, 13.7, 12.2, 11.3 HRMS (ESI) *m+2/2z* Calcd. for $C_{56}H_{97}N_6O_{15}$ [M+2H$^+$]: 546.3461, found 546.3469.

(Clarithromycin-3′-(*N*-(4-triazolylbenzyl)))-*N*-(2-amino-5-(thiophen-2-yl)phenyl)-hexanamide (**22a)**

3′-N-(desmethyl)- 3′-*N*-(4-ethynylbenzyl) clarithromycin **3** (0.08 g, 0.09 mmol) and 2-*N*-(2-amino-5-(thiophen-2-yl)phenyl)-6-azidohexanamide **21a** (0.03 g, 0.10 mmol) are dissolved in anhydrous THF and purged with argon for 10 min. DIPEA (0.03ml, 0.19mmol) and CuI (0.01 g, 0.05 mmol) were then added to the mixture and purged further for another 20 minutes. The resulting suspension was stirred at room temperature for 12 h. Reaction was quenched with a solution of 4:1 satd. Aqueous NH_4Cl/NH_4OH and extracted with a mixture of 10% MeOH in DCM. Combined organic layer was dried over anhydrous Na_2SO_4 and concentrated *in vacuo*. The crude was purified by prep. TLC using Hexanes: EtOAc: ^{i}PrOH: NH_4OH (10:10:0.2:0.01) to give compound **22a** as a brown solid (0.064g, 57%). ^{1}H NMR (400 MHz, $cdcl_3$) δ 7.80 – 7.71 (m, 3H), 7.53 (s, 1H), 7.43 (s, 1H), 7.37 – 7.26 (m, 3H), 7.14 (dd, *J* = 12.4, 4.3 Hz, 2H), 7.04 – 6.97 (m, 1H), 6.77 (d, *J* = 8.2 Hz, 1H), 5.04 (d, *J* = 11.1 Hz, 1H), 4.88 (d, *J* = 4.6 Hz, 1H), 4.40 (t, *J* = 8.0 Hz, 3H), 3.95 (d, *J* = 17.2 Hz, 3H), 3.80 – 3.68 (m, 3H), 3.62 (d, *J* = 6.9 Hz, 1H), 3.48 (s, 3H), 3.33 (d, *J* = 11.4 Hz, 2H), 3.20 (d, *J* = 8.1 Hz, 2H), 3.11 (s, 3H), 3.04 – 2.92 (m, 6H), 2.87 (dd, *J* = 16.3, 8.8 Hz, 2H), 2.57 (s, 2H), 2.40 (dd, *J* = 15.6, 8.4 Hz, 2H), 2.28 (d, *J* = 15.0 Hz, 5H), 2.16

(s, 1H), 2.08 (d, *J* = 10.0 Hz, 2H), 1.96 (dd, *J* = 17.8, 9.8 Hz, 3H), 1.92 – 1.84 (m, 3H), 1.83 – 1.61 (m, 7H), 1.47 (dd, *J* = 20.5, 17.1 Hz, 5H), 1.39 (s, 5H), 1.24 (dt, *J* = 21.5, 10.8 Hz, 10H), 1.19 – 1.13 (m, 5H), 1.14 – 1.01 (m, 18H), 0.83 (t, *J* = 7.3 Hz, 4H). ^{13}C NMR (126 MHz, $CDCl_3$) δ 175.95, 175.78, 172.59, 147.39, 145.00, 129.57, 128.02, 125.78, 124.26, 122.71, 121.07, 119.80, 102.79, 99.96, 95.93, 88.63, 81.00, 78.32, 77.89, 74.27, 72.51, 70.76, 69.08, 65.69, 63.87, 57.67, 50.64, 49.85, 49.42, 45.26, 45.06, 39.26, 39.08, 37.23, 36.87, 34.71, 31.88, 29.71, 29.53, 28.52, 26.51, 25.54, 22.63, 21.48, 21.31, 21.03, 19.83, 18.64, 18.02, 16.03, 15.98, 14.14, 12.33, 10.62, 9.16. HRMS (ESI) *m*+*z* Calcd. for $C_{62}H_{93}O_{14}N_6S$ [M+H$^+$]: 1177.6465, found 1177.6425.

(Clarithromycin-3′-(*N*-(4-triazolylbenzyl)))-N-(2-amino-5-(thiophen-2-yl)phenyl)-heptanamide (22b)

3′-N-(desmethyl)- 3′-*N*-(4-ethynylbenzyl) clarithromycin **3** (0.08 g, 0.09 mmol) and *N*-(2-amino-5-(thiophen-2-yl) phenyl)-7-azidoheptanamide **21b** (0.04 g, 0.10 mmol) are dissolved in anhydrous THF and purged with argon for 10 min. DIPEA (0.02ml, 0.19mmol) and CuI (0.01 g, 0.05 mmol) and left to react as described for compound **22a** above. Crude product was purified by prep. TLC using Hexanes: EtOAc: ^{i}PrOH: NH_4OH (10:10:0.2:0.01) to give compound **22b** as a brown solid (0.046g, 57%). ^{1}H NMR (400 MHz, $cdcl_3$) δ 7.79 – 7.71 (m, 3H), 7.65 (s, 1H), 7.42 (d, *J* = 1.8 Hz, 1H), 7.30 (dd, *J* = 10.3, 4.3 Hz, 3H), 7.14 (dd, *J* = 11.9, 3.8 Hz, 2H), 7.03 – 6.97 (m, 1H), 6.78 (d, *J* = 8.3 Hz, 1H), 5.02 (dt, *J* = 13.1, 6.5 Hz, 1H), 4.88 (d, *J* = 4.6 Hz, 1H), 4.39 (dd, *J* = 10.4, 6.9 Hz, 3H), 3.99 – 3.86 (m, 3H), 3.79 – 3.68 (m, 3H), 3.61 (d, *J* = 7.1 Hz, 2H), 3.43 (s, 2H), 3.31 (dd, *J* = 16.2, 9.0 Hz, 1H), 3.19 (d, *J* = 9.0 Hz, 2H), 3.11 (d, *J* = 11.0 Hz, 3H), 3.03 – 2.90 (m, 6H), 2.90 – 2.81 (m, 1H), 2.58 (d, *J* = 31.0 Hz, 2H), 2.44 – 2.33 (m, 2H), 2.30 – 2.21 (m, 5H), 2.18 – 2.13 (m, 6H), 1.99 – 1.83 (m, 7H), 1.81 – 1.65 (m, 6H), 1.54 – 1.33 (m, 13H), 1.31 – 1.19 (m, 13H), 1.18 – 1.13 (m, 4H), 1.12 – 1.01 (m, 17H), 0.82 (t, *J* = 7.4 Hz, 3H). ^{13}C NMR (126

MHz, $CDCl_3$) δ 175.79, 171.72, 147.39, 144.13, 140.46, 129.56, 129.34, 127.89, 126.21, 125.76, 124.96, 124.59, 123.58, 122.82, 121.90, 118.60, 115.17, 113.31, 102.49, 95.93, 80.97, 78.32, 77.92, 74.27, 72.51, 72.49, 71.29, 70.51, 70.19, 69.07, 65.66, 63.57, 61.88, 57.68, 50.63, 50.11, 49.43, 45.26, 45.06, 39.25, 39.09, 37.23, 36.85, 36.39, 34.82, 31.94, 31.65, 30.01, 29.71, 29.67, 29.37, 28.23, 25.84, 25.21, 22.71, 21.47, 21.29, 21.03, 19.83, 19.27, 18.64, 18.01, 16.02, 15.98, 14.20, 14.14, 13.92, 12.33, 10.62, 9.13. HRMS (ESI) *m+z* Calcd. for $C_{63}H_{95}O_{14}N_6S$ $[M+H^+]$: 1191.6621, found 1191.6620.

(Clarithromycin-3′-(*N*-(4-triazolylbenzyl)))-N-(2-amino-5-(thiophen-2-yl)phenyl)-octanamide (22c)

3′-*N*-(desmethyl)- 3′-*N*-(4-ethynylbenzyl) clarithromycin **3** (0.11 g, 0.09 mmol) and *N*-(2-amino-5-(thiophen-2-yl)phenyl)-8-azidooctanamide **21c** (0.05 g, 0.14 mmol) are dissolved in anhydrous THF and purged with argon for 10 min. DIPEA (0.04 ml, 0.25 mmol) and CuI (0.012 g, 0.064 mmol) and left to react as described for compound **22a** above. Crude product was purified by prep. TLC using DCM: MeOH: NH_4OH (12:1:0.1) to give compound **22c** as a brown solid (0.134g, 87%). ^{1}H NMR (400 MHz, $cdcl_3$) δ 7.76 (d, *J* = 7.8 Hz, 3H), 7.51 (d, *J* = 6.9 Hz, 1H), 7.43 (s, 1H), 7.30 (d, *J* = 6.3 Hz, 3H), 7.17 – 7.10 (m, 2H), 7.04 – 6.97 (m, 1H), 6.78 (d, *J* = 8.1 Hz, 1H), 5.02 (t, *J* = 10.3 Hz, 1H), 4.89 (d, *J* = 4.9 Hz, 1H), 4.44 – 4.30 (m, 3H), 4.00 – 3.85 (m, 3H), 3.76 – 3.67 (m, 3H), 3.62 (d, *J* = 7.0 Hz, 1H), 3.46 (d, *J* = 15.2 Hz, 3H), 3.28 (d, *J* = 20.7 Hz, 1H), 3.19 (d, *J* = 9.1 Hz, 1H), 3.12 (d, *J* = 14.1 Hz, 3H), 3.04 – 2.92 (m, 6H), 2.87 (dd, *J* = 17.9, 9.1 Hz, 2H), 2.51 (d, *J* = 34.1 Hz, 2H), 2.40 (t, *J* = 7.4 Hz, 2H), 2.31 – 2.18 (m, 5H), 2.07 (d, *J* = 9.9 Hz, 1H), 2.00 (d, *J* = 0.7 Hz, 1H), 1.98 – 1.85 (m, 5H), 1.83 – 1.75 (m, 2H), 1.69 (d, *J* = 14.4 Hz, 6H), 1.49 (td, *J* = 15.2, 6.0 Hz, 2H), 1.39 (s, 10H), 1.25 (dd, *J* = 13.2, 6.1 Hz, 10H), 1.17 (d, *J* = 7.1 Hz, 5H), 1.14 – 1.01 (m, 19H), 0.83 (t, *J* = 7.3 Hz, 4H). ^{13}C NMR (101 MHz, $cdcl_3$) δ 175.58,

171.64, 157.80, 152.04, 149.69, 144.17, 129.26, 127.98, 125.85, 124.80, 124.57, 123.29, 122.75, 122.22, 120.41, 118.29, 102.62, 99.74, 95.82, 80.91, 78.25, 74.24, 72.28, 69.10, 68.87, 65.69, 57.60, 50.61, 50.02, 49.50, 43.21, 39.05, 36.92, 36.40, 34.59, 29.90, 28.61, 28.08, 25.94, 25.21, 21.48, 20.74, 19.67, 18.63, 18.09, 15.73, 12.31, 10.60, 8.93. HRMS (ESI) *m*+*z* Calcd. for $C_{64}H_{97}O_{14}N_6S$ [M+H^+]: 1205.6778, found 1205.6795.

2.8.2. *In Vitro* HDAC Inhibition: SAMDI Assay

The maleimide-presenting SAMs and expression of HDAC8 enzyme were prepared as previously reported.[21] To obtain IC_{50} values, we incubated isoform- optimized substrates (50 μM, detailed below) with enzyme (250 nM, detailed below) and inhibitor (at concentrations ranging from .1 nM to 1.0 mM) in HDAC buffer (25.0 mM Tris-HCl, pH 8.0, 140 mM NaCl, 3.0 mM KCl, 1.0 mM $MgCl_2$, and 0.1 mg/mL BSA) in 96-well microtiter plates (60 min, 37 °C). Solution-phase deacetylation reactions were quenched with trichostatin A (TSA) and transferred to SAMDI plates to immobilize the substrate components. SAMDI plates were composed of an array of self-assembled monolayers (SAMs) presenting maleimide in standard 384-well format for high-throughput handling capability. Following immobilization, plates were washed to remove buffer constituents, enzyme, inhibitor, and any unbound substrate and analyzed by MALDI mass spectrometry using automated protocols. Deacetylation yields in each triplicate sample were determined from the integrated peak intensities of the molecular ions for the substrate and the deacetylated product ion by taking the ratio of the former over the sum of both. Yields were plotted with respect to inhibitor concentration and fitted to obtain IC_{50} values for each isoform−inhibitor pair.

Isoform-optimized substrates were prepared by traditional FMOC solid-phase peptide synthesis (reagents supplied by Anaspec) and purified by semi-preparative HPLC on a reverse-phase C18 column (Waters). The peptide GRK^{ac}FGC was prepared for HDAC1 and HDAC8 experiments, whereas the peptide GRK^{ac}YGC was prepared for HDAC6 experiments.

HDAC1, HDAC6, and HDAC2 were purchased from BPS Biosciences. The catalytic domain of HDAC8 was expressed as previously reported.[21e] Briefly, an amplicon was prepared by PCR with the following primers: forward (5′−3′) TATTCTCGAGGA- CCACATGCTTCA and reverse (5′−3′) ATAAGCTAGCATG- GAGGAGCCGGA. A pET21a construct bearing the genetic insert between the NheI and XhoI restriction sites was transformed into Escherichia coli BL21(DE3) (Lucigen) and expressed by standard protocols. Following purification by affinity chromatography, the His- tagged enzyme-containing fractions were purified by FPLC (AKTA) on a superdex size-exclusion column (GE), spin-concentrated, and stored at −80 °C in HDAC buffer with 10% glycerol.

2.8.3. Cell growth inhibition study

A549, MCF-7 and VERO were cultured in DMEM (Lonza, GA) supplemented with 10% fetal bovine serum (FBS) (Atlanta Biologicals, Atlanta, GA) and 1% *Penicillin-Streptomycin*. Cells were incubated in a 96 well plate for 24 h then treated with various drug concentrations and incubated for another 72 h. Cell viability was measured using the MTS assay (CellTiter 96 Aqueous One Solution and CellTiter 96 Non-Radioactive Cell Proliferation Assays, Promega, Madison, WI) protocol as described by the manufacturer. In all experiments, DMSO concentration was maintained at 0.1%.

2.8.4. Anti-inflammatory Activity Assay:

NF-κB activity was measured by luciferase assay. BEAS-2B cells were transfected with NF-κB luciferase reporter construct in pGL3 basic vector.[31] 24 h after transfection, the cells were treated with drugs for 1 h followed by stimulation with NTHi for 5 h. Then cells were lysed with cell lysis buffer (250 mM Tris HCl (pH 7.5), 0.1% Triton-X, 1 mM DTT) and luciferase activity was measured by luciferase assay system (promega). Relative luciferase activity (RLA) was determined using the following equation; RLA = luciferase unit of the cells treated with NTHi and drug / luciferase unit of the cells treated with mock. IC_{50} was determined by treating the cell with a serial dose of the drug followed by luciferase assay. % Inhibition was calculated using the following equation; % inhibition = RLA of the cells treated with indicated concentration of the drug / RLA of the cells treated with mock.

2.8.5. Real-Time quantitative RT-PCR analysis

Total RNA was isolated with TRIzol reagent (Life Technologies) by following the manufacturer's instruction. For the reverse transcription reaction, TaqMan reverse transcription reagents (Life Technologies) were used as described previously. For quantitative RT-PCR analysis, PCR amplifications were performed by using SYBR Green Universal Master Mix (Life Technologies). In brief, reactions were performed in triplicate containing 2×~ Universal Master Mix, 1 μL of template cDNA, 500 nM primers in a final volume of 12.5 μL, and they were analyzed in a 96-well optical reaction plate (USA Scientific). Reactions were amplified and quantified by using a StepOnePlus Real-Time PCR System and the manufacturer's corresponding software (StepOnePlus Software v2.3; Life Technologies). The relative quantities of mRNAs were obtained

by using the comparative Ct method and were normalized by using human cyclophilin as an endogenous control. For semiquantitative RT-PCR analysis, PCR amplifications were performed with PrimeSTAR Max polymerase (Takara) by following the manufacturer's instruction. The primer for TNF-α, IL-1β were described previousery[35,36]. IL-1α :5'-*CGAGCCAATGATCAGTACCTC* -3' and 3'-*CACCCATATATTTCACTG* -5'.

2.8.6. Western blot analysis

MCF-7 cells (10^6 cells/dish) were seeded in petri dishes 24 hour prior to treatment with various concentrations of compounds for 24 hours. Thereafter, media was removed and cells were washed with chilled 1X PBS buffer and resuspended in CelLyticM buffer containing a cocktail of protease inhibitor (Sigma-Aldrich, St. Louis, MO, USA). Protein concentration was determined through Bradford protein assay. Equal amount of protein was then loaded onto an SDS-page gel (Bio-Rad, Hercules, CA, USA) and resolved by electrophoresis at a constant voltage of 100 V for 2 hours. The gel was transfered onto a nitrocellulose membrane and probed for H4 and acetyl H4.

2.9. References

1. Witt, O.; Deubzer, H. E.; Milde, T.; Oehme, I. *Cancer Lett.* **2009,** *277* (1), 8.
2. Mai, A.; Cerbara, I.; Valente, S.; Massa, S.; Walker, L. A.; Tekwani, B. L. *Antimicrob. Agents Chemother.* **2004,** *48* (4), 1435.
3. (a) Jenuwein, T. *Science* **2001,** *293* , 1074 (b) Johnstone, R. W. *Nat. Rev. Drug Discov.* **2002,** *1*, 287 (c) Bolden, J. E.; Peart, M. J.; Johnstone, R. W. *Nat. Rev. Drug Discov.* **2006,**

5, 769 (d) Somech, R.; Izraeli, S.; A, J. S. *Cancer Treat. Rev.* **2004,** *30* , 461 (e) Boyes, J.; Byfield, P.; Nakatani, Y.; Ogryzko, V. *Nature* **1998,** *396*, 594 (f) Gu, W.; Roeder, R. G. *Cell* **1997,** *90*, 595 (g) Jin, S.; Scotto, K. W. *Mol. Cellu. Bio.* **1998,** *18*, 4377 (h) Yang, X. J.; Seto, E. *Nat. Rev. Mol. cell Bio.* **2008,** *9*, 206 (i) Vigushin, D. M.; Coombes, R. C. *Curr. Cancer Drug Targets* **2004,** *4* , 205 (j) Choudhary, C.; Kumar, C.; Gnad, F.; Nielsen, M. L.; Rehman, M.; Walther, T. C.; Olsen, J. V.; Mann, M. *Science* **2009,** *325*, 834.

4. Kelly, W. K.; O'Connor, O. A.; Marks, P. A. *Expt. Opin. Invest. Drugs* **2002,** *11* , 1695.
5. Miller, T. A.; Witter, D. J.; Belvedere, S. *J. Med. Chem.* **2003,** *46*, 5097.
6. Molecule of the month. Vorinostat. *Drug News & Persp.* **2006,** *19*, 352.
7. Grant, S.; Easley, C.; Kirkpatrick, P. *Nat. Rev. Drug Discov.* **2007,** *6*, 21.
8. Campas-Moya, C. *Drugs of Today* **2009,** *45*, 787.
9. RajKumar, S. V. *Lancet Oncology* **2014**, *15*, 1178.
10. Guha, M. *Nat. Rev. Drug Discov.* **2015**, *14*, 225
11. Rashidi, A; Cashen, A. F. *Future Oncology* **2015**, *11*, 1659.
12. Yurek-George, A.; Cecil, A. R.; Mo, A. H.; Wen, S.; Rogers, H.; Habens, F.; Maeda, S.; Yoshida, M.; Packham, G.; Ganesan, A. *J. Med. Chem.* **2007,** *50*, 5720.
13. Mwakwari, S. C.; Patil, V.; Guerrant, W.; Oyelere, A. K. *Curr. Top. Med. Chem.* **2010,** *10*, 1423.
14. Oyelere, A. K.; Chen, P. C.; Guerrant, W.; Mwakwari, S. C.; Hood, R.; Zhang, Y.; Fan, Y. *J. Med. Chem.* **2009,** *52*, 456.
15. Mwakwari, S. C.; Guerrant, W.; Patil, V.; Khan, S. I.; Tekwani, B. L.; Gurard-Levin, Z. A.; Mrksich, M.; Oyelere, A. K. *J. Med. Chem.* **2010,** *53*, 6100.

16. Jakopovic, I. P.; Krajacic, M. B.; Skugor, M. M.; Stimac, V.; Pesic, D.; Vujasinovic, I.; Alihodzic, S.; Cipcic Paljetak, H.; Kragol, G. *Bioorg. Med. Chem. Lett.* **2012,** *22*, 3527.

17. Lee, Y.; Choi, J. Y.; Fu, H.; Harvey, C.; Ravindran, S.; Roush, W. R.; Boothroyd, J. C.; Khosla, C. *J. Med. Chem.* **2011,** *54*, 2792.

18. (a) Rostovtsev, V. V.; Green, L. G.; Fokin, V. V.; Sharpless, K. B. *Angew. Chem.* **2002,** *41*, 2596 (b) Tornoe, C. W.; Christensen, C.; Meldal, M. *J. Org. Chem.* **2002,** *67* , 3057.

19. Cosner, C. C.; Helquist, P. *Org. Lett.* **2011,** *13*, 3564.

20. (a) Denis, A.; Renou, C. *Tetrahedron Lett.* **2002,** *43*, 4171. (b) Mercep, M.; Mesic, M.; Tomaskovic, L.; Markovic, S.; Makaruha, O.; Poljak, V. US 2004014685 (c) M. Miljkovic, Carbohydrates: Synthesis, Mechanisms, and Stereoelectronic Effects. Springer, New York, 2009 (d) Trott, O.; Olson, A. J. *J. Comput. Chem.* **2010**, 31, 455.

21. (a) Min, D. H.; Yeo, W. S.; Mrksich, M. *Anal. Chem.* **2004,** *76* , 3923 (b) Gurard-Levin, Z. A.; Mrksich, M. *Biochemistry* **2008,** *47* , 6242 (c) Mrksich, M. *ACS Nano* **2008,** *2*, 7 (d) Gurard-Levin, Z. A.; Kim, J.; Mrksich, M. *Eur. J. Chem. Biol.* **2009,** *10*, 2159. (e) Gurard-Levin, Z. A.; Kilian, K. A.; Kim, J.; Bahr, K.; Mrksich, M. *ACS Chem. Biol.* **2010**, 5, 863.

22. Vaguliene, N., Zemaitis, M., Lavinskiene, S. *et al. BMC Immunol.* 2013, 14, 36

23. Azad, N., Rojanasakul, Y., Vallyathan, V. *J Tox. Environ. Health B Crit. Rev.* 2008, 11, 1.

24. Lu, H.; Ouyang, W.; Huang C. *Mol Cancer Res.* 2006, 4, 221.

25. Tang, J.; Yan, H.; Zhuang, S. *Clin. Sci.* **2013,** *124* , 651.

26. (a) Shi, Z. J.; Ouyang, D. Y.; Zhu, J. S.; Xu, L. H.; He, X. H. *Int. J. Immunopharmacol.* **2012,** *12* , 580 (b) Wang, D.; Zhao, M.; Chen, G.; Cheng, X.; Han, X.; Lin, S.; Zhang, X.; Yu, X. *Apoptosis : an Int. J. on prog. cell death* **2013,** *18*, 1348.

27. (a) Yoshida, M.; Kijima, M.; Akita, M.; Beppu, T. *J. Bio. Chem.* **1990,** *265*, 17174 (b) Furumai, R.; Ito, A.; Ogawa, K.; Maeda, S.; Saito, A.; Nishino, N.; Horinouchi, S.; Yoshida, M. *Cancer Sci.* **2011,** *102*, 1081.

28. Tong, X.; Yin, L.; Giardina, C. *Biochem. Biophy. Res. Commun.* **2004,** *317*, 463.

29. Choo, Q. Y.; Ho, P. C.; Tanaka, Y.; Lin, H. S. *Molecules* **2013,** *18*, 14085.

30. (a) Blanchard, F.; Chipoy, C. *Drug Discov. Today* **2005,** *10*, 197 (b) Adcock, I. M. *British J. Pharmacology* **2007,** *150*, 829.

31. Ishinaga, H.; Jono, H.; Lim, J. H.; Kweon, S. M.; Xu, H.; Ha, U. H.; Xu, H.; Koga, T.; Yan, C.; Feng, X. H.; Chen, L. F.; Li, J. D. *EMBO J.* **2007,** *26*, 1150.

32. (a) Moghaddam, S. J.; Clement, C. G.; De la Garza, M. M.; Zou, X.; Travis, E. L.; Young, H. W.; Evans, C. M.; Tuvim, M. J.; Dickey, B. F. *Amer. J. Resp. Cell Mol. Bio.* **2008,** *38*, 629 (b) Poolman, J. T.; Bakaletz, L.; Cripps, A.; Denoel, P. A.; Forsgren, A.; Kyd, J.; Lobet, Y. *Vaccine* **2000,** *19 Suppl 1*, S108.

33. (a) Loukides, S.; Bartziokas, K.; Vestbo, J.; Singh, D. *Curr. Drug Targets* **2013,** *14*, 235 (b) Chung, K. F.; Adcock, I. M. *Eur. Resp. J.* **2008,** *31*, 1334.

34. Zhu, D.; Xu, Y.; Liu, Y.; Chen, X.; Zhao, Z.; Lei, P. *Bioorg. Med. Chem. Lett.* **2013,** *23*, 6274.

35. Miyata, M.; Lee, Ji-Y.; Miyata, S.; Wang, W. Y.; Xu, H.; Kai, H.; Kobayashi, K. S.; Flavell, R. A.; Li, J-D. *Nat. Commun.* **2015**, *6*, 6062.

36. Miyata,S.; Miyata, M.; Lee, B-C.; Xu, H.; Kai, H; Yan, C.;Li, J-D. *Proc. Natl. Acad. Sci. USA* **2015**, *112*, E1800.

37. Weichert, W., *Cancer Lett.* **2009,** *280* , 168-176.

38. Müller, B. M.; Jana, L.; Kasajima, A.; Lehmann, A.; Prinzler, J.; Budczies, J.; Winzer, K.-J.; Dietel, M.; Weichert, W.; Denkert, C., *BMC Cancer* **2013,** *13*, 1.

39. Witt, O.; Deubzer, H. E.; Milde, T.; Oehme, I., *Cancer Lett.* **2009,** *277*, 8.

40. Wambua, M. K.; Nalawansha, D. A.; Negmeldin, A. T.; Pflum, M. K. H., *J. Med. Chem.* **2014,** *57*, 642.

41. Methot, J. L.; Chakravarty, P. K.; Chenard, M.; Close, J.; Cruz, J. C.; Dahlberg, W. K.; Fleming, J.; Hamblett, C. L.; Hamill, J. E.; Harrington, P.; Harsch, A.; Heidebrecht, R.; Hughes, B.; Jung, J.; Kenific, C. M.; Kral, A. M.; Meinke, P. T.; Middleton, R. E.; Ozerova, N.; Sloman, D. L.; Stanton, M. G.; Szewczak, A. A.; Tyagarajan, S.; Witter, D. J.; Paul Secrist, J.; Miller, T. A., *Bioorg. Med. Chem. Lett.* **2008,** *18*, 973.

42. Sodji, Q. H.; Kornacki, J. R.; McDonald, J. F.; Mrksich, M.; Oyelere, A. K., *Eur. J. Med. Chem.* **2015,** *96*, 340.

43. Oyelere, A. K.; Chen, P. C.; Guerrant, W.; Mwakwari, S. C.; Hood, R.; Zhang, Y.; Fan, Y., *J. Med. Chem.* **2008,** *52*, 456.

44. Mwakwari, S. C.; Guerrant, W.; Patil, V.; Khan, S. I.; Tekwani, B. L.; Gurard-Levin, Z. A.; Mrksich, M.; Oyelere, A. K., *J. Med. Chem.* **2010,** *53*, 6100.

45. Schroeder, F. A.; Lewis, M. C.; Fass, D. M.; Wagner, F. F.; Zhang, Y.-L.; Hennig, K. M.; Gale, J.; Zhao, W.-N.; Reis, S.; Barker, D. D.; Berry-Scott, E.; Kim, S. W.; Clore, E. L.; Hooker, J. M.; Holson, E. B.; Haggarty, S. J.; Petryshen, T. L., *PLoS One* **2013,** *8*, e71323.

46. Zhang, X.; Kong, Y.; Zhang, J.; Su, M.; Zhou, Y.; Zang, Y.; Li, J.; Chen, Y.; Fang, Y.; Zhang, X.; Lu, W., *Eur. J. Med. Chem.* **2015,** 95, 127.

47. Wagner, F. F.; Zhang, Y. L.; Fass, D. M.; Joseph, N.; Gale, J. P.; Weiwer, M.; McCarren, P.; Fisher, S. L.; Kaya, T.; Zhao, W. N.; Reis, S. A.; Hennig, K. M.; Thomas, M.; Lemercier, B.

C.; Lewis, M. C.; Guan, J. S.; Moyer, M. P.; Scolnick, E.; Haggarty, S. J.; Tsai, L. H.; Holson, E. B., *Chem. Sci.* 2014, 6, 1, 804.

CHAPTER 3

SYNTHESIS AND ANTICANCER ACTIVITY EVALUATION OF MELANOMA-TARGETED HDACI

3.1. Introduction

Melanoma is one of the most prevalent cancers among skin malignancies.[1] As with most cancer types caused by disruption in the homeostatic regulation of cellular processes, melanomas are typified by dysregulation of melanin-producing melanocytes by keratinocytes in the skin epidermis.[2] This dysregulation results in uncontrolled proliferation of melanocytes, hence the high melanin content associated with most melanoma cases. When detected early, melanoma can be corrected by surgery. Therefore, sustained efforts have been on developing effective new tools for early diagnosis of melanoma.

Over the past two decades, benzamides (Figure 3.1A) have emerged as promising class of compounds that can be developed into theranostics for early detection and treatment of melanomas.[3] What makes this class of compounds suitable for this purpose is their high affinity for melanin, which affords them a high residence time in melanoma cells. In phase II clinical trial, *N*-(2-(diethylamino)ethyl)-4-iodobenzamide (Figure 3.1A) showed 100% specificity on a lesion-site basis with little toxicity to the patients.[3a] When incorporated into the structure of a conventional alkylating agent, the resulting alkylating benzamides showed superior selectivity for melanoma cells both *in vitro* and *in vivo*.[4] Moreover, several studies have demonstrated the

suitability of the benzamide template for developing targeted proteasome degradation inhibitors[5]. Hence, benzamides have become "the Holy Grail" for developing melanoma-targeted therapeutics.

Epigenetic dysregulation, exemplified by aberrant regulation of expression of histone deacetylases (HDAC) and histone acetyl transferase (HAT), is one of the root causes of cancer. Several isoforms of HDAC have been implicated in the sustained proliferation of most tumors, with class I and class IIb HDACs being the most prominent.[6] With respect to melanomas, HDAC isoforms 5 and 6 were recently reported to play significant roles in melanoma progression.[7] To further exploit the relevance of HDAC 6 in melanoma progression, Kozikowski *et. al.*[8] made HDAC 6 selective HDAC inhibitors (HDACi) and studied their effects on melanoma cell growth. Though a promising approach, their compounds showed weak cytotoxic effects on B16F10 melanoma cell line.

The structures of the five clinically approved HDACi (Figure 3.1B) conform to a structural model comprising a surface recognition group, linker and a zinc binding group (ZBG) as shown for SAHA in Figure 3.1C. Previous SAR studies on the surface recognition group have identified this part of most HDACi to be the most amenable to modification.[9]

To further demonstrate the broad scope of application of the benzamide template for developing targeted therapies, we designed and synthesized HDACi which have melanin binding benzamide group incorporated unto the surface recognition group (Figure 3.2A and B). We envisaged that this approach will result in selective localization of benzamide-based HDACi within the melanoma cells, and mitigate the off-target toxicities associated with most clinically approved HDACi. Following our previous reports,[9a] we restricted linker lengths in our design to be between 5-7 methylenes separating the hydroxamate (ZBG) from the cap group.

A.

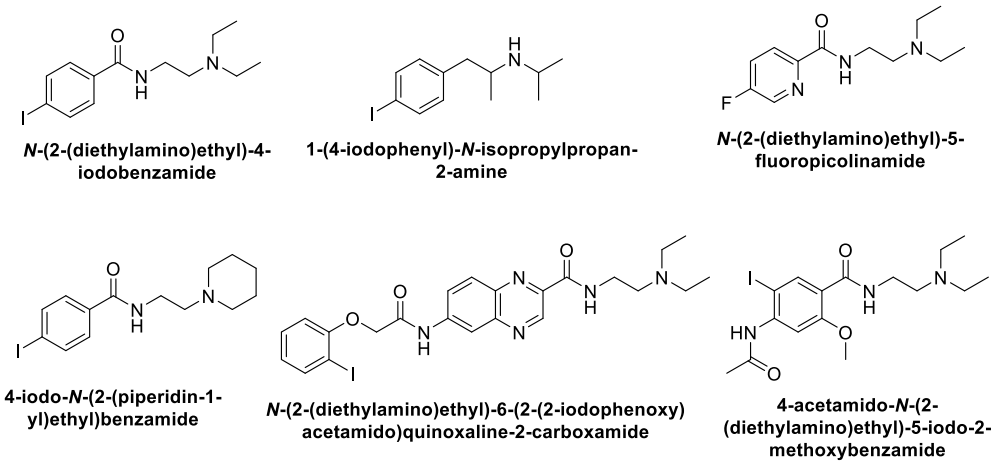

B.

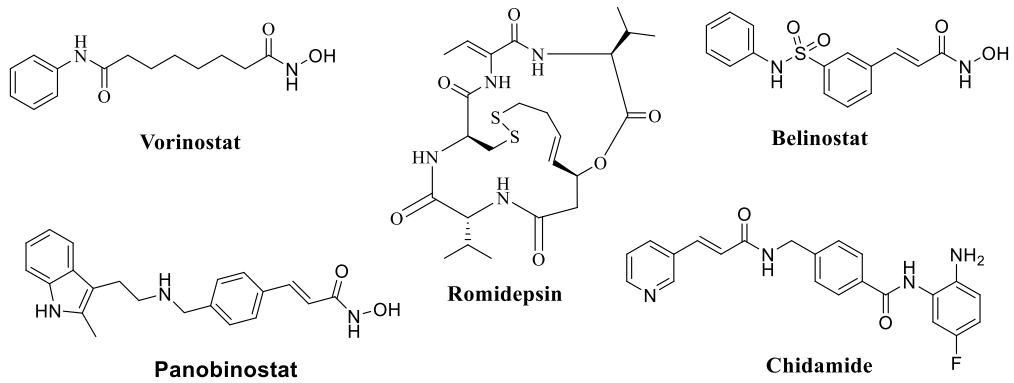

C.

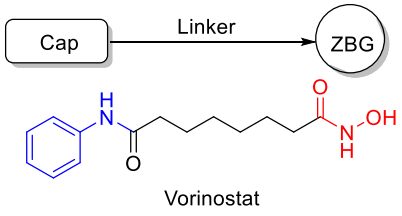

Figure 3.1: **A**) structures of some selected benzamides for imaging tumors[3b, 3c, 11]; **B**) structures of clinically approved HDACi; C) standard HDACi pharmacophoric model.

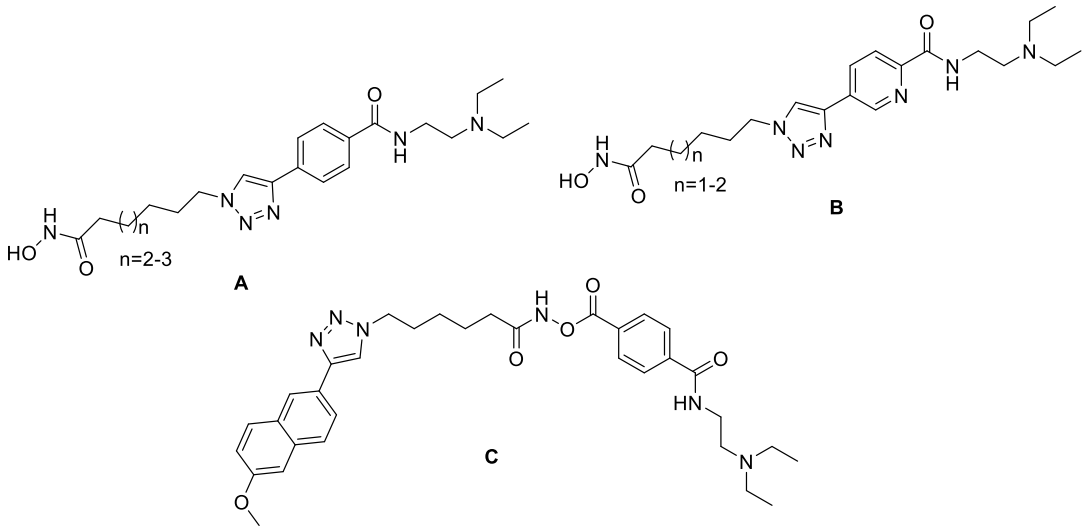

Figure 3.2: General structures of designed compounds.

3.2. Chemistry

Synthesis of target compounds started with the esterification of 4-iodobenzoic acid **1** and 5-bromopyridine-2-carboxylic acid **2**, both of which are commercially, using TMSCl in MeOH to give methyl esters **3** and **4** (Scheme 3.1). Sonogashira coupling[12] of the respective halo-methyl ester (compound **3** or **4**) with TMS-acetylene gave the appropriate TMS-protected ethynyl intermediates **5** and **6**. At this stage, different synthetic pathways were employed to access alkynes **8** and **9**. Subjecting TMS-protected methyl-4-(ethynyl)-benzoate **5** to alkaline hydrolysis, using KOH in isopropanol, resulted in TMS removal and gave the potassium salt of 4-(ethynyl) benzoate **7**. Coupling of **7** to *N*,*N*-diethyl ethane-1,2-diamine using TSTU[3c] afforded compound **8**. In the case of compound **9**, TMS-protected methyl-5-ethynyl picolinate **6** was refluxed with *N*,*N*-diethyl ethane-1,2-diamine in MeOH to give compound **9**. Cu (I) catalyzed cycloaddition reaction[13]

between alkyne **8** or **9** and *O*-trityl protected azido hydroxamates with appropriate linker lengths, followed by trityl deprotection using TFA, gave the target compounds **10a-b** and **11a-b**.

Scheme 3.1: Synthesis of BZA-HDACi

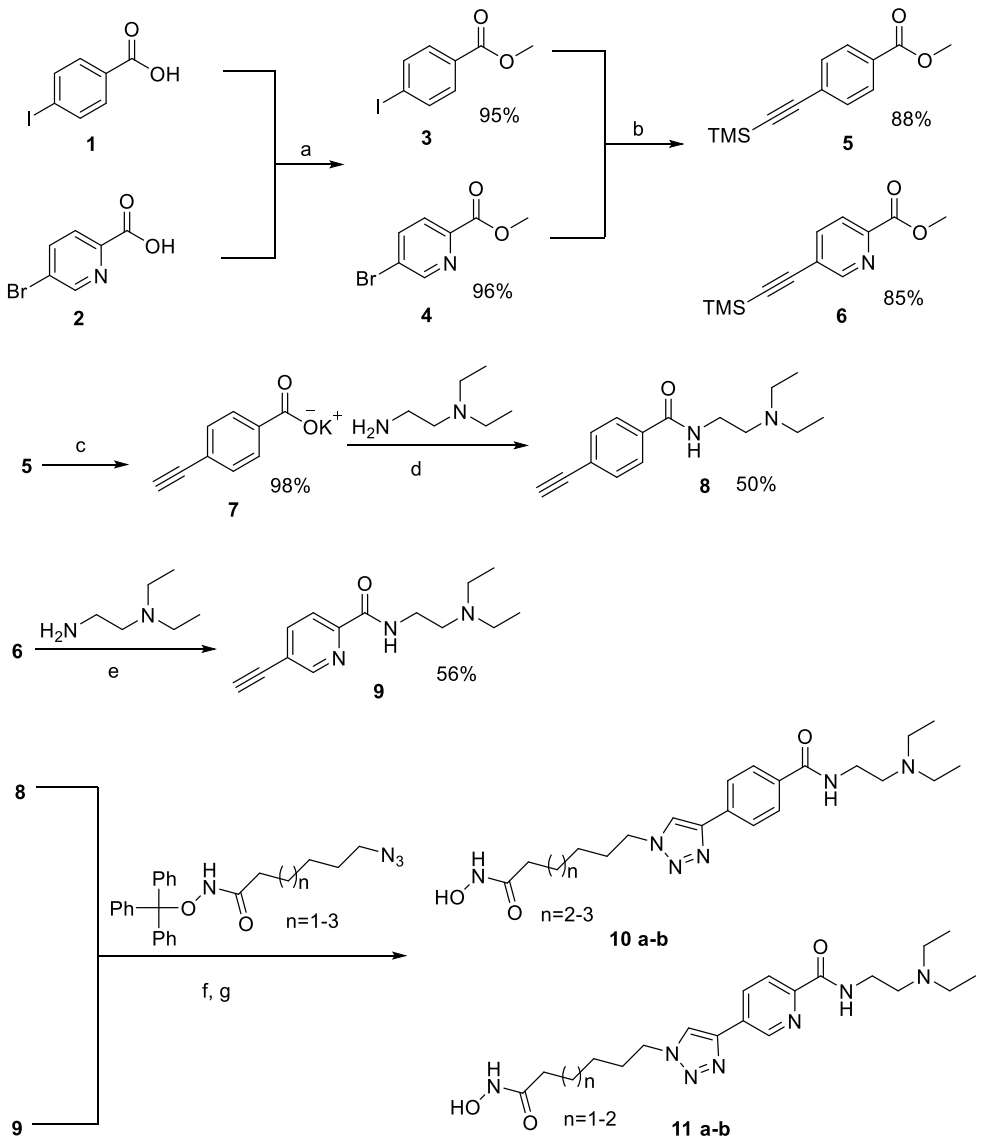

a) TMSCl,MeOH, rt; b) TMS acetylene, $Pd(PPh_3)_2Cl_2$, CuI, TEA, CH_3CN, 90 ^{0}C, overnight; c) KOH, isopropanol, rt, overnight; d) TSTU, DIPEA,DCM, rt; e) MeOH, 120 ^{0}C; f) CuI, DIPEA,THF, rt; g) TFA/TIPS

3.3. HDAC isoform inhibition

Considering the previously reported roles of HDAC6 in sustaining melanoma growth[7-8] and the absolute requirement of HDAC1 inhibition for HDACi to elicit robust antiproliferative effects of HDACi,[8] we profiled compounds **10a-b** and **11a-b** against HDAC1 and HDAC6 in a cell-free assay. All the compounds showed strong inhibitory activities towards the two HDAC isoforms tested, with compound **10a** being ten-fold more potent towards HDAC 1 compared to SAHA (Table 3.1). We observed these compounds to be more potent towards HDAC1 compared to HDAC6, suggesting that they may possess potent *in vitro* anticancer activities. The most potent compound in this series, compound **10a**, showed about four-fold selectivity for HDAC 1 compared to HDAC 6. While the weakest in the series, compound **11a**, is almost indistinguishable in terms of inhibitory activity towards HDAC 1 and HDAC 6. Compounds **10b** and **11b**, despite having seven- and six methylenes, respectively, as linkers are both equipotent towards HDAC 1 and HDAC 6.

Interestingly, the benzyl-based compound with six methylenes as linker, **10a**, is more potent than the analogous pyridyl-based compound, **11b**, in both HDAC1 and HDAC6. This observation is similar to a previous study in our lab in which HDAC inhibitory activities of benzyl-based HDACi and their analogous pyridyl-based HDACi were compared.[14] Likewise, linker-length effects, similar to previous observations,[14-15] was noticeable in the two series of compound.

3.4. Growth inhibition study

Encouraged by the potent cell-free HDAC inhibitory activities of these benzamide-based HDACi, we assayed their growth inhibitory effects on two melanin-producing melanoma cell lines, B16F10 and A375. We were surprised to observe that none of compounds **10a-b** and **11a-b** showed inhibitory effects on the growth of B16F10 and A375 cells at the maximum concentration

Table 3.1: HDAC isoforms inhibition study

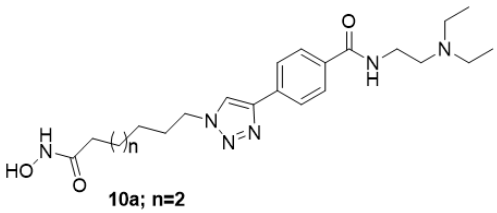

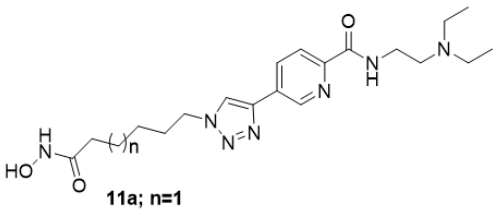

Compound	n	IC_{50} (μM) *	
		HDAC1	HDAC6
10a	2	0.0038	0.016
10b	3	0.012	0.027
11a	1	0.100	0.170
11b	2	0.017	0.034
SAHA	-	0.031	0.011

*values indicate average of three independent experiments

tested (20 μM) (Table 3.2). Previously, the intricate drug efflux system in melanoma, involving melanosomal sequestration and subsequent efflux of cytotoxic agents, was identified to be responsible for resistance of melanoma to chemotherapeutic agents.[10, 16] It is quite possible that our observation is a reflection of this phenomenon. However, it is also possible that melanin

binding might not provide the anticipated advantage. Melanin, being a non-protein polymer,[17] might be unable to release the benzamide-based HDACi upon binding, resulting in their inability to engage HDACs, the therapeutic targets. Furthermore, the observed weak antiproliferative activity might just be a result of the inability of the tested compounds to penetrate the cell membrane.

Intrigued by this observation and determined to unravel the basis for the weak in cellulo activities of these compounds, we extended cell growth inhibition study to LNCaP, an androgen dependent prostate cancer cell line not known to produce melanin. Results obtained from this study should provide insights into the role (s) of melanin in the observed cellular inactivity, and also confirm the ability of these compounds to cross the cell membrane.

As seen in Table 3.2, all of the tested compounds inhibited the growth of LNCaP in a pattern similar to the HDAC inhibitory activity, confirming that these compounds can cross the cell membrane easily. This makes it highly probable that melanin binding or effective drug efflux is impeding access to HDAC enzymes.

Table 3.2: Antiproliferation study in cancer cell lines.

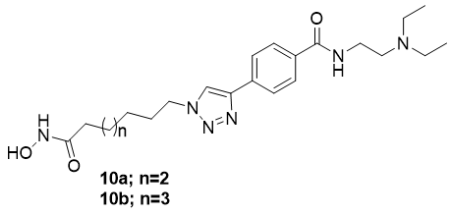

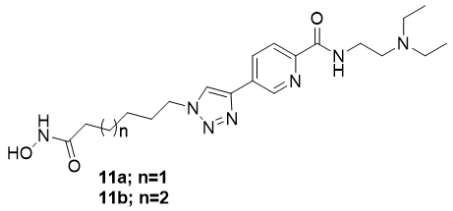

Compound	n	IC_{50} (μM) *		
		B16F10	**A375**	**LNCaP**
10a	2	34.16	23.60	1.2
10b	3	75.91	>100	3.0
11a	1	>100	>100	10.5
11b	2	55.67	47.18	1.5
SAHA	-	13.1	4.1	1.8

*values indicate average of three independent experiments

3.5. Prodrug approach

We then considered exploiting benzamides' affinity for melanin in a slightly different way. For this, a prodrug approach in which the melanin binding benzamide is attached to a hydroxamate-based HDACi, via a labile ester bond that could provide a means of selective delivery of such HDACi to melanoma, was considered. When such compound binds to melanin in melanoma cells, the HDACi component could then be released by hydrolysis, facilitated by cellular esterase. This approach has been successfully used in the past to improve the cellular accessibility of

hydroxamate-based HDACi (Figure 3.3).[18] In addition to this, such a design could mask potential off target interaction of the hydroxamate group with other biological targets in the cells.

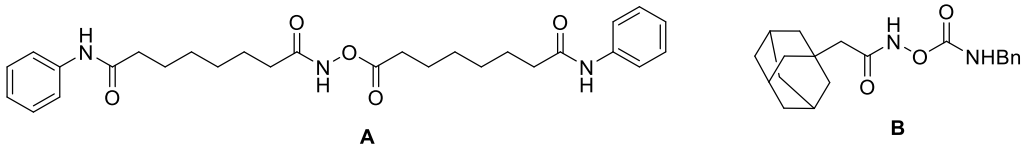

Figure 3.3: Structures of representative hydroxamate-based prodrugs.

Previous work from our lab has identified triazolyl hydroxamate **7u** (scheme 3.2) as a promising HDACi with robust growth inhibitory activity in prostate cancer cell line[14]. Encouraged by this, we incorporated compound **7u** into the design of a releasable benzamide-HDACi prodrug (Figure 3.4).

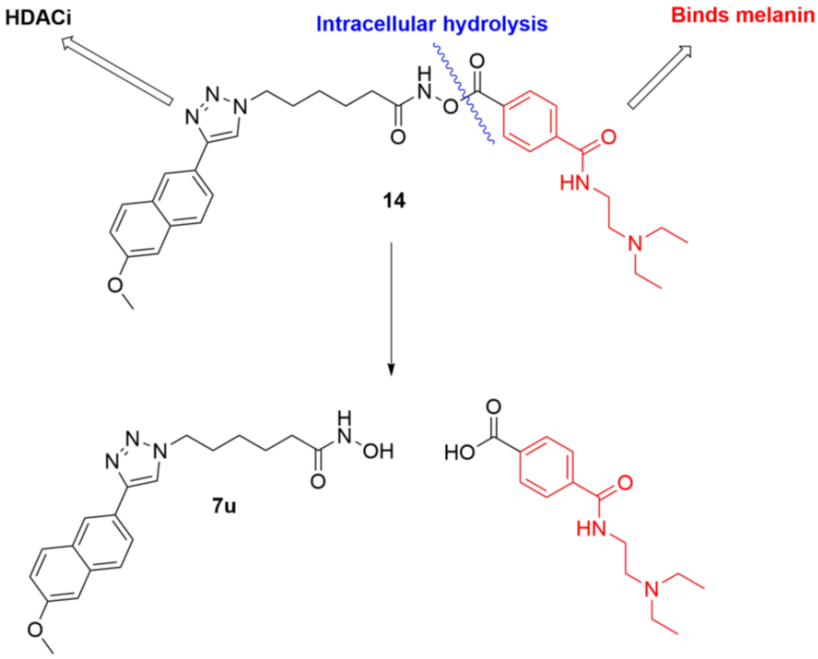

Figure 3.4: Proposed prodrug release mechanism

Potassium 4-((2-(diethylamino) ethyl) carbamoyl) benzoate (**13)** used in the synthesis of prodrug was made as according to Scheme 3.2 (synthesis was previously described in ref. 5c). Coupling of compound **13** to **7u** using TSTU gave the desired prodrug **14**.

Scheme 3.2: Synthesis of releasable BZA-based HDACi

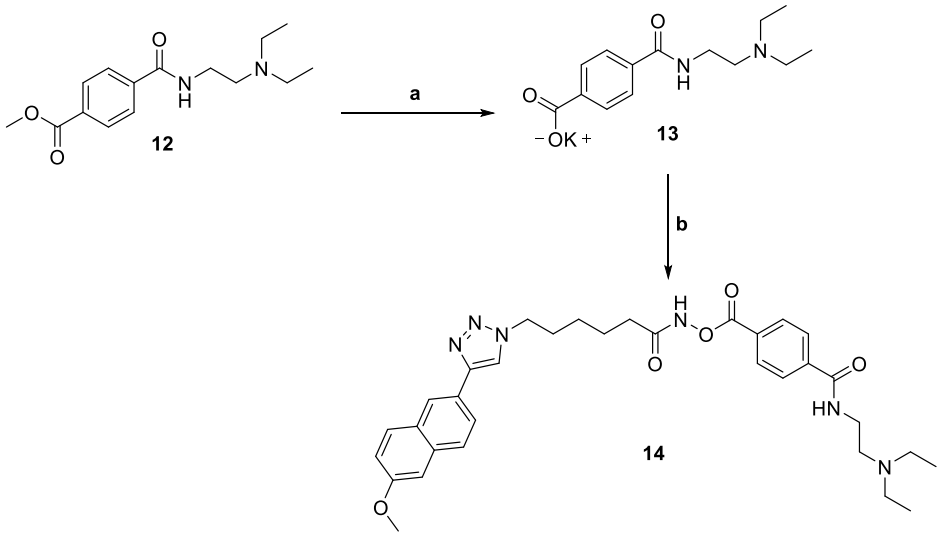

a) KOH, MeOH, rt, overnight; b) Compound **7u**, TSTU, DIPEA, THF/DMF, rt, overnight.

While we do not anticipate any appreciable inhibition of HDAC (because the ZBG is masked), compound **14**, when profiled against HDAC isoforms 1, 6 and 8 at 5 μM, showed 100 percent inhibition against HDAC1, 99 percent inhibition against HDAC6, and 52 percent inhibition against HDAC8. The inhibitory activity shown could be due to hydrolysis of this compound in the HDAC assay buffer leading to the release of compound **7u**, which is a very potent HDACi. A similar observation was reported for some of the compounds by Miller *et al.* in their

patent describing prodrugs of SAHA-like molecules,[18b] though no explanation was given for the observed potency in HDAC assay.

Compounds **7u** and **14** were tested in melanoma cell lines, A375 and B16F10, as shown in Table 3.3. In B16F10, the prodrug **14**, was slightly more potent than compound **10a** and about half as potent as compound **7u.** Similarly, compound **10a** is about half as potent as compound **7u** and equipotent to prodrug **14** in A375 cell line. Interestingly, prodrug **14** showed the same level of potency at 25 μM compared to compound **10a**. The advantage to having the prodrug becomes more obvious at 50 μM, where prodrug **14** becomes more potent than compound **10a** (Figure 3.5). This implies that there may be an advantage to using the benzamide template to design prodrugs rather than having it "permanently" incorporated into the design of compounds targeted towards melanin-producing melanoma cells.

Table 3.3: Anti-proliferation study of prodrug in cancer cell lines.

Compound	**IC_{50} (μM) ***		
	B16F10	**A375**	**LNCaP**
14	27.75	25.95	6.46
7u	10.50	12.61	5.10
10a	34.16	23.60	1.20
SAHA	13.44	4.31	1.80

*values indicate average of three independent experiments

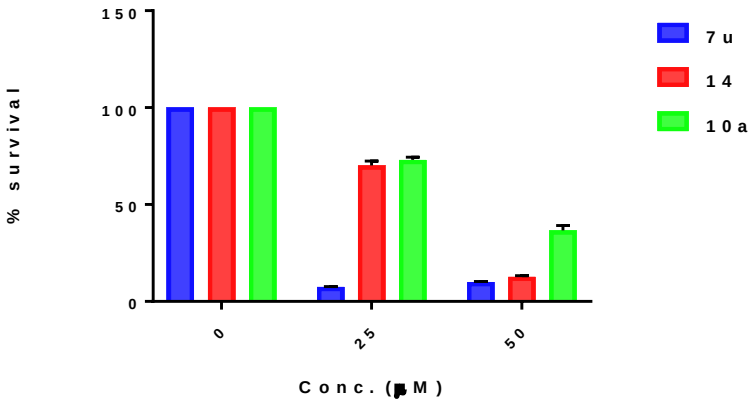

Figure 3.5: Comparison of growth inhibitory effects of prodrug **14** and compound **10a** in B16F10 cell line.

3.6. Cellular target engagement

To gain further insight into the cellular accessibility of the synthesized compounds, and confirm that prodrug **14** releases compound **7u** upon getting into the cells, we used western blot to probe for accumulation of acetyl tubulin upon treating B16F10 cells with compounds **10a**, **7u**, **14**, and SAHA. Accumulation of acetyl tubulin in the cytoplasm is a marker of HDAC 6 inhibition in cells.[19] SAHA and compound **7u** as expected showed significant accumulation of acetyl tubulin at 20 μM (Figure 3.6). Likewise, compound **10a** gave a similar effect at increasing drug concentrations (5-50 μM). Prodrug **14** increasingly shows increase in the level of acetyl tubulin that becomes very significant at 50 μM. This implies that the prodrug is actually releasing compound **17u** once it gets into the cells, validating our prodrug design hypothesis.

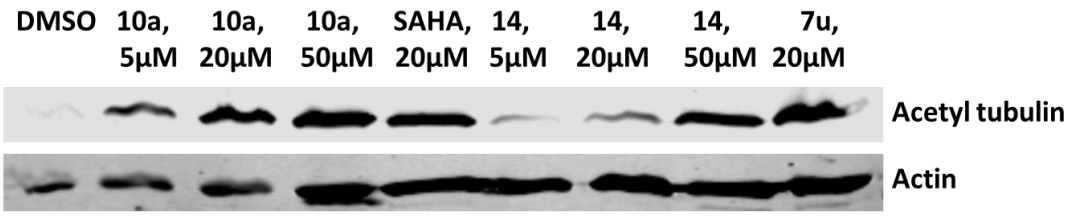

Figure 3.6: Western blot analysis showing acetyl tubulin accumulation

3.7. Conclusion

In conclusion, we have reported a series of HDACi designed to selectively target melanoma cells. Although our compounds have potent HDAC inhibitory activities, they only showed modest cell growth inhibitory activity in melanoma cell lines. Against HDAC 1 and HDAC 6, compounds **10a-b** and **11a-b** showed enzyme inhibitory activities that are largely dependent on the nature of the cap group and the linker length. Preliminary evaluation of the growth inhibitory effects of these compounds on two melanin-rich melanoma cell lines, B16F10 and A375, showed them to have modest effect on the proliferation of these cell lines. An observation that may be attributed to the inability of benzamide-HDACi to engage their HDAC targets after being bound to melanin, and/or the very effective efflux of cytotoxic agents commonly seen with melanoma cells[10]. In androgen-dependent prostate cancer cell line (LNCaP), however, all the compounds showed anticancer activities consistent with their strong HDAC enzyme inhibitory effects.

Effort to adopt a prodrug strategy using the benzamide template to selectively deliver a potent HDACi to melanoma cell lines showed some promise, though the anticipated enhanced cytotoxicity towards melanoma cells was not achieved. While the reason for the low cellular

potency is not readily obvious, the benzamide template should be further explored to develop and/or deliver more potent HDACi to melanoma cells.

3.8. Materials and methods

All commercially available starting materials were used without further purification. Indomethacin was purchased from TCI America (OR, USA). Reaction solvents were either high performance liquid chromatography (HPLC) grade or American Chemical Society (ACS) grade and used without further purification. Analtech silica gel plates (60 F_{254}) were used for analytical TLC, and Analtech preparative TLC plates (UV 254, 2000 μm) were used for purification. UV light was used to examine the spots. 200-400 mesh silica gel was used in column chromatography. For NMR spectra, Varian-Gemini 400 MHz or Bruker 500 MHz magnetic resonance spectrometer was used. ^{1}H NMR spectra were recorded in parts per million (ppm) relative to the peak of $CDCl_3$, (7.26 ppm), CD_3OD (3.31 ppm), or DMSO-d6 (2.49 ppm). ^{13}C spectra were recorded relative to the central peak of the $CDCl_3$ triplet (77.0 ppm), CD_3OD (49.0 ppm), or the DMSO-d6 septet (39.7 ppm) and were recorded with complete heterodecoupling. Multiplicities are described using the abbreviations: s, singlet; d, doublet, t, triplet; q, quartet; m, multiplet. High-resolution mass spectra were recorded at the Georgia Institute of Technology mass spectrometry facility in Atlanta. HPLC was used to establish the purity of the compounds to be >95%. The HPLC analyses were done on a Beckman Coulter instrument with a Phenomenex RP C-18 column (250 mm × 4.6 mm), using 0.1% TFA in water (solvent A) and 0.1% TFA in acetonitrile (solvent B), starting with 70% B for 5 min, then a gradient decrease of 70−10% of B over 20 min. The flow rate was 1.0 mL/min and

detection was at 280 nm. Compounds **3**, **4**, **12**, **13** and all *O*-trityl protected azido linkers were made according to literature protocols.[5c, 15]

B16F10, A375, and LNCaP cell lines were purchased from ATCC (Manassas, VA). Cell cultures were maintained in an incubator at 37 ^{0}C under a 5% CO_2 atmosphere. Mouse antiacetylated α- tubulin antibody was obtained from Invitrogen (Life Technologies, Grand Island, NY, USA), rabbit antiactin, and rabbit antitubulin α antibodies were purchased from Sigma-Aldrich (St. Louis, MO, USA). Secondary antibodies, goat antirabbit conjugated to IRDye680, and goat antimouse conjugated to IRDye800 were purchased from LI-COR Biosciences (Lincoln, NE, USA). The CellTiter 96 Aqueous One Solution Cell Proliferation assay (MTS) kit was purchased from Promega (Madison, WI, USA).

Methyl 4-iodobenzoate (**3**): 4-Iodo benzoic acid (0.500 g, 2.016 mmol) in MeOH (15 mL) and TMSCl (0.510 mL, 4.032 mmol) was added. The reaction mixture was left to stir at room temperature overnight. Water (50 mL) was added to quench the reaction and extracted three times with DCM (50 mL). Organic layer was combined, dried over Na_2SO_4 and concentrated *in vacuo* to give compound **3** as a white solid (0.508g, 95%). The compound was used for the next step without characterization.

Methyl 5-bromopicolinate (**4**): 5-Bromo picolinic acid (0.200 g, 0.990 mmol) in MeOH (5 mL) and TMSCl (0.500 mL, 3.960 mmol) was added. The reaction mixture was left to stir at room temperature overnight. Water (20 mL) was added to quench the reaction and extracted three times with DCM (50 mL). Organic layer was combined, dried over Na_2SO_4 and concentrated *in vacuo*

to give compound **3** as a white solid (0.205g, 94%) ^{1}H NMR (400 MHz, cdcl3) δ 8.81 (s, 1H), 8.03 – 7.97 (m, 2H), 3.96 (s, 3H).

Methyl 4-((trimethylsilyl) ethynyl) benzoate (**5**): A suspension of p-iodo methylbenzoate (0.300g, 1.141 mmol), TMS-acetylene (0.240ml, 1.711mmol), $Pd(PPh_3)_2Cl_2$ (0.024g, 0.034 mmol) and CuI (0.013g, 0.068 mmol) in a 2:1 mixture of deoxygenated Et_3N (4 ml) and THF (2 ml) in a reaction tube was heated while stirring at 80 ^{0}C overnight. The reaction was filtered through celite and solid residue was washed three times with ether. Filtrate was concentrated and the crude residue purified by column using Hexanes: EtOAc (20:1) to give compound (**5**) as a brown solid (0.263g, 99 %). ^{1}H NMR (400 MHz, cdcl3) δ 7.99 (d, 2H), 7.52 (d, 2H), 7.33 – 7.28 (m, 1H), 3.89 (s, 3H), 0.28 – 0.20 (s, 9H). ^{13}C NMR (101 MHz, cdcl3) δ 166.39, 131.76, 129.65, 129.26, 127.73, 104.01, 97.53, 52.15, -0.26.

Methyl 5-((trimethylsilyl) ethynyl) picolinate (**6**): A suspension of **methyl 5-bromopicolinate** (**4**) (2.650 g, 13.100 mmol), TMS-acetylene (3.700 ml, 26.200 mmol), $Pd(PPh_3)_2Cl_2$ (0.460 g, 0.660 mmol) and CuI (0.250 g, 1.310 mmol) in a acetonitrile (25 ml) in a reaction tube was heated while stirring at 90 ^{0}C overnight. The reaction was filtered through celite and solid residue was washed three times with ether. Filtrate was concentrated and the crude residue purified by column using Hexane: EtOAc (5:2) to give compound (**6**) as a brown solid (2.600 g, 85 %). ^{1}H NMR (400 MHz, cdcl3) δ 8.73 (s, 1H), 8.03 – 7.97 (m, 1H), 7.82 (ddd, J = 8.1, 2.0, 0.9 Hz, 1H), 3.94 (s, 3H), 0.27 (s, 9H). ^{13}C NMR (101 MHz, cdcl3) δ 165.13, 152.28, 145.99, 139.74, 124.26, 123.74, 101.79, 100.50, 52.91, -0.45.

Potassium 4-ethynylbenzoate (7): KOH pellets (2.040 g, 36.300 mmol) were added to a solution of compound **5** (2.600 g, 11.190 mmol) in isopropanol (20 ml) and stirred overnight at room

temperature. Reaction mixture was filtered and solid product allowed to dry to give compound 7 as a light brown solid (2.200 g, 100 %). ^{1}H NMR (400 MHz, meod) δ 7.87 (d, 2H), 7.42 (d, 2H).

***N*-(2-(diethylamino) ethyl)-4-ethynylbenzamide** (**8**): Potassium 4-ethynylbenzoate **(7)** (0.200 g, 1.628 mmol) and TSTU (0.360 g, 1.200 mmol) were dissolved in 10ml DCM and left to stir for five minutes. DIPEA (0.200 ml, 1.200 mmol) and DEED (0.17 ml, 1.200 mmol) were then added to the reactive and left to stir at room temperature overnight. Solvent was evaporated and the crude purified by column using EtOAc: Ether: TEA (2:1:0.1) to give compound **8** as a viscous brown oil (0.200 g, 50%). ^{1}H NMR (400 MHz, cdcl3) δ 7.74 (d, 2H), 7.52 (d, 2H), 7.19 (s, 1H), 3.44 (dd, J = 11.7, 5.3 Hz, 2H), 3.17 (s, 1H), 2.65 – 2.57 (m, 2H), 2.57 – 2.48 (m, 4H), 1.04 – 0.96 (m, 6H). ^{13}C NMR (101 MHz, cdcl3) δ 166.42, 134.48, 131.91, 126.88, 125.10, 82.71, 79.33, 51.28, 46.62, 37.24, 11.58. HRMS (ESI) $[M + H]^+$ calculated for $[C_{15}H_{21}ON_2]^+$ was 245.1648, found 245.1647.

***N*-(2-(diethylamino) ethyl)-5-ethynylpicolinamide** (**9**): DEED (3 ml, 21.800 mmol) was added to a solution of methyl 5-((trimethylsilyl) ethynyl) picolinate (**6**) (2.520 g, 10.900 mmol) in MeOH (25 ml) and heated at 120 ^{0}C overnight. Solvent was evaporated off and the crude product was purified by column using Hexanes: EtOAc: TEA (2:1:1) to give a brown solid (1.380 g, 56 %). ^{1}H NMR (400 MHz, cdcl3) δ 8.59 (dd, J = 2.0, 0.8 Hz, 1H), 8.30 (s, 1H), 8.10 (dt, J = 8.1, 1.8 Hz, 1H), 7.88 – 7.82 (m, 1H), 3.47 (dd, J = 12.0, 6.3 Hz, 2H), 3.31 (s, 1H), 2.64 – 2.57 (t, 2H), 2.53 (q, J = 7.1 Hz, 4H), 1.03 – 0.94 (m, 6H). ^{13}C NMR (101 MHz, cdcl3) δ 163.53, 150.98, 149.18, 140.24, 121.38, 82.40, 79.84, 51.32, 46.85, 37.23, 11.81. HRMS (ESI) $[M + H]^+$ calculated for $[C_{14}\ H_{20}\ O\ N_3]^+$ was 246.1601, found 246.1602.

***N*-(2-(diethylamino) ethyl)-4-(1-(7-(hydroxyamino)-7-oxoheptyl)-*1H*-1, 2, 3-triazol-4-yl) benzamide** (**10a**): *N*-(2-(diethylamino) ethyl)-4-ethynylbenzamide (**8**) (0.070 g, 0.286 mmol),

trityl-protected 7-azidoheptanehydroxamic acid (0.140 g, 0.315 mmol) and DIPEA (0.090 ml, 0.573 mmol) were dissolved in anhydrous THF (10 ml) and purged for 10 minutes at room temperature while stirring. CuI (0.027 g, 0.143 mmol) was then added while purging continued for another 20 minutes, after which the reaction was left to stir overnight. Reaction was concentrated and the crude purified by prep TLC using 10:4:0.1 DCM: Ether: TEA to give *N*-(2-(diethylamino)ethyl)-4-(1-(7-oxo-7-((trityloxy)amino)heptyl)-*1H*-1,2,3-triazol-4-yl)benzamide (0.130 g, 67 %), which was used immediately for the next reaction (trityl deprotection) without characterization.

Removal of trityl group was done by dissolving *N*-(2-(diethylamino)ethyl)-4-(1-(7-oxo-7-((trityloxy)amino)heptyl)-*1H*-1,2,3-triazol-4-yl)benzamide (0.130 g, 0.193 mmol) in anhydrous DCM (10 ml) after which 1.0 ml TFA and 0.5 ml TIPS were added and the reaction was left to stir for 2 hours. Solvent and excess TFA were evaporated off, and 20 ml of anhydrous ether was added to the residue. Due to lack of success with ether precipitation, crude was purified using 10:1 DCM:MeOH to give compound **10a** as a white solid (0.010 g, 12 %). ^{1}H NMR (500 MHz, MeOD) δ 8.46 (s, 1H), 7.95 (t, J = 6.5 Hz, 4H), 4.49 (t, J = 6.5 Hz, 2H), 3.59 (t, J = 6.4 Hz, 2H), 2.86 (d, J = 18.5 Hz, 2H), 2.81 (dd, J = 13.8, 6.8 Hz, 4H), 2.11 (t, J = 6.9 Hz, 2H), 2.00 (s, 2H), 1.65 (s, 2H), 1.38 (d, J = 33.3 Hz, 4H), 1.17 (t, J = 7.0 Hz, 6H). ^{13}C NMR (126 MHz, MeOD) δ 171.56, 168.50, 146.37, 133.69, 133.47, 127.49, 125.18, 121.63, 51.22, 49.94, 36.59, 32.16, 29.56, 29.35, 28.00, 25.69, 24.94, 9.75. HRMS (ESI) $[M + H]^+$ calculated for $[C_{22}\ H_{35}\ O_3\ N_6]^+$ was 431.2765, found 431.2762.

***N*-(2-(diethylamino) ethyl)-4-(1-(8-(hydroxyamino)-8-oxooctyl)-*1H*-1, 2, 3-triazol-4-yl) benzamide** (**10b**): *N*-(2-(diethylamino) ethyl)-4-ethynylbenzamide (**8**) (0.200 g, 0.818 mmol),

trityl-protected 8-azidooctanehydroxamic acid (0.400 g, 0.900 mmol) and DIPEA (0.28 ml, 1.636 mmol) were dissolved in anhydrous THF (10 ml) and purged for 10 minutes at room temperature while stirring. CuI (0.080 g, 0.409 mmol) was then added while purging continued for another 20 minutes, after which the reaction was left to stir overnight. Reaction was concentrated and the crude purified prep TLC using 10:4:0.1 DCM: Ether: TEA to give *N*-(2-(diethylamino)ethyl)-4-(1-(8-oxo-8-((trityloxy)amino)octyl)-*1H*-1,2,3-triazol-4-yl)benzamide (0.170g, 31 %), which was used immediately for the next reaction (trityl deprotection) without characterization.

Removal of trityl group was done by dissolving *N*-(2-(diethylamino)ethyl)-4-(1-(8-oxo-8-((trityloxy)amino)octyl)-*1H*-1,2,3-triazol-4-yl)benzamide (0.170 g, 0.25 mmol) in anhydrous DCM (10 ml) after which 1.0 ml TFA and 0.5 ml TIPS were added and the reaction was left to stir for 2 hours. Solvent and excess TFA were evaporated off, and 20 ml of anhydrous ether was added to the residue. Precipitate obtained was filtered, and the residue washed sequentially with 20 ml anhydrous ether (twice), and 40 ml of 1:1 mixture of anhydrous ether and DCM. The resulting residue was left to dry to give compound **10b** as a white solid (0.070 g, 64 %). ^{1}H NMR (500 MHz, MeOD) δ 8.48 (s, 1H), 7.97 (d, J = 9.1 Hz, 4H), 4.49 (t, J = 7.1 Hz, 2H), 3.80 (t, J = 6.1 Hz, 2H), 3.43 (t, J = 6.1 Hz, 2H), 3.40 – 3.34 (m, 4H), 2.10 (s, 2H), 2.02 – 1.94 (m, 2H), 1.66 – 1.57 (m, 2H), 1.44 – 1.31 (m, 12H). ^{13}C NMR (126 MHz, MeOD) δ 177.23, 169.39, 146.22, 134.20, 132.50, 127.84, 125.24, 121.75, 51.60, 50.12, 35.06, 29.74, 28.45, 28.23, 25.87, 25.14, 7.76. HRMS (ESI) $[M + H]^+$ calculated for $[C_{23}\ H_{37}\ O_3\ N_6]^+$ was 445.2922, found 445.2918.

***N*-(2-(diethylamino) ethyl)-5-(1-(6-(hydroxyamino)-6-oxohexyl)-*1H*-1, 2, 3-triazol-4-yl) picolinamide** (**11a**): *N*-(2-(diethylamino) ethyl)-5-ethynylpicolinamide (**9**) (0.100 g, 0.408 mmol), trityl-protected 6-azidohexanehydroxamic acid (0.190 g, 0.448 mmol) and DIPEA (0.150 ml,

0.815 mmol) were dissolved in anhydrous THF (10 ml) and purged for 10 minutes at room temperature while stirring. CuI (0.040 g, 0.204 mmol) was then added while purging continued for another 20 minutes, after which the reaction was left to stir overnight. Reaction was concentrated and the crude purified by prep TLC using 10:4:0.1 DCM: Ether: TEA to give *N*-(2-(diethylamino)ethyl)-5-(1-(6-oxo-6-((trityloxy)amino)hexyl)-*1H*-1,2,3-triazol-4-yl)picolinamide (0.190 g, 71 %), which was used immediately for the next reaction (trityl deprotection) without characterization.

Removal of trityl group was done by dissolving *N*-(2-(diethylamino)ethyl)-5-(1-(6-oxo-6-((trityloxy)amino)hexyl)-*1H*-1,2,3-triazol-4-yl)picolinamide (0.110 g, 0.167 mmol)in anhydrous DCM (10 mL) after which 1.0 ml TFA and 0.5 ml TIPS were added and the reaction was left to stir for 2 hours. Solvent and excess TFA were evaporated off, and 20 ml of anhydrous ether was added to the residue. Due to lack of success with ether precipitation, crude was purified using 10:1 DCM: MeOH to give compound **11a** as a white solid (0.010 g, 14 %). ^{1}H NMR (500 MHz, MeOD) δ 9.16 (s, 1H), 8.63 (s, 1H), 8.43 (d, 1H), 8.20 (d, 1H), 4.53 (t, *J* = 7.0 Hz, 2H), 3.83 (t, *J* = 6.2 Hz, 2H), 3.51 (q, *J* = 7.3 Hz, 2H), 3.42 – 3.37 (m, 2H), 3.31 (t, *J* = 7.3 Hz, 4H), 2.14 (t, *J* = 7.3 Hz, 2H), 2.06 – 1.98 (m, 2H), 1.72 (dt, *J* = 15.1, 7.4 Hz, 2H), 1.39 (dt, *J* = 7.2, 3.4 Hz, 6H). ^{13}C NMR (126 MHz, MeOD) δ 171.22, 166.25, 148.30, 145.48, 143.54, 133.72, 129.67, 122.42, 122.17, 52.20, 51.19, 49.99, 34.59, 32.03, 29.44, 25.47, 24.58, 7.95. HRMS (ESI) $[M + H]^+$ calculated for $[C_{20}\ H_{32}\ O_3\ N_7]^+$ was 418.2561, found 418.2558.

***N*-(2-(diethylamino) ethyl)-5-(1-(7-(hydroxyamino)-7-oxoheptyl)-1H-1, 2, 3-triazol-4-yl) picolinamide** (**11b**)

N-(2-(diethylamino) ethyl)-5-ethynylpicolinamide (**9**) (0.100 g, 0.408 mmol), trityl-protected 7-azidoheptanehydroxamic acid (0.190 g, 0.448 mmol) and DIPEA (0.150 mL, 0.815 mmol) were dissolved in anhydrous THF (10 mL) and purged for 10 minutes at room temperature while stirring. CuI (0.040 g, 0.204 mmol) was then added while purging continued for another 20 minutes, after which the reaction was left to stir overnight. Reaction was concentrated and the crude purified by prep TLC using 10:4:0.1 DCM: Ether: TEA to give *N*-(2-(diethylamino)ethyl)-5-(1-(7-oxo-7-((trityloxy)amino)heptyl)-1H-1,2,3-triazol-4-yl)picolinamide (0.194 g, 71 %), which was used immediately for the next reaction (trityl deprotection) without characterization.

Removal of trityl group was done by dissolving *N*-(2-(diethylamino)ethyl)-5-(1-(7-oxo-7-((trityloxy)amino)heptyl)-1H-1,2,3-triazol-4-yl)picolinamide (0.194g, 0.288 mmol) in anhydrous DCM (10 mL) after which 1.0 mL TFA and 0.5 mL TIPS were added and the reaction was left to stir for 2 hours. Solvent and excess TFA were evaporated off, and 20 mL of anhydrous ether was added to the residue. Due to lack of success with ether precipitation, crude was purified using 10:1 DCM: MeOH to give compound **11b** as a white solid (0.015g, 12 %). ^{1}H NMR (500 MHz, MeOD) δ 9.13 (d, J = 1.5 Hz, 1H), 8.59 (s, 1H), 8.38 (dd, J = 8.1, 2.0 Hz, 1H), 8.17 (d, J = 8.1 Hz, 1H), 4.51 (t, J = 7.1 Hz, 2H), 3.57 (t, J = 6.9 Hz, 2H), 2.75 (t, J = 6.9 Hz, 2H), 2.67 (q, J = 7.2 Hz, 4H), 2.09 (t, J = 7.4 Hz, 2H), 2.03 – 1.96 (m, 2H), 1.68 – 1.57 (m, 2H), 1.44 – 1.35 (m, 4H), 1.12 (t, J = 7.2 Hz, 6H). ^{13}C NMR (126 MHz, MeOD) δ 178.94, 164.99, 148.88, 145.41, 143.64, 133.63, 129.29, 122.25, 121.84, 51.17, 50.13, 36.58, 32.38, 29.67, 29.39, 28.07, 25.72, 25.33, 22.83, 10.38. HRMS (ESI) $[M + H]^+$ calculated for $[C_{21} H_{34} O_3 N_7]^+$ was 432.2718, found 432.2712.

***N*-(2-(diethylamino) ethyl)-4-(((6-(4-(6-methoxynaphthalen-2-yl)-1H-1, 2, 3-triazol-1-yl) hexanamido) oxy) carbonyl) benzamide** (**15**): Compound (**14**) (0.050 g, 0.166 mmol) and TSTU (0.050 g, 0.166 mmol) were dissolved and left to stir at room temperature for 30 min. Afterwards compound **7u** (0.058 g, 0.166 mmol) dissolved in 1ml DMF containing DIPEA (0.03 ml, 0.166 mmol) was added to the reaction and left to stir overnight. Solvent was evaporated off and the crude purified by prep. TLC using 10:1 DCM: MeOH as an off white waxy solid (0.040 g, 40 %). ^{1}H NMR (500 MHz, DMSO) δ 8.80 (s, 1H), 8.67 – 8.61 (m, 1H), 8.32 (s, 1H), 8.11 – 8.02 (m, 2H), 8.02 – 7.96 (m, 2H), 7.92 (dt, J = 13.4, 4.7 Hz, 1H), 7.87 (d, J = 9.2 Hz, 1H), 7.34 (d, J = 2.5 Hz, 1H), 7.21 – 7.15 (m, 1H), 4.44 (dd, J = 14.7, 7.7 Hz, 2H), 3.89 (d, J = 4.3 Hz, 3H), 3.00 (d, J = 6.9 Hz, 2H), 2.75 (d, J = 6.4 Hz, 6H), 2.24 (t, J = 7.2 Hz, 1H), 1.65 (dt, J = 14.8, 7.3 Hz, 2H), 1.37 (dt, J = 21.7, 10.8 Hz, 2H), 1.19 – 1.14 (m, 2H), 1.04 (dt, J = 20.3, 6.5 Hz, 6H). ^{13}C NMR (126 MHz, DMSO) δ 186.16, 173.19, 170.41, 165.63, 157.82, 146.92, 134.33, 129.96, 129.56, 128.99, 128.33, 128.05, 127.74, 126.61, 124.60, 123.82, 121.64, 119.63, 106.50, 70.30, 55.61, 49.70, 47.41, 46.06, 32.19, 29.58, 25.70, 24.43, 11.30. HRMS (ESI) $[M + H]^+$ calculated for $[C_{33} H_{41} O_5 N_6]^+$ was 601.3133, found 601.3118.

3.8.1. Cell viability assay

All cell lines used in this study (B16F10, A375 LNCaP and Vero) were maintained in the respective media recommended by ATCC. All the culture media used were supplemented with 10 % fetal bovine serum (FBS) (Atlanta Biologicals, Atlanta, GA) and 1 % *Pen. Strep*. Prior to treatment with various drug concentrations and subsequent incubation for 72 hours, cells were incubated in a 96 well plate for 24 hours. Cell viability was measured using the MTS assay protocol

as described by the manufacturer. For all drugs tested, DMSO concentration was maintained at 0.1 % for experiments in LNCaP and at 1 % for experiments in other cell lines. Data was analyzed using GRAPHPAD prism software.

3.8.2. Western blots analysis

B16F10 cells (10^6 cells/dish) were seeded in petri dishes 24 hour prior to treatment with various concentrations of compounds for 24h. Thereafter, media was removed and cells were washed with chilled 1X PBS buffer and resuspended in CelLyticM buffer containing a cocktail of protease inhibitor (Sigma-Aldrich, St. Louis, MO, USA). Protein concentration was determined through Bradford protein assay. Equal amount of protein was then loaded onto an SDS-page gel (Bio-Rad, Hercules, CA, USA) and resolved by electrophoresis at a constant voltage of 100 V for 2 h. The gel was transfered onto a nitrocellulose membrane and probed for acetylated tubulin, acetyl H4, and actin as loading control.

3.8.3. HDAC inhibition

HDAC inhibition study was done under contractual agreement by BPS Bioscience.

3.9. References

1. Siegel, R. L.; Miller, K. D.; Jemal, A., Cancer statistics, 2015. *CA Cancer J. Clin.* **2015,** *65* (1), 5-29.

2. (a) Gray-Schopfer, V.; Wellbrock, C.; Marais, R., Melanoma biology and new targeted therapy. *Nature* **2007,** *445* (7130), 851-857; (b) Haass, N. K.; Smalley, K. S.; Herlyn, M., The role of altered cell-cell communication in melanoma progression. *J Mol Histol* **2004,** *35* (3), 309-18.

3. (a) Michelot, J. M.; Moreau, M. F. C.; Veyre, A. J.; Bonafous, J. F.; Bacin, F. J.; Madelmont, J. C.; Bussiere, F.; Souteyrand, P. A.; Mauclaire, L. P.; Chossat, F. M.; Papon, J. M.; Labarre, P. G.; Kauffmann, P.; Plagne, R. J., Phase II Scintigraphic Clinical Trial of Malignant Melanoma and Metastases with Iodine-123-N-(2-Diethylaminoethyl 4-Iodobenzamide). *J. Nucl. Med.* **1993,** *34* (8), 1260-1266; (b) Oltmanns, D.; Eisenhut, M.; Mier, W.; Haberkorn, U., Benzamides as Melanotropic Carriers for Radioisotopes, Metals, Cytotoxic Agents and as Enzyme Inhibitors. *Curr. Med. Chem.* **2009,** *16* (17), 2086-2094; (c) Liu, H.; Liu, S.; Miao, Z.; Deng, Z.; Shen, B.; Hong, X.; Cheng, Z., Development of 18F-Labeled Picolinamide Probes for PET Imaging of Malignant Melanoma. *J. Med. Chem.* **2013,** *56* (3), 895-901.

4. Wolf, M.; Bauder-Wüst, U.; Mohammed, A.; Schönsiegel, F.; Mier, W.; Haberkorn, U.; Eisenhut, M., Alkylating benzamides with melanoma cytotoxicity. *Melanoma Res.* **2004,** *14* (5), 353-360.

5. (a) Vivier, M.; Rapp, M.; Galmier, M.-J.; Jarrousse, A.-S.; Miot-Noirault, E.; Leal, F.; Weber, V.; Métin, J.; Sauzière, J.; Chezal, J.-M.; Madelmont, J.-C., New aldehyde and vinylsulfone proteasome inhibitors for targeted melanoma therapy. *Eur. J. Med. Chem.* **2011,** *46* (11), 5705-5710; (b) Vivier, M.; Rapp, M.; Papon, J.; Labarre, P.; Galmier, M.-J.; Sauzière, J.; Madelmont, J.-C., Synthesis, Radiosynthesis, and Biological Evaluation of New Proteasome Inhibitors in a Tumor Targeting Approach. *J. Med. Chem.* **2008,** *51* (4), 1043-1047; (c) Vivier, M.; Jarrousse, A.-S.; Bouchon, B.; Galmier, M.-J.; Auzeloux, P.; Sauzieres, J.; Madelmont, J.-C.,

Preliminary Studies of New Proteasome Inhibitors in the Tumor Targeting Approach: Synthesis and in Vitro Cytotoxicity. *J. Med. Chem.* **2005,** *48* (21), 6731-6740.

6. (a) Weichert, W., HDAC expression and clinical prognosis in human malignancies. *Cancer Lett.* **2009,** *280* (2), 168-176; (b) West, A. C.; Johnstone, R. W., New and emerging HDAC inhibitors for cancer treatment. *J. Clin. Invest.* **2014,** *124* (1), 30-39.

7. Liu, J.; Gu, J.; Feng, Z.; Yang, Y.; Zhu, N.; Lu, W.; Qi, F., Both HDAC5 and HDAC6 are required for the proliferation and metastasis of melanoma cells. *J. Transl. Med.* **2016,** *14* (1), 1-13.

8. Bergman, J. A.; Woan, K.; Perez-Villarroel, P.; Villagra, A.; Sotomayor, E. M.; Kozikowski, A. P., Selective Histone Deacetylase 6 Inhibitors Bearing Substituted Urea Linkers Inhibit Melanoma Cell Growth. *J. Med. Chem.* **2012,** *55* (22), 9891-9899.

9. (a) Oyelere, A. K.; Chen, P. C.; Guerrant, W.; Mwakwari, S. C.; Hood, R.; Zhang, Y.; Fan, Y., Non-Peptide Macrocyclic Histone Deacetylase Inhibitors. *J. Med. Chem.* **2008,** *52* (2), 456-468; (b) De Vreese, R.; Van Steen, N.; Verhaeghe, T.; De Smet, T.; Bougarne, N.; De Bosscher, K.; Benoy, V.; Haeck, W.; Van den Bosch, L.; D'Hooghe, M., Synthesis of benzothiophene-based hydroxamic acids as potent and selective HDAC6 inhibitors. *Chem. Comm.* **2015**; (c) Valente, S.; Trisciuoglio, D.; De Luca, T.; Nebbioso, A.; Labella, D.; Lenoci, A.; Bigogno, C.; Dondio, G.; Miceli, M.; Brosch, G.; Del Bufalo, D.; Altucci, L.; Mai, A., 1,3,4-Oxadiazole-Containing Histone Deacetylase Inhibitors: Anticancer Activities in Cancer Cells. *J. Med. Chem.* **2014**.

10. Chen, K. G.; Valencia, J. C.; Lai, B.; Zhang, G.; Paterson, J. K.; Rouzaud, F.; Berens, W.; Wincovitch, S. M.; Garfield, S. H.; Leapman, R. D.; Hearing, V. J.; Gottesman, M. M., Melanosomal sequestration of cytotoxic drugs contributes to the intractability of malignant melanomas. *PNAS* **2006,** *103* (26), 9903-9907.

11. El Aissi, R.; Liu, J.; Besse, S.; Canitrot, D.; Chavignon, O.; Chezal, J.-M.; Miot-Noirault, E.; Moreau, E., Synthesis and Biological Evaluation of New Quinoxaline Derivatives of ICF01012 as Melanoma-Targeting Probes. *ACS Med. Chem. Lett.* **2014,** *5* (5), 468-473.

12. Sonogashira, K.; Tohda, Y.; Hagihara, N., A convenient synthesis of acetylenes: catalytic substitutions of acetylenic hydrogen with bromoalkenes, iodoarenes and bromopyridines. *Tetrahedron Lett.* **1975,** *16* (50), 4467-4470.

13. (a) Rostovtsev, V. V.; Green, L. G.; Fokin, V. V.; Sharpless, K. B., A Stepwise Huisgen Cycloaddition Process: Copper(I)-Catalyzed Regioselective "Ligation" of Azides and Terminal Alkynes. *Ang. Chem. Int. Ed.* **2002,** *41* (14), 2596-2599; (b) Kislukhin, A. A.; Hong, V. P.; Breitenkamp, K. E.; Finn, M. G., Relative Performance of Alkynes in Copper-Catalyzed Azide–Alkyne Cycloaddition. *Bioconjug. Chem.* **2013,** *24* (4), 684-689.

14. Chen, P. C.; Patil, V.; Guerrant, W.; Green, P.; Oyelere, A. K., Synthesis and structure–activity relationship of histone deacetylase (HDAC) inhibitors with triazole-linked cap group. *Bioorg. Med. Chem.* **2008,** *16* (9), 4839-4853.

15. Mwakwari, S. C.; Guerrant, W.; Patil, V.; Khan, S. I.; Tekwani, B. L.; Gurard-Levin, Z. A.; Mrksich, M.; Oyelere, A. K., Non-Peptide Macrocyclic Histone Deacetylase Inhibitors Derived from Tricyclic Ketolide Skeleton. *J. Med. Chem.* **2010,** *53* (16), 6100-6111.

16. Huang, Y.-Y.; Vecchio, D.; Avci, P.; Yin, R.; Garcia-Diaz, M.; Hamblin, M. R., Melanoma resistance to photodynamic therapy: new insights. *Biol. Chem.* **2013,** *394* (2), 239-250.

17. Sarangarajan, R.; Apte, S. P., The polymerization of melanin: a poorly understood phenomenon with egregious biological implications. *Melanoma Res.* **2006,** *16* (1), 3-10.

18. (a) Šilhár, P.; Eubanks, L. M.; Seki, H.; Pellett, S.; Javor, S.; Tepp, W. H.; Johnson, E. A.; Janda, K. D., Targeting Botulinum A Cellular Toxicity: A Prodrug Approach. *J. Med. Chem.* **2013,**

56 (20), 7870-7879; (b) Miller, T. A.; Witter, D. J.; Belvedere, S. Preparation of histone deacetylase inhibitor prodrugs useful for the treatment of proliferation of neoplastic cells. WO2005097747A1, 2005.

19. Butler, K. V.; Kalin, J.; Brochier, C.; Vistoli, G.; Langley, B.; Kozikowski, A. P., Rational Design and Simple Chemistry Yield a Superior, Neuroprotective HDAC6 Inhibitor, Tubastatin A. *J. Am. Chem. Soc.* **2010,** *132* (31), 10842-10846.

CHAPTER 4

BIFUNCTIONAL CONJUGATES WITH POTENT INHIBITORY ACTIVITY TOWARDS CYCLOOXYGENASE AND HISTONE DEACETYLASE

4.1. INTRODUCTION

Aberrant epigenetic regulation and inflammation play significant roles in tumor development and progression. Posttranslational acetylation and deacetylation of histones, both epigenetic events regulated by histone acetyl transferases (HAT) and histone deacetylases (HDAC), respectively, control the expression and/or silencing of tumor suppressor genes.[1] While these two epigenetic regulators exist in equilibrium in non-transformed cells, HDAC activity predominates in most malignant tumors, effectively leading to silencing of tumor suppressor genes and uncontrolled proliferation of cancer cells.[2] Eighteen isoforms of HDAC are known, eleven of which depend on zinc for their catalytic activities and are group into: class I (HDACs 1-3 and 8); class II (subdivided into class II A (HDACs 4, 5, 7 and 9) and class IIB (HDACs 6 and 10)); and class IV (HDAC 11).[3] Class III HDACs, also known as sirtuins, are non-zinc dependent and require NAD^+ for their catalytic activity.[3b] The expression profiles of HDAC isoforms in different tumors vary with each isoform playing unique roles in driving tumorigenesis.[4] The therapeutic potential of HDAC inhibition has been validated by the US food and drugs administration's (FDA) approval of HDAC inhibitors (HDACi), vorinostat, romidepsin, belinostat and panabinostat (Figure 4.1) for the treatment of cutaneous T-cell lymphoma, peripheral T-cell lymphoma and multiple myeloma.[5]

Cardiotoxicity, short half-life, and inactivity towards solid tumors are few of many challenges faced by HDACi in the clinic.[3a, 6]

Among the several drivers of inflammation in tumors, the inducible isoform of cyclooxygenases (COX), COX-2, plays a crucial role by ensuring a continuous supply of prostaglandin E2 (PGE_2) to the tumors.[7] The other COX isoform, COX-1, is constitutively expressed in the body where it performs housekeeping functions.[8] In contrast to COX-1, COX-2 expression is short-lived[9] and is upregulated in most tumors to meet up with the requirement for PGE_2 in the rapidly proliferating cells.[7b] Both COX isoforms facilitate the conversion of arachidonic acid to prostaglandin H2, which is in turn transformed to prostaglandins, by specific synthases, as required by the cells.[7b, 10] Several COX inhibitors (Figure 4.2), also known as non-steroidal anti-inflammatory drugs (NSAIDs), have been approved by the FDA for managing inflammation associated with pains and fever.

Due to high expression of COX-2 in most tumors, it has been suggested that NSAIDs could someday find applications in the prevention and/or cure of some cancers, especially colon and prostate cancer.[11] Several mechanisms of cytotoxicity of NSAIDs towards cancer cells have been reported; most are believed to be independent of COX-2 inhibition. In androgen dependent prostate cancer cell line (LNCaP), celecoxib exerts its cytotoxic effect via induction of c-jun[12] and EP2 signaling leading to suppression of androgen receptor (AR)[13]. Induction of apoptosis[14], Wnt/beta-catenin pathway suppression,[15] cell cycle arrest[16] and inhibition of angiogenesis[17] are some of the other mechanisms through which NSAIDs exert their anticancer activity. In addition to being a possible therapeutic target, COX-2 upregulation in tumors has been exploited for tumor imaging through the use of contrast agents containing COX-2-selective NSAIDs.[18]

Recently, there has been enormous interest in the development of dual-acting compounds comprising of an HDACi and another cytotoxic component.[19] In such compounds, one of the components is usually the surface recognition group (cap) of the HDACi (see pharmacophoric model in Figure 4.1). While dual-acting compounds comprising NSAIDs and other agents exist,[20] none contain HDACi and NSAIDs combined as a single component. Moreover, results from *in vitro* studies suggest that enhanced cytotoxic effect could be achieved by combining NSAIDs and HDACi in cancer cell lines.[21] In this study, we designed and synthesized bifunctional compounds with HDAC and COX-2 inhibitory activities. These compounds are capable of harnessing the cytotoxic effects of HDAC inhibition, COX-2 inhibition, and perturbation of other non-COX dependent pathways. Our design has indomethacin or celecoxib as the cap, methylenes as linkers, and hydroxamate as the zinc binding group (ZBG) (Figure 4.4 b-e). These compounds potently inhibited the HDAC isoforms tested and retained COX-2 inhibitory activity comparable to both celecoxib and indomethacin. The potent HDAC and COX-2 inhibitory activities of these conjugates are reflected in their growth inhibitory activities in MCF-7 (breast cancer), A549 (non-small cell lung cancer), HCT-116 (colon cancer), DU-145 (androgen independent prostate cancer) and LNCaP (androgen dependent prostate cancer) cell lines. They are also less toxic towards healthy cell (VERO) compared to vorinostat.

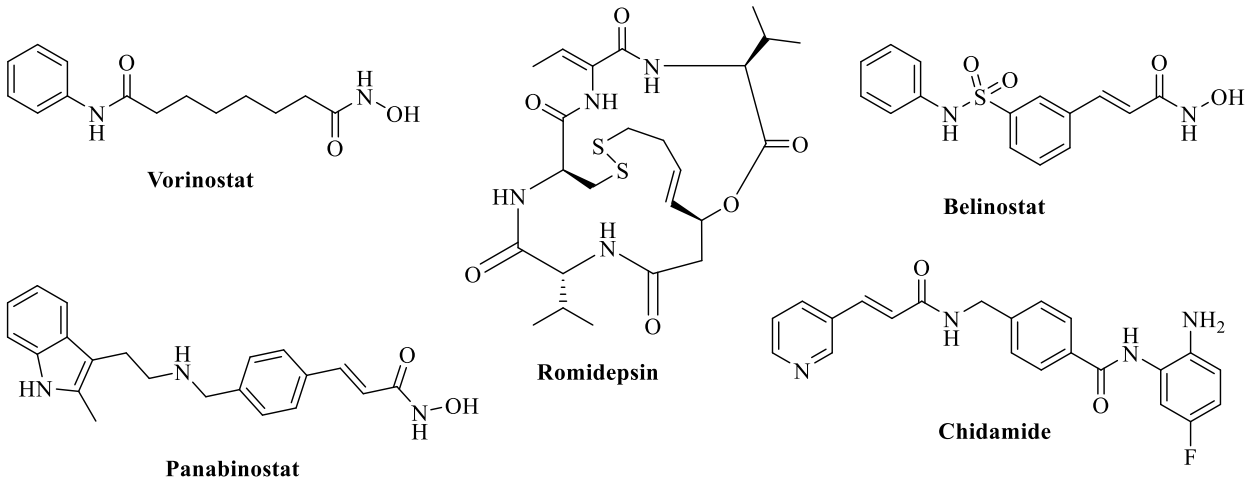

Figure 4.1: HDACi in use in the clinic

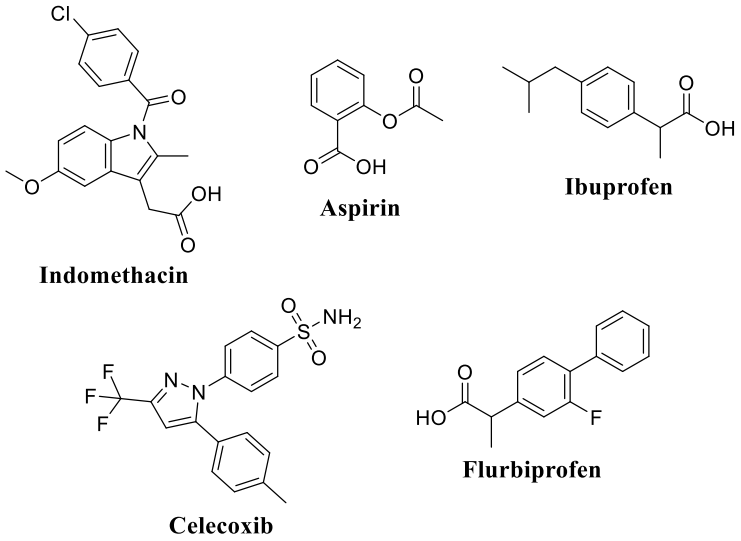

Figure 4.2: Representative examples of US FDA approved NSAIDs

4.2. Results and discussion

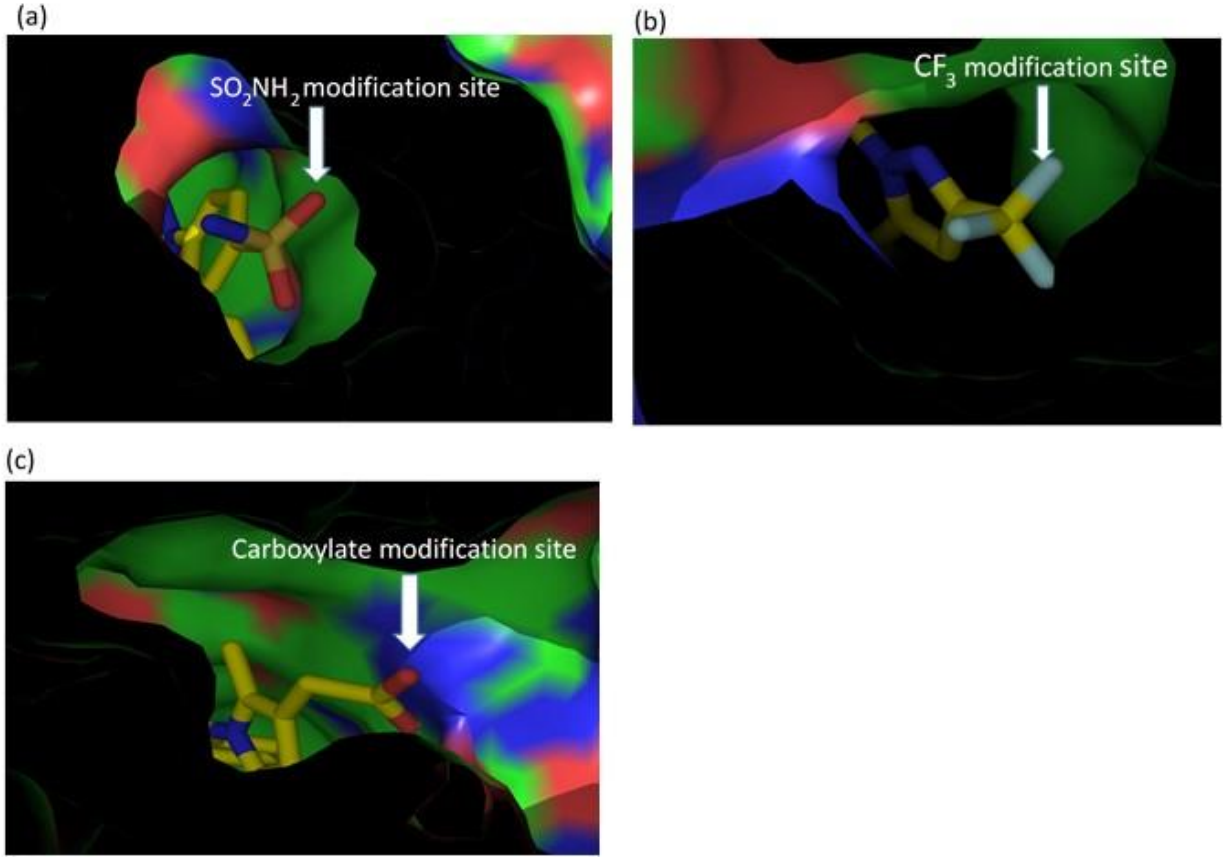

Figure 4.3: Crystal structures showing (a) binding of celecoxib within COX-2 (PDB code 3LN1) showing SO_2NH_2 modification site, and (b) binding of celecoxib within COX-2 (PDB code 3LN1) showing CF_3 modification site, (c) bindining of indomethacin within COX-2 (PDB code 4COX) showing carboxylate modification site.

4.2.1. Design rationale

The residues presented at the outer rim of HDAC enzymes form rugged landscapes designed to flexibly accommodate a diverse class of substrates. This may explain the tolerance of the HDAC outer rim for incorporation of various surface recognition groups into the design of

structurally dissimilar HDACi. Taking this into consideration, we hypothesized that incorporation of celecoxib (a COX-2 selective inhibitor) and indomethacin (a non-selective inhibitor of COX isoforms) into the surface recognition cap group of an HDACi may result in dual-acting agents that inhibit both HDAC and COX-2. Such agents are likely to show enhanced tumor cell cytotoxicity and superior therapeutic index compared to the individual HDACi and COX-2 inhibitors.

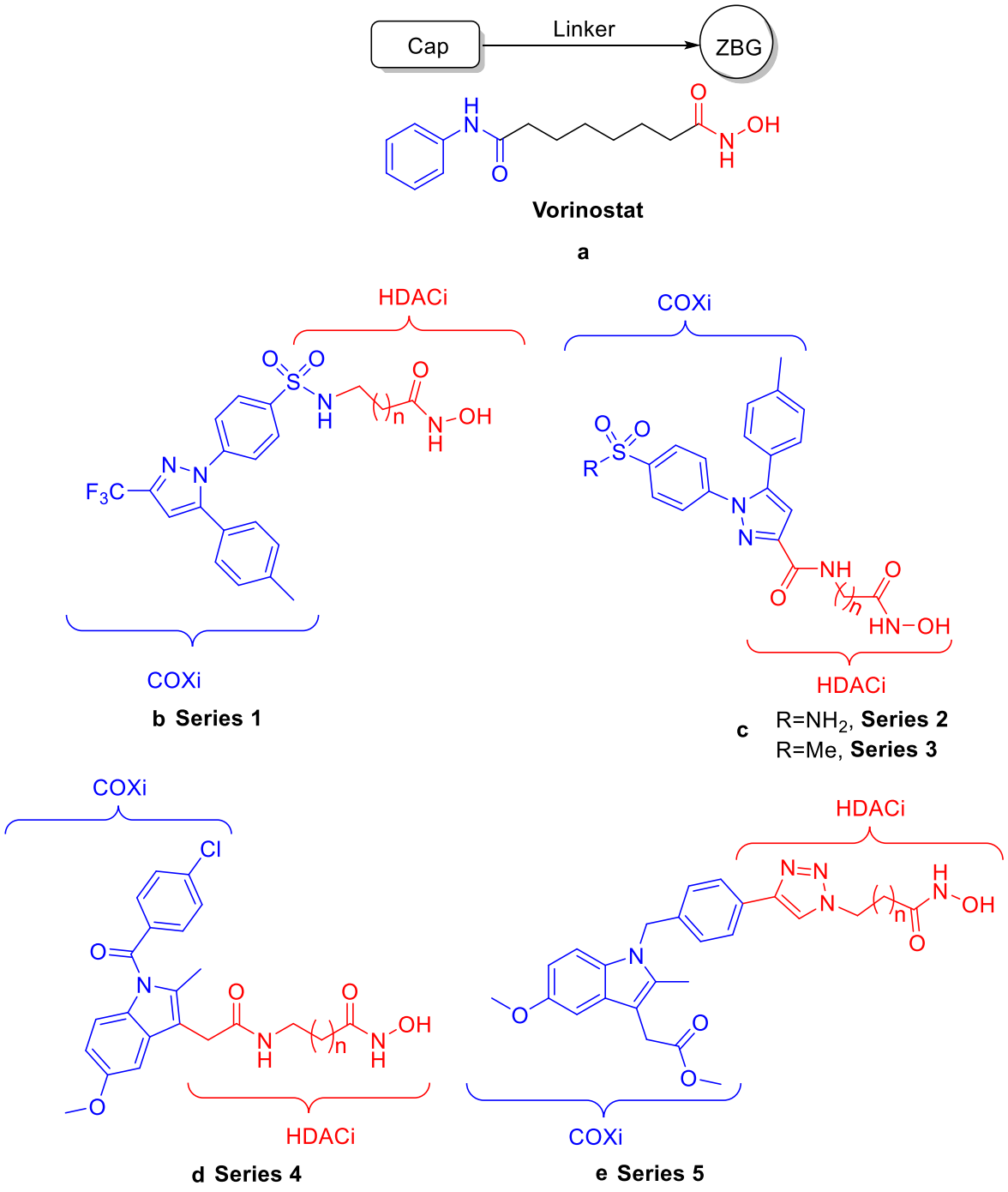

Figure 4.4: (a) HDACi pharmacophoric model integrated in vorinostat structure. (b) Designed dual-acting COXi-HDACi compounds – (i) Celecoxib-based HDACi (series 1), (ii and iii) Celecoxib-based HDACi (series 2 and 3) (iv and v) Indomethacin-based HDACi (series 4 and 5).

To determine which site to modify on celecoxib, we analyzed the orientation of celecoxib in the COX-2 active site. We found that the sulfonamide (SO_2NH_2) and trifluoromethyl (CF_3) moieties of celecoxib are projected towards different solvent exposed regions of the enzyme (Figure 4.3 a-b). Based on this analysis, the sulfonamide and trifluoromethyl moieties could be suitable points for the attachment of HDAC-inhibiting pharmacophores. Modifications at these two ends should minimally perturb the binding of celecoxib-based conjugates to the COX-2 active site, as shown in previous studies.[20b, 22] Because of the relaxed specificity for hydrophobic groups at the HDAC outer rims, the celecoxib aromatic moiety of the resulting dual-acting agents is expected to be accommodated as a surface recognition group when bound to HDAC enzymes. To test this deduction, we designed and synthesized celecoxib-HDACi conjugates in which: i) HDACi template is attached to the sulfonamide (Series 1, Figure 4.4) ii), the "CF_3" is replaced by HDACi template (Series 2, Figure 4.4) and iii) the sulfonamide is replaced with a methyl sulfone (SO_2Me) and "CF_3" is replaced by HDACi template (Series 3, Figure 4.4).

Similarly for indomethacin, the carboxylic acid moiety is projected towards the solvent exposed region (Figure 4.3c) of COX-2. Modification of this moiety is known to convert indomethacin from a non-selective COX inhibitor to a COX-2 selective inhibitor.[23] This prompted us to design and synthesize indomethacin-HDACi conjugates in which the HDACi template is attached to the carboxylic acid end (Series 4, Figure 4.4). Further modifications of indomethacin yielded conjugates in which the chlorobenzoyl is replaced by HDACi template, and carboxylic acid is either esterified or left unmodified (Series 5, Figure 4.4).

In all the NSAID-HDACi conjugates, linker lengths were restricted to five, six and seven methylenes separating the ZBG from the cap groups, in accordance with a previous study in our lab showing these lengths to be optimal for HDAC inhibition.[24]

Scheme 4.1: Synthesis of series 1 celecoxib-HDACi conjugates

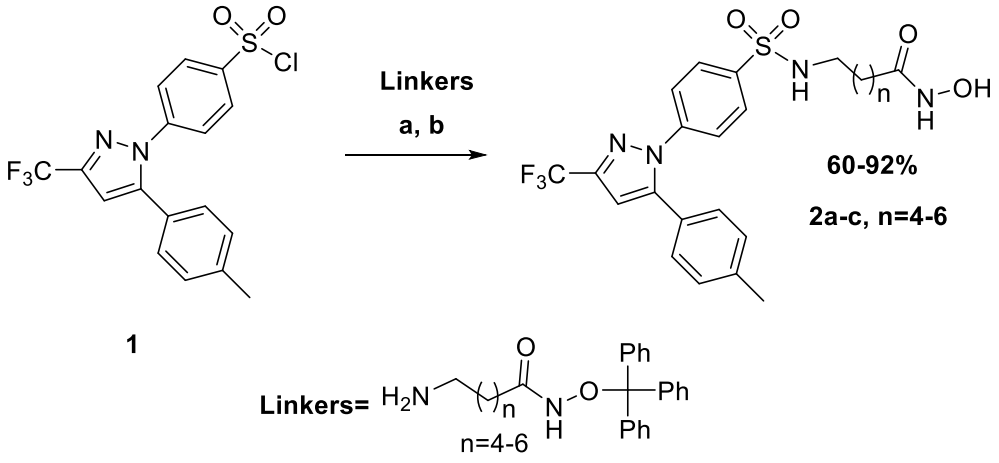

Reagents and conditions:

(a) TEA, DCM, rt,12hrs (b) TFA, TIPS, DCM, rt, 2hr

4.2.2. Chemistry

The sulfonyl chloride **1**, a vital intermediate required in the synthesis of sulfonamide-modified celecoxib-HDACi conjugates, was made according to a previously reported protocol[25]. The desired conjugates **2a-c** were thereafter made by displacement of chloride from compound **1** with trityl-protected primary amine having methylene linkers of appropriate lengths, followed by removal of trityl-protection with TFA (scheme 4.1).

To access the series 2 conjugates, the 1-(4-sulfamoylphenyl)-5-(*p*-tolyl)-*1H*-pyrazole-3-carboxylic acid intermediate **5** was made by hydrolysis of ethyl 1-(4-sulfamoylphenyl)-5-(p-tolyl)-1H-pyrazole-3-carboxylate **4**, whose synthesis had been previously reported,[26] using lithium hydroxide (Scheme 4.2). Subsequent coupling of compound **5** to trityl-protected primary amine having methylene linkers of appropriate lengths followed by trityl deprotection furnished the desired celecoxib-HDACi conjugates **7a-c** in decent yields. Likewise, the methyl sulfone analog **8** (Series 3) was made from **6** using the same chemistry.

Scheme 4.2: Synthesis of series 2 and 3 celecoxib-HDACi conjugates

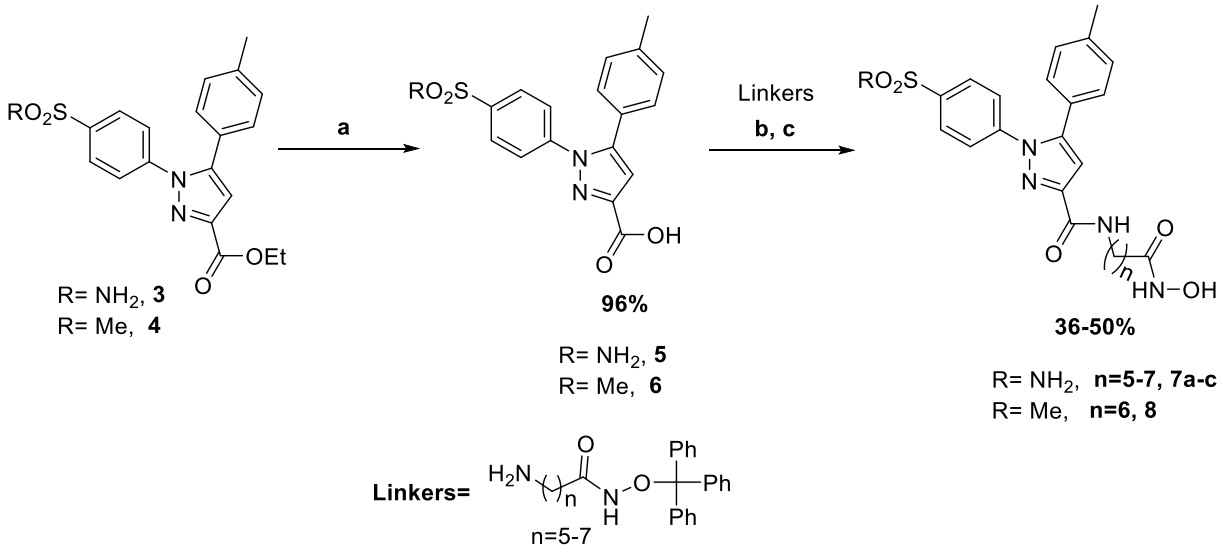

a) $LiOH.H_2O$, THF/H_2O, rt, 12hrs, b) EDCI, HOBT, $CHCl_3$, rt, 12 hrs c) TFA, TIPS, DCM, rt, 1 hr

The first series of indomethacin-based COXi-HDACi conjugates (Series 4) were made from the NHS-activated indomethacin intermediate **10**, which was obtained by reacting indomethacin with disuccinimidyl carbonate (Scheme 4.3). Displacement of NHS by trityl-protected primary amine having methylene linkers of appropriate lengths and subsequent trityl removal furnished conjugates **11a-c** in good yields.

Scheme 4.3: Synthesis of series 4 celecoxib-HDACi conjugates

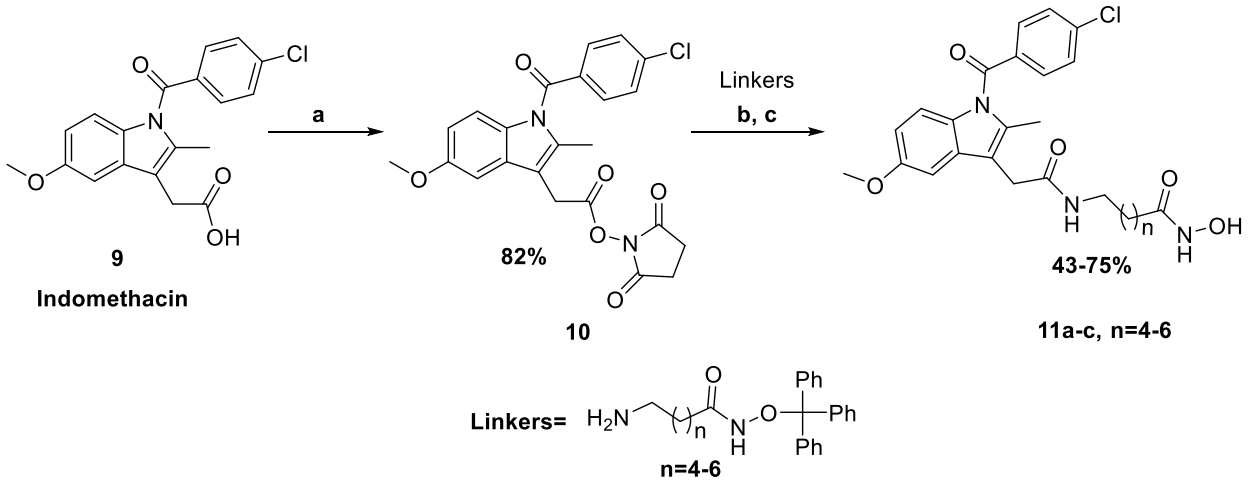

Reagents and conditions:

(a) Disuccinimidylcarbonate, DCM, rt, 6hrs (b) TEA, DCM, rt, 12hrs (c) TFA, TIPS, DCM, rt, 2hr

The esterified indole **12** required to synthesize the second series of indomethacin-HDACi conjugates was obtained by hydrolysis of indomethacin using NaOH followed by esterification using TMSCl in MeOH. Reaction of **12** with 4-ethynylbenzyl mesylate **13** in the presence of sodium hydride, gave the *N*-alkylated alkyne intermediate **14** (Scheme 4.4). Via Cu (I)-catalyzed azide-alkyne cyclo-addition reaction between alkyne **14** and trityl-protected azide having methylene linkers of appropriate lengths **15a-c**, trityl-protected precursors to the final compounds **16** and **17a-c** were made. Ester hydrolysis with lithium hydroxide followed by trityl deprotection using TFA furnished the NSAID-HDACi conjugate **16** while methyl ester compounds **17a-c** were obtained by trityl deprotection of precursors to the final compounds.

Scheme 4.4: Synthesis of series 5 celecoxib-HDACi conjugates

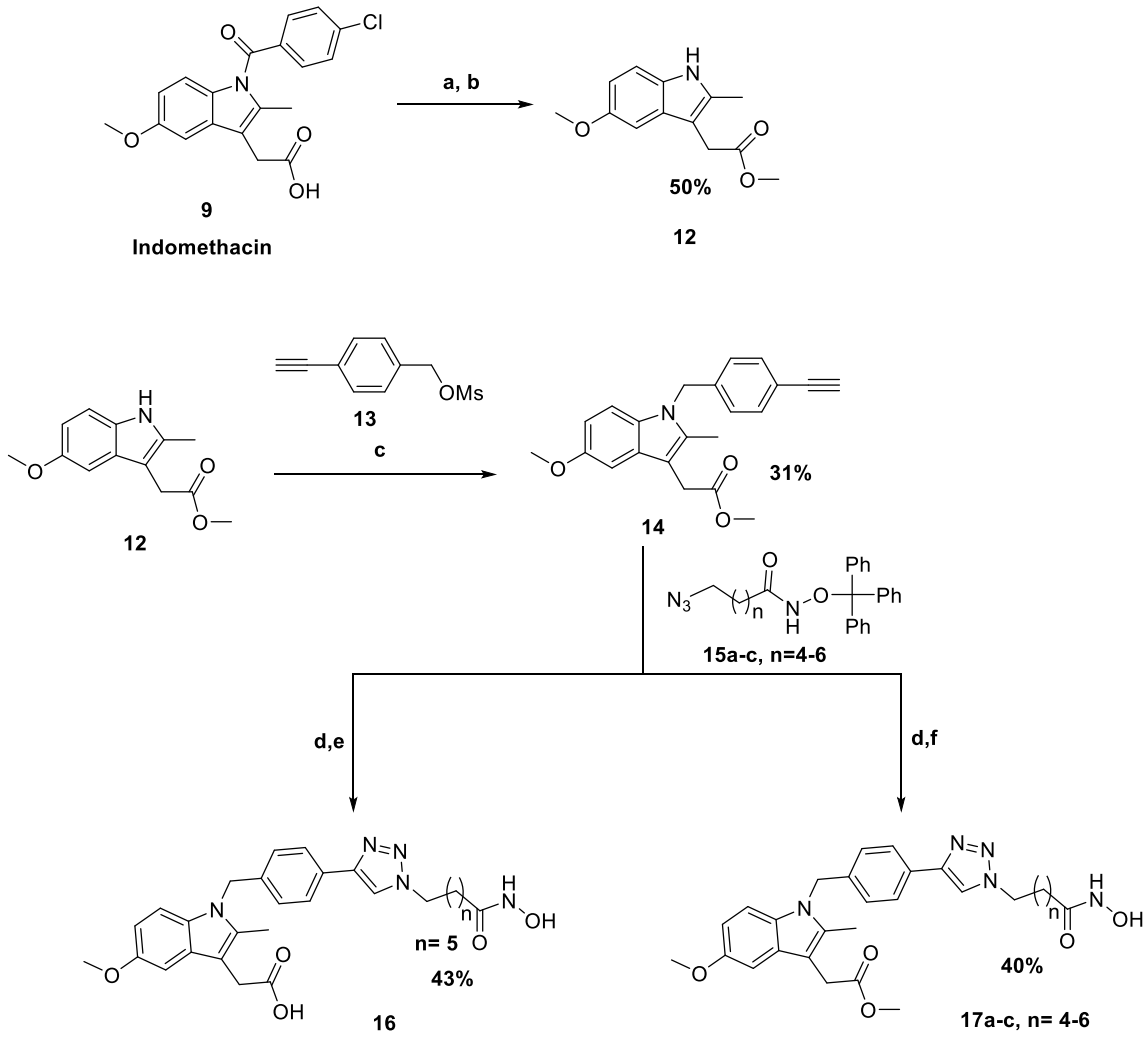

Reagents and conditions:
(a)NaOH, rt, 12 hrs (b) TMSCl, MeOH, rt, 12 hrs (c) NaH, THF, 0^0C-rt (d) CuI, DIPEA, THF, rt, 12 hrs (e) LiOH, THF/H_2O, rt, 12hrs (f) TFA, TIPS, DCM, rt, 2hr

4.2.3. HDAC isoforms inhibition screening

We screened all of the synthesized dual-acting COXi-HDACi compounds against all class I HDACs (HDACs 1-3 and HDAC 8) and HDAC6 (class IIB HDAC). These conjugates potently

inhibited all the HDAC isoforms screened. A closer look at the enzyme inhibitory activities reveals a linker length dependency which generally favors longer methylene linkers with few key exceptions (Table 4.1). Across all the five HDAC isoforms tested, these conjugates showed the strongest inhibitory effect towards HDAC 6, with IC_{50} as low as 5 nM for **17c**. Among the celecoxib-based series (series 1-2), compounds **7a-c** (series 2) showed more potency towards HDACs 1-3 compared to those of series 1 with the same linker lengths. This may be due to more favorable interaction of the 3'-amide and the free sulfonamide group, at the surface recognition group of conjugates, with potential H-bond donor/acceptor residues at the outer rim of the enzyme. In addition to the strong inhibitory effects towards HDAC 6 seen within the series 1 conjugates (compounds **2a-c**), **2b** also strongly inhibited HDACs 3 and 8, while **2c** showed preference for HDAC 3 compared to **2a** which has a strong inhibitory effect against HDAC 8. The only member of series 3 conjugates, compound **8**, is slightly more potent than compound **7b**, the corresponding conjugate in series 2 with the same linker length.

In the indomethacin-based series, conjugates with triazolyl connecting the linker to the head group, compounds **17a-c** (series 5), show greater inhibition of HDACs 1-3 and HDAC 6, compared to the amide-linked conjugates compounds **11a-c** (series 4). Compounds **11a-c** are equipotent towards HDAC 6, while they show varying activities towards other HDAC isoforms. We observed compounds **11a** and **11c** to be modestly active towards HDAC 1 (1810 nM and 1760 nM respectively), with almost no activity towards HDAC 2. An important observation, considering the level of similarity in the sequence composition at the active site of the two HDAC isoforms. We probed this observation by molecular docking (see Appendix I, Figures 3 and 4), but did not see any obvious differences in the manner of interaction of the two compounds with HDAC 1 and HDAC 2. It is noteworthy to point out that compound **16** and its methyl ester analog **17b** show

similar activity in all the HDAC isoforms screened, suggesting that modifying the carboxylic acid group in the series 5 conjugates does not result in loss of enzyme inhibitory activity. The remaining members of this series, **17a** and **17c**, have vastly varied anti-HDAC activities. Compound **17a** is moderately active against HDACs 3 and 8 with little activity against HDACs 1, 2 and 6. Conversely, **17c** is broadly active against all HDAC isoforms tested and it is the most potent HDAC 6 inhibitor among the dual-acting COXi-HDACi compounds herein disclosed.

Table 4.1: HDAC isoforms inhibition screening (IC_{50} in nM)[a] of NSAIDs-HDACi conjugates

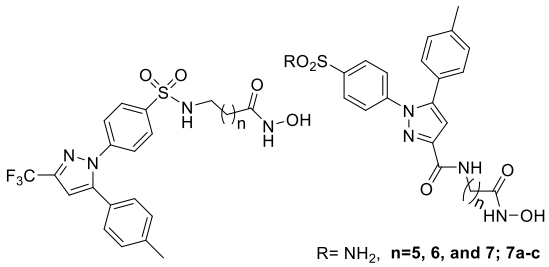

2a-c; n=4, 5 and 6

R= NH_2, **n=5, 6, and 7; 7a-c**
R= Me, **n=6; 8**

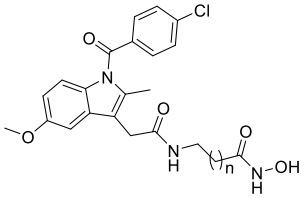

11a-c; n=4, 5, and 6

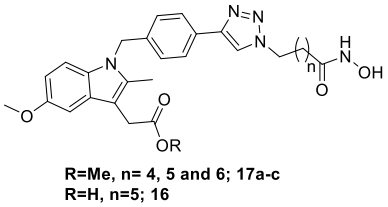

R=Me, n= 4, 5 and 6; 17a-c
R=H, n=5; 16

Compound	n	HDAC1	HDAC2	HDAC3	HDAC6	HDAC8
2a	4	1870 ± 280	2060 ± 400	1020 ± 160	76 ± 26	226 ± 90
2b	5	1030 ± 70	4050 ± 130	424 ± 53	66 ± 6	412 ± 43
2c	6	968 ± 160	929 ± 164	256 ± 35	61 ± 11	989 ± 142
7a	5	400 ± 60	232 ± 40	191 ± 44	92 ± 9	544 ± 76
7b	6	208 ± 52	294 ± 46	333 ± 79	83 ± 8	520 ± 110
7c	7	60 ± 7	32 ± 3	32.6 ± 7.5	183 ± 12	697 ± 55
8	6	261 ± 35	163 ± 8	338 ± 130	50 ± 16	345 ± 43
11a	4	1810 ± 330	41±12%	722 ± 119	49 ± 10	345 ± 95

11b	5	980 ± 75	854 ± 280	356 ± 48	49 ± 9	109 ± 41
11c	6	1760 ± 190	43 ± 3%	283 ± 54	50 ± 14	707 ± 86
16	5	111 ± 15	302 ± 40	59 ± 10	22 ± 5	116 ± 32
17a	4	778 ± 105	1360 ± 530	224 ± 60	6830 ± 430	672 ± 77
17b	5	89 ± 13	407 ± 97	35 ± 6	10 ± 1	135 ± 35
17c	6	251 ± 80	209 ± 18	181 ± 71	5 ± 3	394 ± 172

% values refer to % inhibition at 10 μM. [a] average of three independent experiments.

4.2.4. Molecular docking analysis

To gain an insight into the specific interactions that may exist between our compounds and HDACs, which may explain the pattern of the observed HDAC inhibition, we docked all the compounds against HDAC 6. In all the series, we observed zinc chelation, typical of all hydroxamate-based HDACi, while the COX-binding moieties sit at surface of the enzyme (Appendix I, Figure 1).

In all the celecoxib-based conjugates (series 1-3), the "*para* tolyl" group makes a stabilizing pi-stacking interaction with PHE 680 residue at the surface of the enzyme. We observed that compound **2a**, analog with the shortest linker among the series 1 compounds, had the phenyl at the headgroup and the linker pushed further down the active site to maximize chelation with Zn at the bottom of the active site (Appendix I, Figure 1(i)). This slightly offset the pi-stacking interaction with PHE 680 at the surface of the enzyme, and may explain the slightly weaker activity against HDAC 6 compared to **2b and 2c**. Compound **7b** had a slightly different orientation at the surface of the enzyme, with its "*para* tolyl" group and "phenyl sulfonamide groups flipped, but

still maintained pi-stacking interaction with PHE 680 and Zn chelation shown by compounds **7a**, **7c** and **8** (Appendix I, Figure 1(iii)).

Among the indomethacin-based compounds, the series 4 conjugates (**11a-c**) adopt a similar binding pose within the HDAC 6 active site, except for **11c** (Appendix I, Figure 1(v)). Despite this, compounds **11a-c** have similar inhibitory effects on HDAC 6 (Table 4.1). All the series 5 conjugates, on the other hand, elicit a completely different interaction at the surface of the enzyme ((Appendix I, Figure 1(vii)).

i

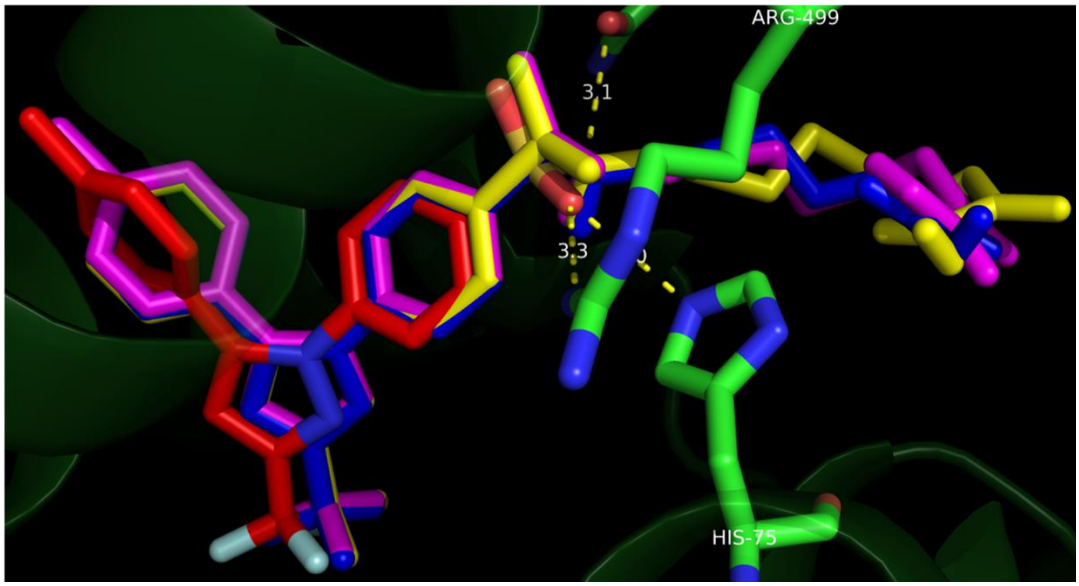

ii

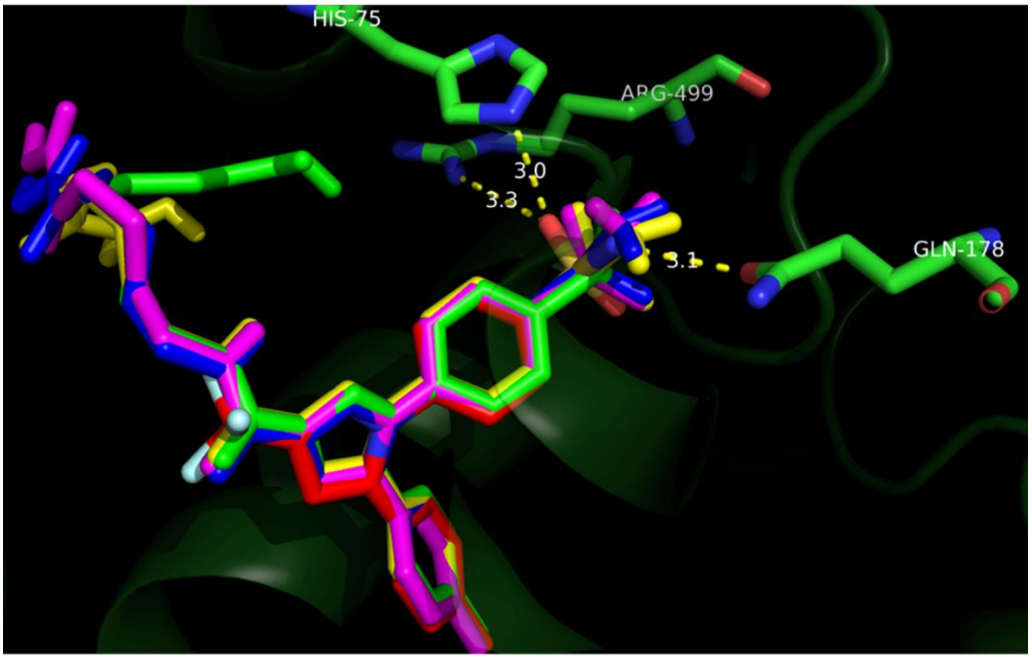

iii

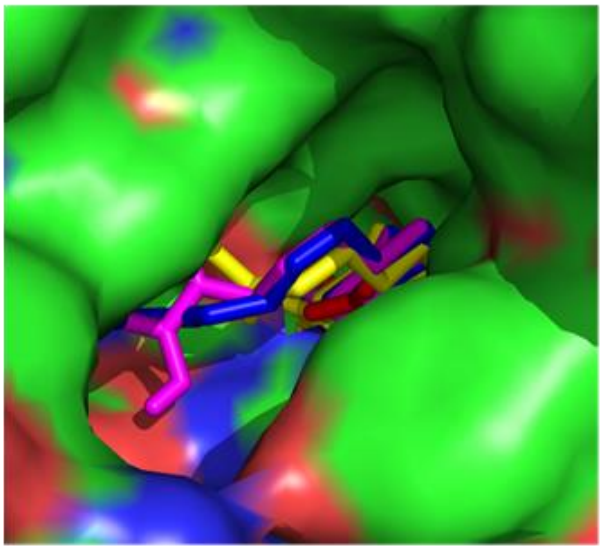

iv

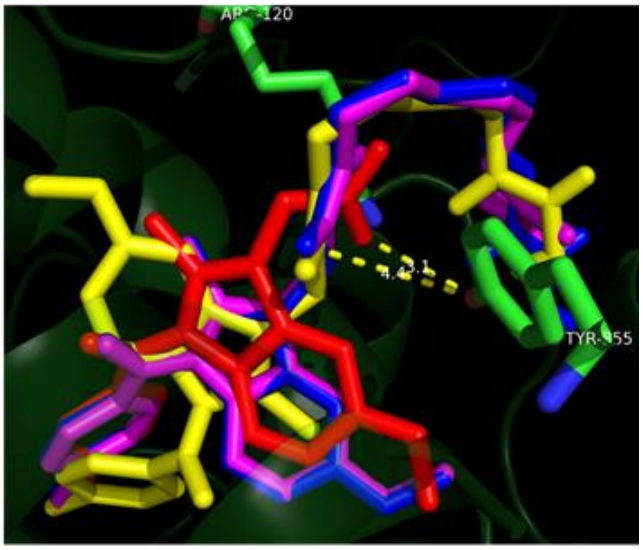

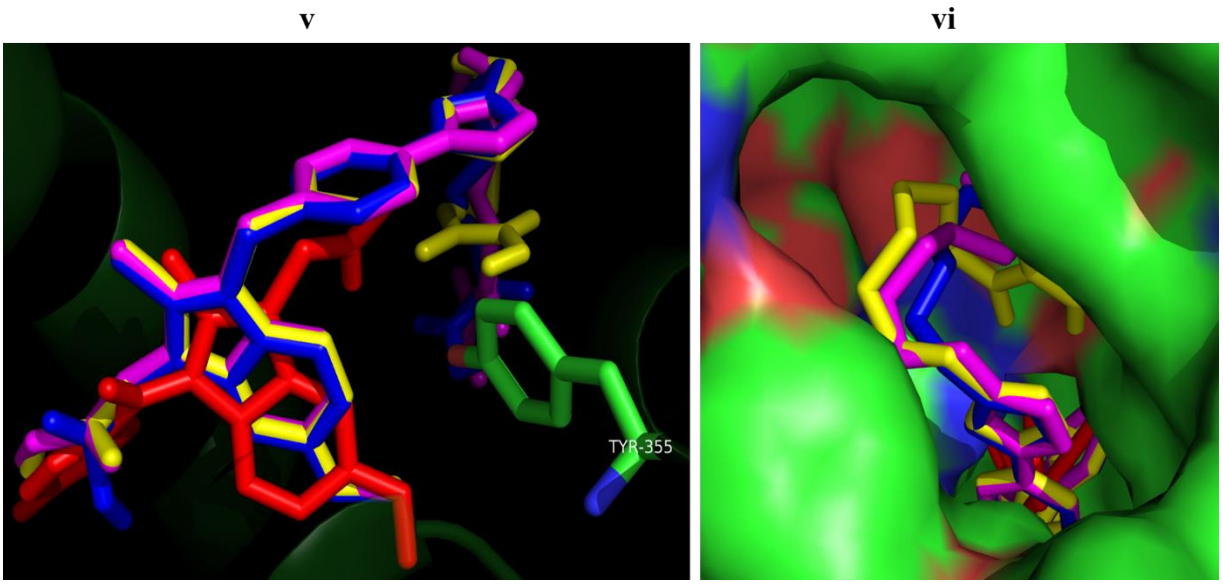

Figure 4.5: Docking output of NSAID-HDACi conjugates overlaid with crystal structure of celecoxib and indomethacin in COX-2: i) series 1 conjugates: **2a** (blue), **2b** (magenta), **2c** (yellow) and celecoxib (red); ii) series 2 and 3 conjugates: **7a** (blue), **7b** (magenta), **7c** (yellow), **8** (green); iii) series 4 conjugates: **11a** (blue), **11b** (magenta), **11c** (yellow), and indomethacin (red); iv) surface representation of series 4 conjugates: **11a** (blue), **11b** (magenta), **11c** (yellow), and indomethacin (red); v) series 5 conjugates: **17a** (blue), **17b** (magenta), **17c** (yellow), and indomethacin (red); vi) surface representation of series 5 conjugates: **17a** (blue), **17b** (magenta), **17c** (yellow), and indomethacin (red).

We also docked the conjugates against COX-2 to confirm that the structural modifications made on celecoxib and indomethacin do not appreciably compromise their interactions with COX-2. The selectivity of celecoxib towards COX-2 is attributed to its sulfonamide group forming four polar contacts (two H-bonding and two salt bridges) with His75, Arg499, Leu338 and Ser339 of COX-2, while the "*para* tolyl" group is projected towards the hydrophobic region in the active

site.[27] Docking output of celecoxib-based series (series 1-3) show that the conjugates overlay perfectly with celecoxib in the COX-2 active site with the HDACi moiety projected towards the solvent exposed region. Among the series 1 conjugates, the "*para* tolyl" group is twisted perpendicularly to the plane of the "*para* tolyl" group of celecoxib (Figure 4.5 (i)), perhaps, to compensate for the modification at the sulfonamide end. The series 2 conjugates on the other hand, align perfectly with celecoxib in the COX-2 active site, with the appended HDACi template projecting towards the solvent exposed region (Figure 4.5 (ii)). All the conjugates bind COX-2 similarly, irrespective of the length of the appended HDACi template.

A similar observation was seen with the indomethacin-based series 4 conjugates, wherein all the conjugates align with indomethacin, except for compound **11c**, with the HDACi appendage projected towards a pocket at the surface of the enzyme (Figures 4.5 (iii) and (iv)). We believe the misalignment of compound **11c**, relative to indomethacin and other conjugates, is due to the length of the HDACi appendage. In order for the HDACi appendage to fit the pocket at the enzyme's surface, there has to be a distortion in the binding mode within the active site leading to the misalignment (Figure 4.5 (iii)). The series 5 conjugates present a different binding mode, with the methyl ester group projected towards the hydrophobic region occupied by the chlorobenzoyl group of indomethacin. Consistent with previous observation in other series, all series 5 conjugates bind to the COX-2 active site in a similar fashion regardless of the length of the HDACi template.

Table 4.2: COX isoforms inhibition study

Compound	COX-1 % inhibition [a]	COX-2 % inhibition [a]	COX-1 IC_{50} (µM) [b]	COX-2 IC_{50} (µM) [b]	SI
2a	16.25	97.69	ND	ND	-
2b	61.43	100.00	3.57 ± 0.34	0.30 ± 0.03	>11
2c	26.05	95.57	ND	ND	-
7a	NI	19.06	ND	ND	-
7b	26.36	71.11	ND	ND	-
7c	NI	66.87	ND	ND	-
8	NI	60.25	23.09 ± 0.70	4.44 ± 0.06	>5.20
11a	40.22	95.13	ND	ND	-
11b	22.81	98.13	21.00 ± 9.07	0.33 ± 0.06	>60
11c	42.76	96.20	ND	ND	-
16	NI	40.59	ND	ND	-
17a	NI	11.51	ND	ND	-
17b	NI	50.77	ND	ND	-
17c	7.076	78.16	11.97 ± 1.10	4.58 ± 0.06	>2
Celecoxib	-	-	7.70[28]	0.07[28]	>100
Indomethacin	-	-	0.05[29]	0.20[29]	0.25

[a] percent inhibition at 10µM; [b] average of three independent experiments; NI represents no inhibition; ND represents not determined; SI represents selectivity index (COX-1 IC_{50}/COX-2 IC_{50}).

4.2.5. COX inhibition study

We performed a preliminary screening (at 10μM) of all the bifunctional compounds against COX-1 and COX-2 enzymes using Cayman fluorescent inhibitor screening assay kit. Based on the preliminary screen, representative members from each series were selected for IC_{50} determination in both COX isoforms (Table 4.2). In most cases, compounds within the same series showed similar percent inhibitory activities towards COX-1 and COX-2, validating our observation from docking which suggests that conjugates' within the same series should have similar interactions with COX-2, independent of the length of the HDACi appendage.

The celecoxib based conjugate **2b** retained selectivity towards COX-2 akin to celecoxib, though with reduced potency. Compound **7c** was surprisingly less potent compared to **2b** in the preliminary screen, despite having a near perfect alignment with celecoxib in the COX-2 active site (Figure 4.4 (ii)) compared to the alignment of **2b** (Figure 4.4 (i)). The only indomethacin-based compound evaluated for IC_{50}, **11b**, shows comparable level of potency towards COX-2 as indomethacin. Interestingly, the COX-2 selectivity of **11b** rivals that of celecoxib, an FDA-approved COX-2-selective inhibitor. The COX-2-selectivity seen with compound **11b** is consistent with observations in the literature on indomethacin modified at the carboxylic acid group.[23] Despite the drastic structural modifications to celecoxib and indomethacin templates which furnished compounds **8** and **17c** respectively, these compounds still showed decent activity towards COX-2 (Table 4.2).

Table 4.3: Cell growth inhibitory activity (IC_{50} in µM) of bifunctional COXi-HDACi conjugates in cancer and healthy cell lines.[a]

Compound	MCF-7	A549	HCT-116	LNCaP	DU-145	Vero
2a	7.77 ± 1.20	10.44 ± 0.96	8.74 ± 0.23	8.88 ± 1.76	NT	6.83 ± 0.74
2b	5.70 ± 0.55	8.00 ± 0.23	3.38 ± 0.09	2.19 ± 0.21	6.41 ± 0.51	5.53 ± 0.40
2c	4.58 ± 0.23	8.15 ± 0.44	6.29 ± 0.15	2.11 ± 0.07	10.10 ± 0.33	6.61 ± 0.42
7a	>100	>100	NT	NT	NT	>100
7b	>100	>100	24.97 ± 1.95	>20	NT	>100
7c	59.48 ± 3.40	34.14 ± 7.43	7.12 ± 0.86	>20	NT	12.14 ± 0.34
8	16.34 ± 1.40	23.38 ± 2.60	2.62 ± 0.32	1.89 ± 0.11	18.30 ± 0.80	20.94 ± 1.26
11a	>100	31.93 ± 1.95	16.13 ± 0.79	>20	NT	40.67 ± 2.67
11b	29.30 ± 1.47	14.46 ± 1.76	11.21 ± 0.44	2.71 ± 0.52	7.26 ± 0.46	19.36 ± 1.36
11c	25.10 ± 9.38	33.02 ± 0.64	24.85 ± 1.11	6.46 ± 0.67	>20	34.74 ± 0.28

16	47.84%	NT	9.90 ± 1.95	NT	NT	NT
17a	14.16 ± 2.02	37.44 ± 1.03	9.31 ± 0.85	>20	NT	37.82 ± 1.26
17b	9.61 ± 1.45	8.22 ± 0.61	1.67 ± 0.09	1.35 ± 0.30	8.17 ± 0.05	5.82 ± 0.16
17c	5.94 ± 0.29	4.43 ± 0.14	1.28 ± 0.13	1.53 ± 0.51	12.54 ± 0.54	5.73 ± 0.29
SAHA	3.27 ± 0.05	5.00 ± 0.24	1.4	1.22 ± 0.06	3.45 ± 0.16	1.03 ± 0.09
Celecoxib	NT	NT	NT	32.60[12]	NT	NT
Indomethacin	5.20%	NT	NT	>300[12]	NT	NT

% represents percent inhibition at 100µM, NT represents not tested, average of three independent experiments.[a]

4.2.6. *In vitro* anticancer activity study

Encouraged by the impressive HDAC and COX inhibitory activities of our conjugates, we tested their growth inhibitory activities in a panel of cancer cell lines: breast (MCF-7), lung (A549), colon (HCT-116), androgen-dependent (LNCaP) and -independent (DU-145) prostate cancer cell lines. Healthy monkey kidney epithelial cells (VERO) were used as a positive control. Our choice of cancer cell lines was based on the expression profiles of different HDAC isoforms and COX-2 in the cell lines. All class I HDACs and HDAC 6 (a class IIb HDAC) play crucial roles in the

survival of the chosen cancer cell lines.[2, 4] While COX-2 is ubiquitously expressed in the MCF-7[18a] and A549[30] cell lines, its expression is barely discernible in the HCT-116[22b] cell line. Prostate cancer cell lines (LNCaP and DU-145) were chosen to evaluate the selectivity of our compounds towards androgen dependent prostate cancer. COX-2-specific NSAIDs perturb androgen receptor (AR)-mediated functions which are critical for the survival of LNCaP.[12] Most of the conjugates show strong antiproliferative effects in all the cancer cell lines used in this study, and are less cytotoxic towards VERO compared to SAHA. More specifically, we observed the compounds to be considerably more potent towards androgen dependent prostate (LNCaP) and HCT-116 (with no COX-2 expression).

Among the conjugates based on celecoxib (Series 1-3), compounds **2a-c** show increasing activity with increase in methylene linker lengths in MCF-7 and A549 cell lines, consistent with the trend observed in their HDACs 1-3 and 6 inhibition activities. A different trend is observed for these series of compounds in HCT-116 and LNCaP cell lines, as compound **2b** potently inhibit the proliferation of both cell lines while **2c** is less potent against HCT-116 but equipotent as **2b** against LNCaP (Table 4.3). Surprisingly, sulfonamide compounds **7a-c** were barely cytotoxic across all cell lines (except for compound **7c**), despite their impressive anti-HDAC activities. The inactivity of the sulfonamide-based compounds **7a-c** may be due to lack of cell penetration to an appreciable extent. This deduction was supported by the fact that the methyl sulfone congener of inactive compound **7b**, compound **8**, showed anti-proliferative activity that is consistent with its HDAC inhibitory activity and with exquisite selectivity toward AR-positive LNCaP and HCT-116 cells.

Most of the indomethacin-based conjugates potently inhibited the growth of all the cancer cell lines, with the effect more pronounced within the series 5 conjugates (**17a-c**). Notably, compound

17c showed IC_{50} comparable to vorinostat in A549 cell line and it is more cytotoxic towards LNCaP and HCT-116 in similar manner to the other active celecoxib-based compounds. Considering their strong anti-HDAC and weak COX-2 inhibitory effect within the series 5 conjugates, mechanism of cytotoxicity in HCT-116 could be attributed, predominantly, to HDAC inhibition. The series 4 conjugates **11b** and **11c** showed reduced anticancer effect in all cell lines, except LNCaP against which they are still potently active. Compound **11a**, the other member of this series, is poorly active or inactive against all cell lines tested. The cytotoxic effects of **11b** and **11c** towards LNCaP may be due to a combined effect of HDAC inhibition and inherent downregulation of AR associated with COX-2 selective NSAIDs.

In healthy cells (VERO), these compounds are significantly less toxic when compared to vorinostat. Specifically, compound **8** is about ten-fold more selective towards prostate cancer cells (LNCaP) compared to VERO. Likewise, compounds **11b**, **11c**, **17b** and **17c** displayed varying level of selective cytotoxicity towards LNCaP compared to VERO.

4.2.7. Comparison of antiproliferative activity of bifunctional compounds and combination therapy of NSAIDs and HDACi

To investigate if there is an advantage in having bifunctional compounds compared to just a combination of the individual components (SAHA + Celecoxib; or SAHA + Indomethacin), we tested an equimolar concentration of the individual components, and compared their growth inhibitory activities to those of lead bifunctional compounds **2b** and **11b** in LNCaP, DU-145 and VERO.

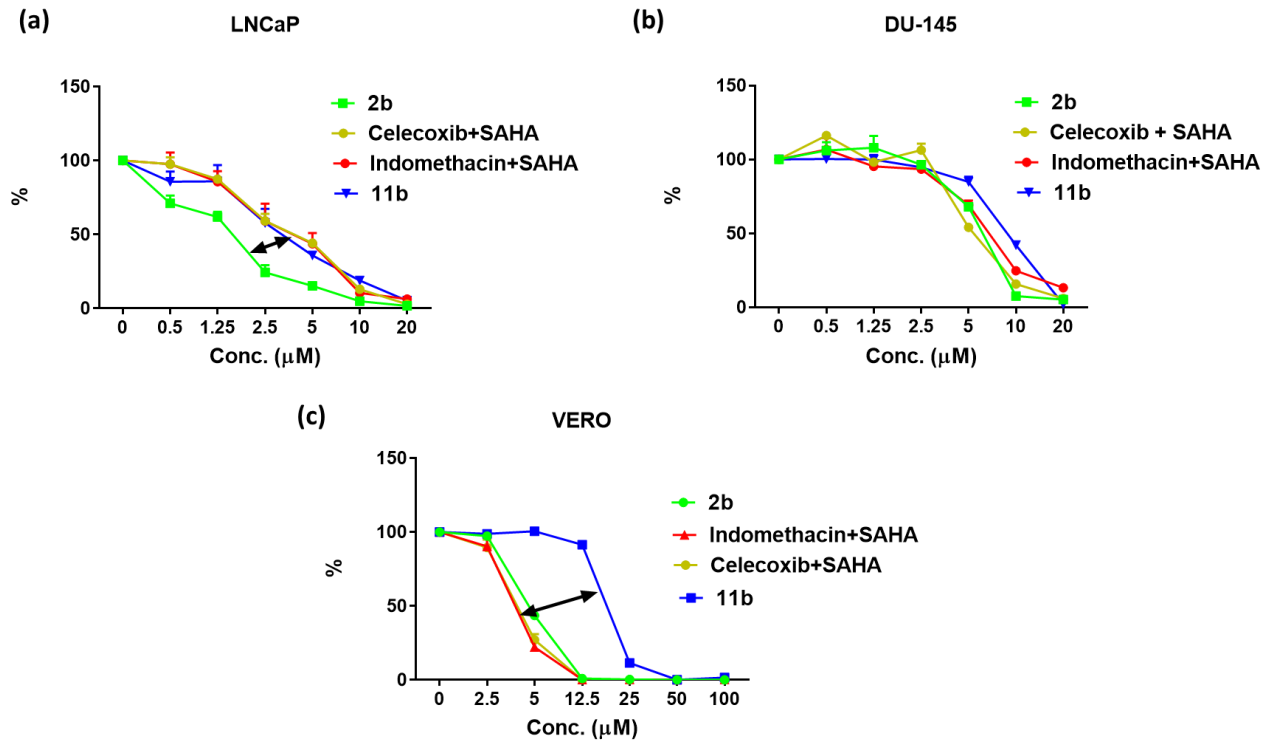

Figure 4.6: Antiproliferative activity of combination of equimolar concentration of respective NSAIDs and SAHA compared to equal concentration of appropriate bifunctional compounds in a) LNCaP; b) DU-145; and c) VERO cell lines.

As shown in Figure 4.6a above, compound **2b**, bifunctional compound derived from celecoxib template, is significantly more potent than a combination of celecoxib and SAHA in LNCaP, with no observable differences in DU-145 and VERO (Figures 4.6, b and c respectively). This confirms compound **2b** as a more selective and potent compound to treat AR positive prostate cancer. Indomethacin derived compound **11b** on the other hand, while equipotent to a combination of indomethacin and SAHA in both LNCaP and DU-147 (Figures 4.6 a and b respectively), is significantly less toxic to healthy cells, VERO (Figure 4.6c). Hence, a hybrid of indomethacin and

HDACi, **11b**, has a superior therapeutic index when compared to a combination of equimolar concentrations of indomethacin and SAHA.

Overall, compound **2b** is more potent (Figure 4.6a) and selective towards LNCaP (Appendix I, Figure 3a) compared to compound **11b** and a combination of SAHA and the respective NSAID, while compound **11b** has the highest *in vitro* selective toxicity index.

4.2.8. Intracellular target validation

Using western blot, we probed for evidence of intracellular HDAC inhibition among our compounds in LNCaP. Inhibition of HDAC 6 is known to result in accumulation of acetylated tubulin in the cytosol.[31] In this experiment, we chose compound **2b** as a representative of all celecoxib-based conjugates (Series 1-3), while compounds **11b** and **17b** were selected as representatives of series 4 and 5 conjugates respectively. SAHA was used as the positive control. As expected, all the tested compounds showed accumulation of acetylated tubulin in a concentration dependent manner (Figure 4.6, panel 1). Compound **17b**, a highly potent HDAC 6 inhibitor ($IC_{50} \approx 10$ nM), showed about the same level of acetyl tubulin at 1.5 μM (Figure 4.6, panel 1, lane **7**) as SAHA at 10 μM (Figure 4.6, panel 1, lane 2). A similar trend was observed with histone H4 acetylation (a marker of class 1 HDAC inhibition) (see Appendix I, Figure 4).

According to Yamaguchi *et al*,[32] HDAC inhibition causes downregulation of PMA-induced COX-2 expression in cancer cell lines. A similar observation was obtained when we treated LNCaP cells with SAHA at 10 μM (Figure 4.7, panel 3, lane 2). Our observation, following treatment with compounds **11b** and **17b**, was contrary to this, as we saw sustained COX-2

expression levels at the tested concentrations (Figure 4.7, panel 3, lanes 5-7). Compound **2b**, on the other hand, showed COX-2 downregulation at low concentration (2 μM) and a slight upregulation a higher concentration (10 μM) (Figure 4.7, panel 3, lanes 3-4). The implication of this may be that the cytotoxic effect of these compounds in LNCaP may be less dependent on their effects on COX-2 expression. This is not without precedence, as other selective COX-2 inhibitors are known to induce apoptosis independent of COX-2 expression.[14, 33] However, the sustained COX-2 expression level observed with our compounds, clearly distinguishes them from SAHA. This may prove to be advantageous in *in vivo* experiments with prostate cancer, as the COX-2 binding component of our compounds may confer selective localization in the tumor.

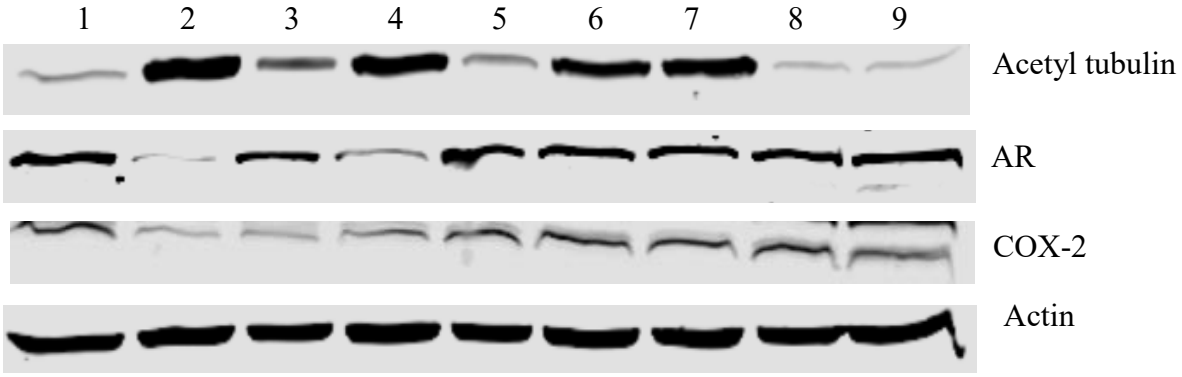

Figure 4.7: Western blot analysis of acetylated tubulin, AR and COX-2 in LNCaP following treatment for 24hr. Lanes: 1, Control (DMSO); 2, SAHA (10 μM); 3, **2b** (2 μM); 4, **2b** (10 μM); 5, **11b** (2 μM); 6, **11b** (10 μM); 7, **17b** (1.5 μM); 8, celecoxib (10 μM); 9, indomethacin (10 μM).

AR upregulation is critical to the survival of LNCaP[34]. In our study with LNCaP, SAHA significantly suppressed AR expression at 10 μM (Figure 4.7, panel 2, lane 2), consistent with the literature.[35] Compounds **2b** showed a similar effect in a concentration dependent manner (Figure

4.7, panel 2, lanes 3-4). Quite unexpectedly, AR downregulation was much weaker for compound **11b** (Figure 4.7, panel 2, lanes 5-6)**,** while compound **17b** showed no noticeable effect at the single concentration tested (Figure 4.7, panel 2, lane **7**). Both celecoxib and indomethacin showed no effects on AR regulation at 10 μM (Figure 4.7, panel 2, lanes 8 and 9). All together, these observations suggest that our compounds might be perturbing distinct pathways to elicit anti-proliferative activities against LNCaP cells. Compound **2b** acts more like a typical HDACi via induction protein acetylation and downregulation of AR. In contrast, **11b** and **17b** are atypical as they have no effect on AR expression. They most likely derived their potent anti-proliferative effect on LNCaP cells through a combination of COX-2-facilitated cell uptake, HDAC inhibition and perturbation of other pathways unique to prostate cancer.

4.2.9. Effect of bifunctional compounds on PGE_2 expression

One of the consequences on intracellular COX inhibition is decreased production of prostaglandin E2 (PGE_2).[36] To confirm that the strong COX-2 inhibitory effects of our compounds is maintained in cells, we treated HeLa cells with compounds **2b**, **11b**, celecoxib and indomethacin for 24 hours then measured the level of PGE_2 produced in the cell culture supernatant. HeLa cell line was chosen for this study because it has been previously used for a similar study[36] (see Appendix I, Table 1 for the IC_{50} of these compounds in HeLa cells). As shown in Figure 4.8, both compounds **2b** and **11b** significantly inhibited PGE_2 production, confirming that these NSAID-HDACi conjugates possess intracellular COX-2 inhibitory activities as well.

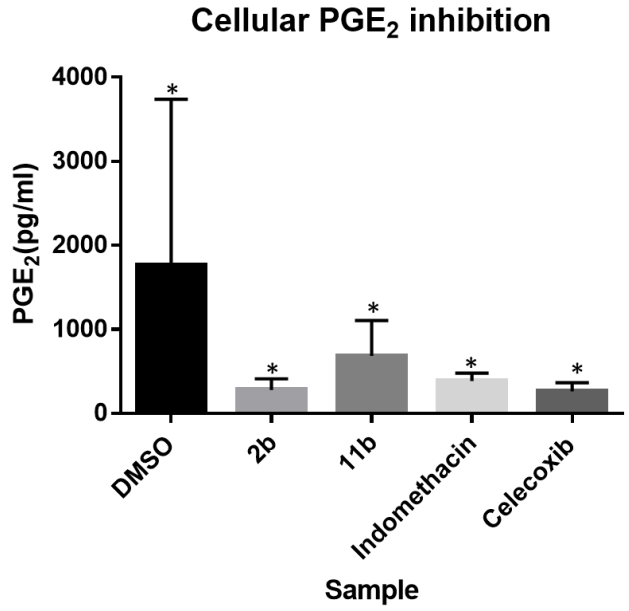

Figure 4.8: Intracellular COX-2 inhibition is evidenced by attenuation of prostaglandin E2 (PGE_2) production. HeLa cells were treated with each of the tested compounds at 10X IC_{50} for 24hrs and PGE_2 level was measured. *$p<0.05$. Statistical analysis was performed using Student's *t*-test. Data are representative of three independent experiments.

4.2.10. Effect of lead compound on cell cycle progression

To determine if the potent cell proliferation inhibition activities of these compounds result from their perturbation of the cell cycle pattern, we evaluated the effect of compounds **2a**, **8**, **11b** and **17b** on LNCaP cell cycle progression using SAHA, celecoxib and indomethacin as controls. We observed that the effect of celecoxib and indomethacin (both at 40 μM) was not significantly different from the DMSO control. SAHA at 2.5 μM induced a G_0/G_1 phase arrest as reported previously in the literature[35] (Figure 4.9). Compound **8**, at 2.5 μM, displayed a similar G_0/G_1 phase arrest as SAHA. This is not unexpected, since **8** has a broad HDAC inhibition activity and only

weak inhibitory effect against COX- 2 (Table 4.2). Compared to **8**, compounds **2a**, **11b** and **17b**, have a distinct effect on cell cycle progression. At 2.5 μM, they induced a significant S phase arrest. This may be as a result of their combined HDAC and COX-2 inhibitory effects.

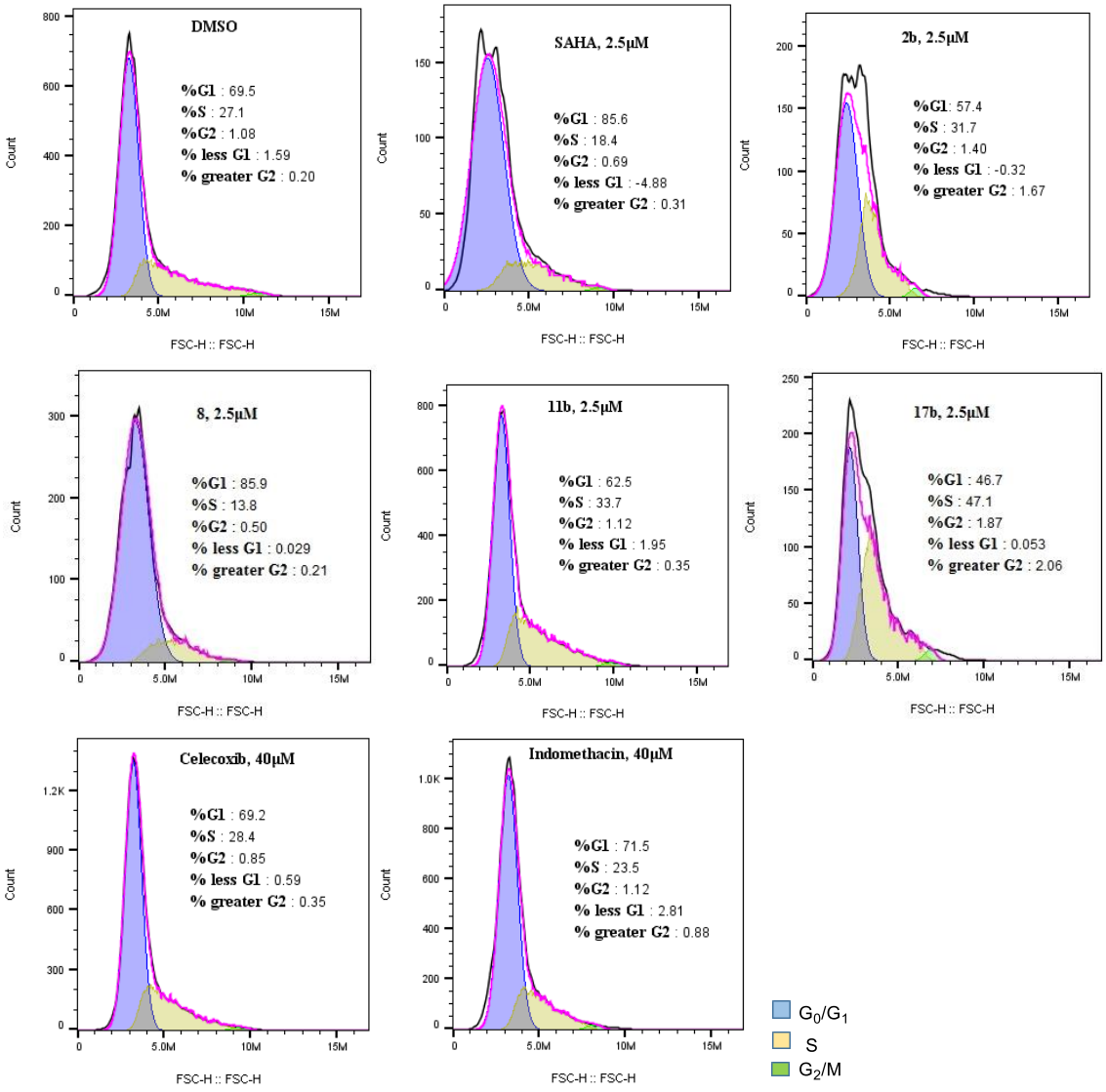

Figure 4.9: Effect of SAHA, **2b**, **8**, **11b**, **17b**, celecoxib and indomethacin on LNCaP cell cycle progression.

4.2.11. Bifunctional compounds suppress NTHi-induced NF-κB activation

NF-κB activation drives inflammation and tumorigenesis in cancer. The two pathways involved in NF-κB activation (canonical and non-canonical pathways) are initiated by pro-inflammatory cytokines such as TNFα and interleukins.[37] We recently reported that HDACi downregulate inflammatory cytokines release and NF-κB activation.[38] Likewise, there is evidence for non-COX inhibition dependent downregulation of NF-κB activation by NSAIDs.[39] In view of these, we investigated the ability of our bifunctional compounds to suppress NF-κB activation in BEAS-2B cells treated with nontypeable *Haemophilus influenzae* (NTHi) using NF-κB luciferase assay. NTHi is a Gram-negative bacterium which causes infection in the human respiratory tract. NF-κB is potently activated upon NTHi infection in human epithelial cells, and induces pro-inflammatory mediators such as IL-1β, IL-6 and TNF-α.

We screened representative NSAID-HDACi conjugates with potent HDAC inhibition activities and observed that compounds **8** and **17b** suppressed NTHi-induced NF-κB activation in BEAS-2B cells almost to the same extent as SAHA (Figure 4.10). In this assay, compound **2c**, celecoxib and indomethacin also showed some level of suppression of NF-κB (Appendix I, Figure 5). Considering the fact that compounds **8** and **17b** have moderate COX and strong HDAC inhibitory activities, their ability to downregulate NF-κB activation is likely a consequence of their HDAC inhibitory capability. In summary, these results demonstrate that representative NSAID-HDACi conjugates could suppress inflammation due to their ability to inhibit NF-κB activation.

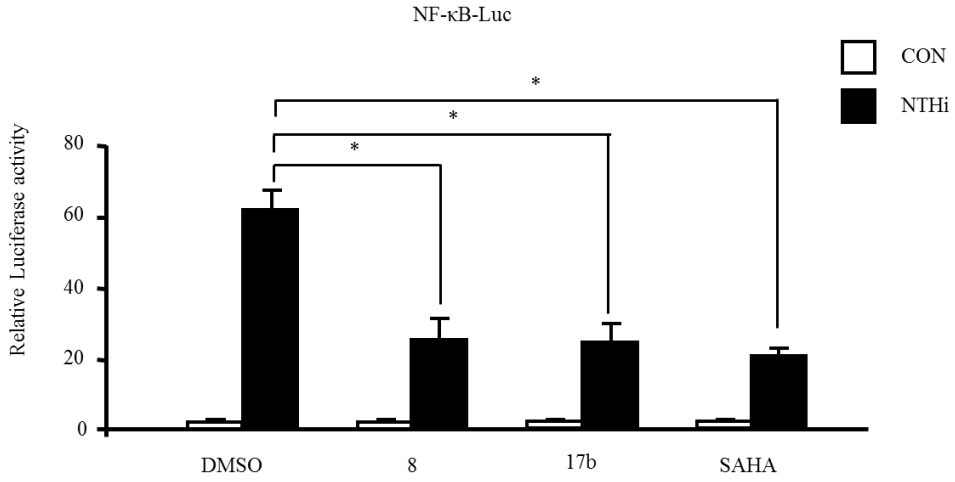

Figure 4.10: Representative NSAID-HDACi conjugates inhibit NF-κB activation. BEAS-2B cells, transfected with NF-κB luciferase construct, were pre-treated with compounds **8**, **17b** or SAHA at 1 μM for 1hr and stimulated with NTHi for 5hr, and NF-kB promoter activity was then measured by performing luciferase assay. Data are mean ± SD (n=3). *$p<0.05$. Statistical analysis was performed using Student's *t*-test. Data are representative of three independent experiments. CON = BEAS-2B cells treated with PBS control; NTHi = BEAS-2B cells treated with NTHi.

4.3. Conclusion

The clinical success of HDACi as a single agent in the treatment of solid tumors continues to remain elusive. Approaches currently exploited to make this achievable include: i) using a non-hydroxamate ZBG[40], ii) having a targeting group attached to the surface recognition group,[19a] iii) making dual acting conjugates comprising a cytotoxic component and HDACi template,[19a] and iv) using a prodrug approach.[41] Herein, we described compounds that potently and selectively inhibit COX-2 while also maintaining strong anti-HDAC activity. In addition to exploiting the anticancer effects of the two enzyme inhibitory templates in our design, we anticipate that these compounds

may show selective localization in tumors as seen with other conjugates comprising a COX-2-selective inhibitor and a fluorophore.[18a, 18c, 22b, 42] This approach has led to the discovery of compounds with strong growth inhibitory activities in various cancer cell lines with a strong preference for androgen-dependent prostate cancer cell line (LNCaP). While the selectivity towards LNCaP is not fully understood, we postulate that it could be a consequence of the effect of COX-2 and HDAC inhibition on AR functions. Previous studies on the effect of NSAIDs on AR in LNCaP suggest that COX-2 inhibition led to induction of the transcription factor c-jun, which in turn results in inhibition of AR activity.[12] HDAC inhibition on the other hand, leads to decreased AR expression.[35]

Compared to SAHA, our lead compounds (**2b**, **2c**, **8**, **11b**, **17b** and **17c**) showed superior *in vitro* therapeutic index in all cancer cell lines relative to the positive control VERO. Compounds **8** and **11b** are particularly impressive in this regard, with about a ten-fold increase in selective cytotoxicity towards LNCaP relative to VERO. Lastly, we observed significant differences in the perturbation of cell cycle progression by compounds **2b**, **11b** and **17b**, compared to SAHA, celecoxib and indomethacin that may be due to their combined effects on COX-2 and HDAC.

4.4. Materials and methods

All commercially available starting materials were used without further purification. Indomethacin was purchased from TCI America (OR, USA). Reaction solvents were either high performance liquid chromatography (HPLC) grade or American Chemical Society (ACS) grade and used without further purification. Analtech silica gel plates (60 F_{254}) were used for analytical TLC, and Analtech preparative TLC plates (UV 254, 2000 μm) were used for purification. UV

light was used to examine the spots. 200-400 mesh silica gel was used in column chromatography. For NMR spectra, Varian-Gemini 400 MHz or Bruker 500 MHz magnetic resonance spectrometer was used. ^{1}H NMR spectra were recorded in parts per million (ppm) relative to the peak of $CDCl_3$, (7.26 ppm), CD_3OD (3.31 ppm), or DMSO-d6 (2.49 ppm). ^{13}C spectra were recorded relative to the central peak of the $CDCl_3$ triplet (77.0 ppm), CD_3OD (49.0 ppm), or the DMSO-d6 septet (39.7 ppm) and were recorded with complete heterodecoupling. Multiplicities are described using the abbreviations: s, singlet; d, doublet, t, triplet; q, quartet; m, multiplet. High-resolution mass spectra were recorded at the Georgia Institute of Technology mass spectrometry facility in Atlanta. HPLC was used to establish the purity of the compounds to be >95 %. The HPLC analyses were done on a Beckman Coulter instrument with a Phenomenex RP C-18 column (250 mm × 4.6 mm), using 0.1% TFA in water (solvent A) and 0.1 % TFA in acetonitrile (solvent B), starting with 70% B for 5 min, then a gradient decrease of 70−10 % of B over 20 min. The flow rate was 1.0 ml/min and detection was at 280 nm. 4-Ethynyl-benzyl methylsulfonate **13**, trityl-protected azide and amine linkers were made as previously described[43].

Du-145, LNCaP, Vero and A549 cell lines were purchased from ATCC (Manassas, VA), while MCF-7 and HCT-116 were generous a gifts from Dr. Al Merrill's and Dr. Julia Kubanek's laboratories respectively, at Georgia Institute of technology, Atlanta, GA. Cell cultures were maintained in an incubator at 37 ^{0}C under a 5 % CO_2 atmosphere. Mouse antiacetylated α- tubulin antibody was obtained from Invitrogen (Life Technologies, Grand Island, NY, USA), rabbit antiactin, and rabbit antitubulin α antibodies were purchased from Sigma-Aldrich (St. Louis, MO, USA), AR antibody was purchased from Cell Signaling, while COX-2 antibody was purchased from Cayman chemicals. Secondary antibodies, goat antirabbit conjugated to IRDye680, and goat antimouse conjugated to IRDye800 were purchased from LI-COR Biosciences (Lincoln, NE,

USA). The CellTiter 96 Aqueous One Solution Cell Proliferation assay (MTS) kit was purchased from Promega (Madison, WI, USA).

4.4.1. Cell viability assay

All cell lines used in this study (Du-145, LNCaP, HCT-116, A549, MCF-7 and Vero) were maintained in the respective media recommended by ATCC. All the media used were supplemented with 10% fetal bovine serum (FBS) (Atlanta Biologicals, Atlanta, GA) and 1% *Pen. Strep*. Prior to treatment with various drug concentrations and subsequent incubation for 72 hours, cells were incubated in a 96 well plate for 24 hours. Cell viability was measured using the MTS assay protocol as described by the manufacturer. For all drugs tested, DMSO concentration was maintained at 0.1% for experiments in LNCaP, HCT-116 and DU-145; and at 1% for experiments in other cell lines. Data was analyzed using the LOGIT function. GRAPHPAD prism software was used to generate all growth-inhibition curves.

4.4.2. Cell cycle analysis

LNCaP cells were seeded onto 6-well plates at a density of 1×10^6 cells in 5 mL of media, and incubated in a humidified 5% CO_2 atmosphere at 37 °C overnight. Following aspiration of media, fresh media containing drugs were added to the cells and incubated for 24 h. After incubation, cells were trypsinized, harvested and fixed with 70% EtOH. Fixed cells were stained with freshly prepared PI solution containing RNAse A, and then analyzed on flow cytometer (BD

FACS Acuri, BD Bioscience, San Jose, CA, USA). Unstained cells were used as control. Each experiment was performed in triplicate.

4.4.3. Western blots analysis

LNCaP cells (10^6 cells/dish) were seeded in petri dishes 24 hour prior to treatment with various concentrations of compounds for 24h. Thereafter, media was removed and cells were washed with chilled 1X PBS buffer and resuspended in CelLyticM buffer containing a cocktail of protease inhibitor (Sigma-Aldrich, St. Louis, MO, USA). Protein concentration was determined through Bradford protein assay. Equal amount of protein was then loaded onto an SDS-page gel (Bio-Rad, Hercules, CA, USA) and resolved by electrophoresis at a constant voltage of 100 V for 2 h. The gel was transfered onto a nitrocellulose membrane and probed for acetylated tubulin, acetyl H4, AR, COX-2 and actin as loading control.

4.4.4. HDAC inhibition

The HDAC activity in presence of our compounds was assessed using the SAMDI mass spectrometry. As a label-free technique, SAMDI is compatible with a broad range of native peptide substrates without requiring potentially disruptive fluorophores. To obtain IC_{50} values, we incubated isoform-optimized substrates (20 μM for HDACs 1-2, 6 and 50 μM for HDAC 8) with enzyme (70 nM (HDAC 1), 100 nM (HDAC 2), 50 nM (HDAC 3), 60 nM (HDAC 6), 500 nM (HDAC 8)) and inhibitor (at concentrations ranging from 10 nM to 1.0 mM) in 96-well microtiter plates at 30 °C (24 h (HDAC 1), 24 h (HDAC 2), 5 h (HDAC 3), 20 h (HDAC 6), 2.5 h (HDAC

8)). Solution-phase deacetylation reactions were quenched with trichostatin A (TSA) and transferred to SAMDI plates to immobilize the substrate components. SAMDI plates were composed of an array of self-assembled monolayers (SAMs) presenting maleimide in standard 384-well format for high-throughput handling capability. Following immobilization, plates were washed to remove buffer constituents, enzyme, inhibitor, and any unbound substrate and analyzed by MALDI mass spectrometry using automated protocols[44]. Deacetylation yields in each triplicate sample were determined from the integrated peak intensities of the molecular ions for the substrate and the deacetylated product ion by taking the ratio of the former over the sum of both. Yields were plotted with respect to inhibitor concentration and fitted to obtain IC_{50} values for each isoform−inhibitor pair.

4.4.5. COX inhibition assay

In vitro COX inhibitory activity was evaluated using Cayman's COX Fluorescent Inhibitor Screening Assay Kit (Cayman Chemical Company, Ann Arbor, MI, USA) following the manufacturer's protocol. Briefly, ovine COX-1 and human recombinant COX-2 enzymes were incubated with stock solutions of our compounds and heme for 15 minutes at room temperature, after which a resorufin precursor was added and incubated for another 15 minutes at room temperature. The reaction was started by the adding arachidonic acid and left to proceed for 2 minutes. Fluorescence was measured at a 530 nm excitation wavelength and a 595 nm emission wavelength using a micro plate reader (Envision, PerkinElmer). Data was analyzed using the LOGIT function.

4.4.6. Molecular Docking Analysis

In silico docking was performed using Autodock Vina[45] run through PyRx to manage the workflow and PyMol to visualize the results, as described previously.[19d] Briefly, ligands were prepared by first generating an energy minimized 3D structure in ChemBioDraw3D. This was followed by processing with Autodock Tools 1.5.4. Docking runs were performed within a 25−30 Å cubic search space surrounding the binding pocket.

4.4.7. Intracellular PGE_2 measurement

HeLa cells ($3x10^5$ cells/dish) were seeded in 6-well plates 24 hours prior to treatment with various concentrations of tested compounds. After incubation for 24 hours, the cell culture media was taken and centrifuged at 14,000 x g for 10 minutes, to remove cellular debris. PGE_2 concentration was determined by using PGE_2 ELISA Kit-monoclonal (catalog number 514010). The assay was performed as recommended by the manufacturer. Briefly, serial dilution of PGE_2 standard and 50 µL of each sample were added to the recommended amount PGE_2 antiserum and acetylcholinesterase tracer and incubated at 4 ^{0}C for 18 hours. The wells were emptied and washed five times with wash buffer. Thereafter, 200 µL of Ellman's reagent containing substrate for acetylcholinesterase was added. The reaction was developed at room temperature for 2 hours on a slow shaker. Plates was read at 405 nm on a micro plate reader (Envision, PerkinElmer). Data was analyzed using the LOGIT function. GRAPHPAD prism software was used to generate graph and perform statistical analyses.

4.4.8. Anti-inflammatory activity assay

NF-κB activity was measured using luciferase assay. BEAS-2B cells were transfected with NF-κB luciferase reporter construct in pGL3 basic vector[46]. Forty hours after transfection, the cells were treated with test compounds for 1 hour followed by stimulation with NTHi for 5 hours. The cells were then lysed with cell lysis buffer (250 mM Tris-HCl (pH 7.5), 0.1% Triton-X, 1 mM DTT) and luciferase activity was measured by using luciferase assay system (Promega). Relative luciferase activity (RLA) was determined using the following equation: RLA = luciferase unit of the cells treated with NTHi and inhibitors/ luciferase unit of the cells treated with mock.

***N*-Hydroxy-6-((4-(5-(p-tolyl)-3-(trifluoromethyl)-*1H*-pyrazol-1-yl) phenyl) sulfonamido) hexanamide (2a)**. Triethylamine (0.02 ml, 0.175 mmol) was added to a solution of trityl-protected 6-aminohexanehydroxamic acid (0.05 g, 0.13 mmol) in $CHCl_3$ (10 ml) and left to stir under argon for 5 minutes. Thereafter, a solution of 4-(5-(p-tolyl)-3-(trifluoromethyl)-1H-pyrazol-1-yl) benzenesulfonyl chloride (0.05 g, 0.13 mmol) in anhydrous $CHCl_3$ (5 ml) was added and the reaction left to stir overnight. Reaction was quenched with water (20 ml) and extracted with DCM (20 ml) three times. Combined organic layers were dried over anhydrous sodium sulfate and concentrated in vacuo. Residue was purified with prep TLC to give 6-((4-(5-(p-tolyl)-3-(trifluoromethyl)-1H-pyrazol-1-yl) phenyl)sulfonamido)-*N*-(trityloxy)hexanamide an off-white solid (0.08 g, 0.10 mmol) which was immediately used for the next reaction without characterization.

To a solution of 6-((4-(5-(p-tolyl)-3-(trifluoromethyl)-*1H*-pyrazol-1-yl) phenyl)sulfonamido)-N-(trityloxy)hexanamide (0.08 g, 0.10 mmol) in anhydrous DCM (10 ml)

were added TFA (1.5 ml) and TIPS (0.75 ml). Reaction was stirred at room temperature for one hour. Solvent was evaporated and the resulting residue purified by prep TLC using DCM:Acetone:AcOH (2:1:0.1) to give **2a** as an off-white solid (0.03 g, 60%). HPLC retention time 16.22 minutes. ^{1}H NMR (400 MHz, CD_3OD) δ 7.90 (d, *J* = 8.5 Hz, 2H), 7.54 (d, *J* = 8.5 Hz, 2H), 7.21 (q, *J* = 8.2 Hz, 4H), 6.94 (s, 1H), 2.90 (t, *J* = 6.8 Hz, 2H), 2.38 (s, 3H), 2.09 (m, 2H), 1.60 (m, 2H), 1.54 – 1.45 (m, 2H), 1.34 (m, 2H).^{13}C NMR (101 MHz, CD_3OD) δ 145.7, 143.5, 142.6, 142.1, 140.7, 139.8, 129.2, 128.6, 127.6, 125.7, 124.4, 122.3, 105.6, 42.5, 28.9, 25.8, 25.6, 24.8, 19.9. HRMS (ESI) $[M + H]^+$ calculated for $[C_{23}H_{26}O_4N_4F_3S]^+$ was 511.1621, found 511.1608.

***N*-Hydroxy-7-((4-(5-(p-tolyl)-3-(trifluoromethyl)-*1H*-pyrazol-1-yl)phenyl)sulfonamido) heptanamide (2b)**. Trityl-protected 7-aminoheptanehydroxamic acid (0.05 g, 0.14 mmol) was reacted with 4-(5-(p-tolyl)-3-(trifluoromethyl)-*1H*-pyrazol-1-yl) benzenesulfonyl chloride (0.05 g, 0.13 mmol) in anhydrous $CHCl_3$ (5 ml) containing TEA (0.03 ml, 1.87 mmol) similar to compound **2a** above, to give 7-((4-(5-(p-tolyl)-3-(trifluoromethyl)-1H-pyrazol-1-yl)phenyl)sulfonamido)-*N*-(trityloxy) hexanamide as an off-white solid (0.08 g, 0.11 mmol) which was used for the next reaction (trityl deprotection) without characterization.

Trityl deprotection was done as described for **2a** in a DCM (10 ml) solution containing TFA (1.5 ml) and TIPS (0.75 ml). Purification was by prep TLC using DCM:Acetone:AcOH (2:1:0.1) to give **2b** as an off-white solid (0.05 g, 92%). HPLC retention time 16.22 minutes. ^{1}H NMR (500 MHz, CD_3OD) δ 7.89 (d, *J* = 8.1 Hz, 2H), 7.53 (d, *J* = 8.1 Hz, 2H), 7.21 (dd, *J* = 18.5, 7.7 Hz, 4H), 6.93 (s, 1H), 2.89 (t, *J* = 6.5 Hz, 2H), 2.37 (s, 3H), 2.10 (s, 2H), 1.60 (s, 2H), 1.47 (s, 2H), 1.32 (s, 5H). ^{13}C NMR (126 MHz, MeOD) δ 145.7, 143.7, 143.3, 142.2, 140.8, 139.7, 129.1,

128.7, 127.7, 125.8, 122.4, 120.2, 105.5, 42.6, 29.1, 28.2, 27.8, 25.9, 25.2, 19.9. HRMS (ESI) [M + H]$^+$ calculated for $[C_{24}H_{28}O_4N_4F_3S]^+$ was 525.1778, found 525.1771.

***N*-Hydroxy-7-((4-(5-(p-tolyl)-3-(trifluoromethyl)-*1H*-pyrazol-1-yl)phenyl)sulfonamido) octanamide (2c)**. Trityl-protected 8-aminooctanehydroxamic acid (0.06 g, 0.14 mmol) was reacted with 4-(5-(p-tolyl)-3-(trifluoromethyl)-1H-pyrazol-1-yl) benzenesulfonyl chloride (0.05 g, 0.13 mmol) in anhydrous $CHCl_3$ (5 ml) containing TEA (0.03 ml, 1.87 mmol) similar to compound **2a** above, to give 8-((4-(5-(p-tolyl)-3-(trifluoromethyl)-*1H*-pyrazol-1-yl)phenyl)sulfonamido)-*N*-(trityloxy) octanamide an off-white solid (0.09 g, 0.11mmol) which was used for the next reaction (trityl deprotection) without characterization.

Trityl deprotection was done as described for **2a** in a DCM (10 mL) solution containing TFA (1.5 ml) and TIPS (0.75 ml). Purification was by prep TLC using DCM:Acetone:AcOH (2:1:0.1) to give **2c** as an off-white solid (0.04 g, 71%). HPLC retention time 16.82 minutes. ^{1}H NMR (400 MHz, CD_3OD) δ 7.86 (d, *J* = 7.3 Hz, 2H), 7.50 (d, *J* = 7.6 Hz, 2H), 7.17 (dd, *J* = 14.9, 8.0 Hz, 4H), 6.91 (s, 1H), 2.85 (s, 2H), 2.34 (s, 3H), 1.58 (m, 2H), 1.43 (m, 2H), 1.26 (m, *J* = 14.1 Hz, 8H).^{13}C NMR (101 MHz, cd_3od) δ 145.7, 143.4, 143.1, 142.1, 140.7, 139.6, 129.2, 128.6, 127.6, 125.7, 122.5, 119.9, 105.5, 42.6, 29.1, 28.5, 28.4, 26.2, 25.7, 19.9. HRMS (ESI) [M + H]$^+$ calculated for $[C_{25}H_{30}O_4N_4F_3S]^+$ was 539.1934, found 539.1928.

1-(4-Sulfamoylphenyl)-5-(p-tolyl)-*1H*-pyrazole-3-carboxylic acid (5). Ethyl 1-(4-sulfamoylphenyl)-5-(p-tolyl)-*1H*-pyrazole-3-carboxylate (1.33 g, 3.31 mmol) was dissolved in THF (30 ml) and $LiOH.H_2O$ (0.21 g, 4.97 mmol) was added followed by 6 ml of H_2O. The reaction was left to stir at room temperature overnight. THF was evaporated off and product was precipitated off the resulting solution with 1N HCl. Precipitate was filtered and washed severally

with H_2O to give **(5)** as a white solid (1.14 g, 96%). ^{1}H NMR (400 MHz, DMSO-*d6*) δ 13.15 (s, 1H), 7.91 (d, *J* = 8.6 Hz, 2H), 7.56 (d, *J* = 8.8 Hz, 4H), 7.23 (q, *J* = 8.2 Hz, 4H), 7.09 (s, 1H), 2.34 (s, 3H). ^{13}C NMR (101 MHz, DMSO-*d6*) δ 163.9, 146.2, 145.6, 144.5, 142.6, 139.7, 130.4, 129.7, 127.8, 127.0, 126.8, 111.1, 21.8.

1-(4-(Methylsulfonyl)phenyl)-5-(p-tolyl)-*1H*-pyrazole-3-carboxylic acid (6). Ethyl 1-(4-(methylsulfonyl)phenyl)-5-(*p*-tolyl)-*1H*-pyrazole-3-carboxylate (0.42 g, 1.08 mmol) was reacted with $LiOH.H_2O$ (0.09 g, 2.16 mmol) following the same procedure for **5** above to give **6** as a white solid (0.38 g, 100 %). ^{1}H NMR (400 MHz, DMSO-*d6*) δ 8.03 (d, *J* = 8.7 Hz, 2H), 7.61 (d, *J* = 8.6 Hz, 2H), 7.26 – 7.17 (m, 4H), 7.09 (s, 1H), 3.31 (s, 3H), 2.33 (s, 3H). ^{13}C NMR (101 MHz, DMSO-*d6*) δ 163.4, 145.8, 145.1, 143.5, 140.6, 139.3, 129.9, 129.2, 128.7, 126.5, 126.3, 110.8, 43.7, 21.2.

***N*-(6-(Hydroxyamino)-6-oxohexyl)-1-(4-sulfamoylphenyl)-5-(*p*-tolyl)-*1H*-pyrazole-3-carboxamide (7a)**. EDCI (0.03 g, 0.17 mmol) and HOBT (0.02 g, 0.17 mmol) were added to a solution of 1-(4-sulfamoylphenyl)-5-(p-tolyl)-1H-pyrazole-3-carboxylic acid (**5**) (0.05 g, 0.14 mmol) in $CHCl_3$ (10 ml). The mixture was stirred at room temperature for 30 minutes after which trityl-protected 6-aminohexanehydroxamic acid (0.06 g, 0.154 mmol) was added, then left to stir overnight. The reaction was quenched with $NaHCO_3$ (20 ml) and extracted three times with DCM (20 ml). Combined organic layer was dried over anhydrous Na_2SO_4 and concentrated *in vacuo*. Crude product was purified by prep TLC using DCM:Acetone:AcOH (5:1:0.1) to give *N*-(6-oxo-6-(trityloxy)amino)hexyl)-1-(4-sulfamoylphenyl)-5-(p-tolyl)-*1H*-pyrazole-3-carboxamide, which was used for the next reaction (trityl deprotection) without characterization.

To a solution of *N*-(6-oxo-6-(trityloxy)amino)hexyl)-1-(4-sulfamoylphenyl)-5-(p-tolyl)-*1H*-pyrazole-3-carboxamide (0.06 g, 0.08 mmol) in anhydrous DCM (10 ml), TFA (1.5 ml) and

TIPS (0.75 ml) were added. Reaction was stirred at room temperature for one hour. Solvent was evaporated and the resulting residue purified by prep TLC using DCM:MeOH:AcOH (10:1:0.1) to give **7a** as an off white solid (0.03 g, 50 %). HPLC retention time 9.47 minutes ^{1}H NMR (500 MHz, DMSO-*d6*) δ 8.58 (s, 1H), 8.09 (d, *J* = 8.1 Hz, 2H), 7.75 (d, *J* = 8.4 Hz, 2H), 7.42 (dd, *J* = 18.1, 7.9 Hz, 4H), 7.20 (s, 1H), 5.98 (s, 1H), 3.47 (d, *J* = 5.5 Hz, 2H), 2.54 (s, 3H), 1.73 (m, *J* = 6.7 Hz, 3H), 1.47 (m, *J* = 14.0 Hz, 3H). ^{13}C NMR (126 MHz, DMSO-*d6*) δ 161.6, 148.7, 145.3, 144.3, 142.6, 139.3, 130.2, 129.5, 127.4, 126.6, 108.8, 55.8, 30.1, 29.8, 27.5, 26.8, 25.7, 25.1, 21.7. HRMS (ESI) $[M + H]^+$ calculated for $[C_{23}H_{28}O_5N_5S]^+$ was 486.1806, found 486.1804.

***N*-(7-(Hydroxyamino)-7-oxoheptyl)-1-(4-sulfamoylphenyl)-5-(*p*-tolyl)-*1H*-pyrazole-3-carboxamide (7b)**. Trityl-protected 7-aminoheptanehydroxamic acid (0.08 g, 0.16 mmol) was reacted with a solution of 1-(4-sulfamoylphenyl)-5-(p-tolyl)-1H-pyrazole-3-carboxylic acid (**5**) (0.05 g, 0.14 mmol), HOBT (0.02 g, 0.17 mmol) and EDCI (0.03 g, 0.17 mmol) in $CHCl_3$ (10 ml) similar to compound **7a** above, to give N-(7-oxo-7-((trityloxy)amino)heptyl)-1-(4-sulfamoylphenyl)-5-(p-tolyl)-*1H*-pyrazole-3-carboxamide as an brown solid (0.08 g, 0.11 mmol) which was used for the next reaction (trityl deprotection) without characterization.

Trityl deprotection was done as described for **7a**. Purification was by prep TLC using DCM:MeOH:AcOH (10:1:0.1) to give **7b** as a brown solid (0.02 g, 36 %). HPLC retention time 10.13 minutes ^{1}H NMR (500 MHz, DMSO-*d6*) δ 8.34 (s, 1H), 7.87 (d, *J* = 8.4 Hz, 2H), 7.53 (d, *J* = 8.4 Hz, 2H), 7.20 (dd, *J* = 18.1, 8.1 Hz, 4H), 6.98 (s, 1H), 3.25 (d, *J* = 3.3 Hz, 2H), 2.32 (s, 3H), 1.95 (m, 2H), 1.50 (m, 4H), 1.26 (m, *J* = 19.3 Hz, 4H). ^{13}C NMR (126 MHz, DMSO) δ 161.9, 149.1, 145.7, 144.5, 142.8, 139.7, 130.5, 129.7, 127.7, 127.3, 126.9, 109.2, 39.6, 30.3, 29.5, 27.3,

26.3, 26.2, 21.9. HRMS (ESI) $[M + H]^+$ calculated for $[C_{24}H_{30}O_5N_5S]^+$ was 500.1962, found 500.1956.

***N*-(8-(Hydroxyamino)-8-oxooctyl)-1-(4-sulfamoylphenyl)-5-(*p*-tolyl)-*1H*-pyrazole-3-carboxamide (7c)**. Trityl-protected 8-aminooctanehydroxamic acid (0.06 g, 0.15 mmol) was reacted with a solution of 1-(4-sulfamoylphenyl)-5-(p-tolyl)-1H-pyrazole-3-carboxylic acid (**5**) (0.05 g, 0.14 mmol), HOBT (0.02 g, 0.17 mmol) and EDCI (0.03 g, 0.17cmmol) in $CHCl_3$ (10 ml), as described for compound **7a** above, to give *N*-(8-oxo-8-((trityloxy)amino)octyl)-1-(4-sulfamoylphenyl)-5-(*p*-tolyl)-*1H*-pyrazole-3-carboxamide as an brown solid (0.08 g, 0.11 mmol) which was used for the next reaction (trityl deprotection) without characterization.

Trityl deprotection was done as described for **7a**. Purification was by prep TLC using DCM:MeOH:AcOH (10:1:0.1) to give **7c** as a brown solid (0.02 g, 36 %). HPLC retention time 10.92 minutes. ^{1}H NMR (500 MHz, DMSO-*d6*) δ 8.37 (s, 1H), 7.90 (d, *J* = 8.1 Hz, 2H), 7.56 (d, *J* = 8.1 Hz, 2H), 7.23 (dd, *J* = 18.1, 7.9 Hz, 4H), 7.01 (s, 1H), 3.28 (s, 2H), 2.35 (s, 3H), 1.97 (m, 2H), 1.54 (m, 4H), 1.29 (m, *J* = 21.0 Hz, 8H). ^{13}C NMR (126 MHz, DMSO) δ 161.3, 148.5, 144.9, 143.8, 142.1, 139.1, 129.9, 129.1, 127.2, 126.7, 126.2, 108.4, 35.3, 31.9, 29.6, 29.0, 28.2, 26.8, 21.3. HRMS (ESI) $[M + H]^+$ calculated for $[C_{25}H_{32}O_5N_5S]^+$ was 514.2119, found 514.2106.

***N*-(7-(Hydroxyamino)-7-oxoheptyl)-1-(4-(methylsulfonyl)phenyl)-5-(*p*-tolyl)-*1H*-pyrazole-3-carboxamide (8)**. Trityl-protected 7-aminoheptanehydroxamic acid (0.12 g, 0.31 mmol) was reacted with a solution of 1-(4-(methylsulfonyl)phenyl)-5-(*p*-tolyl)-*1H*-pyrazole-3-carboxylic acid **(6)** (0.10 g, 0.28 mmol), HOBT (0.04 g, 0.31 mmol) and EDCI (0.06 g, 0.30 mmol) in $CHCl_3$ (10 ml) as described for compound **7a** above, to give 1-(4-(methylsulfonyl)phenyl)-N-(7-oxo-7-

((trityloxy)amino)heptyl)-5-(p-tolyl)-1H-pyrazole-3-carboxamide as an brown solid (0.08 g, 0.11 mmol) which was used for the next reaction (trityl deprotection) without characterization.

Trityl deprotection was done as described for **7a**. Purification was by prep TLC using DCM:MeOH:AcOH (10:1:0.1) to give **8** as a brown solid (0.02 g, 36 %). HPLC retention time 11.13 minutes. ^{1}H NMR (400 MHz, dmso) δ 8.41 (s, 1H), 8.03 (d, *J* = 8.4 Hz, 2H), 7.63 (d, *J* = 8.4 Hz, 2H), 7.24 (q, *J* = 8.3 Hz, 4H), 7.01 (s, 1H), 3.31 (s, 3H), 2.35 (s, 3H), 2.04 (m, 2H), 1.93 (m, 2H), 1.54 (m, 4H), 1.31 (m, 4H). ^{13}C NMR (101 MHz, DMSO-*d6*) δ 156.2, 148.5, 144.9, 143.5, 140.4, 139.2, 129.9, 129.1, 128.5, 126.6, 126.3, 109.0, 105.0, 43.8, 32.3, 29.6, 28.7, 26.6, 25.6, 21.3. HRMS (ESI) $[M + H]^+$ calculated for $[C_{25}H_{31}O_5N_4S]^+$ was 499.2010, found 499.2010.

NHS-activated indomethacin (10). Disuccinimidyl carbonate (0.86 g, 3.35 mmol) was added to a mixture of indomethacin (1.00 g, 2.79 mmol) and TEA (0.50 ml, 3.35 mmol) in DCM (20 ml). The reaction was stirred at room temperature overnight. Solvent was evaporated off and the residue purified by column chromatography using DCM: Acetone (10:1) to give **10** as a white solid (1.04 g, 82 %). ^{1}H NMR (400 MHz, $CDCl_3$) δ 7.68 – 7.63 (m, 2H), 7.49 – 7.43 (m, 2H), 6.97 (d, *J* = 2.5 Hz, 1H), 6.94 – 6.89 (m, 1H), 6.69 (dd, *J* = 9.0, 2.5 Hz, 1H), 3.96 (s, 2H), 3.85 (s, 3H), 2.80 (s, 4H), 2.37 (s, 3H). ^{13}C NMR (101 MHz, $CDCl_3$) δ 169.1, 168.6, 166.5, 156.4, 139.6, 136.6, 133.9, 131.6, 130.9, 130.2, 129.3, 115.3, 112.8, 110.4, 100.9, 55.9, 27.4, 25.8, 13.7.

6-(2-(1-(4-Chlorobenzoyl)-5-hydroxy-2-methyl-*1H*-indol-3-yl)acetamido)-*N*-hydroxyhexanamide (11a). TEA (0.02 ml, 0.16 mmol) was added to a solution of NHS-activated indomethacin **10** (0.05 g, 0.11 mmol) and trityl-protected 7-aminoheptanehydroxamic acid (0.05 g, 0.12 mmol) in DCM (10 ml). The reaction was left to stir at room temperature for 3 hours. The reaction was quenched with water (20 ml) and extracted three times with DCM (20 ml). Combined

organic layer was dried over Na_2SO_4 and concentrated *in vacuo*. Residue obtained was purified by prep TLC using DCM: Acetone (10:1) to give 6-(2-(1-(4-chlorobenzoyl)-5-methoxy-2-methyl-*1H*-indol-3-yl)acetamido)-*N*-(trityloxy)hexanamide (0.07 g, 81 %) which was used for the next reaction (trityl deprotection) without characterization.

Trityl group deprotection was done by dissolving 6-(2-(1-(4-chlorobenzoyl)-5-methoxy-2-methyl-1H-indol-3-yl)acetamido)-*N*-(trityloxy)hexanamide in anhydrous DCM (10 ml) after which 1.5 mL TFA and 0.5 ml TIPS were added and the reaction was left to stir for 2 hours. Saturated $NaHCO_3$ solution (40 ml) was added to the reaction and extracted three times with DCM (20 ml) after gas evolution had ceased. Combined organic layer was dried over Na_2SO_4 and concentrated *in vacuo*. Crude residue was purified by prep TLC using DCM:Acetone:AcOH (2:1:0.1) to give **11a** as a light brown solid (0.07 g, 75 %). HPLC retention time 12.82 minutes. ^{1}H NMR (400 MHz, CD_3OD) δ 7.72 (d, *J* = 8.4 Hz, 2H), 7.58 (d, *J* = 8.4 Hz, 2H), 7.03 (d, *J* = 2.2 Hz, 1H), 6.95 (d, *J* = 9.0 Hz, 1H), 6.70 (dd, *J* = 9.0, 2.3 Hz, 1H), 3.86 – 3.80 (m, 3H), 3.62 (s, 2H), 3.22 (t, *J* = 6.7 Hz, 2H), 2.34 (s, 3H), 2.08 (s, 2H), 1.58 (d, *J* = 33.3 Hz, 4H), 1.32 (d, *J* = 9.7 Hz, 2H). ^{13}C NMR (101 MHz, CD_3OD) δ 168.6, 164.9, 156.2, 138.7, 135.7, 134.3, 131.0, 130.7, 128.8, 114.5, 113.5, 111.1, 104.4, 101.0, 54.8, 52.8, 39.1, 30.9, 28.6, 26.0, 24.9, 12.3. HRMS (ESI) $[M + H]^+$ calculated for $[C_{25}H_{29}O_5N_3Cl]^+$ was 486.1790, found 486.1782.

7-(2-(1-(4-Chlorobenzoyl)-5-methoxy-2-methyl-*1H*-indol-3-yl)acetamido)-*N*-hydroxyheptanamide (11b). Reaction of NHS-activated indomethacin **10** (0.10 g, 0.22 mmol) with trityl-protected 7-aminoheptanehydroxamic acid (0.10 g, 0.24 mmol) in DCM (10 ml) containing TEA (0.04 ml, 0.26 mmol), as described for **11a**, gave 7-(2-(1-(4-chlorobenzoyl)-5-methoxy-2-methyl-*1H*-indol-3-yl)acetamido)-*N*-(trityloxy)heptanamide (0.14 g, 87 %). Trityl

deprotection was achieved as described for **11a** to give **11b** as a light brown solid (0.14 g, 87 %). HPLC retention time 13.25 minutes. ^{1}H NMR (400 MHz, DMSO-*d6*) δ 10.40 (s, 1H), 8.77 (s, 1H), 8.09 (s, 1H), 7.70 (dd, *J* = 17.6, 8.5 Hz, 4H), 7.15 (d, *J* = 2.3 Hz, 1H), 6.97 (d, *J* = 9.0 Hz, 1H), 6.74 (dd, *J* = 9.0, 2.4 Hz, 1H), 3.83 – 3.76 (m, 3H), 3.52 (s, 2H), 3.40 (s, 1H), 3.07 (d, *J* = 5.9 Hz, 2H), 2.32 – 2.21 (m, 3H), 1.95 (t, *J* = 7.3 Hz, 2H), 1.46 (dd, *J* = 18.5, 11.6 Hz, 4H), 1.25 (m, 4H). ^{13}C NMR (101 MHz, DMSO-*d6*) δ 169.7, 169.1, 168.3, 156.0, 138.0, 135.6, 134.8, 131.6, 131.2, 131.0, 130.7, 129.6, 114.9, 111.6, 102.4, 55.8, 49.9, 32.7, 31.6, 29.4, 28.9, 26.6, 25.7, 14.0. HRMS (ESI) $[M + H]^+$ calculated for $[C_{26}H_{31}O_5N_3Cl]^+$ was 500.1947, found 500.1935.

8-(2-(1-(4-Chlorobenzoyl)-5-methoxy-2-methyl-*1H*-indol-3-yl)acetamido)-*N*-hydroxyoctanamide (11c). Reaction of NHS-activated indomethacin **10** (0.05 g, 0.11 mmol) with trityl-protected 7-aminoheptanehydroxamic acid (0.05 g, 0.12mmol) in DCM (10 ml) containing TEA (0.02 ml, 0.16 mmol), as described for **11a**, gave 8-(2-(1-(4-chlorobenzoyl)-5-methoxy-2-methyl-*1H*-indol-3-yl)acetamido)-*N*-(trityloxy)octanamide (0.08 g, 91 %). Trityl deprotection was achieved as described for **11a** to give **11c** as a light brown solid (0.02 g, 47 %). HPLC retention time 13.95 minutes. ^{1}H NMR (400 MHz, CD_3OD) δ 7.69 (d, *J* = 8.1 Hz, 2H), 7.55 (d, *J* = 8.1 Hz, 2H), 7.00 (s, 1H), 6.92 (d, *J* = 8.9 Hz, 1H), 6.67 (d, *J* = 8.7 Hz, 1H), 5.49 (s, 2H), 3.80 (s, 3H), 3.59 (s, 2H), 3.19 (d, *J* = 5.5 Hz, 2H), 2.31 (s, 3H), 1.52 (m, *J* = 28.6 Hz, 4H), 1.26 (m, *J* = 14.7 Hz, 8H). ^{13}C NMR (101 MHz, CD_3OD) δ 170.9, 169.2, 162.8, 158.5, 149.8, 147.4, 141.0, 138.0, 136.6, 133.2, 131.1, 116.8, 115.7, 113.6, 103.3, 57.1, 55.7, 44.5, 43.8, 41.4, 33.4, 31.0, 30.8, 28.8, 14.5. HRMS (ESI) $[M + H]^+$ calculated for $[C_{27}H_{33}O_5N_3Cl]^+$ was 514.2103, found 514.2087.

Methyl 2-(5-methoxy-2-methyl-*1H*-indol-3-yl)acetate (12). Indomethacin (3.00 g, 8.39 mmol) was dissolved in 1M NaOH (200 ml) and left to stir overnight. The reaction was acidified with 1M HCl and the precipitate filtered off. Filtrate was then extracted three times with DCM (100 ml). Combined organic layer was dried over Na_2SO_4 and concentrated *in vacuo* to give crude 2-(5-methoxy-2-methyl-*1H*-indol-3-yl)acetic acid (1.12 g, 5.15 mmol). The crude intermediate was dissolved in MeOH (50 ml) and TMSCl (1.86 ml, 14.73 mmol) was added. The reaction mixture was left to stir at room temperature overnight. Water (50 ml) was added to quench the reaction and extracted three times with DCM (50 ml). Organic layer was combined, dried over Na_2SO_4 and concentrated *in vacuo*. Residue obtained was purified by column chromatography using $CHCl_3$:EtOAc (10:1) to give **12** as a brown solid (0.99 g, 83 %). ^{1}H NMR (400 MHz, $CDCl_3$) δ 7.92 (s, 1H), 7.07 (d, *J* = 8.7 Hz, 1H), 7.01 (d, *J* = 2.0 Hz, 1H), 6.81 – 6.75 (m, 1H), 3.87 (d, *J* = 1.1 Hz, 3H), 3.68 (d, *J* = 1.0 Hz, 5H), 2.32 (s, 3H). ^{13}C NMR (101 MHz, $CDCl_3$) δ 172.8, 154.1, 133.7, 130.2, 129.0, 111.1, 110.8, 104.1, 100.4, 55.9, 51.9, 30.3, 11.7.

Methyl 2-(1-(4-ethynylbenzyl)-5-methoxy-2-methyl-*1H*-indol-3-yl)acetate (14). A solution of methyl 2-(5-methoxy-2-methyl-1H-indol-3-yl)acetate (**12**) (0.10 g, 0.43 mmol) and NaH (60 % dispersion in mineral oil) (0.03 g, 0.64 mmol) in anhydrous THF (10 ml) was cooled to 0 ^{0}C and left to stir for 20 minutes. The reaction was brought to room temperature, after which 4-ethynylbenzyl methanesulfonate (0.11 g, 0.51 mmol) was added, and left to stir overnight. Reaction mixture was poured into sat. NH_4Cl (10 ml) and extracted three times with DCM (15 ml). Combined organic layer was dried over Na_2SO_4 and concentrated *in vacuo*. Purification was by prep TLC using $CHCl_3$:Ether (20:1) to give **14** as a yellow solid (0.05 g, 31 %). ^{1}H NMR (400 MHz, $CDCl_3$) δ 7.41 (d, *J* = 8.0 Hz, 2H), 7.15 – 7.10 (m, 2H), 6.85 (d, *J* = 8.0 Hz, 2H), 6.80– 6.78 (m, 1H), 5.36 (s, 2H), 3.87 (s, 3H), 3.73 (s, 2H), 3.69 (s, 3H), 3.08 (s, 1H), 2.31 (s, 3H). ^{13}C NMR

(101 MHz, $CDCl_3$) δ 172.8, 154.1, 138.1, 135.0, 133.7, 130.2, 129.0, 128.0, 125.0, 121.6, 111.1, 110.8, 104.1, 100.4, 83.4, 55.9, 51.9, 46.8, 30.3, 11.7. HRMS (ESI) $[M + H]^+$ calculated for $[C_{22}H_{21}NO_3]^+$ was 347.1521, found 347.1529.

2-(1-(4-(1-(7-(Hydroxyamino)-7-oxoheptyl)-*1H*-1,2,3-triazol-4-yl)benzyl)-5-methoxy-2-methyl-*1H*-indol-3-yl)acetic acid (16). Methyl 2-(1-(4-ethynylbenzyl)-5-methoxy-2-methyl-*1H*-indol-3-yl)acetate (**14**) (0.074 g, 0.21 mmol), trityl-protected 7-azidoheptanehydroxamic acid (0.11 g, 0.26 mmol) and DIPEA (0.07 ml, 0.43 mmol) were dissolved in anhydrous THF (10 ml) and purged for 10 minutes at room temperature while stirring. CuI (0.02 g, 0.11 mmol) was then added with purging continued for another 20 minutes. The reaction was left to stir overnight. Reaction was quenched with a solution of 4:1 sat. NH_4Cl/NH_4OH (20 ml) and extracted with a mixture of 10% MeOH in DCM (3X) (20 ml). Combined organic layer was dried over anhydrous Na_2SO_4 and concentrated *in vacuo*. Purification was by prep TLC using 10:1 DCM:MeOH to give methyl 2-(5-methoxy-2-methyl-1-(4-(1-(7-oxo-7-((trityloxy)amino)heptyl)-*1H*-1,2,3-triazol-4-yl)benzyl)-*1H*-indol-3-yl)acetate (0.08 g, 51 %), which was used for the next reaction.

The product of the first step above was dissolved in a 4:1 $MeOH/H_2O$ mixture (5 ml). $LiOH.H_2O$ (0.0065 g, 0.16 mmol) was added to the solution which was left to stir for 6 hours. Solvent was evaporated off and the residue purified by prep TLC using EtOAc:hexanes:AcOH (2:1:0.1) to give 2-(5-methoxy-2-methyl-1-(4-(1-(7-oxo-7-((trityloxy)amino)heptyl)-*1H*-1,2,3-triazol-4-yl)benzyl)-*1H*-indol-3-yl)acetic acid (0.035 g, 45 %) as a yellow solid. Trityl deprotection was done as described for **11a**. Purification was done using 10:1:0.1 DCM:MeOH:AcOH to give **16** as a yellow solid (0.023 g, 96 %). HPLC retention time 10.62 minutes ^{1}H NMR (500 MHz, DMSO-*d6*) δ 10.38 (s, 1H), 8.53 (s, 1H), 7.76 (s, 2H), 7.29 (s, 1H),

7.06 (d, *J* = 18.4 Hz, 3H), 6.70 (d, *J* = 7.5 Hz, 1H), 5.40 (s, 2H), 4.40 (s, 2H), 3.80 (d, *J* = 22.4 Hz, 3H), 3.55 (s, 2H), 2.32 (s, 3H), 1.92 (d, *J* = 30.5 Hz, 2H), 1.49 (s, 2H), 1.28 (s, 5H). ^{13}C NMR (126 MHz, DMSO-*d6*) δ 184.2, 175.2, 171.2, 163.3, 156.1, 148.5, 144.5, 139.8, 136.8, 135.4, 131.5, 129.9, 124.8, 120.1, 115.3, 110.8, 91.9, 65.6, 59.5, 56.1, 39.6, 35.9, 35.0, 22.4, 15.0. HRMS (ESI) $[M + H]^+$ calculated for $[C_{28}H_{34}O_5N_5]^+$ was 520.2554, found 520.2549.

Methyl 2-(1-(4-(1-(6-(hydroxyamino)-6-oxohexyl)-*1H*-1,2,3-triazol-4-yl)benzyl)-5-methoxy-2-methyl-*1H*-indol-3-yl)acetate (17a). Reaction of methyl 2-(1-(4-ethynylbenzyl)-5-methoxy-2-methyl-*1H*-indol-3-yl)acetate (**14**) (0.070 g, 0.20 mmol) with trityl-protected 6-azidohexanehydroxamic acid (0.10 g, 0.24 mmol) in the presence of DIPEA (0.070 ml, 0.43 mmol) and CuI (0.019 g, 0.10 mmol) in THF (10 ml), as described above for **16**, gave methyl 2-(5-methoxy-2-methyl-1-(4-(1-(6-oxo-6-((trityloxy)amino)hexyl)-*1H*-1,2,3-triazol-4-yl)benzyl)-*1H*-indol-3-yl)acetate (0.075 g, 49 %). Trityl deprotection was achieved as described for **11a**. Purification was done by prep TLC using 10:1 DCM:MeOH to give **17a** as a brown solid (0.042 g, 40 %). HPLC retention time 12.88 minutes ^{1}H NMR (400 MHz, CD_3OD) δ 8.13 (s, 1H), 7.62 (d, J = 8.1 Hz, 2H), 7.08 (d, *J* = 8.8 Hz, 1H), 6.96 (dd, *J* = 11.0, 5.2 Hz, 3H), 6.67 (dd, *J* = 8.8, 2.3 Hz, 1H), 5.26 (s, 2H), 4.33 (t, *J* = 6.9 Hz, 2H), 3.76 (s, 3H), 3.71 – 3.65 (m, 2H), 3.62 (s, 3H), 2.25 (s, 3H), 2.03 (t, *J* = 7.2 Hz, 2H), 1.60 (dt, *J* = 14.9, 7.3 Hz, 2H), 1.32 – 1.18 (m, 4H). ^{13}C NMR (101 MHz, CD_3OD) δ 173.2, 171.5, 153.9, 138.4, 134.9, 131.8, 128.1, 126.3, 125.3, 120.6, 110.1, 109.3, 100.0, 54.8, 50.9, 49.9, 45.7, 31.7, 29.9, 29.7, 25.4, 24.5, 8.9. HRMS (ESI) $[M + H]^+$ calculated for $[C_{28}H_{34}O_5N_5]^+$ was 520.2554, found 520.2543.

Methyl 2-(1-(4-(1-(7-(hydroxyamino)-7-oxoheptyl)-*1H*-1,2,3-triazol-4-yl)benzyl)-5-methoxy-2-methyl-*1H*-indol-3-yl)acetate (17b). Trityl deprotection of methyl 2-(5-methoxy-2-methyl-1-(4-(1-(7-oxo-7-((trityloxy)amino)heptyl)-*1H*-1,2,3-triazol-4-yl)benzyl)-*1H*-indol-3-yl)acetate (0.074 g, 0.095 mmol), an intermediate obtained during the synthesis of **16** above, was achieved as described for **11a**. Purification was done by prep TLC using 10:1 DCM:MeOH to give **17b** as a brown solid (0.025 g, 49 %). HPLC retention time 8.48 minutes ^{1}H NMR (500 MHz, CD_3OD) δ 8.24 (s, 1H), 7.69 (d, *J* = 8.0 Hz, 2H), 7.14 (d, *J* = 8.8 Hz, 1H), 7.04 – 6.98 (m, 3H), 6.72 (dd, *J* = 8.8, 2.1 Hz, 1H), 5.36 (s, 2H), 4.40 (t, *J* = 6.8 Hz, 2H), 3.81 (s, 3H), 3.75 (s, 2H), 3.67 (s, 3H), 2.32 (s, 3H), 2.06 (m, 2H), 1.60 (m, 2H), 1.35 (m, 5H). ^{13}C NMR (126 MHz, CD_3OD) δ 173.4, 171.3, 154.3, 147.3, 138.6, 135.0, 131.8, 129.4, 128.2, 126.3, 125.5, 120.7, 110.3, 109.5, 104.2, 100.2, 55.0, 51.3, 50.0, 45.9, 29.7, 28.9, 28.0, 25.8, 25.1, 9.0. HRMS (ESI) $[M + H]^+$ calculated for $[C_{29}H_{36}O_5N_5]^+$ was 534.2711, found 534.2705.

Methyl 2-(1-(4-(1-(8-(hydroxyamino)-8-oxooctyl)-*1H*-1,2,3-triazol-4-yl)benzyl)-5-methoxy-2-methyl-*1H*-indol-3-yl)acetate (17c). Reaction of methyl 2-(1-(4-ethynylbenzyl)-5-methoxy-2-methyl-1H-indol-3-yl)acetate (**14**) (0.074 g, 0.21 mmol) with trityl-protected 8-azidooctanehydroxamic acid (0.11 g, 0.26 mmol) in the presence of DIPEA (0.07 ml, 0.43 mmol) and CuI (0.02 g, 0.11 mmol) in THF (10 ml), as described above for **16**, gave methyl 2-(5-methoxy-2-methyl-1-(4-(1-(8-oxo-8-((trityloxy)amino)octyl)-*1H*-1,2,3-triazol-4-yl)benzyl)-*1H*-indol-3-yl)acetate (0.026 g, 16 %). Trityl deprotection was achieved as described for **11a**. Purification was done by prep TLC using 10:1 DCM:MeOH to give **17c** as a brown solid (0.017 g, 92 %). HPLC retention time 9.92 minutes ^{1}H NMR (500 MHz, CD_3OD) δ 8.26 (s, 1H), 7.72 (d, *J* = 7.2 Hz, 2H), 7.16 (d, *J* = 8.7 Hz, 1H), 7.04 (s, 3H), 6.74 (d, *J* = 8.6 Hz, 1H), 5.38 (s, 2H), 4.42 (s, 2H), 3.83 (s, 3H), 3.77 (s, 2H), 3.69 (s, 3H), 2.34 (s, 4H), 1.95 (s, 2H), 1.61 (s, 2H), 1.34 (ms, *J* = 24.6 Hz, 8H).

^{13}C NMR (126 MHz, CD_3OD) δ 175.3, 170.3, 156.4, 149.2, 140.7, 137.1, 133.8, 131.5, 130.3, 128.4, 127.5, 122.8, 112.4, 111.6, 106.2, 102.3, 57.1, 53.1, 52.1, 48.0, 31.8, 30.8, 30.3, 28.1, 27.4, 24.7, 11.1. HRMS (ESI) $[M + H]^+$ calculated for $[C_{30}H_{38}O_5N_5]^+$ was 548.2867, found 548.2855.

4.5. References

1. (a) Bowman, G. D.; Poirier, M. G., Post-Translational Modifications of Histones That Influence Nucleosome Dynamics. *Chem. Rev.* **2014**, 115 (6) 2274-2295; (b) Minucci, S.; Pelicci, P. G., Histone deacetylase inhibitors and the promise of epigenetic (and more) treatments for cancer. *Nat. Rev. Cancer* **2006,** *6* (1), 38-51.

2. West, A. C.; Johnstone, R. W., New and emerging HDAC inhibitors for cancer treatment. *The Journal of Clinical Investigation* **2014,** *124* (1), 30-39.

3. (a) Gryder, B. E.; Sodji, Q. H.; Oyelere, A. K., Targeted cancer therapy: giving histone deacetylase inhibitors all they need to succeed. *Future Med. Chem.* **2012,** *4* (4), 505-524; (b) Zhang, L.; Han, Y.; Jiang, Q.; Wang, C.; Chen, X.; Li, X.; Xu, F.; Jiang, Y.; Wang, Q.; Xu, W., Trend of Histone Deacetylase Inhibitors in Cancer Therapy: Isoform Selectivity or Multitargeted Strategy. *Med. Res. Rev.* **2015,** *35* (1), 63-84.

4. Weichert, W., HDAC expression and clinical prognosis in human malignancies. *Cancer Lett.* **2009,** *280* (2), 168-176.

5. Ratner, M., Small biotech steers HDAC inhibitor to clinic. *Nat Biotech* **2014,** *32* (9), 853-854.

6. Shah, M. H.; Binkley, P.; Chan, K.; Xiao, J.; Arbogast, D.; Collamore, M.; Farra, Y.; Young, D.; Grever, M., Cardiotoxicity of Histone Deacetylase Inhibitor Depsipeptide in Patients with Metastatic Neuroendocrine Tumors. *Clin. Cancer Res.* **2006,** *12* (13), 3997-4003.

7. (a) Tondera, C.; Ullm, S.; Laube, M.; Meister, S.; Neuber, C.; Mosch, B.; Kniess, T.; Pietzsch, J., Optical imaging of COX-2: Studies on an autofluorescent 2,3-diaryl-substituted indole-based cyclooxygenase-2 inhibitor. *Biochem. Biophys. Res. Commun.* **2015,** (0); (b) Toomey, D. P.; Murphy, J. F.; Conlon, K. C., COX-2, VEGF and tumour angiogenesis. *The Surgeon* **2009,** *7* (3), 174-180.

8. Smith, W. L.; Garavito, R. M.; DeWitt, D. L., Prostaglandin Endoperoxide H Synthases (Cyclooxygenases)-1 and −2. *J. Biol. Chem.* **1996,** *271* (52), 33157-33160.

9. Yuan, C.; Smith, W. L., A Cyclooxygenase-2 Dependent Prostaglandin E2 Biosynthetic System in the Golgi Apparatus. *J. Biol. Chem.* **2014**.

10. Funk, C. D., Prostaglandins and Leukotrienes: Advances in Eicosanoid Biology. *Science* **2001,** *294* (5548), 1871-1875.

11. Fischer, S. M.; Hawk, E. T.; Lubet, R. A., Coxibs and Other Nonsteroidal Anti-Inflammatory Drugs in Animal Models of Cancer Chemoprevention. *Cancer Prevention Research* **2011,** *4* (11), 1728-1735.

12. Pan, Y.; Zhang, J.-S.; Gazi, M. H.; Young, C. Y. F., The Cyclooxygenase 2-specific Nonsteroidal Anti-inflammatory Drugs Celecoxib and Nimesulide Inhibit Androgen Receptor Activity via Induction of c-Jun in Prostate Cancer Cells. *Cancer Epidemiology Biomarkers & Prevention* **2003,** *12* (8), 769-774.

13. (a) Kashiwagi, E.; Shiota, M.; Yokomizo, A.; Inokuchi, J.; Uchiumi, T.; Naito, S., EP2 signaling mediates suppressive effects of celecoxib on androgen receptor expression and cell

proliferation in prostate cancer. *Prostate Cancer Prostatic Dis.* **2014,** *17* (1), 10-17; (b) Kashiwagi, E.; Shiota, M.; Yokomizo, A.; Itsumi, M.; Inokuchi, J.; Uchiumi, T.; Naito, S., Prostaglandin receptor EP3 mediates growth inhibitory effect of aspirin through androgen receptor and contributes to castration resistance in prostate cancer cells. *Endocr. Relat. Cancer* **2013,** *20* (3), 431-441.

14. Jendrossek, V., Targeting apoptosis pathways by Celecoxib in cancer. *Cancer Lett.* **2013,** *332* (2), 313-324.

15. Li, N.; Xi, Y.; Tinsley, H. N.; Gurpinar, E.; Gary, B. D.; Zhu, B.; Li, Y.; Chen, X.; Keeton, A. B.; Abadi, A. H.; Moyer, M. P.; Grizzle, W. E.; Chang, W.-C.; Clapper, M. L.; Piazza, G. A., Sulindac Selectively Inhibits Colon Tumor Cell Growth by Activating the cGMP/PKG Pathway to Suppress Wnt/β-Catenin Signaling. *Mol. Cancer Ther.* **2013,** *12* (9), 1848-1859.

16. Patel, M. I.; Subbaramaiah, K.; Du, B.; Chang, M.; Yang, P.; Newman, R. A.; Cordon-Cardo, C.; Thaler, H. T.; Dannenberg, A. J., Celecoxib Inhibits Prostate Cancer Growth: Evidence of a Cyclooxygenase-2-Independent Mechanism. *Clin. Cancer Res.* **2005,** *11* (5), 1999-2007.

17. Masferrer, J. L.; Leahy, K. M.; Koki, A. T.; Zweifel, B. S.; Settle, S. L.; Woerner, B. M.; Edwards, D. A.; Flickinger, A. G.; Moore, R. J.; Seibert, K., Antiangiogenic and Antitumor Activities of Cyclooxygenase-2 Inhibitors. *Cancer Res.* **2000,** *60* (5), 1306-1311.

18. (a) Zhang, H.; Fan, J.; Wang, J.; Zhang, S.; Dou, B.; Peng, X., An Off-On COX-2-Specific Fluorescent Probe: Targeting the Golgi Apparatus of Cancer Cells. *J. Am. Chem. Soc.* **2013,** *135* (31), 11663-9; (b) Zhang, H.; Fan, J.; Wang, J.; Dou, B.; Zhou, F.; Cao, J.; Qu, J.; Cao, Z.; Zhao, W.; Peng, X., Fluorescence Discrimination of Cancer from Inflammation by Molecular Response to COX-2 Enzymes. *J. Am. Chem. Soc.* **2013**; (c) Uddin, M. J.; Crews, B. C.; Ghebreselasie, K.;

Daniel, C. K.; Kingsley, P. J.; Xu, S.; Marnett, L. J., Targeted imaging of cancer by fluorocoxib C, a near-infrared cyclooxygenase-2 probe. *BIOMEDO* **2015,** *20* (5), 050502-050502.

19. (a) Musso, L.; Dallavalle, S.; Zunino, F., Perspectives in the development of hybrid bifunctional antitumour agents. *Biochem. Pharmacol.* **2015,** *96* (4), 297-305; (b) Guerrant, W.; Patil, V.; Canzoneri, J. C.; Oyelere, A. K., Dual Targeting of Histone Deacetylase and Topoisomerase II with Novel Bifunctional Inhibitors. *J. Med. Chem.* **2012,** *55* (4), 1465-1477; (c) Gryder, B. E.; Akbashev, M. J.; Rood, M. K.; Raftery, E. D.; Meyers, W. M.; Dillard, P.; Khan, S.; Oyelere, A. K., Selectively targeting prostate cancer with antiandrogen equipped histone deacetylase inhibitors. *ACS Chem. Biol.* **2013,** *8* (11), 2550-60; (d) Gryder, B. E.; Rood, M. K.; Johnson, K. A.; Patil, V.; Raftery, E. D.; Yao, L.-P. D.; Rice, M.; Azizi, B.; Doyle, D. F.; Oyelere, A. K., Histone Deacetylase Inhibitors Equipped with Estrogen Receptor Modulation Activity. *J. Med. Chem.* **2013,** *56* (14), 5782-5796.

20. (a) Neumann, W.; Crews, B. C.; Sarosi, M. B.; Daniel, C. M.; Ghebreselasie, K.; Scholz, M. S.; Marnett, L. J.; Hey-Hawkins, E., Conjugation of cisplatin analogues and cyclooxygenase inhibitors to overcome cisplatin resistance. *ChemMedChem* **2015,** *10* (1), 183-92; (b) Zhang, G.; Panigrahy, D.; Hwang, S. H.; Yang, J.; Mahakian, L. M.; Wettersten, H. I.; Liu, J.-Y.; Wang, Y.; Ingham, E. S.; Tam, S.; Kieran, M. W.; Weiss, R. H.; Ferrara, K. W.; Hammock, B. D., Dual inhibition of cyclooxygenase-2 and soluble epoxide hydrolase synergistically suppresses primary tumor growth and metastasis. *Proceedings of the National Academy of Sciences* **2014**.

21. Wang, X.; Li, G.; Wang, A.; Zhang, Z.; Merchan, J. R.; Halmos, B., Combined histone deacetylase and cyclooxygenase inhibition achieves enhanced antiangiogenic effects in lung cancer cells. *Mol. Carcinog.* **2013,** *52* (3), 218-228.

22. (a) Uddin, M. J.; Crews, B. C.; Ghebreselasie, K.; Tantawy, M. N.; Marnett, L. J., [123I]-Celecoxib Analogues as SPECT Tracers of Cyclooxygenase-2 in Inflammation. *ACS Med. Chem. Lett.* **2010,** *2* (2), 160-164; (b) Bhardwaj, A.; Kaur, J.; Wuest, F.; Knaus, E. E., Fluorophore-Labeled Cyclooxygenase-2 Inhibitors for the Imaging of Cyclooxygenase-2 Overexpression in Cancer: Synthesis and Biological Studies. *ChemMedChem* **2014,** *9* (1), 109-116.

23. Uddin, M. J.; Crews, B. C.; Ghebreselasie, K.; Marnett, L. J., Design, Synthesis, and Structure-Activity Relationship Studies of Fluorescent Inhibitors of Cycloxygenase-2 as Targeted Optical Imaging Agents. *Bioconjug. Chem.* **2013,** *24* (4), 712-723.

24. Mwakwari, S. C.; Guerrant, W.; Patil, V.; Khan, S. I.; Tekwani, B. L.; Gurard-Levin, Z. A.; Mrksich, M.; Oyelere, A. K., Non-Peptide Macrocyclic Histone Deacetylase Inhibitors Derived from Tricyclic Ketolide Skeleton. *J. Med. Chem.* **2010,** *53* (16), 6100-6111.

25. Szabó, G.; Fischer, J.; Kis-Varga, Á.; Gyires, K., New Celecoxib Derivatives as Anti-Inflammatory Agents. *J. Med. Chem.* **2007,** *51* (1), 142-147.

26. Rogez-Florent, T.; Meignan, S.; Foulon, C.; Six, P.; Gros, A.; Bal-Mahieu, C.; Supuran, C. T.; Scozzafava, A.; Frédérick, R.; Masereel, B.; Depreux, P.; Lansiaux, A.; Goossens, J.-F.; Gluszok, S.; Goossens, L., New selective carbonic anhydrase IX inhibitors: Synthesis and pharmacological evaluation of diarylpyrazole-benzenesulfonamides. *Bioorg. Med. Chem.* **2013,** *21* (6), 1451-1464.

27. Dwivedi, A. K.; Gurjar, V.; Kumar, S.; Singh, N., Molecular basis for nonspecificity of nonsteroidal anti-inflammatory drugs (NSAIDs). *Drug Discovery Today* **2015,** *20* (7), 863-873.

28. Bhardwaj, A.; Kaur, J.; Sharma, S. K.; Huang, Z.; Wuest, F.; Knaus, E. E., Hybrid fluorescent conjugates of COX-2 inhibitors: Search for a COX-2 isozyme imaging cancer biomarker. *Bioorg. Med. Chem. Lett.* **2013,** *23* (1), 163-168.

29. Liedtke, A. J.; Adeniji, A. O.; Chen, M.; Byrns, M. C.; Jin, Y.; Christianson, D. W.; Marnett, L. J.; Penning, T. M., Development of Potent and Selective Indomethacin Analogues for the Inhibition of AKR1C3 (Type 5 17 beta-Hydroxysteroid Dehydrogenase/Prostaglandin F Synthase) in Castrate-Resistant Prostate Cancer. *J. Med. Chem.* **2013,** *56* (6), 2429-2446.

30. Gadgeel, S. M., Cyclooxygenase 2 inhibition in patients with non-small cell lung cancer: Is this still a valid target for therapy? *Cancer* **2015**, n/a-n/a.

31. Tang, G.; Wong, J. C.; Zhang, W.; Wang, Z.; Zhang, N.; Peng, Z.; Zhang, Z.; Rong, Y.; Li, S.; Zhang, M.; Yu, L.; Feng, T.; Zhang, X.; Wu, X.; Wu, J. Z.; Chen, L., Identification of a Novel Aminotetralin Class of HDAC6 and HDAC8 Selective Inhibitors. *J. Med. Chem.* **2014**.

32. Yamaguchi, K.; Lantowski, A.; Dannenberg, A. J.; Subbaramaiah, K., Histone Deacetylase Inhibitors Suppress the Induction of c-Jun and Its Target Genes Including COX-2. *J. Biol. Chem.* **2005,** *280* (38), 32569-32577.

33. Agarwal, B.; Swaroop, P.; Protiva, P.; Raj, S. V.; Shirin, H.; Holt, P. R., Cox-2 is needed but not sufficient for apoptosis induced by Cox-2 selective inhibitors in colon cancer cells. *Apoptosis 8* (6), 649-654.

34. Feldman, B. J.; Feldman, D., The development of androgen-independent prostate cancer. *Nat. Rev. Cancer* **2001,** *1* (1), 34-45.

35. Marrocco, D. L.; Tilley, W. D.; Bianco-Miotto, T.; Evdokiou, A.; Scher, H. I.; Rifkind, R. A.; Marks, P. A.; Richon, V. M.; Butler, L. M., Suberoylanilide hydroxamic acid (vorinostat) represses androgen receptor expression and acts synergistically with an androgen receptor antagonist to inhibit prostate cancer cell proliferation. *Mol. Cancer Ther.* **2007,** *6* (1), 51-60.

36. Lu, X.-Y.; Wang, Z.-C.; Ren, S.-Z.; Shen, F.-Q.; Man, R.-J.; Zhu, H.-L., Coumarin sulfonamides derivatives as potent and selective COX-2 inhibitors with efficacy in suppressing cancer proliferation and metastasis. *Bioorg. Med. Chem. Lett.* **2016,** *26* (15), 3491-3498.

37. Lawrence, T., The Nuclear Factor NF-κB Pathway in Inflammation. *Cold Spring Harb. Perspect. Biol.* **2009,** *1* (6).

38. Tapadar, S.; Fathi, S.; Raji, I.; Omesiete, W.; Kornacki, J. R.; Mwakwari, S. C.; Miyata, M.; Mitsutake, K.; Li, J.-D.; Mrksich, M.; Oyelere, A. K., A structure–activity relationship of non-peptide macrocyclic histone deacetylase inhibitors and their anti-proliferative and anti-inflammatory activities. *Bioorg. Med. Chem.* **2015,** *23* (24), 7543-7564.

39. (a) Takada, Y.; Bhardwaj, A.; Potdar, P.; Aggarwal, B. B., Nonsteroidal anti-inflammatory agents differ in their ability to suppress NF-[kappa]B activation, inhibition of expression of cyclooxygenase-2 and cyclin D1, and abrogation of tumor cell proliferation. *Oncogene* **2004,** *23* (57), 9247-9258; (b) TEGEDER, I.; PFEILSCHIFTER, J.; GEISSLINGER, G., Cyclooxygenase-independent actions of cyclooxygenase inhibitors. *The FASEB Journal* **2001,** *15* (12), 2057-2072.

40. Schroeder, F. A.; Lewis, M. C.; Fass, D. M.; Wagner, F. F.; Zhang, Y.-L.; Hennig, K. M.; Gale, J.; Zhao, W.-N.; Reis, S.; Barker, D. D.; Berry-Scott, E.; Kim, S. W.; Clore, E. L.; Hooker, J. M.; Holson, E. B.; Haggarty, S. J.; Petryshen, T. L., A Selective HDAC 1/2 Inhibitor Modulates Chromatin and Gene Expression in Brain and Alters Mouse Behavior in Two Mood-Related Tests. *PLoS One* **2013,** *8* (8), e71323.

41. (a) Daniel, K. B.; Sullivan, E. D.; Chen, Y.; Chan, J. C.; Jennings, P. A.; Fierke, C. A.; Cohen, S. M., Dual-Mode HDAC Prodrug for Covalent Modification and Subsequent Inhibitor Release. *J. Med. Chem.* **2015,** *58* (11), 4812-4821; (b) Ueki, N.; Lee, S.; Sampson, N. S.; Hayman,

M. J., Selective cancer targeting with prodrugs activated by histone deacetylases and a tumour-associated protease. *Nat Commun* **2013,** *4*.

42. Uddin, M. J.; Crews, B. C.; Blobaum, A. L.; Kingsley, P. J.; Gorden, D. L.; McIntyre, J. O.; Matrisian, L. M.; Subbaramaiah, K.; Dannenberg, A. J.; Piston, D. W.; Marnett, L. J., Selective Visualization of Cyclooxygenase-2 in Inflammation and Cancer by Targeted Fluorescent Imaging Agents. *Cancer Res.* **2010,** *70* (9), 3618-3627.

43. (a) Sodji, Q. H.; Kornacki, J. R.; McDonald, J. F.; Mrksich, M.; Oyelere, A. K., Design and structure activity relationship of tumor-homing histone deacetylase inhibitors conjugated to folic and pteroic acids. *Eur. J. Med. Chem.* **2015,** *96* (0), 340-359; (b) Oyelere, A. K.; Chen, P. C.; Guerrant, W.; Mwakwari, S. C.; Hood, R.; Zhang, Y.; Fan, Y., Non-Peptide Macrocyclic Histone Deacetylase Inhibitors. *J. Med. Chem.* **2008,** *52* (2), 456-468.

44. Gurard-Levin, Z. A.; Scholle, M. D.; Eisenberg, A. H.; Mrksich, M., High-Throughput Screening of Small Molecule Libraries using SAMDI Mass Spectrometry. *ACS Combinatorial Science* **2011,** *13* (4), 347-350.

45. Trott, O.; Olson, A. J., AutoDock Vina: Improving the speed and accuracy of docking with a new scoring function, efficient optimization, and multithreading. *J. Comput. Chem.* **2010,** *31* (2), 455-461.

46. (a) Miyata, M.; Lee, J.-Y.; Susuki-Miyata, S.; Wang, W. Y.; Xu, H.; Kai, H.; Kobayashi, K. S.; Flavell, R. A.; Li, J.-D., Glucocorticoids suppress inflammation via the upregulation of negative regulator IRAK-M. *Nature Communications* **2015,** *6*, 6062; (b) Ishinaga, H.; Jono, H.; Lim, J. H.; Kweon, S.-M.; Xu, H.; Ha, U.-H.; Xu, H.; Koga, T.; Yan, C.; Feng, X.-H.; Chen, L.-F.; Li, J.-D., TGF-β induces p65 acetylation to enhance bacteria-induced NF-κB activation. *The EMBO Journal* **2007,** *26* (4), 1150-1162.

CHAPTER 5

FORMULATION AND PRELIMINARY EVALUATION OF CELLULAR UPTAKE OF LIGAND-FUNCTIONALIZED LIPOSOMES

5.1. Introduction

Targeting of drug delivery systems (DDS), using small molecules or antibodies, continues to be an attractive approach employed to improve on the bioavailability of drugs, and mitigate the toxic effects that may limit the clinical use of promising therapeutics. Liposomes are attractive as DDS because of their biodegradability and amphiphilic nature, which enables them to cross cell membranes with little resistance. What used to be a major challenge in the field is making liposomes with long circulation time in systemic circulation, while resisting uptake by the mononuclear phagocyte system and still maintain structural integrity.[1] This challenge was resolved with the introduction of stealth liposomes,[2] having PEG coating on their surfaces. Stealth liposomes get to tumor sites by leaching through defects in the tumor blood vessels, by a process known as enhanced permeability and retention effect (EPR).[3]

To enhance the amount of liposomes getting to tumor sites, liposomes are often functionalized with ligands that have affinity for receptors ubiquitously expressed in tumors.[4] Such liposomes are called actively-targeted liposomes, and have been proposed to get to tumors through a combination of EPR effect and receptor-facilitated uptake.[4-5] In designing ligand targeted liposomes, the location of the ligand on the surface of the liposomes relative to the PEG coating is an important factor to consider. Ligands at the distal end of PEG on liposomes are expected to

bind to their receptors with minimal hindrance[6]. On the other hand, ligands buried within PEG coating are likely to encounter hindrance in the ligand-receptor interaction needed to facilitate their uptake.[6]

In continuation of our effort to assess the suitability of macrolides as targeting ligands on the surface of nanoparticles,[7-8] we functionalized a phospholipid, 1,2-distearoyl-sn-glycero-3-phosphoethanolamine (DSPE), with clarithromycin and formulated liposomes with the functionalized DSPE. Three types of these clarithromycin-functionalized DSPE were made: one in which clarithromycin was directly attached to the phospholipid head group (compound **3**), another one with a short linker (PEG_8) as connecting unit between clarithromycin and DSPE (compound **6**); and lastly, one with long linker (PEG_{2000}) separating DSPE from clarithromycin (compound **10**). Liposomes made with these compounds were used to encapsulate propidium iodide (PI), and their cellular uptake was assessed in macrophage cell line (RAW 264.7).

Similarly, we appended tamoxifen, an estrogen receptor (ER) antagonist, to DSPE (compound **12**), and formulated liposomes with the functionalized DSPE. Cellular uptake was also assessed in ER positive breast cancer cell line (MCF-7), with tamoxifen functionalized liposomes carrying propidium iodide.

5.2. Materials and methods

1,2-distearoyl-sn-glycero-3-phosphoethanolamine (DSPE), DSPE-$mPEG_{2000}$, DSPE-$mPEG_{2000}$-NHS, and 1,2-distearoyl-sn-glycero-3-phosphocholine (DSPC) were purchased from NOF America. Cholesterol was purchased from Avanti lipids (USA). Propidium iodide (PI) was

purchased via VWR from EMD Millipore (Biosciences. Murine macrophage cells RAW 264.7 and breast cancer cell line MCF-7 were obtained from ATCC, USA. All solvents used in this study were either of HPLC grade or analytical grade, and were used without further purification.

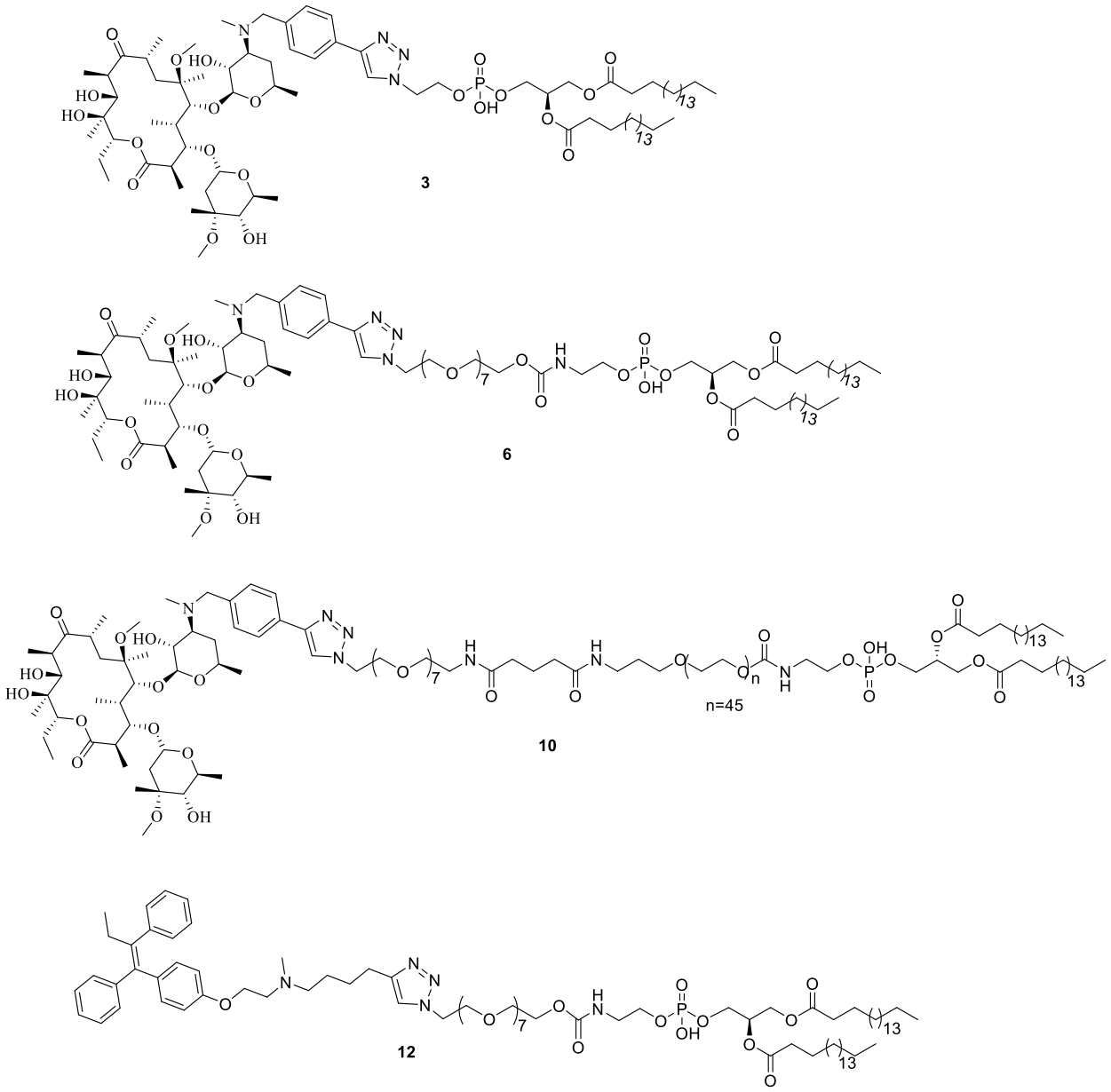

Figure 5.1: Structures of clarithromycin- and tamoxifen-modified phospholipids being investigated.

5.3. Chemistry

Clarithromycin-DSPE (**3**) was made using Cu (I) catalyzed Huisgen 1, 3-cycloaddition reaction between DSPE-azide (**1**) and clarithromycin benzyl alkyne (**2**) (scheme 5.1). The two intermediates (compounds **1** and **2**) used in this synthesis were made as described previously.[9]

Scheme 5.1: Synthesis of DSPE-clarithromycin (Compound **3**)

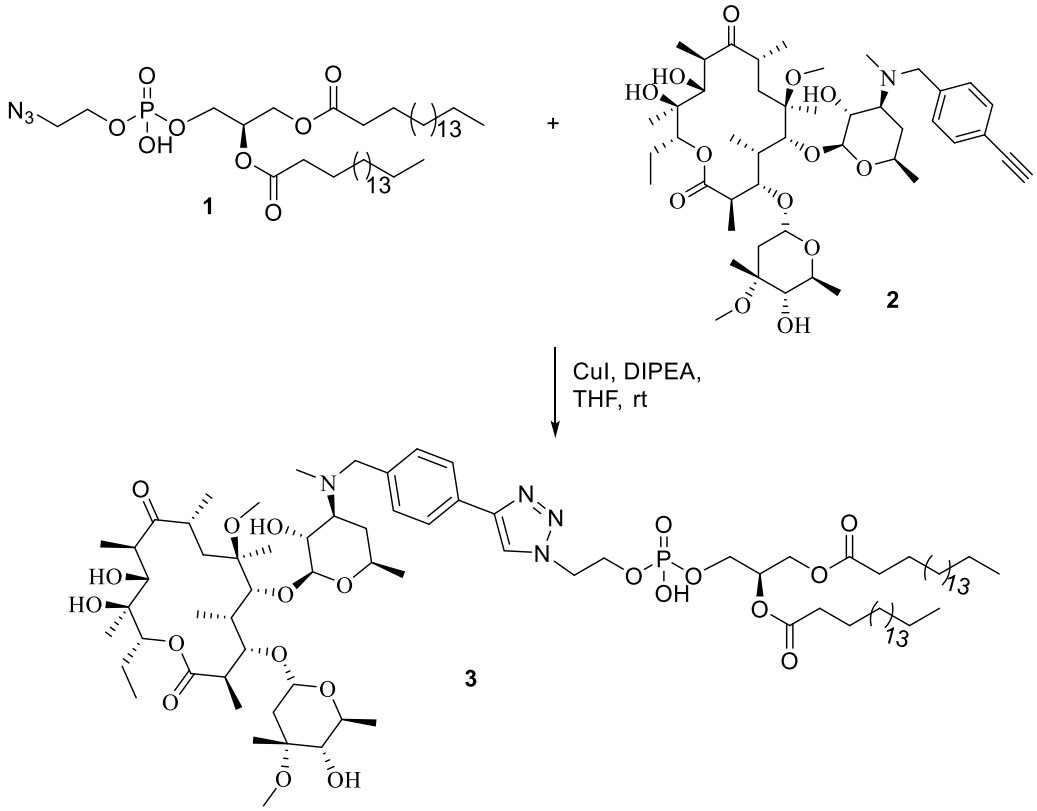

In making compound **6**, we converted PEG-monoazide (**4**) to azide-PEG-carbonate, which was immediately reacted with DSPE to give azido-PEG-DSPE (**5**). The desired compound **6** was thereafter made by Cu(I)-catalyzed 1, 3-cycloaddition reaction between clarithromycin alkyne (**2**) and compound **5** (scheme 5.2).

Scheme 5.2: Synthesis of DSPE-PEG$_8$-clarithromycin (Compound **6**)

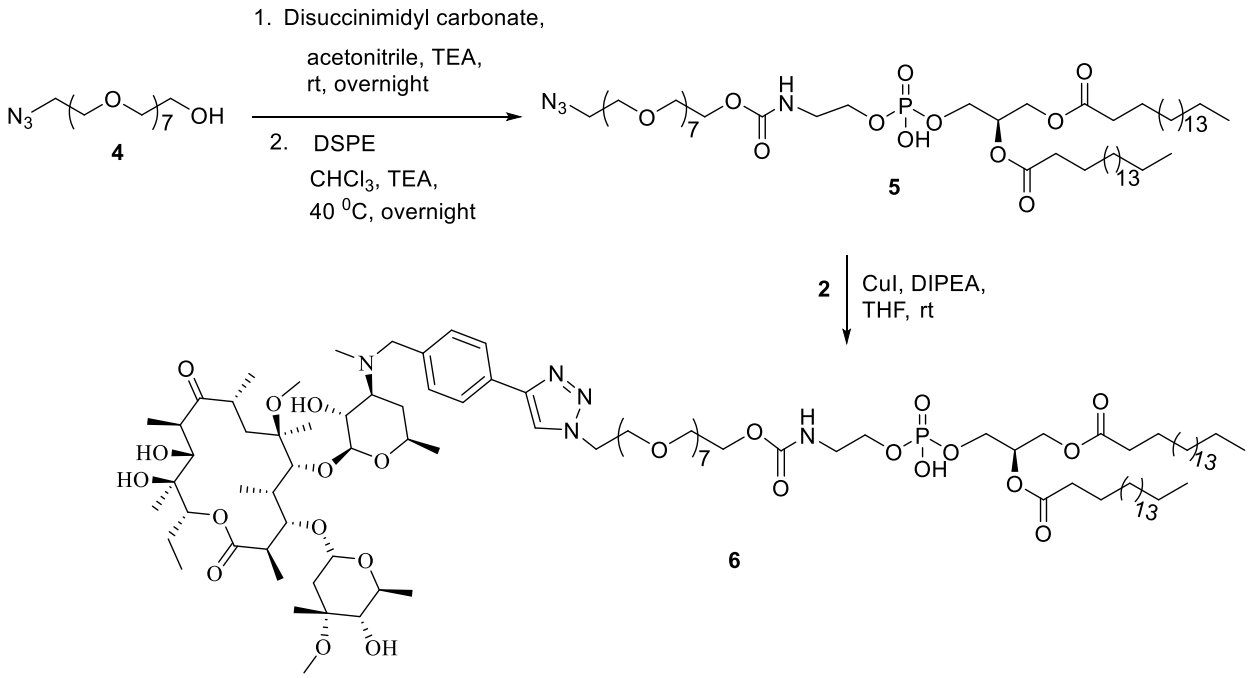

Synthesis of compound **10** was achieved via a multistep synthesis involving making of intermediate compound **8**. Access to compound **8** was achieved by Cu(I)-catalyzed cycloaddition reaction between azide-PEG-amine (**7**) and clarithromycin-alkyne compound **2** (scheme 5.3). Refluxing compound **8** with commercially available NHS-activated DSPE-PEG$_{2000}$ (**9**) in $CHCl_3$ furnished the desired compound **10**. Due to the polydispersed nature of the commercially available intermediate **9**, compound **10** was also obtained in the polydispersed form. Product synthesis was thus confirmed using mass spectrometry (Figure 5.2).

Scheme 5.3: Synthesis of DSPE-PEG$_{2000}$-clarithromycin (compound **10**)

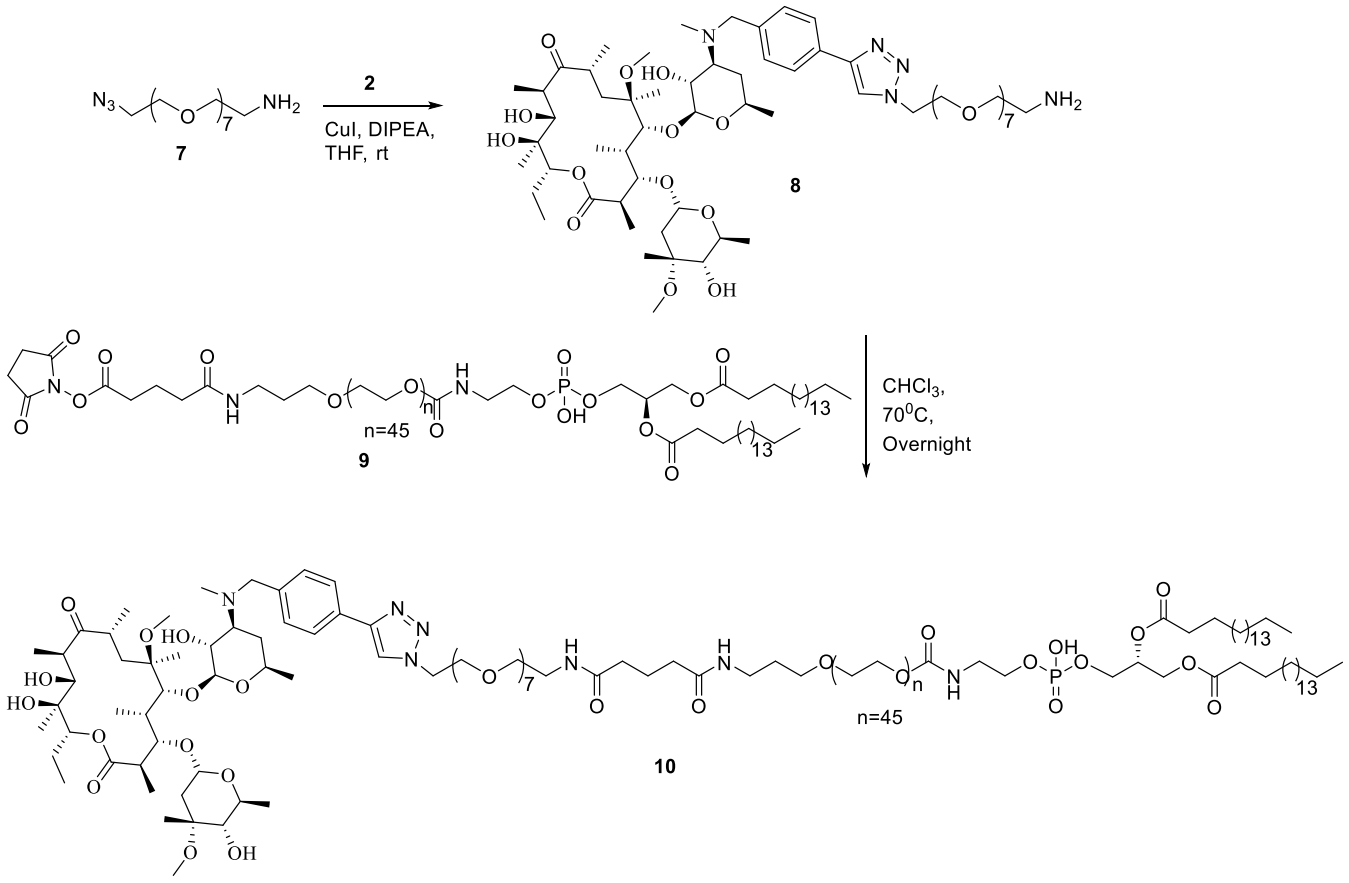

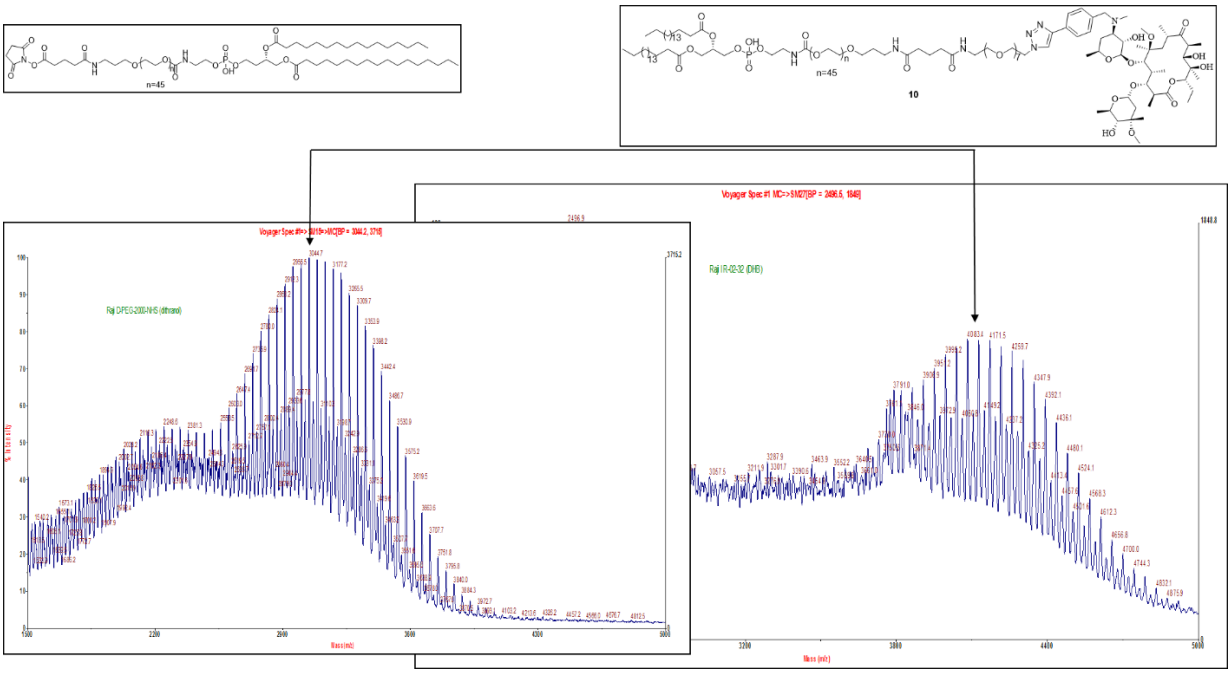

Figure 5.2: Mass spec confirmation of synthesis of DSPE-PEG_{2000}-clarithromycin (compound **10**)

Scheme 5.4: Synthesis of DSPE-PEG_8-tamoxifen **12**

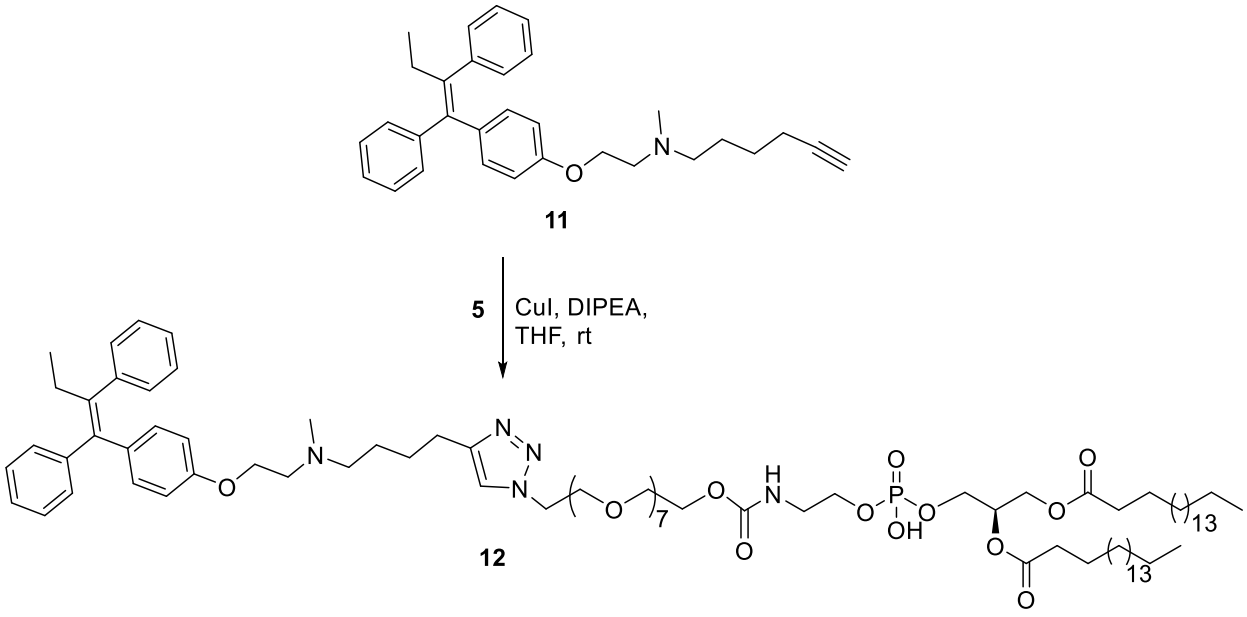

Similar to compounds **3** and **6**, tamoxifen-functionalized DSPE (**12**) was successfully made using Cu(I)-catalyzed cycloaddition reaction between compound **11** and compound **5** (scheme 5.4).

Table 5.1: Various liposome formulations

Formulation	Lipid composition	Molar ratio
C1	DSPC: DSPE-mPEG$_{2000}$: cholesterol	11:1:7
C2	DSPC: DSPE-mPEG$_{2000}$: cholesterol: compound **3**	11:1:7:0.1
C3	DSPC: DSPE-mPEG$_{2000}$: cholesterol: compound **6**	11:1:7:0.1
C4	DSPC: DSPE-mPEG$_{2000}$: cholesterol: compound **10**	11:1:7:0.025
C5	DSPC: DSPE-mPEG$_{2000}$: cholesterol: compound **12**	11:1:7:0.1

5.4. Preparation of liposomes

Liposomes were prepared were prepared by the thin film hydration method.[10] Briefly, DSPC, DSPE-mPEG$_{2000}$, cholesterol and the respective clarithromycin- or tamoxifen-modified DSPE, in molar ratios shown in table 4.1, were dissolved in chloroform in a round bottom flask to give a clear solution. If a clear solution is not obtained, a mixture of chloroform and methanol (2:1) was used to dissolved the components. Organic solvents were removed using the rotary evaporator until a thin film is obtained, and the flask is left on the high vacuum overnight to remove residual solvent. The thin film is thereafter hydrated with 1X phosphate-buffered saline (PBS, pH 7.4)

containing 10 µM propidium iodide (PI) at 55^0 C, followed by intermittent sonication, in a bath-type sonicator, for 10 minutes at 100W. The resulting suspension was extruded seventeen times through an extruder (Avanti mini extruder, Avanti Lipids) with a polycarbonate membrane (100 nm) to obtain a clear solution of unilamellar liposomes. Dialysis through Slide-A-Lyzer dialysis cassette G2 (Thermo Scientific) (with molecular weight cut-off 10 KDa) was used to removed unencapsulated PI and unincorporated lipids. Pure liposomes were stored at 4 ^{0}C until used.

5.5. Characterization of liposomes

The sizes of liposomes (Table 5.2) were measured using dynamic light scattering.

5.6. Encapsulation efficiency (EE) of liposomes

EE was determined by lysis followed by absorbance measurement. To determine the amount of PI encapsulated in liposomes, 50µL of liposome was lysed using Triton-X (Sigma, USA) and absorbance of the solution measured. This was then compared to a standard curve of absorbance vs varying concentrations of PI. Encapsulation efficiency was calculated using the equation:

EE (%)= (amount of PI encapsulated in liposome/ concentration of PI solution used in hydration) ×100 %

Table 5.2: Characteristics of various liposome formulations

Formulation	Radius (nm)	Polydispersity	EE (%)
C1	55.7	0.08	10.3
C2	51.7	0.19	ND
C3	54.5	0.11	15.3
C4	ND	ND	ND
C5	54.9	0.21	10

ND= not determined

5.7. *In vitro* cellular uptake

RAW 264.7 and MCF-7 cells were grown in DMEM supplemented with 10% fetal bovine serum (FBS) and 1% *pen. Strep*. in a humidified incubator with 5% CO_2 at 37 ^{0}C in petri dishes. Prior to experiment, cells were seeded in a 12-well plate containing a cover slip at $5*10^5$ plating density. The following day, media was aspirated and replaced with fresh media containing appropriate concentrations of PI or liposomes encapsulating PI. 24 hours after incubation at 37 ^{0}C, media was aspirated and the wells washed twice with chilled PBS, pH 7.4. Cells were thereafter fixed with 4% paraformaldehyde. For MCF-7 experiment, 300 nM solution of DAPI was added to the wells, after which cover slips were removed from the wells and mounted on slides using glycerol. Slides were imaged immediately using confocal microscope (Zeiss LSM 700-405).

5.8. Results and discussion

5.8.1. Characterization: clarithromycin-functionalized liposome

Liposomes were successfully formulated using the molar ratios of individual components shown in Table 5.1. For a typical stealth liposome (C1), molar ratio of 11:1:7 of DSPC: DSPE-mPEG$_{2000}$: cholesterol was sufficient to give the desired formulation, and this formed the basis on which other liposomes were made. The major challenge in making ligand-bearing liposomes is determining the optimum amount of ligand-functionalized DSPE that can be incorporated into the lipid mix. For each of the clarithromycin-targeted liposomes, we added varying amounts of each of the three clarithromycin modified DSPE, and chose the optimum ratio that gave a stable liposome formulation. As shown in Table 5.1, compounds **3** (without linker) and **6** (with PEG$_8$ linker) (Figure 5.1) were doped into the lipid mix at 0.1 mol equivalent of DSPE-mPEG$_{2000}$ to give formulations C2 and C3 respectively. This was the optimum level of incorporation of the two compounds that gave a stable formulation. For formulation C4, however, we could not exceed 0.025 mol (relative to DSPE-mPEG$_{2000}$) of compound **10** to form liposomes. The reason for this is not very clear.

The hydrodynamic radius was determined for three of our formulations (C1-C3), as a measure of size of liposomes. For a typical unilamellar liposome for tumor drug delivery purpose, sizes in the range of 50-100 nm (radius) are desirable[11]. All the three liposomes analyzed have radius of 55.7, 51.7 and 54.5 nm for C1, C2, and C3 formulations respectively (Table 5.2). The two ligand functionalized liposomes, C2 and C3, have radii within the 50-100 nm range, suggesting that they may be suitable for cancer drug delivery applications. Comparing the sizes of the ligand functionalized liposomes, C2 and C3, to the one without ligand, C1, we observe that

there was no significant difference in the size of C1 and C3, suggesting that incorporating clarithromycin-PEG_8-DSPE into the liposome do not lead to visible change in size of the liposome. Liposome formulation C2, on the other hand, appear to be smaller than the formulation without ligand, C1. This is an unusual observation, as most ligand functionalized liposomes turn out to be bigger in sizes that the non-functionalized ones. Since clarithromycin is directly attached to the lipid's phosphate group for compound **3** (incorporated into C2), it is quite possible that clarithromycin in this location compresses the liposome, which then leads to the decrease in size compared to non-modified liposome.

Analysis of EE for the stealth liposome, C1, and one of the clarithromycin-functionalized liposomes, C3, showed that they both have low EE (Table 5.2) 15.3 and 10.3 respectively. The low EE obtained could be due to the thin film hydration method used in formulating these liposomes.

5.8.2. Characterization: tamoxifen-functionalized liposome

The liposome formulation containing tamoxifen-PEG_8-DSPE (**12**), C5, was made by doping the lipid mix with compound **12** at a 0.1 mol equivalent of DSPE-$mPEG_{2000}$ (Table 5.2). This formulation gave liposome with a radius (54.9 nm) not significantly different from the size of liposome without ligand, C1, (55.7 nm). This also suggests that tamoxifen-PEG_8-DSPE do not significantly affect the size of the liposome made, and that the liposome obtained may be suitable for drug delivery applications for reasons stated *vide supra*.

Similar to the clarithromycin-based liposome, tamoxifen functionalized liposome also had a low EE (Table 5.2), though about the same as that for stealth liposome.

5.8.3. Cellular uptake study: uptake of clarithromycin-functionalized liposomes in RAW 264.7 macrophage cells

Having successfully made and characterize liposomes encapsulating PI with clarithromycin on their surfaces, we evaluated the effect of having clarithromycin on the surface of liposomes on cell uptake. For this, we used confocal microscopy to track the fluorescence due to PI within the liposomes in murine macrophage cell line, RAW 264.7. For this study, we treated RAW 264.7 cells with free PI and liposomes from C1 and C3 formulations for 24 hours. Confocal images obtained are shown in Figure **5.3**. We can clearly see that cells treated with liposome having clarithromycin-PEG_8-DSPE incorporated (formulation C3) have the highest amount of PI internalized compared to cells treated with free PI and liposome without ligand (formulation C1). This observation is consistent with our previous study[7], where we showed that macrolides facilitate substantial accumulation of gold nanoparticles in RAW 264.7 cells. Although this data is preliminary, we can safely assume that clarithromycin could be used as a targeting ligand on the surface of liposomes for drug delivery applications.

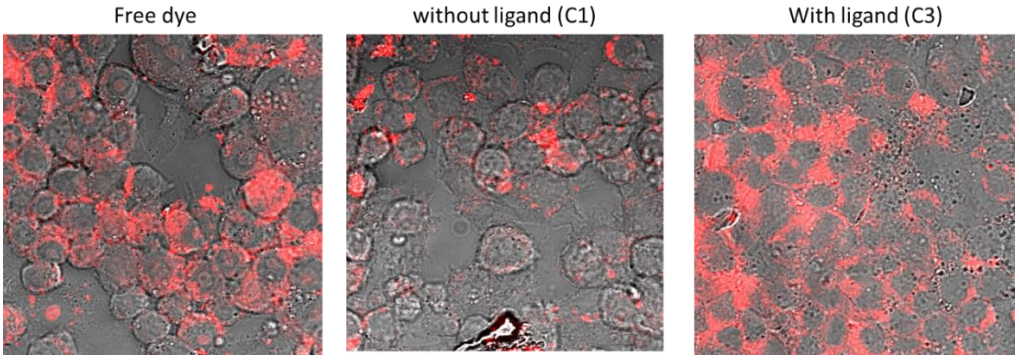

Figure 5.3: Confocal microscope images of RAW 264.7 cellular uptake of PI encapsulated in non-targeted- and targeted liposomes, as well as unencapsulated PI (free dye)

Further evaluation is required to reproduce this observation, and also explore other formulations (C2 and C4) to see which one will give the highest amount of intracellular liposomal PI.

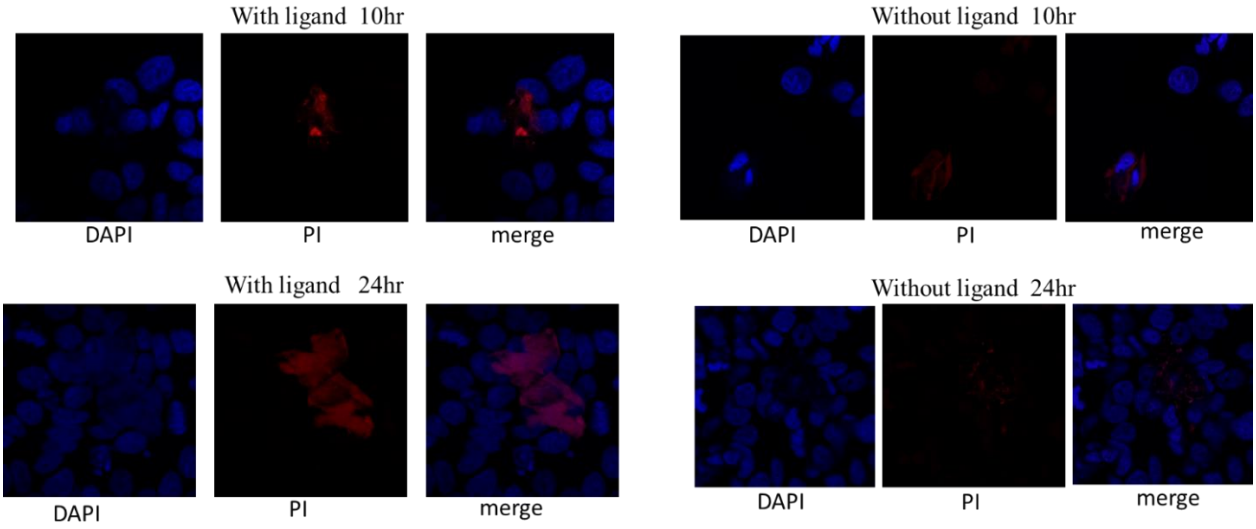

Figure 5.4: Confocal microscope images of MCF-7 cellular uptake of PI encapsulated in non-targeted- and tamoxifen-targeted liposomes.

5.8.4. Cellular uptake study: uptake of tamoxifen-functionalized liposomes in MCF-7 cells

Tamoxifen is an ER-binder currently FDA approved for ER+ breast cancer. Our lab and others have exploited tamoxifen's affinity for ER to facilitate delivery of gold nanoparticles[12] and liposomes[13] to ER-expressing breast cancer cell line, MCF-7. Though the previous study using tamoxifen as ligand to guide liposome[13] showed some promise, tamoxifen was not covalently linked to any of the lipids that constitute the liposome. In our study, we treated MCF-7 cells with tamoxifen-functionalized liposome and non-targeted liposome (both encapsulating PI) for 10- and 24 hours, after which the cells nuclei were stained with DAPI. The images taken with confocal microscope are shown in Figure 5.4 above. At 10 hours, we saw more of PI in the cells treated with Tamoxifen-functionalized liposome compared to the non-functionalized one, with some of the dye already in the nucleus. The observation was more pronounced at 24 hours.

5.9. Conclusion

We have reported our synthetic efforts towards making phospholipids carrying targeting ligands. With our approach, we were able to make DSPE functionalized with clarithromycin and tamoxifen. Liposomes made with phospholipids having clarithromycin attached showed some promise in facilitating delivery of PI to RAW 264.7 macrophage cells. Likewise, liposome made with DSPE functionalized with tamoxifen was assessed for cellular uptake in RAW 264.7 macrophage cells. Though promising, it is not very clear from the current study if there is an advantage to having tamoxifen-DSPE incorporated into liposomes. A more extensive study will be required to verify the utility of tamoxifen as a targeting ligand on liposomes.

5.10. Description of compound synthesis

Compounds **1**, **4** and **7** were made following literature protocols[7].

Clarithromycin triazolyl DSPE (3):

DSPE azide **1** (0.30 g, 0.39 mmol) and ethynyl benzyl clarithromycin **2** (0.36 g, 0.43 mmol) are dissolved in anhydrous THF (20 ml) and purged with argon for 10 min. DIPEA (0.13ml, 0.78 mmol) and CuI (0.04 g, 1.94 mmol) were then added to the mixture and purged further for another 20 minutes. The resulting suspension was stirred at room temperature for 12 h. Reaction was quenched with a solution of 4:1 satd. Aqueous NH_4Cl/NH_4OH and extracted with a mixture of 10% MeOH in DCM. Combined organic layer was dried over anhydrous Na_2SO_4 and concentrated *in vacuo*. The crude was purified by prep. TLC using $CHCl_3$: MeOH: NH_4OH (10:2:0.1) to give compound **3** as an off white solid (0.46g, 72 %). ^{1}H NMR (400 MHz, cdcl$_3$) δ 8.10 (s, 1H), 7.74 (d, *J* = 7.8 Hz, 2H), 7.38 (s, 2H), 5.17 (d, *J* = 18.5 Hz, 1H), 4.84 (d, *J* = 15.8 Hz, 1H), 4.60 (d, *J* = 20.2 Hz, 2H), 4.44 – 4.36 (m, 1H), 4.25 (d, *J* = 28.4 Hz, 3H), 4.07 (d, *J* = 29.5 Hz, 1H), 3.93 (d, *J* = 20.6 Hz, 4H), 3.78 – 3.66 (m, 3H), 3.66 – 3.54 (m, 2H), 3.47 (d, *J* = 7.1 Hz, 2H), 3.42 – 3.32 (m, 1H), 3.17 (s, 1H), 3.09 (s, 2H), 3.04 – 2.91 (m, 7H), 2.80 (d, *J* = 30.7 Hz, 1H), 2.57 (s, 1H), 2.41 (s, 2H), 2.31 – 2.13 (m, 7H), 1.98 – 1.72 (m, 2H), 1.61 – 1.42 (m, 5H), 1.36 (d, *J* = 11.8 Hz, 3H), 1.32 – 1.14 (m, 97H), 1.08 (dd, *J* = 28.3, 6.2 Hz, 27H), 0.90 – 0.77 (m, 16H). HRMS (ESI) *m+z* Calcd. for $C_{87}H_{154}O_{21}N_4P$ [$M+H^+$]: 1622.0838, found 1622.0778.

DSPE-PEG$_8$ azide (5):

PEG azide **4** (0.57 ml, 1.43 mmol), TEA (0.60 ml, 4.29 mmol), and disuccinimidyl carbonate (0.73 g, 2.86 mmol) were dissolved in acetonitrile (20 ml) and left to stir at room temperature overnight. Solvent was evaporated and azido-PEG-carbonate was recovered by prep TLC using DCM:Acetone (1:2) as a colorless viscous liquid (0.70 g, 90 %) and used for the next step without characterization. The recovered azido-PEG-carbonate (0.24 g, 0.44 mmol), DSPE (0.25 g, 0.34 mmol) and TEA (0.14 ml, 1.02 mmol) were dissolved in $CHCl_3$ (15 ml) and stirred at 40 ^{0}C overnight. Solvent was evaporated off, and the crude purified by prep TLC using DCM: MeOH (10:1) to give compound **5** as a waxy solid (0.17 g, 56 %). ^{1}H NMR (400 MHz, cdcl$_3$) δ 6.23 (s, 1H), 5.14 (s, 1H), 4.31 (d, *J* = 9.5 Hz, 2H), 4.18 (s, 2H), 4.12 – 4.03 (m, 2H), 3.92 – 3.81 (m, 5H), 3.69 – 3.59 (m, 30H), 2.68 (s, 6H), 2.25 (dd, *J* = 12.8, 7.4 Hz, 5H), 1.53 (s, 5H), 1.19 (d, *J* = 12.5 Hz, 74H), 0.84 (t, *J* = 6.8 Hz, 7H). ^{31}P NMR (162 MHz, cdcl$_3$) δ -1.98.

Clarithromycin triazolyl PEG$_8$ DSPE (6):

DSPE-PEG$_8$ azide **5** (0.17 g, 0.15 mmol), ethynyl benzyl clarithromycin **2** (0.14 g, 0.16 mmol), DIPEA (0.06 ml, 0.29 mmol) and CuI (0.01 g, 0.07 mmol) were reacted in anhydrous THF (10 ml) as described for compound **3** above. Due to PEG's solubility in water, no aqueous workup was done. Solvent was evaporated and the crude was purified by prep. TLC using $CHCl_3$: MeOH: NH_4OH (10:2:0.1) to give compound **6** as an off white solid (0.16 g, 53 %). ^{1}H NMR (400 MHz, cd$_3$od) δ 8.28 (s, 1H), 7.78 (d, *J* = 8.2 Hz, 2H), 7.41 (d, *J* = 8.1 Hz, 2H), 5.42 – 5.38 (m, 1H), 5.17 (d, *J* = 19.1 Hz, 1H), 5.06 (dt, *J* = 16.2, 8.1 Hz, 1H), 4.86 (t, *J* = 11.1 Hz, 1H), 4.61 (t, *J* = 5.0 Hz, 2H), 4.48 (t, *J* = 8.5 Hz, 1H), 4.40 (dt, *J* = 12.6, 6.4 Hz, 1H), 4.21 – 4.11 (m, 3H), 4.09 – 4.00 (m, 1H), 3.94 (dt, *J* = 10.0, 5.1 Hz, 5H), 3.86 (t, *J* = 10.1 Hz, 4H), 3.72 (d, *J* = 10.7 Hz, 2H), 3.67 –

3.51 (m, 39H), 3.37 – 3.26 (m, 8H), 3.20 – 3.10 (m, 7H), 3.04 – 2.96 (m, 5H), 2.94 – 2.85 (m, 1H), 2.76 (d, *J* = 24.4 Hz, 1H), 2.53 (d, *J* = 30.4 Hz, 1H), 2.37 (s, 1H), 2.36 – 2.23 (m, 10H), 1.94 – 1.76 (m, 5H), 1.69 (d, *J* = 12.9 Hz, 1H), 1.63 – 1.49 (m, 8H), 1.42 – 1.31 (m, 31H), 1.31 – 1.16 (m, 100H), 1.16 – 1.06 (m, 18H), 0.85 (dt, *J* = 13.8, 7.1 Hz, 12H). ^{31}P NMR (162 MHz, cdcl$_3$) δ 0.85. HRMS (ESI) *m+2/2z* Calcd. for $C_{104}H_{188}O_{30}N_5P$ [M+2H$^+$]: 1009.1533, found 1009.1544.

Clarithromycin triazolyl PEG$_8$ amine (8):

Azide PEG amine **7** (0.11 g, 0.27 mmol) and ethynyl benzyl clarithromycin **2** (0.15 g, 0.18 mmol), DIPEA (0.06 ml, 0.35 mmol) and CuI (0.02 g, 0.09 mmol) were reacted in anhydrous THF (10 ml) as described for compound **6**. The crude was purified by prep. TLC using DCM: MeOH: NH_4OH (10:2:0.1) to give compound **8** as a light yellow viscous liquid (0.12g, 37 %). ^{1}H NMR (400 MHz, cdcl$_3$) δ 8.17 (s, 1H), 7.96 (d, *J* = 8.2 Hz, 2H), 7.51 (d, *J* = 8.1 Hz, 2H), 5.21 (dd, *J* = 11.1, 2.0 Hz, 1H), 5.05 (t, *J* = 8.4 Hz, 1H), 4.76 (t, *J* = 4.9 Hz, 2H), 4.58 (t, *J* = 10.3 Hz, 1H), 4.14 – 4.03 (m, 3H), 3.98 – 3.84 (m, 3H), 3.85 – 3.72 (m, 36H), 3.70 (dd, *J* = 15.2, 10.0 Hz, 5H), 3.67 – 3.52 (m, 4H), 3.52 – 3.42 (m, 2H), 3.31 (d, *J* = 9.2 Hz, 2H), 3.31 (d, *J* = 11.7 Hz, 4H), 3.23 – 3.11 (m, 6H), 3.09 – 2.99 (m, 4H), 2.85 – 2.64 (m, 5H), 2.50 – 2.37 (m, 5H), 2.33 (d, *J* = 0.7 Hz, 1H), 2.08 (dd, *J* = 13.3, 6.5 Hz, 3H), 2.02 – 1.80 (m, 4H), 1.73 – 1.63 (m, 2H), 1.54 (d, *J* = 16.0 Hz, 3H), 1.41 (dt, *J* = 18.5, 9.3 Hz, 9H), 1.38 – 1.20 (m, 31H), 1.00 (t, *J* = 7.4 Hz, 3H).

Clarithromycin triazolyl PEG$_{2000}$ DSPE (10):

DSPE-PEG$_{2000}$-NHS **9** (0.35 g, 0.15 mmol) and compound **8** (0.12 g, 0.10 mmol) were dissolved in $CHCl_3$ and stirred at 70 ^{0}C overnight. Solvent was evaporated off and the crude purified by prep TLC using DCM: MeOH: NH4OH (12:1:0.1) to give compound **10** (0.24 g, 40 %) as an off white solid. Product synthesis was confirmed by MALDI (see Figure 5.2).

Tamoxifen triazolyl PEG_8 DSPE (12):

DSPE-PEG_8 azide **5** (0.59 g, 0.50 mmol), tamoxifen alkyne **2** (0.20 g, 0.50 mmol), DIPEA (0.16 ml, 0.914 mmol) and CuI (0.04 g, 0.23 mmol) were reacted in anhydrous THF (20 ml) as described for compound **3** above. Due to PEG's solubility in water, no aqueous workup was done. Solvent was evaporated and the crude was purified by prep. TLC using DCM: MeOH (10:1) to give compound **12** as an off white solid (0.51 g, 63 %). ^{1}H NMR (400 MHz, $cdcl_3$) δ 7.50 (t, *J* = 9.6 Hz, 1H), 7.25 (dd, *J* = 9.7, 4.9 Hz, 2H), 7.19 – 7.10 (m, 2H), 7.11 – 7.05 (m, 2H), 7.05 – 6.97 (m, 3H), 6.89 (t, *J* = 6.7 Hz, 1H), 6.82 – 6.73 (m, 1H), 6.69 (d, *J* = 8.7 Hz, 1H), 6.44 (d, *J* = 8.7 Hz, 1H), 6.33 (s, 1H), 5.13 (s, 1H), 4.71 (s, 1H), 4.46 – 4.35 (m, 2H), 4.28 (d, *J* = 11.5 Hz, 2H), 4.05 (d, *J* = 19.4 Hz, 5H), 3.83 (d, *J* = 31.8 Hz, 4H), 3.76 (t, *J* = 4.7 Hz, 3H), 3.57 – 3.44 (m, 33H), 3.28 (s, 3H), 3.13 (s, 1H), 2.99 (q, *J* = 7.5 Hz, 2H), 2.85 (s, 1H), 2.69 – 2.61 (m, 3H), 2.59 (s, 2H), 2.42 – 2.29 (m, 1H), 2.19 (dd, *J* = 13.4, 6.7 Hz, 4H), 1.63 (t, *J* = 16.9 Hz, 3H), 1.46 (d, *J* = 19.4 Hz, 5H), 1.43 – 1.28 (m, 15H), 1.16 (s, 65H), 0.81 (dt, *J* = 13.5, 7.3 Hz, 9H). ^{31}P NMR (162 MHz, $cdcl_3$) δ -3.98. HRMS (ESI) *m*+*z* Calcd. for $C_{89}H_{149}N_5O_{18}P$ [$M+H^+$]: 1607.0635, found 1607.0629.

5.11. References

1. Pattni, B. S.; Chupin, V. V.; Torchilin, V. P., New Developments in Liposomal Drug Delivery. *Chem. Rev.* **2015**.

2. Ishida, T.; Harada, M.; Wang, X. Y.; Ichihara, M.; Irimura, K.; Kiwada, H., Accelerated blood clearance of PEGylated liposomes following preceding liposome injection: Effects of lipid dose and PEG surface-density and chain length of the first-dose liposomes. *J. Control. Release* **2005,** *105* (3), 305-317.

3. Theek, B.; Gremse, F.; Kunjachan, S.; Fokong, S.; Pola, R.; Pechar, M.; Deckers, R.; Storm, G.; Ehling, J.; Kiessling, F.; Lammers, T., Characterizing EPR-mediated passive drug targeting using contrast-enhanced functional ultrasound imaging. *J. Control. Release* **2014,** *182* (0), 83-89.

4. Sanna, V.; Pala, N.; Sechi, M., Targeted therapy using nanotechnology: focus on cancer. *International Journal of Nanomedicine* **2014,** *9*, 467-483.

5. Cheng, C. J.; Tietjen, G. T.; Saucier-Sawyer, J. K.; Saltzman, W. M., A holistic approach to targeting disease with polymeric nanoparticles. *Nat Rev Drug Discov* **2015,** *14* (4), 239-247.

6. Kaasgaard, T.; Andresen, T. L., Liposomal cancer therapy: exploiting tumor characteristics. *Expert Opinion on Drug Delivery* **2010,** *7* (2), 225-243.

7. Dreaden, E. C.; Mwakwari, S. C.; Austin, L. A.; Kieffer, M. J.; Oyelere, A. K.; El-Sayed, M. A., Small Molecule–Gold Nanorod Conjugates Selectively Target and Induce Macrophage Cytotoxicity towards Breast Cancer Cells. *Small* **2012,** *8* (18), 2819-2822.

8. Dreaden, E. C.; Raji, I. O.; Austin, L. A.; Fathi, S.; Mwakwari, S. C.; Humphries, W. H.; Kang, B.; Oyelere, A. K.; El-Sayed, M. A., P-Glycoprotein-Dependent Trafficking of Nanoparticle-Drug Conjugates. *Small* **2014,** *10* (9), 1719-1723.

9. Oyelere, A. K.; Chen, P. C.; Guerrant, W.; Mwakwari, S. C.; Hood, R.; Zhang, Y.; Fan, Y., Non-Peptide Macrocyclic Histone Deacetylase Inhibitors. *J. Med. Chem.* **2008,** *52* (2), 456-468.

10. Emmetiere, F.; Irwin, C.; Viola-Villegas, N. T.; Longo, V.; Cheal, S. M.; Zanzonico, P.; Pillarsetty, N.; Weber, W. A.; Lewis, J. S.; Reiner, T., 18F-Labeled-Bioorthogonal Liposomes for In Vivo Targeting. *Bioconjug. Chem.* **2013**.

11. Ernsting, M. J.; Murakami, M.; Roy, A.; Li, S. D., Factors controlling the pharmacokinetics, biodistribution and intratumoral penetration of nanoparticles. *J. Control. Release* **2013,** *172* (3), 782-94.

12. Dreaden, E. C.; Mwakwari, S. C.; Sodji, Q. H.; Oyelere, A. K.; El-Sayed, M. A., Tamoxifen−Poly(ethylene glycol)−Thiol Gold Nanoparticle Conjugates: Enhanced Potency and Selective Delivery for Breast Cancer Treatment. *Bioconjug. Chem.* **2009,** *20* (12), 2247-2253.

13. Jain, A. S.; Goel, P. N.; Shah, S. M.; Dhawan, V. V.; Nikam, Y.; Gude, R. P.; Nagarsenker, M. S., Tamoxifen guided liposomes for targeting encapsulated anticancer agent to estrogen receptor positive breast cancer cells: in vitro and in vivo evaluation. *Biomed. Pharmacother.* **2014,** *68* (4), 429-38.

CHAPTER 6

CONCLUSION/FUTURE STUDIES

With the recent US FDA approvals of Belinostat and Panobinostat, the future of HDACi drug discovery field looks promising. Several other HDACi are in different stages of preclinical and clinical development to address the shortcomings of the clinically approved HDACi.

In my thesis work, I have successfully explored different approaches to making new series of HDACi with exceptional *in vitro* therapeutic index (a measure of toxicity towards cancer cells relative to healthy cells). In chapter two, I described effort towards expanding the SAR studies on macrolide-based HDACi derived from clarithromycin, as a continuation of studies in our lab towards making lung tissue- selective HDACi.[1-2] In this project, SAR studies were focused on the points of attachment of HDACi template to clarithromycin and the zinc binding group (ZBG). In the former, modifications were made on both desosamine and cladinose sugars of clarithromycin. Among the new series of compounds made, the cladinose-modified series afforded us the lead compound (with six methylenes as connecting unit between the triazolyl end and hydroxamate), thereby justifying modification at this end of clarithromycin. However, it is yet to be shown that synthetic transformations on cladinose sugar do not significantly affect lung tissue accumulation profile of clarithromycin. Hence, future studies will focus on the *in vivo* bio-distribution study and therapeutic effect of my lead compound in animal models of lung cancer. In the latter part of this project, I adopted a biaryl ZBG into the design of clarithromycin-based HDACi as an extension of the SAR studies. This resulted in compounds that potently and selectively inhibit HDAC 1 and HDAC 2, consistent with previous studies that adopted the same ZBG.[3] Surprisingly though, none of the isoform-selective compounds showed cytotoxic effects towards cancer cell lines at the

maximum concentration tested. The lack of cytotoxicity observed might be due to the inability of the compounds to efficiently penetrate the cell membrane, hence the modest to moderate changes to the acetylation status of H4, a marker of intracellular class I HDAC inhibition observed in the cells. Studies that shed light on efflux of these compounds from the cells may help explain the discrepancy observed between the in vitro HDAC inhibition and the antiproliferative activities of these compounds.

Using design-multiple ligands approach, I also explored the beneficial effects of having bifunctional compounds as compared to combination therapy. It is a common clinical practice for patients to be prescribed two or more drugs with the goal of achieving synergistic therapeutic effects resulting from the action of the individual drugs. In such cases though, there is the challenge of dealing with issues such as the individual toxicity associated with each drugs, different pharmacological profiles of each drugs also requires that the dosage be optimized, which further makes combination therapy complicated. To avoid these bottlenecks, the bifunctional approach that incorporates two "warheads" into a single compound is currently being explored as a safer and probably more cost-effective approach.[4] In my approach, I generated bifunctional COX-HDAC inhibitors, that showed impressive cytotoxic effects in prostate cancer cell lines, with selectivity towards AR-dependent prostate cancer cell line. Lead compounds from this study showed unprecedented selective cytotoxicity towards prostate cancer cell lines relative to healthy control cell line Vero. What makes this concept more appealing is that some of the bifunctional compounds significantly downregulate activation of NF-kB, a driver of inflammation in tumors. Future work on this project will involve *in vivo* study in animal model of prostate cancer.

While the roles of individual HDAC isoforms in melanoma progression has not been fully characterized, some studies have shown that upregulation of HDAC 5 and HDAC 6 are important in melanoma survival.[5-6] Using a targeted approach, I made HDACi by incorporating a group with high affinity for melanin to further study the roles of HDACs in melanoma survival. High melanin production is a common phenomenon in many melanoma cases. The lead compound from this work is about ten-fold more potent than SAHA towards HDAC 1, and has about the same activity towards HDAC6 as SAHA. Surprisingly, none of the compounds were significantly cytotoxic towards melanoma cell lines, B16F10 and A375. In order to improve on the cellular potency of the compounds, I made a prodrug bearing the benzamide template linked by a labile bond to a hydroxamate-based HDACi. The prodrug showed some promise, but did not show the anticipated benefit in melanoma cell lines. Both the benzamide HDACi and the prodrug may be redesigned in future studies to optimize for potency in cell lines.

Lastly, lipid nanoparticles have emerged as important drug delivery systems for drugs with poor pharmacokinetic profiles, and those with significant off-target toxicities. One approach to improve the specificity of nanoparticle for tumors is to have targeting ligands appended to their surface to further enhance their ability to localize in tumors. I carried out preliminary studies evaluating the suitability of clarithromycin and tamoxifen as targeting ligands on liposomes. Liposomes incorporating clarithromycin-functionalized phospholipid showed promising results in terms of uptake into macrophage cells. However, this needs to be reproduced and optimized to improve on the cellular uptake. Likewise, phospholipid functionalized with tamoxifen showed some promise in facilitating uptake of liposomes into MCF-7, an estrogen receptor positive breast cancer cell line. Further studies are required to affirm this observation and also use both

clarithromycin- and tamoxifen- functionalized liposomes to deliver chemotherapeutic agents to cancer cells, and ultimately to tumors *in vivo*.

References

1. Oyelere, A. K.; Chen, P. C.; Guerrant, W.; Mwakwari, S. C.; Hood, R.; Zhang, Y.; Fan, Y., Non-Peptide Macrocyclic Histone Deacetylase Inhibitors. *J. Med. Chem.* **2008,** *52* (2), 456-468.

2. Mwakwari, S. C.; Guerrant, W.; Patil, V.; Khan, S. I.; Tekwani, B. L.; Gurard-Levin, Z. A.; Mrksich, M.; Oyelere, A. K., Non-Peptide Macrocyclic Histone Deacetylase Inhibitors Derived from Tricyclic Ketolide Skeleton. *J. Med. Chem.* **2010,** *53* (16), 6100-6111.

3. Witter, D. J.; Harrington, P.; Wilson, K. J.; Chenard, M.; Fleming, J. C.; Haines, B.; Kral, A. M.; Secrist, J. P.; Miller, T. A., Optimization of biaryl Selective HDAC1&2 Inhibitors (SHI-1:2). *Bioorg. Med. Chem. Lett.* **2008,** *18* (2), 726-731.

4. Musso, L.; Dallavalle, S.; Zunino, F., Perspectives in the development of hybrid bifunctional antitumour agents. *Biochem. Pharmacol.* **2015,** *96* (4), 297-305.

5. Liu, J.; Gu, J.; Feng, Z.; Yang, Y.; Zhu, N.; Lu, W.; Qi, F., Both HDAC5 and HDAC6 are required for the proliferation and metastasis of melanoma cells. *J. Transl. Med.* **2016,** *14* (1), 1-13.

6. Bergman, J. A.; Woan, K.; Perez-Villarroel, P.; Villagra, A.; Sotomayor, E. M.; Kozikowski, A. P., Selective Histone Deacetylase 6 Inhibitors Bearing Substituted Urea Linkers Inhibit Melanoma Cell Growth. *J. Med. Chem.* **2012,** *55* (22), 9891-9899.

Appendix I

Table 1: Growth inhibitory activity of selected bifunctional compounds in HeLa cells

Compound	**HeLa IC_{50} (μM)** [a]
2b	**6.50**
11b	**8.87**
17b	**4.02**
SAHA	**2.12**

[a] average of three independent experiments.

Docking against HDAC6:

i

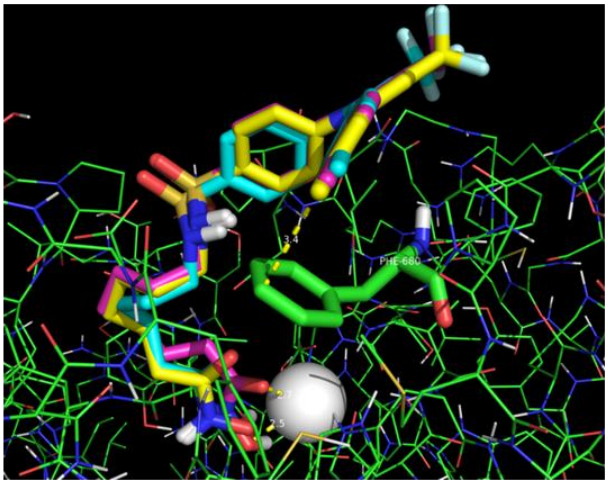

ii

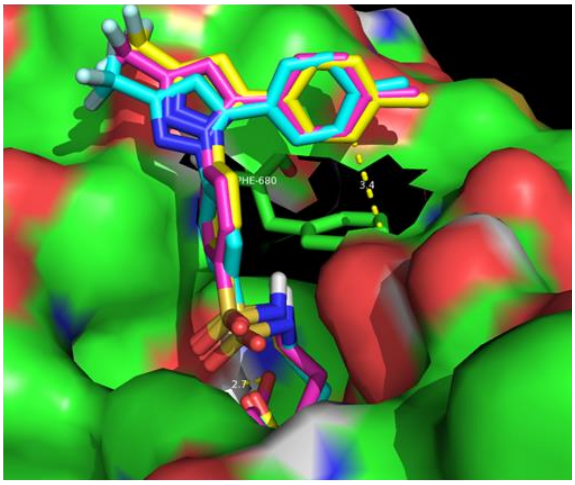

iii

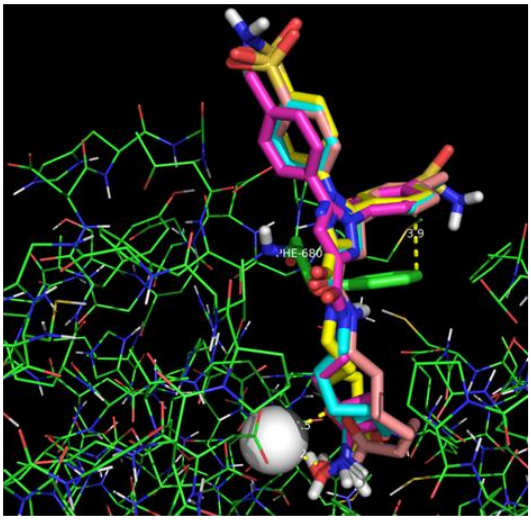

iv

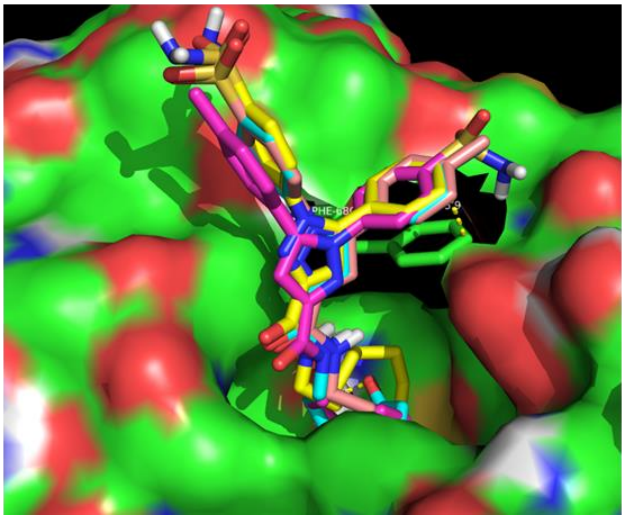

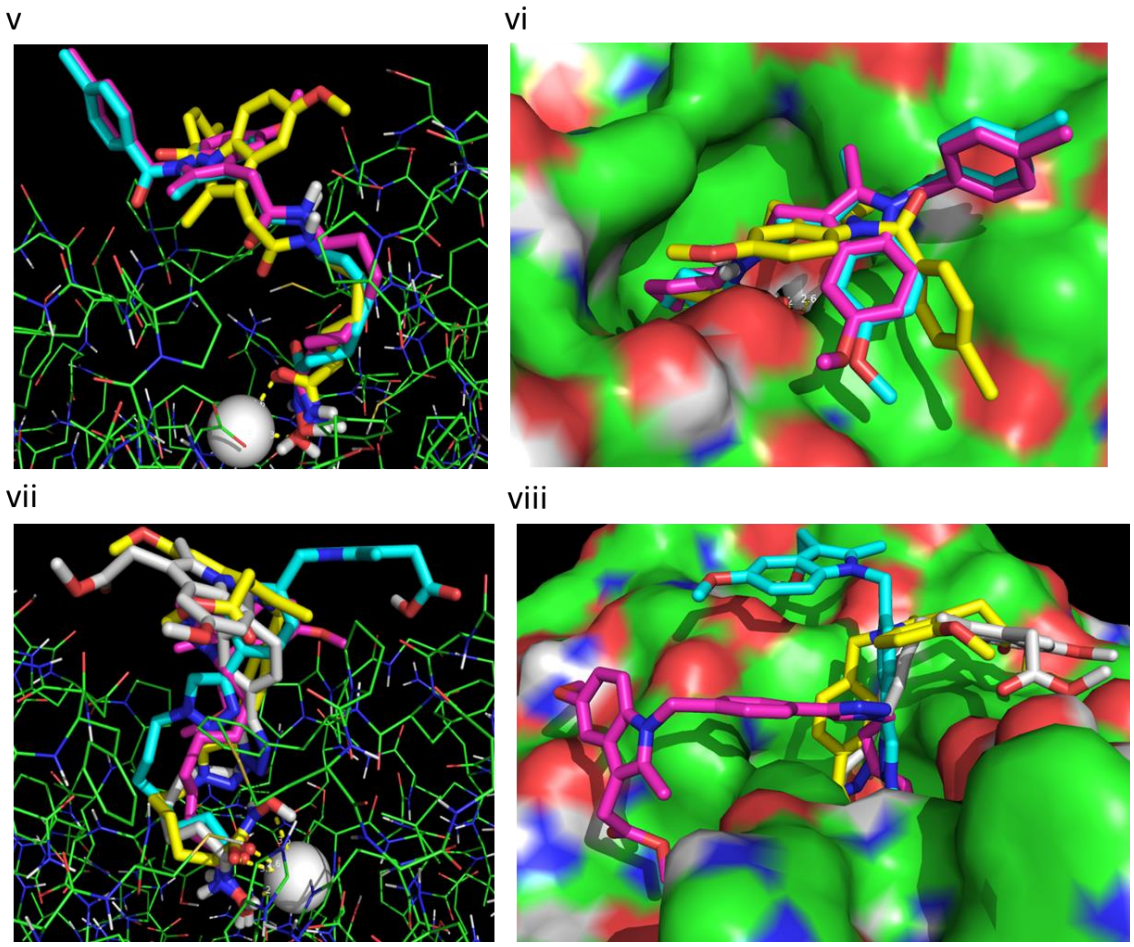

Figure 1: Docking against HDAC6; i) series 1 in HDAC6: 2a= light blue, 2b= yellow, 2c= magenta; ii) space fill model representation of (i), iii) series 2 & 3 in HDAC6: 7a= light blue, 7b= magenta, 7c= yellow, 8= brown; iv) space fill model representation of (iii); v) series 4 in HDAC6: 11a= blue, 11b= magenta, 11c= yellow; vi) space fill model representation of (v); vii) series 5 in HDAC6: 16=blue, 17a=yellow, 17b=gray, and 17c=magenta.

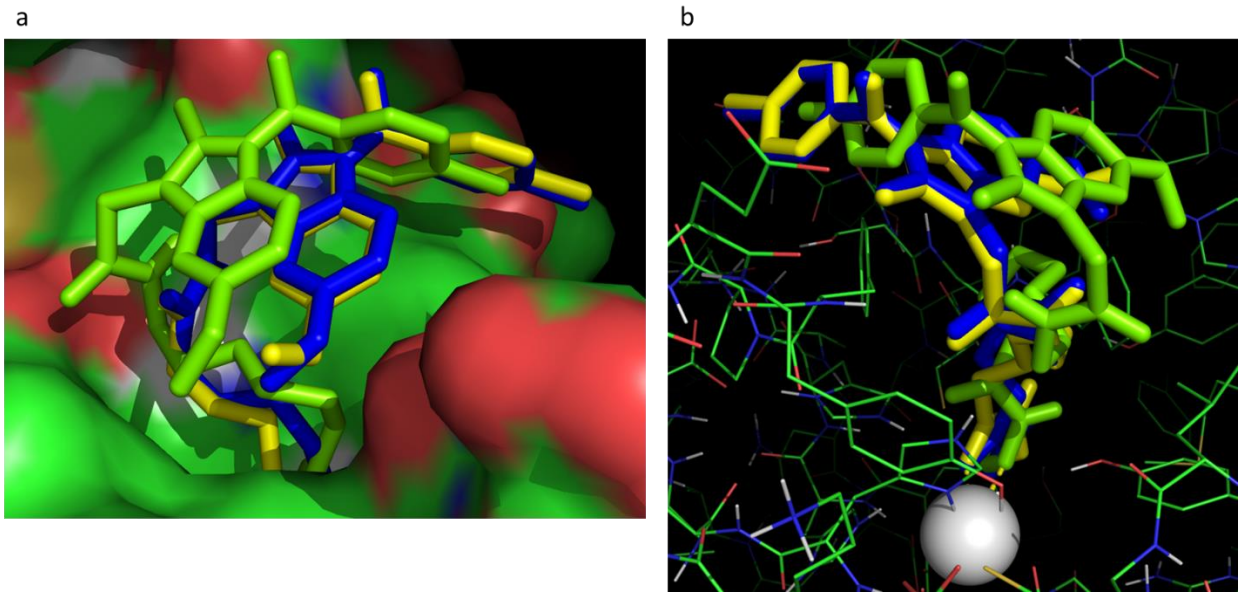

Figure 2: Docked structures of compounds 11a-c in the HDAC 1 active site: 11a= yellow, 11b= blue, 11c= green.

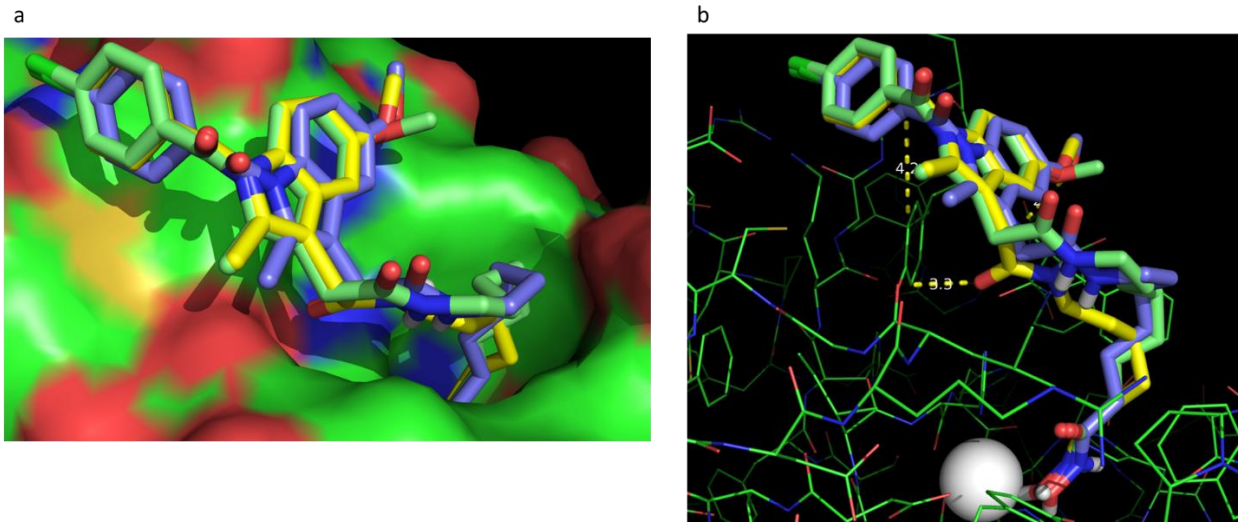

Figure 3: Docked structures of compounds 11a-c in the HDAC 2 active site: 11a= yellow, 11b= blue, 11c= green.

Intracellular target validation:

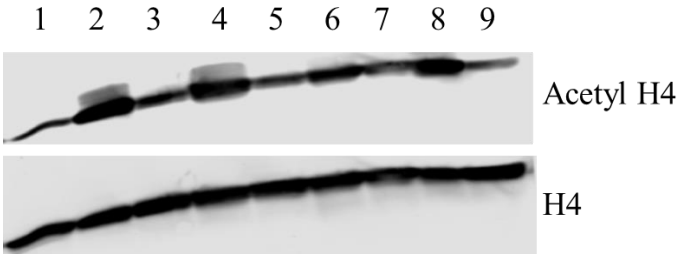

Figure 4: Western blot analysis of histone H4 acetylation in LNCaP cell line. Lanes: 1, Control (DMSO); 2, SAHA (10 μM); 3, **2b** (2 μM); 4, **2b** (10 μM); 5, **11b** (2 μM); 6, **11b** (10 μM); 7, **17b** (1.5 μM); 8, **17b** (10 μM); 9, indomethacin (10 μM).

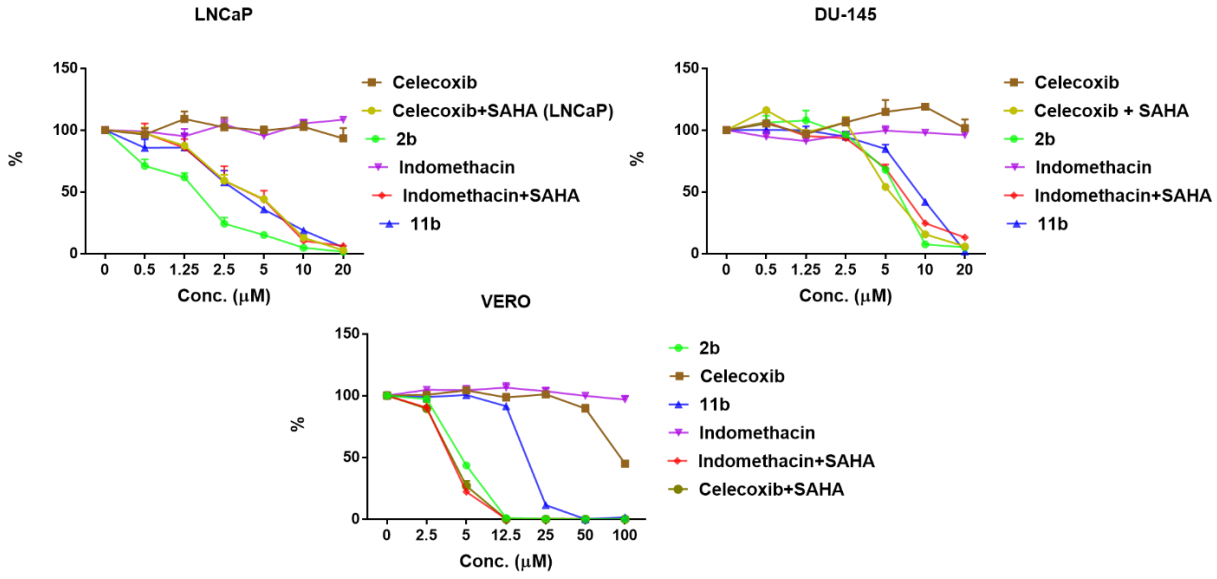

Figure 5: Comparison of antiproliferative activities of compounds **2b** and **11b**, and combinations of SAHA and the respective NSAIDs in LNCaP, DU-145 and VERO.

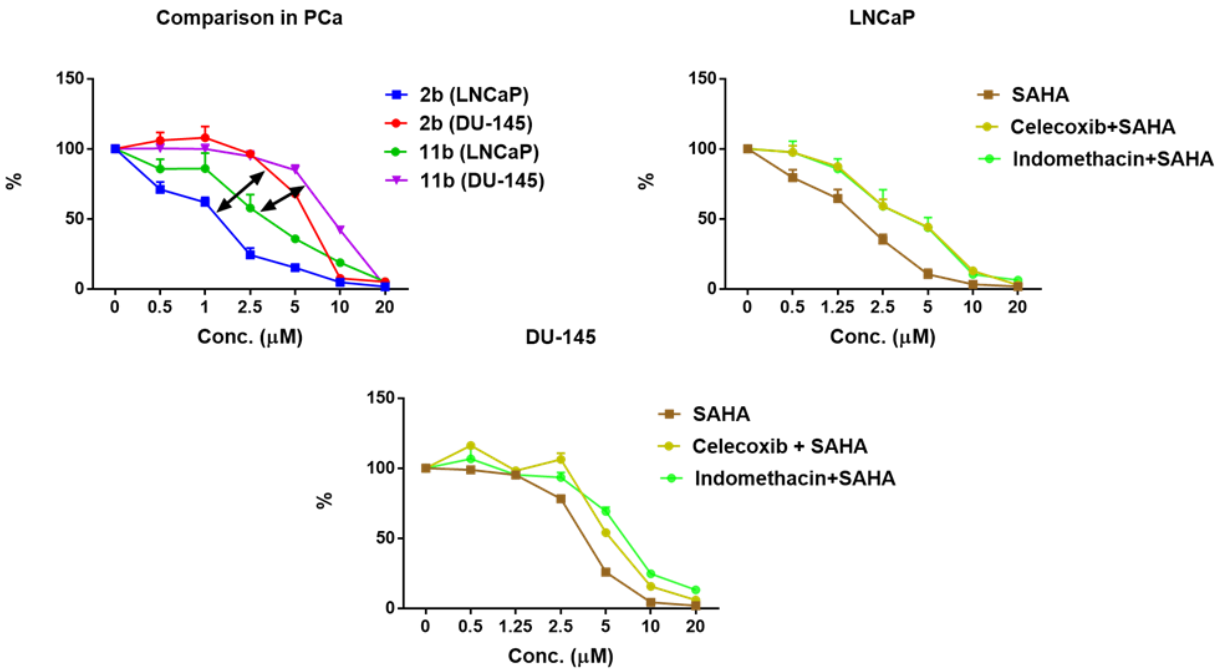

Figure 6: Degree of selectivity towards LNCaP shown by compounds **2b** and **11b**.

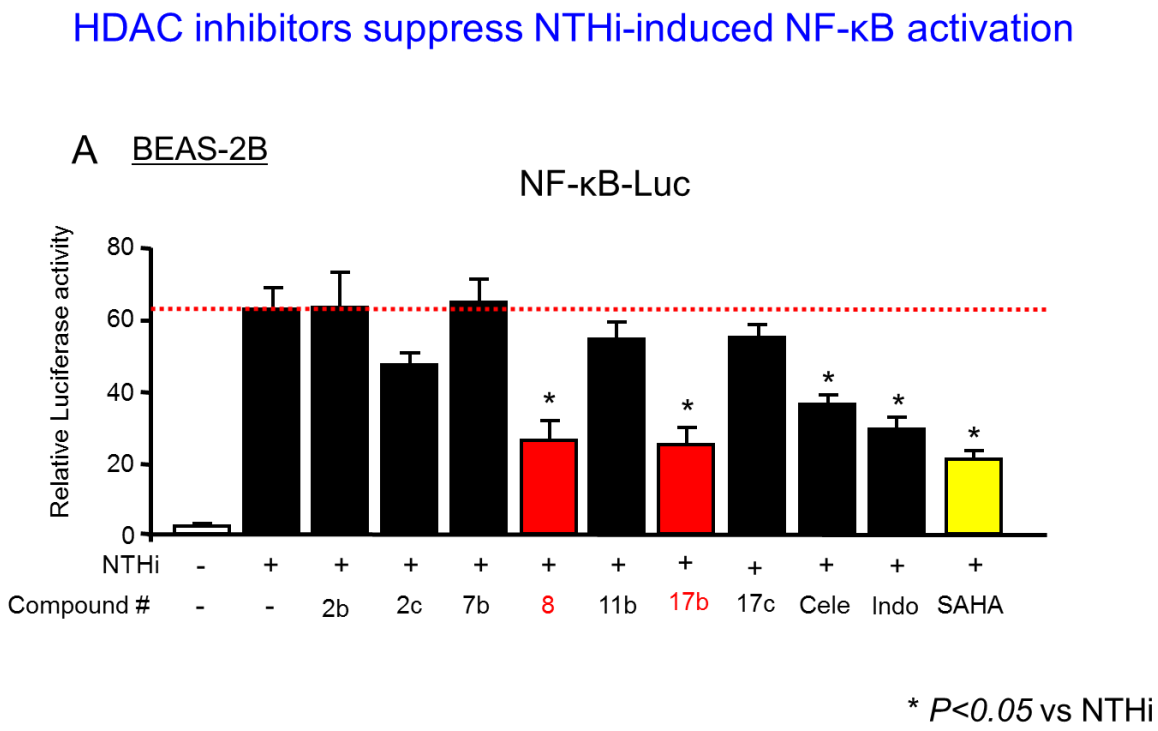

Figure 7: BEAS-2B cells, transfected with NF-κB luciferase construct, were pre-treated with tested compounds at 1 μM for 1hr and stimulated with NTHi for 5hr, and NF-kB promoter activity was then measured by performing luciferase assay. Data are mean ± SD (n=3). *$p<0.05$. Statistical analysis was performed using Student's *t*-test. Data are representative of three independent experiments. CON = BEAS-2B cells treated with PBS control; NTHi = BEAS-2B cells treated with NTHi

COMPOUND ^{1}H- AND ^{13}C-NMR

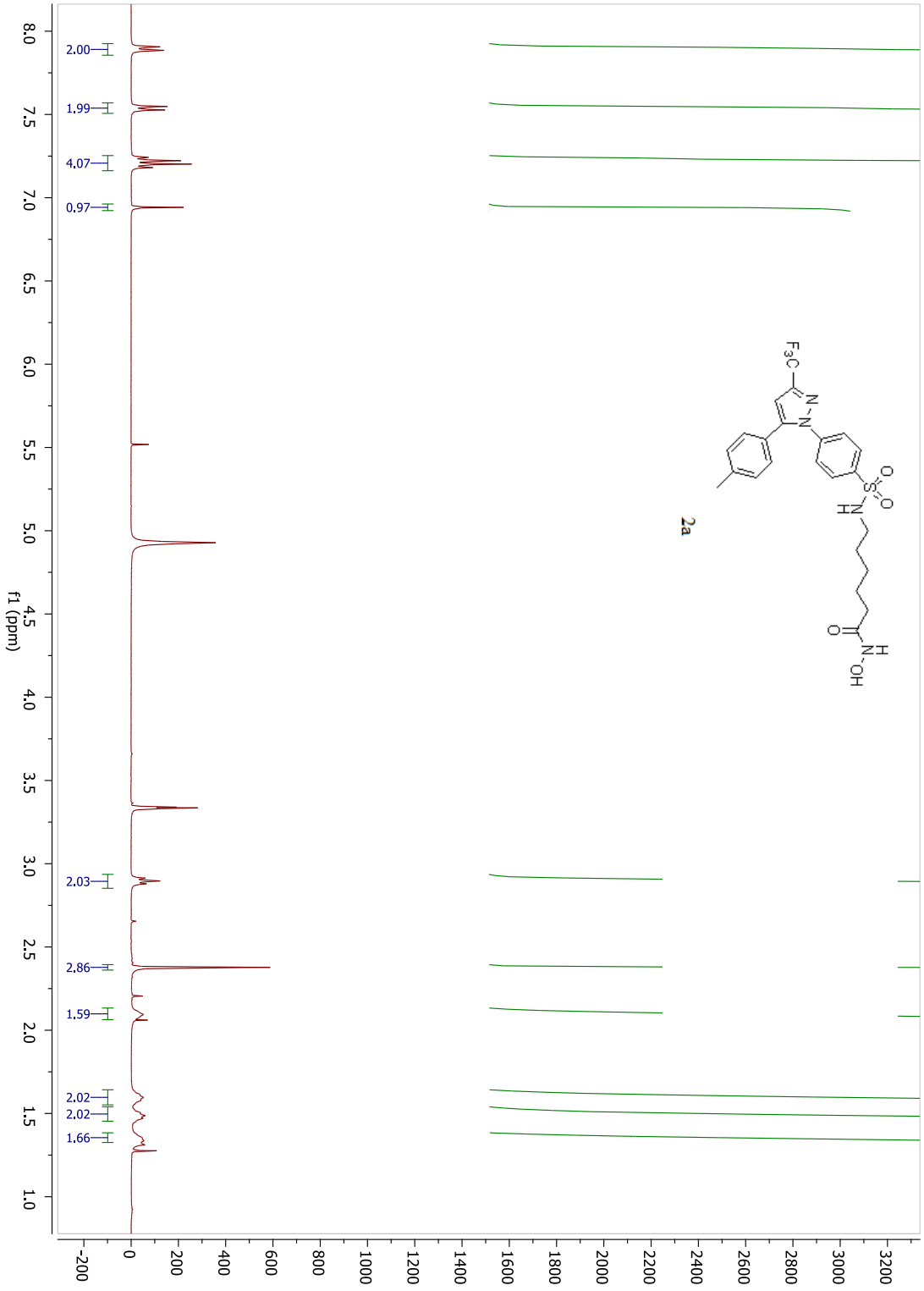

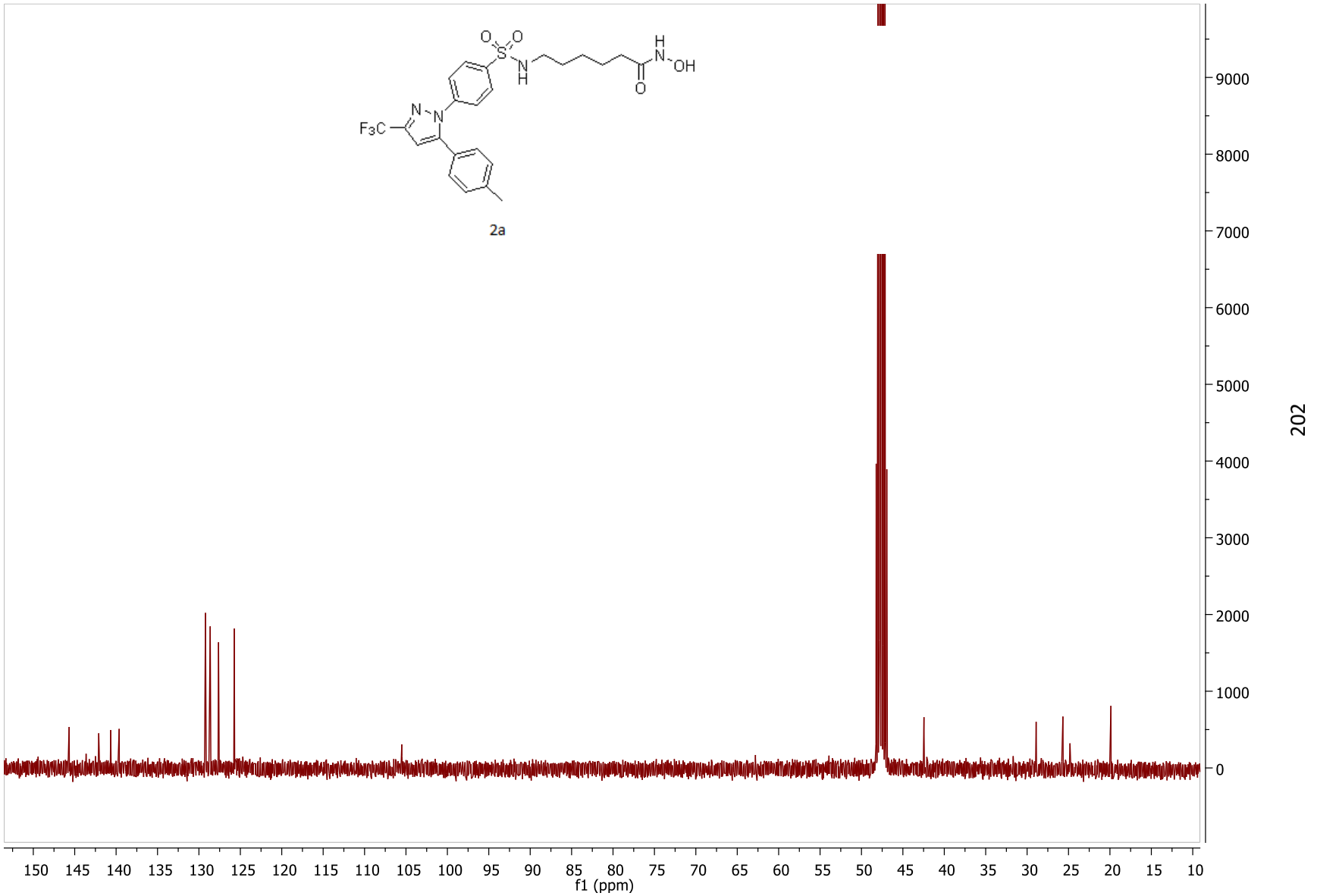
2a
9000
8000
7000
6000
5000
4000
3000
2000
1000
0
150 145 140 135 130 125 120 115 110 105 100 95 90 85 80 75 70 65 60 55 50 45 40 35 30 25 20 15 10
f1 (ppm)
202

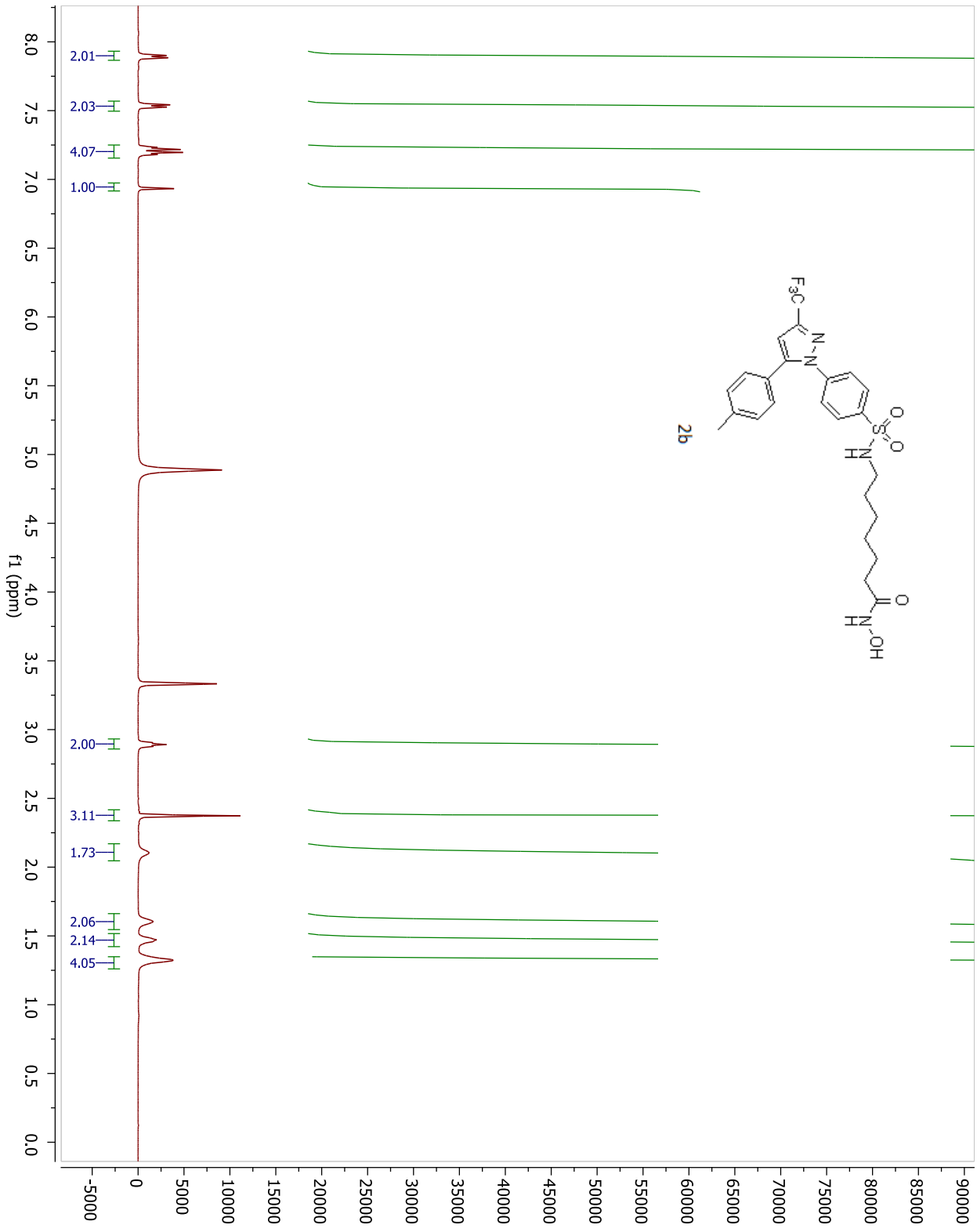
2.01
2.03
4.07
1.00
2.00
3.11
1.73
2.06
2.14
4.05
f1 (ppm)
2b

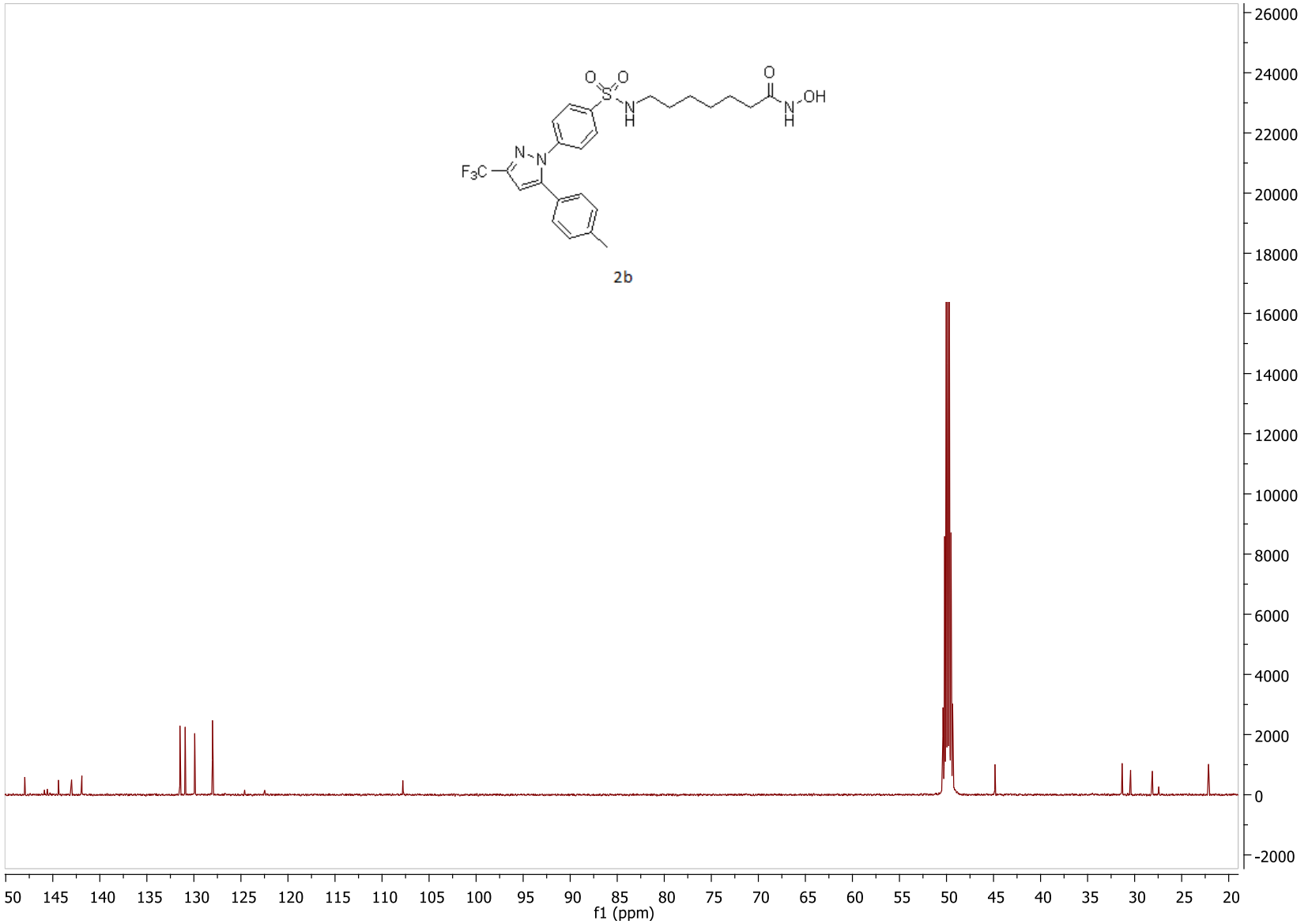
O
O
S
N
H
O
N
OH
H
N
N
F3C
2b
26000
24000
22000
20000
18000
16000
14000
12000
10000
8000
6000
4000
2000
0
-2000
50 145 140 135 130 125 120 115 110 105 100 95 90 85 80 75 70 65 60 55 50 45 40 35 30 25 20
f1 (ppm)

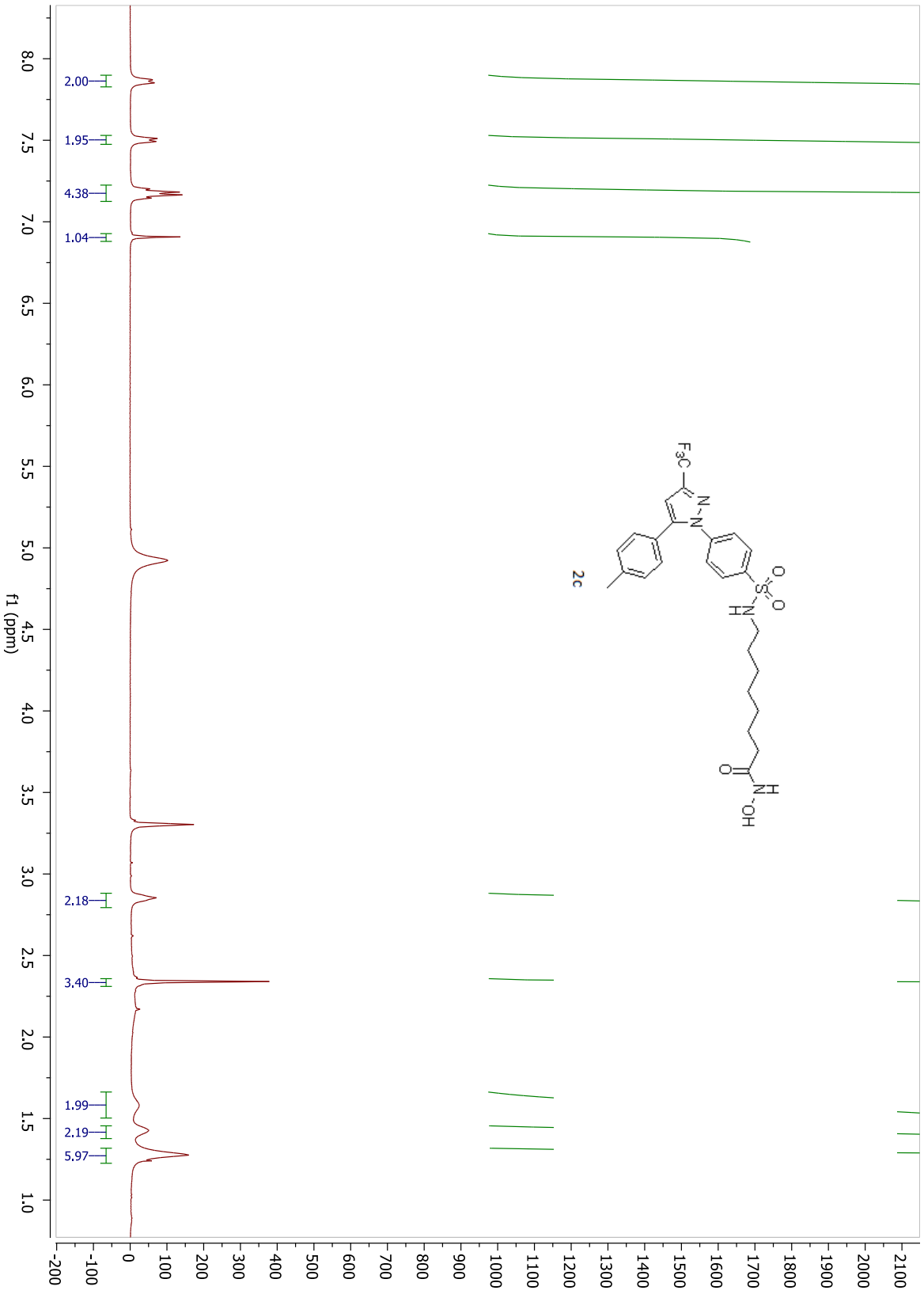
2.00
1.95
4.38
1.04
2.18
3.40
1.99
2.19
5.97
f1 (ppm)
2c

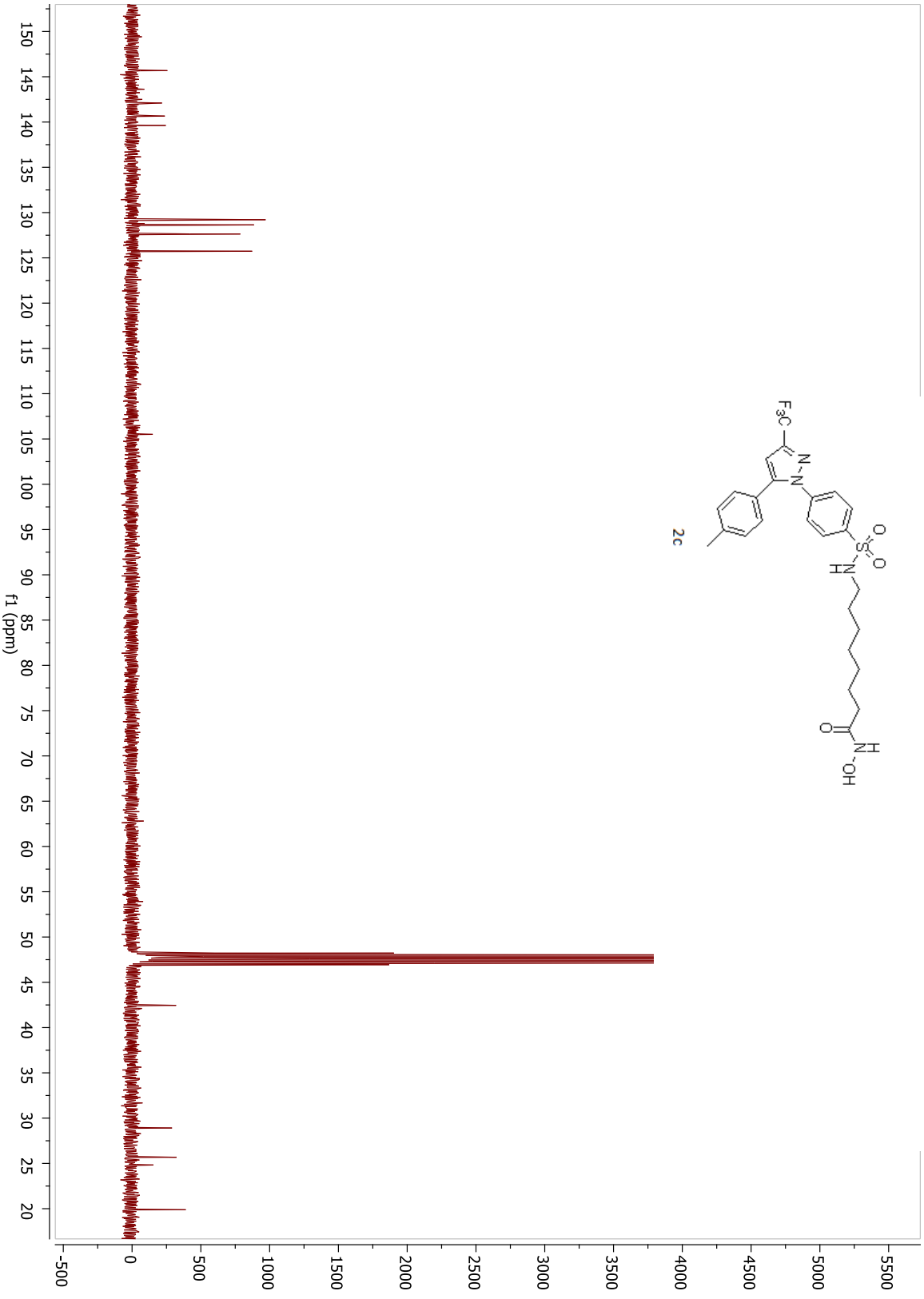
2c
F3C
N
N
O
S
O
H
N
O
H
N
OH
f1 (ppm)
150 145 140 135 130 125 120 115 110 105 100 95 90 85 80 75 70 65 60 55 50 45 40 35 30 25 20
-500 0 500 1000 1500 2000 2500 3000 3500 4000 4500 5000 5500

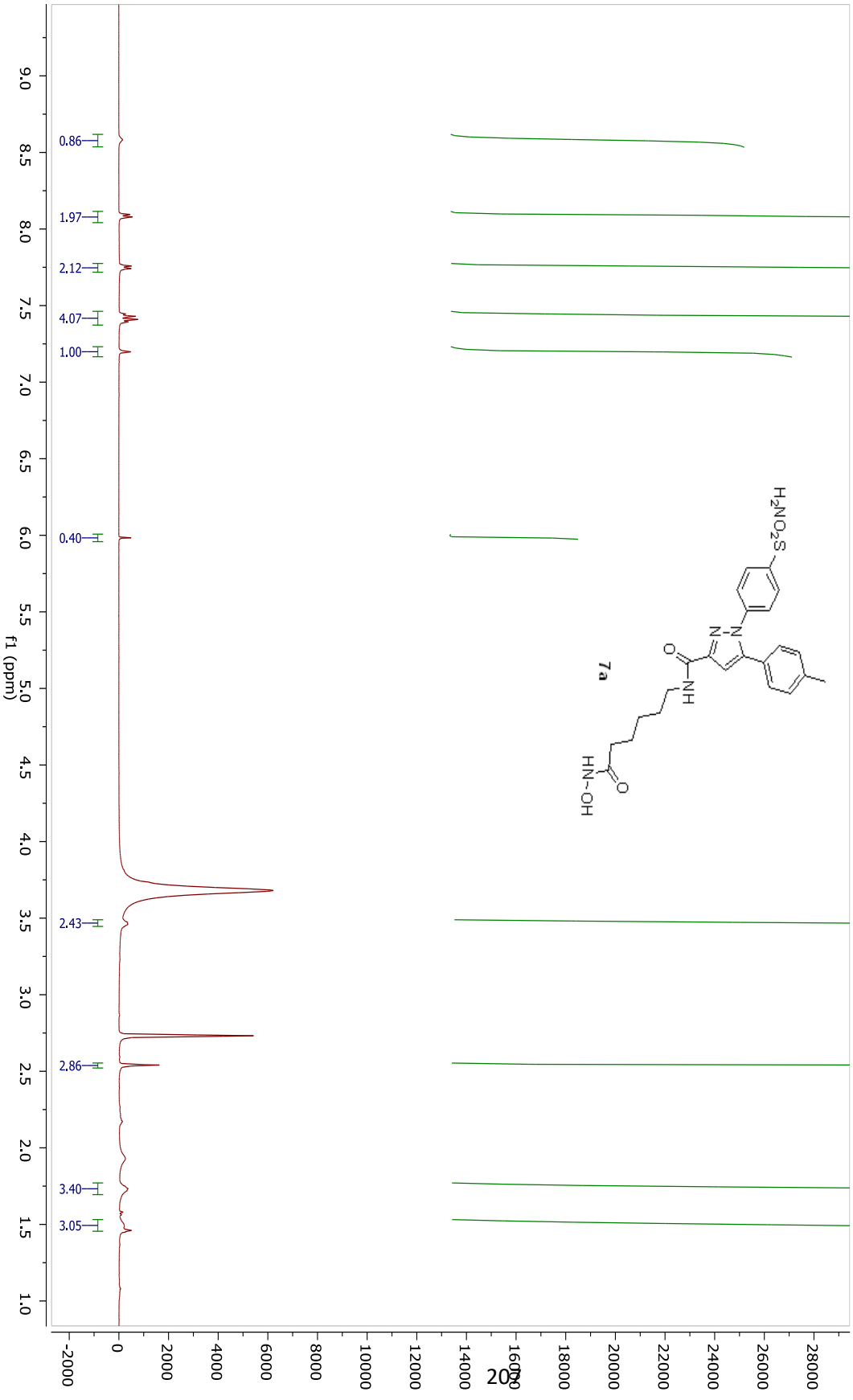
0.86
1.97
2.12
4.07
1.00
0.40
2.43
2.86
3.40
3.05
f1 (ppm)
7a
H2NO2S
NH
HN-OH
O

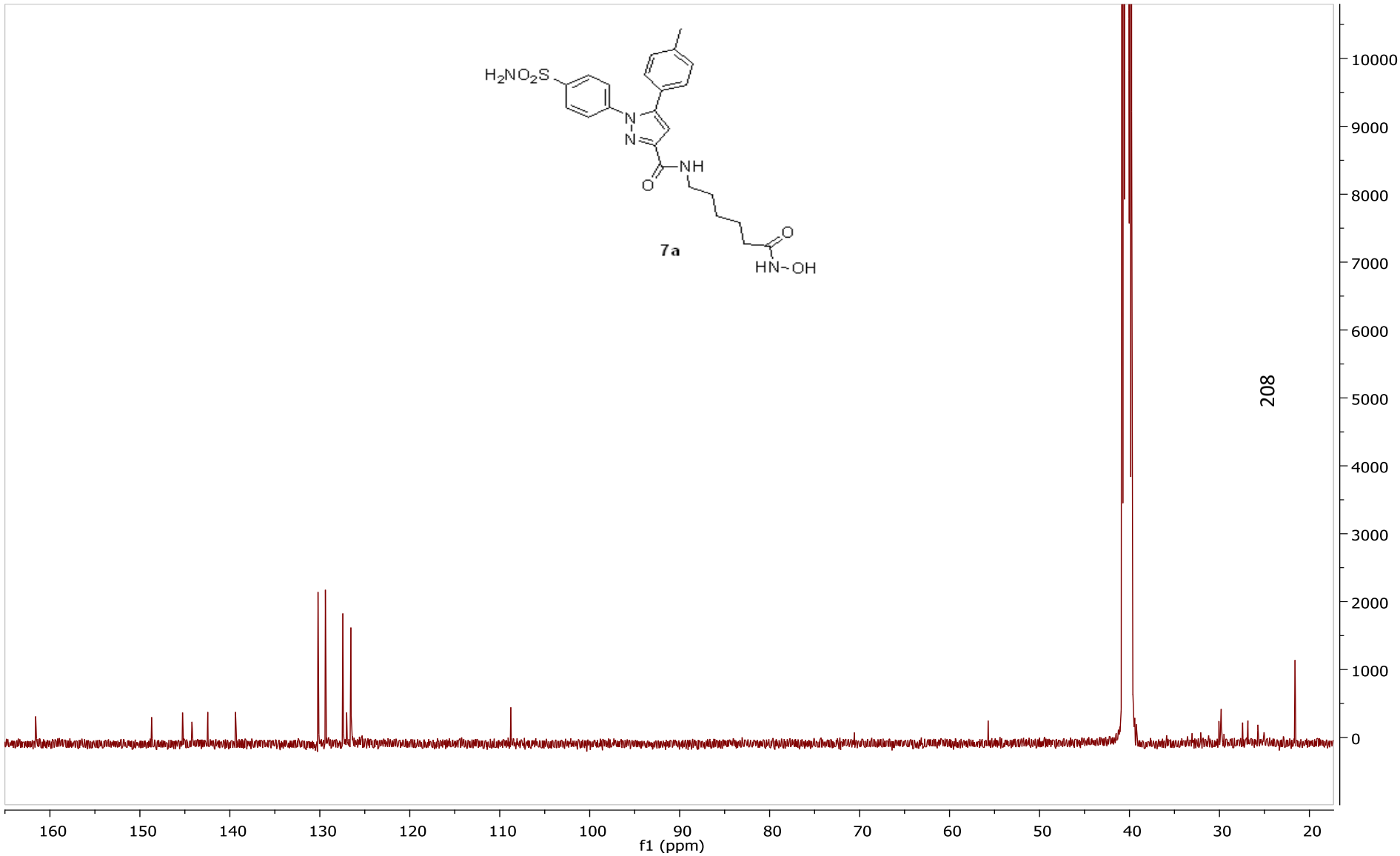
H2NO2S
N
N
NH
O
O
HN~OH
7a
208
10000
9000
8000
7000
6000
5000
4000
3000
2000
1000
0
160
150
140
130
120
110
100
90
80
70
60
50
40
30
20
f1 (ppm)

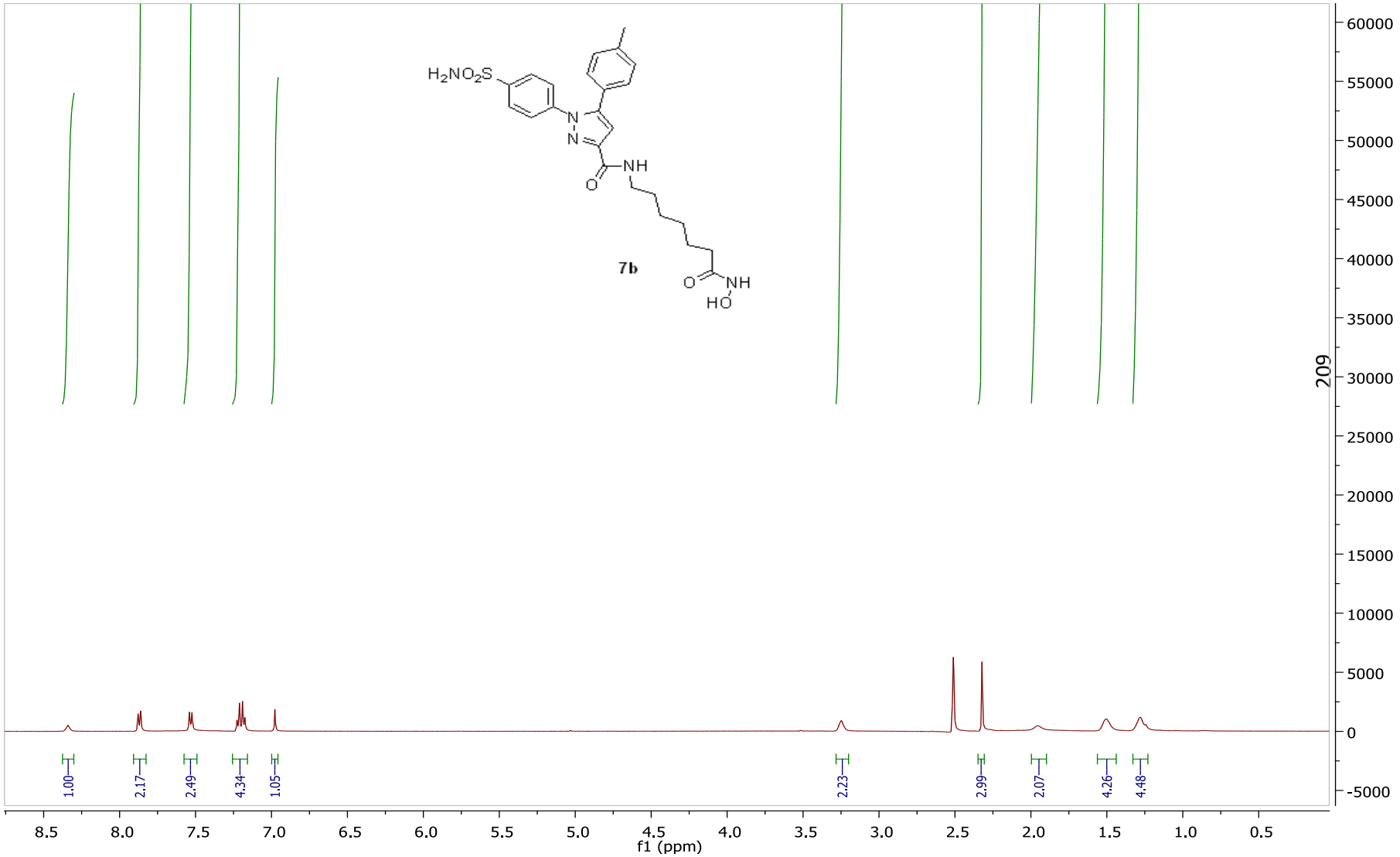
H2NO2S
N
N
NH
O
7b
O
NH
HO
209
60000
55000
50000
45000
40000
35000
30000
25000
20000
15000
10000
5000
0
-5000
1.00
2.17
2.49
4.34
1.05
2.23
2.99
2.07
4.26
4.48
8.5
8.0
7.5
7.0
6.5
6.0
5.5
5.0
4.5
4.0
3.5
3.0
2.5
2.0
1.5
1.0
0.5
f1 (ppm)

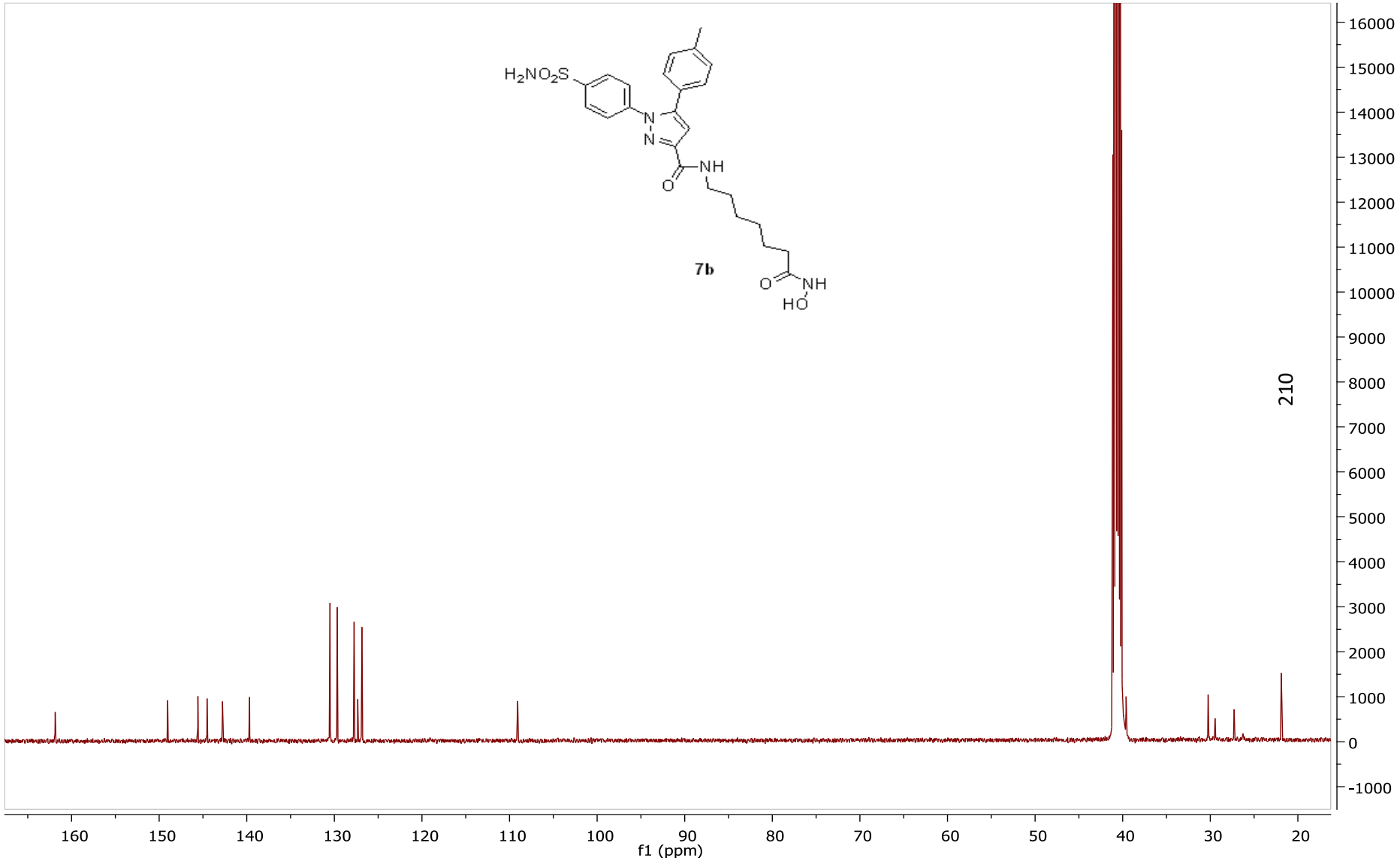
H2NO2S
N
N
NH
O
7b
O
NH
HO
210
16000
15000
14000
13000
12000
11000
10000
9000
8000
7000
6000
5000
4000
3000
2000
1000
0
-1000
160
150
140
130
120
110
100
90
80
70
60
50
40
30
20
f1 (ppm)

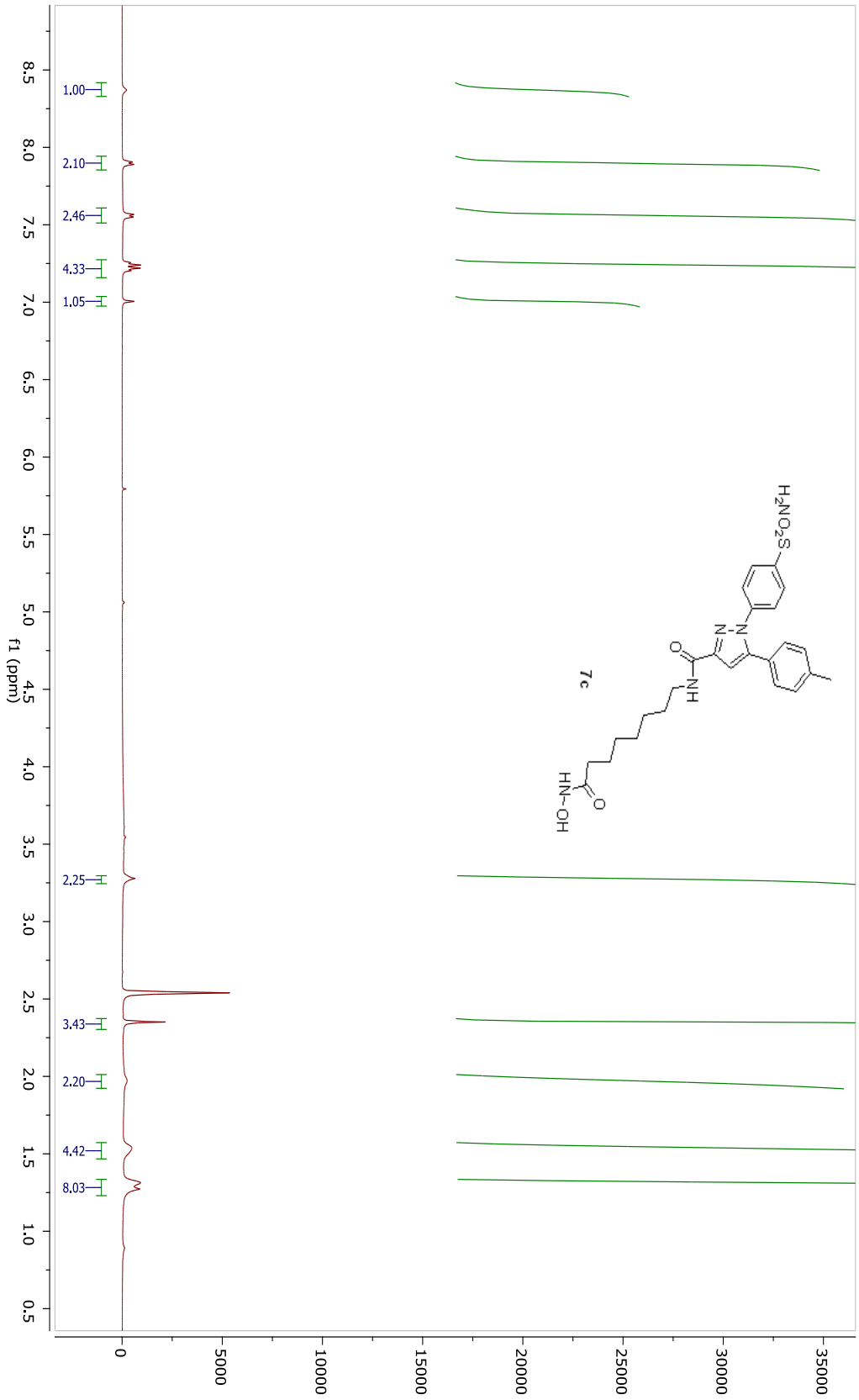
1.00
2.10
2.46
4.33
1.05
2.25
3.43
2.20
4.42
8.03
f1 (ppm)
7c

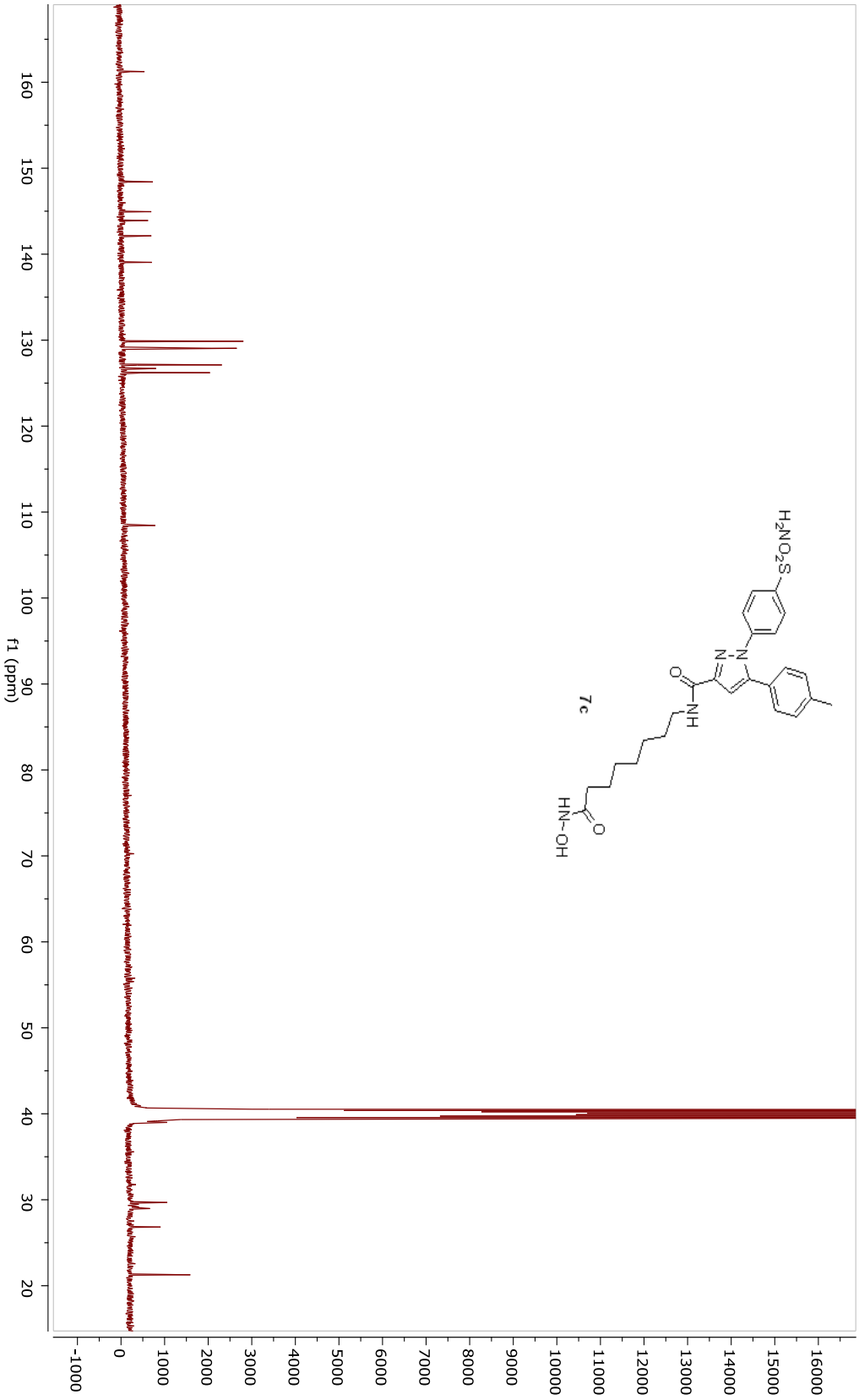
7c
H2NO2S
HN
O
HN-OH
O
f1 (ppm)

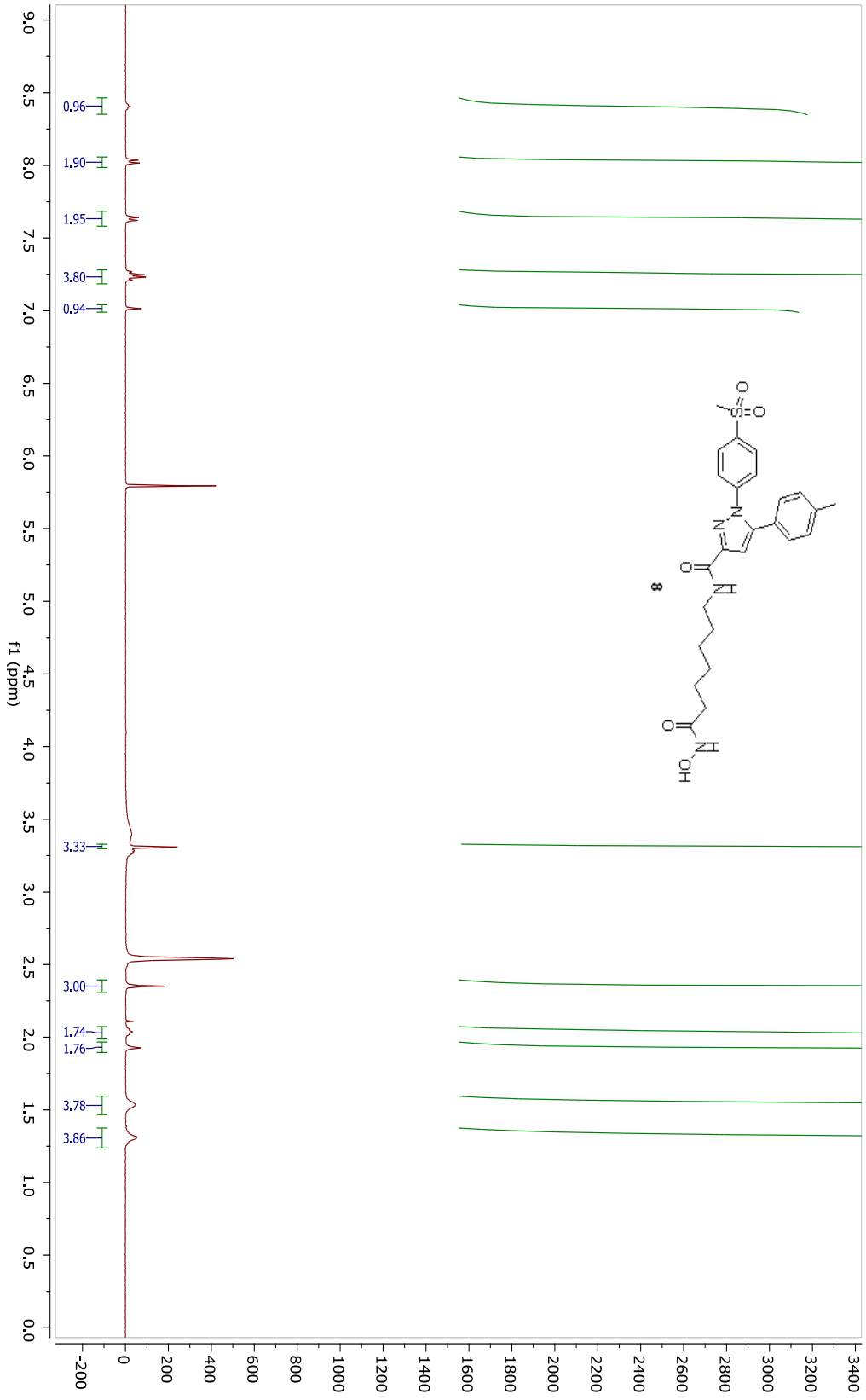
0.96
1.90
1.95
3.80
0.94
3.33
3.00
1.74
1.76
3.78
3.86
f1 (ppm)
8

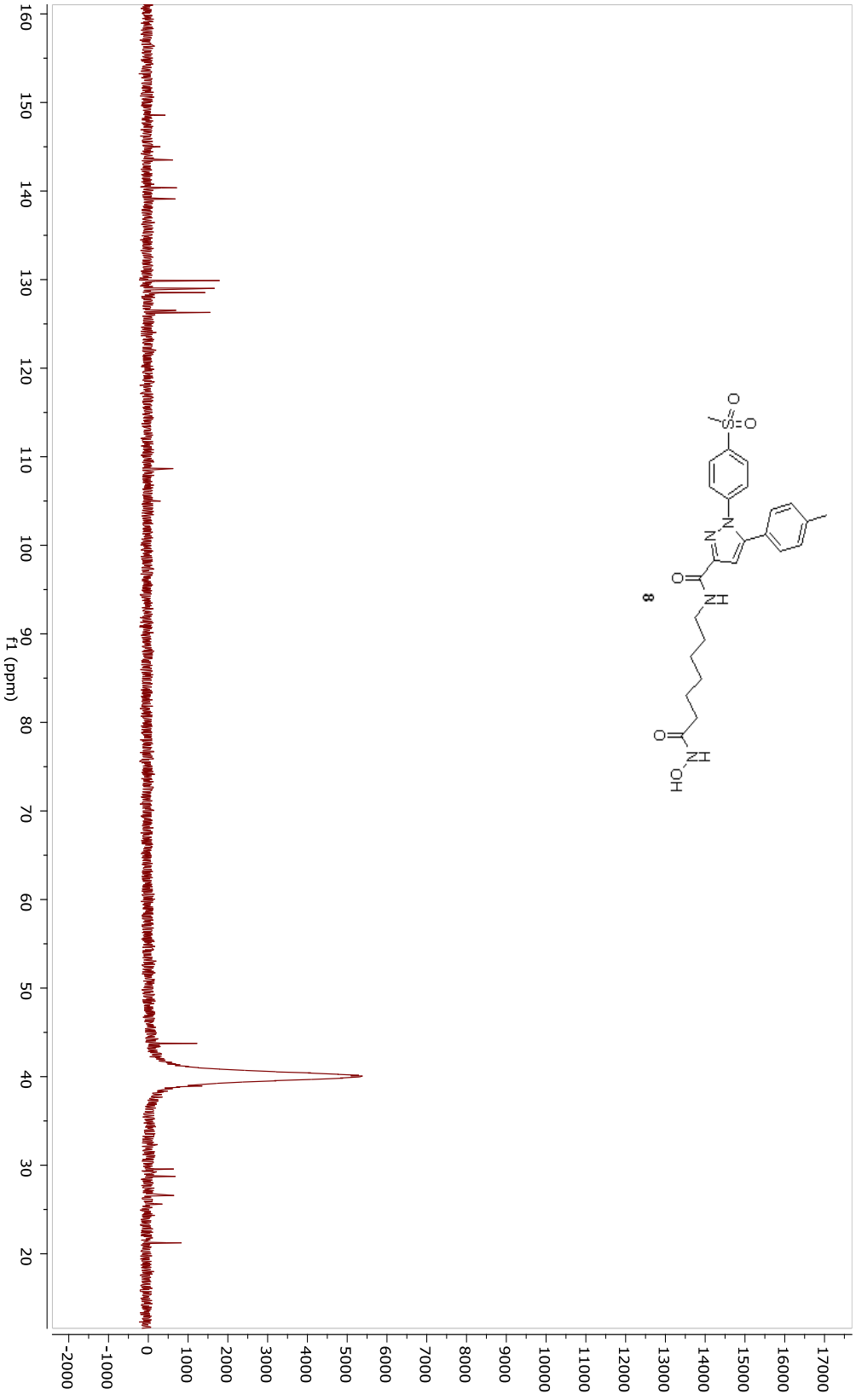
f1 (ppm)
8

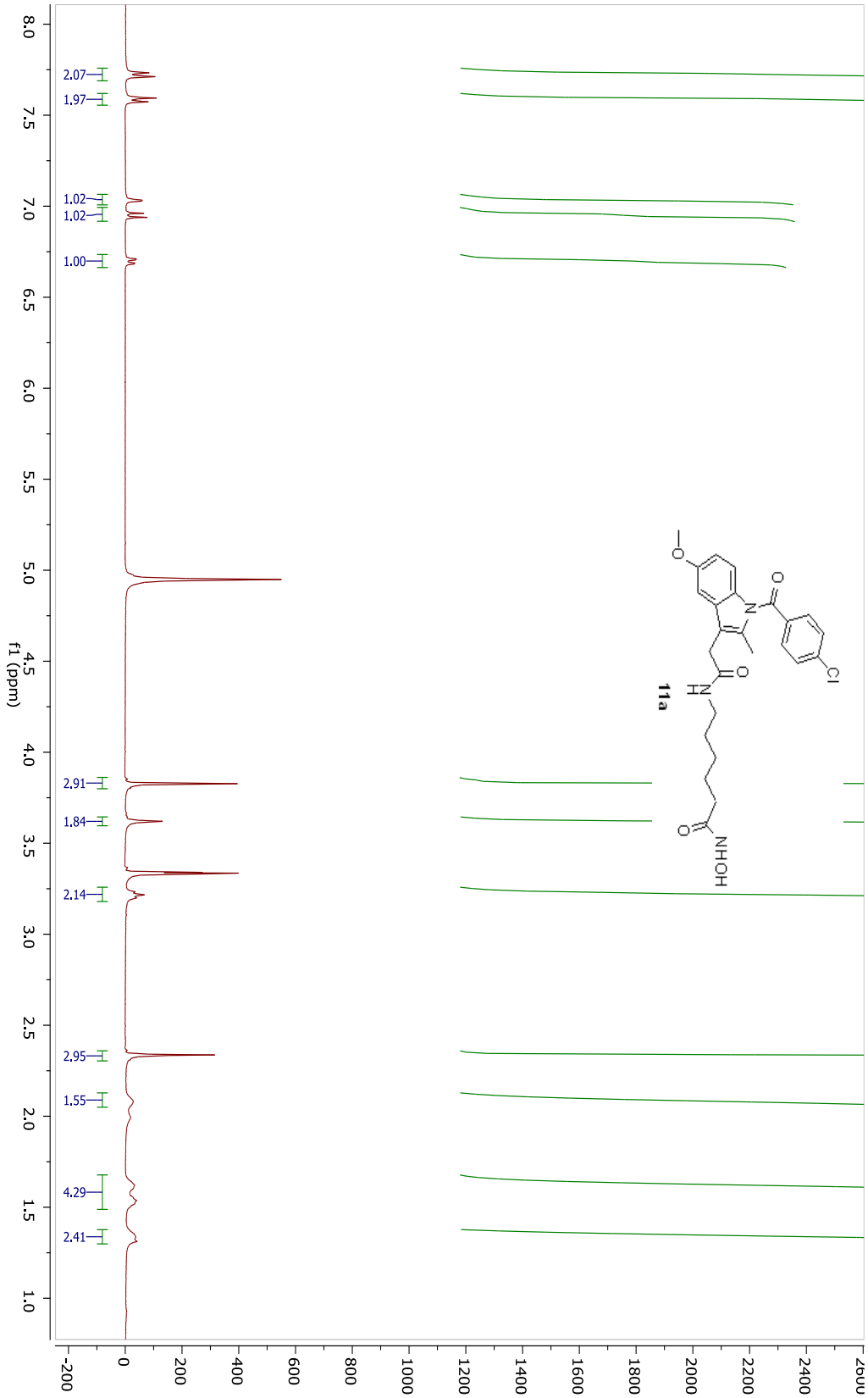
2.07
1.97
1.02
1.02
1.00
2.91
1.84
2.14
2.95
1.55
4.29
2.41
f1 (ppm)
11a
NHOH

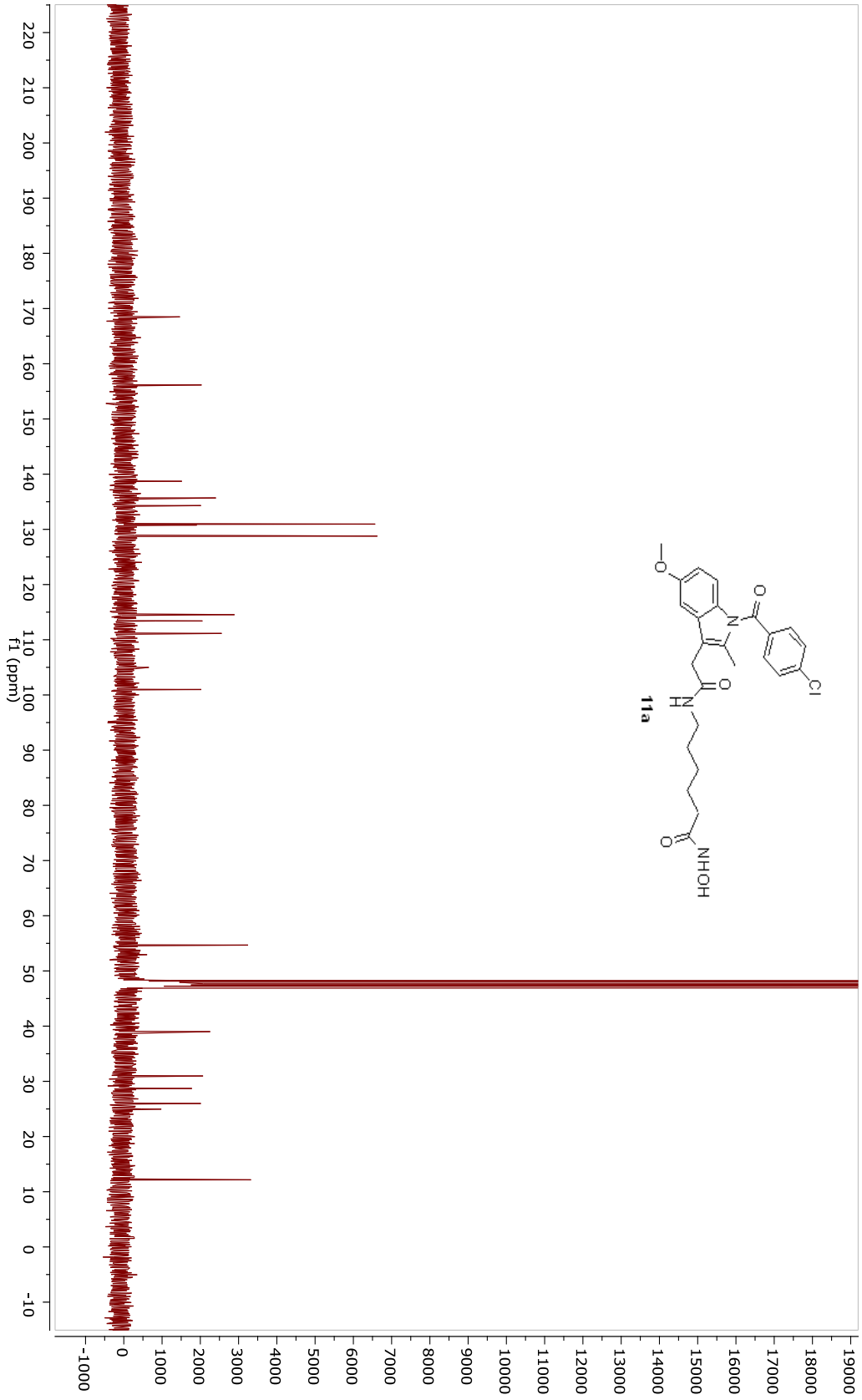
f1 (ppm)
11a

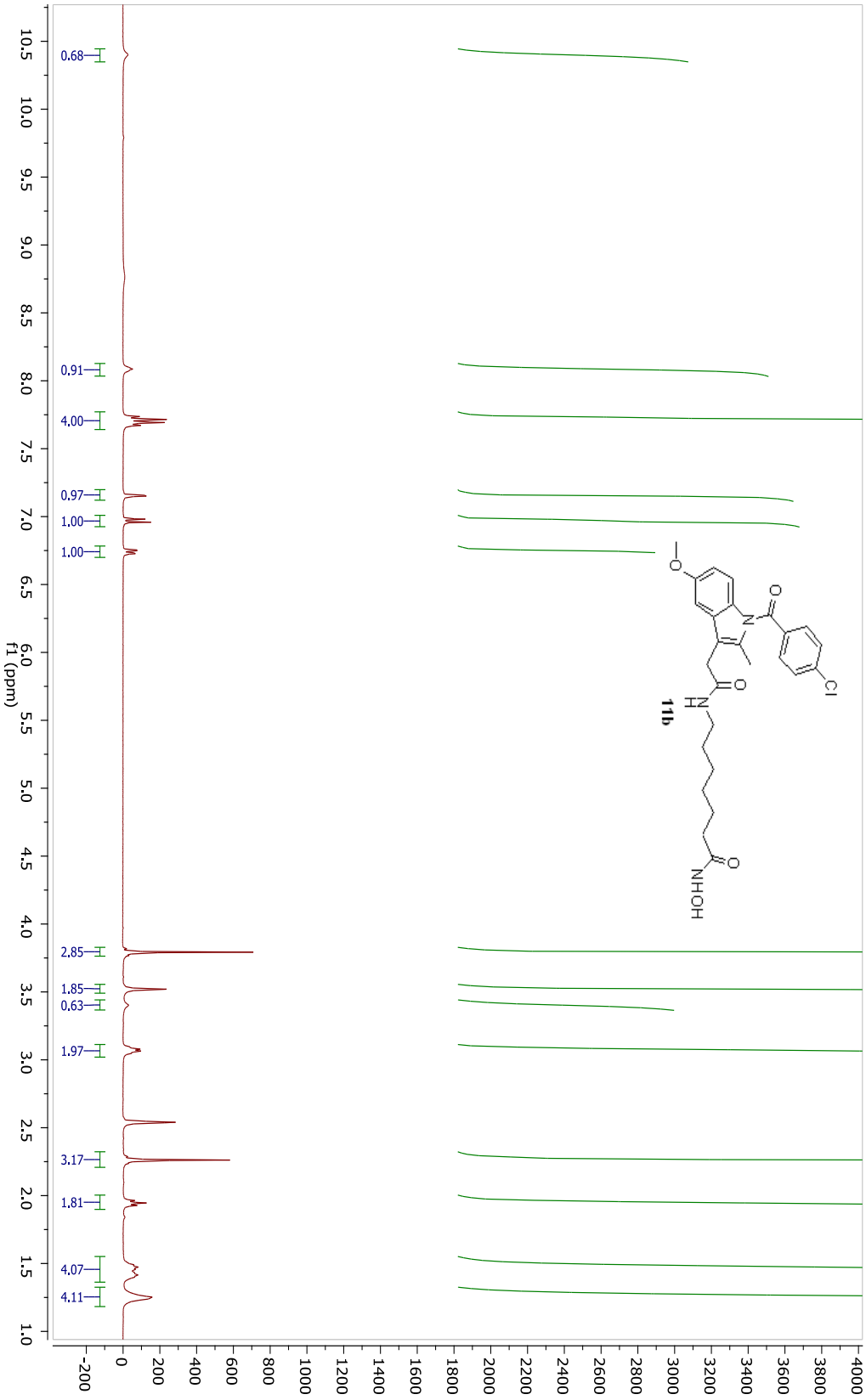
0.68
0.91
4.00
0.97
1.00
1.00
2.85
1.85
0.63
1.97
3.17
1.81
4.07
4.11
f1 (ppm)
11b

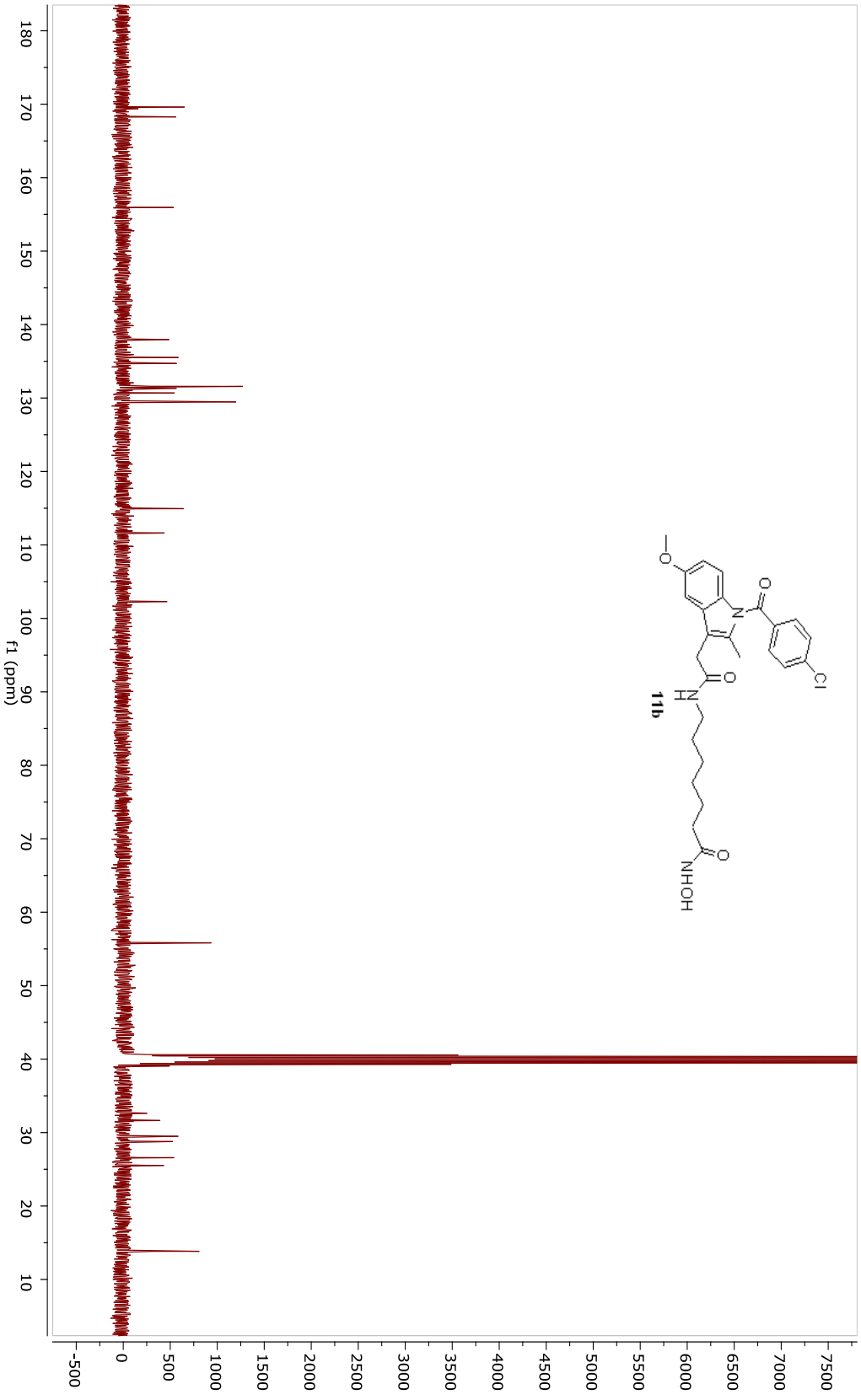
f1 (ppm)
11b

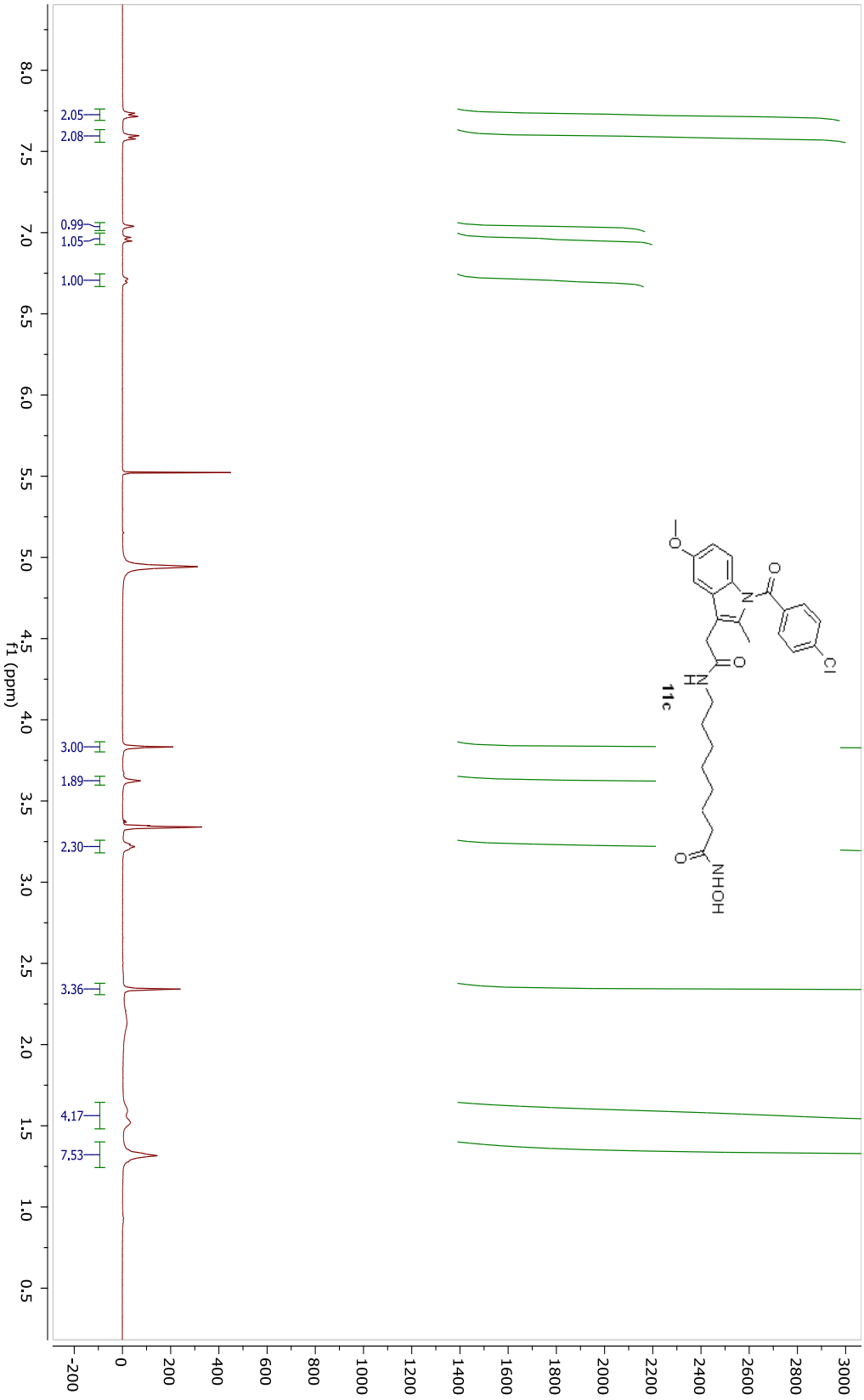
2.05
2.08
0.99
1.05
1.00
3.00
1.89
2.30
3.36
4.17
7.53
f1 (ppm)
11c
NHOH
Cl

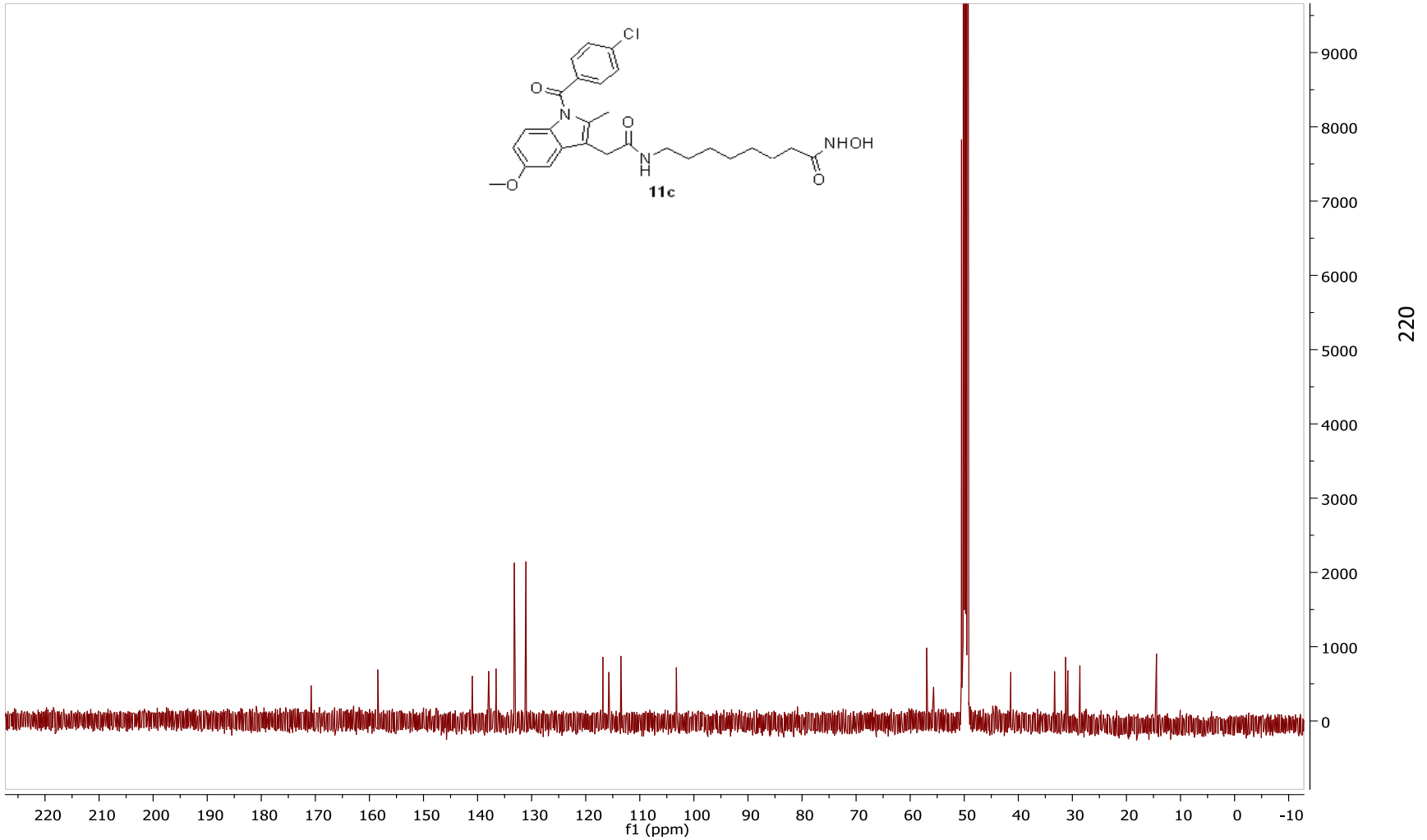
Cl
O
N
O
N
H
NHOH
O
O
11c
9000
8000
7000
6000
5000
4000
3000
2000
1000
0
220
220 210 200 190 180 170 160 150 140 130 120 110 100 90 80 70 60 50 40 30 20 10 0 -10
f1 (ppm)

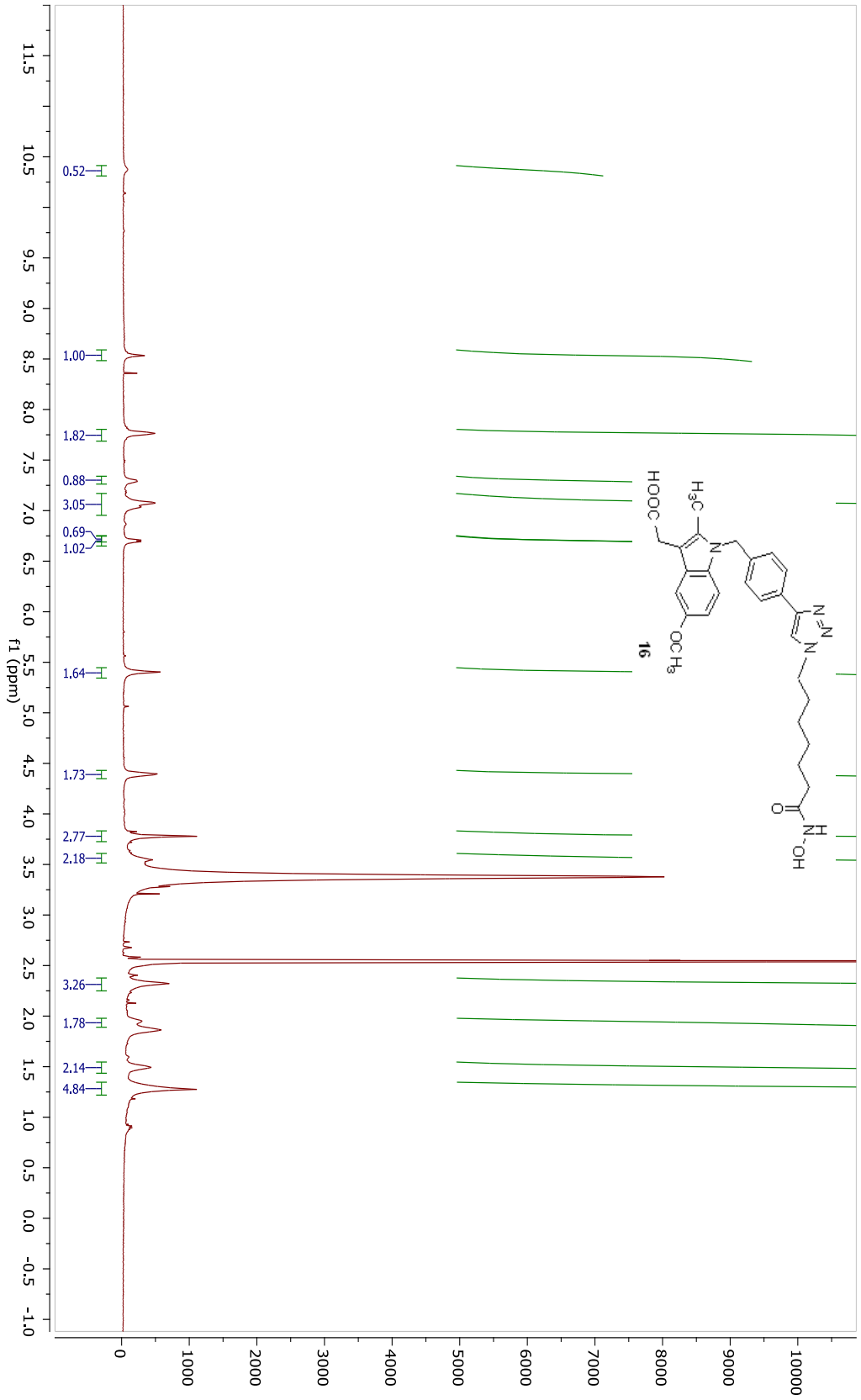
0.52
1.00
1.82
0.88
3.05
0.69
1.02
1.64
1.73
2.77
2.18
3.26
1.78
2.14
4.84
f1 (ppm)
HOOC
H3C
OCH3
16
N
N
N
O
H
N
OH

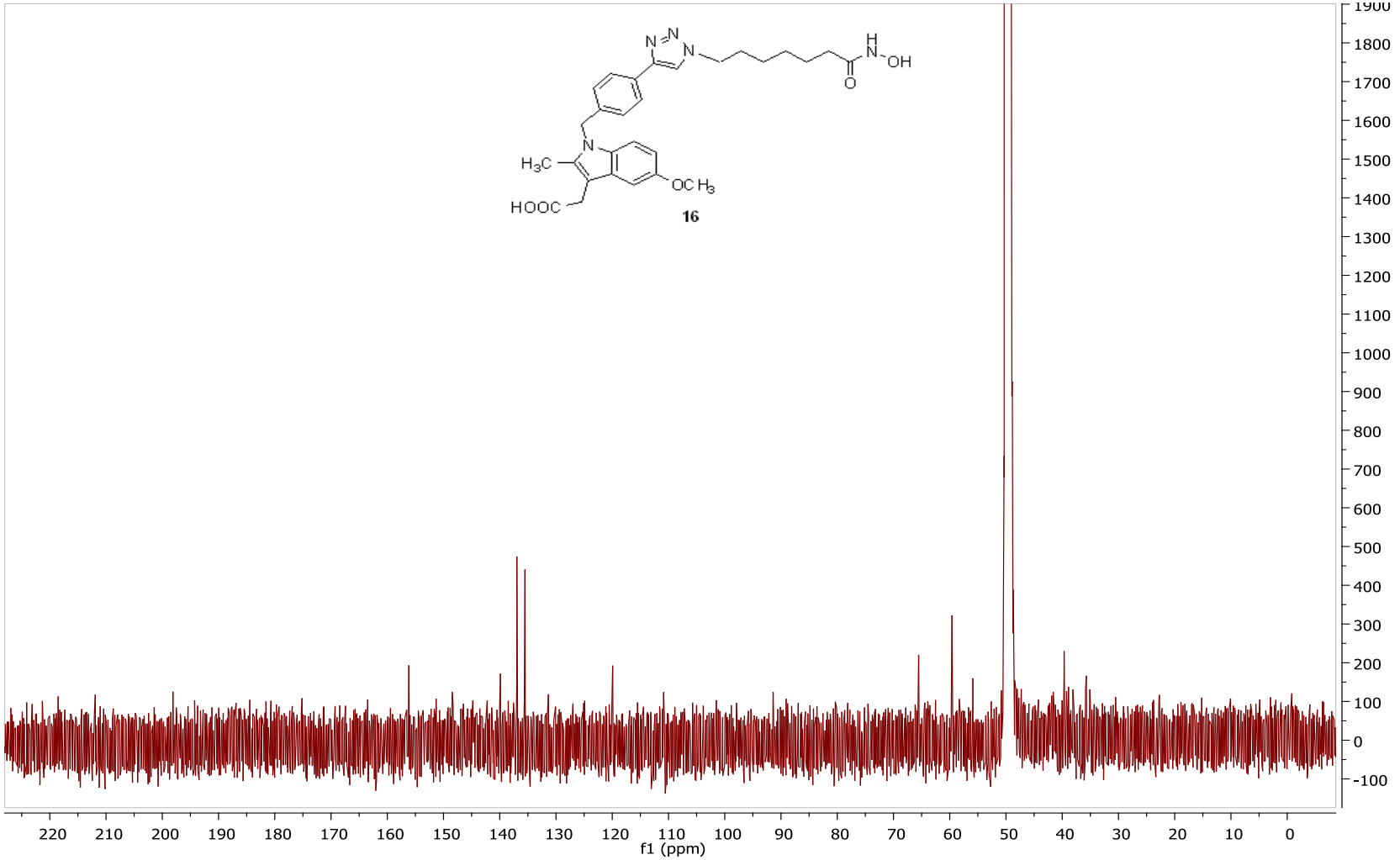
H3C
OCH3
HOOC
16
f1 (ppm)

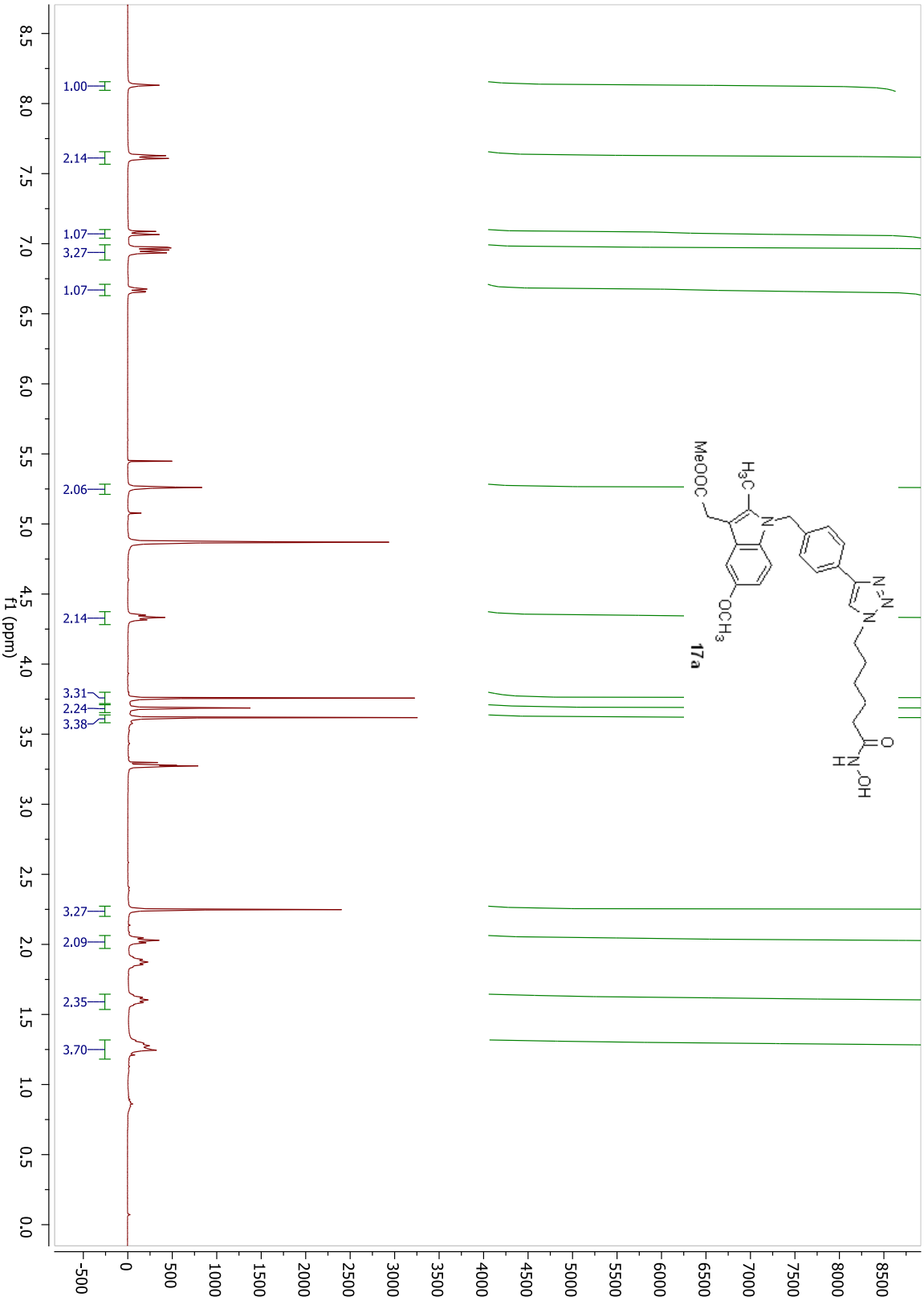
1.00
2.14
1.07
3.27
1.07
2.06
2.14
3.31
2.24
3.38
3.27
2.09
2.35
3.70
f1 (ppm)
MeOOC
H3C
OCH3
17a
O
H
N
OH

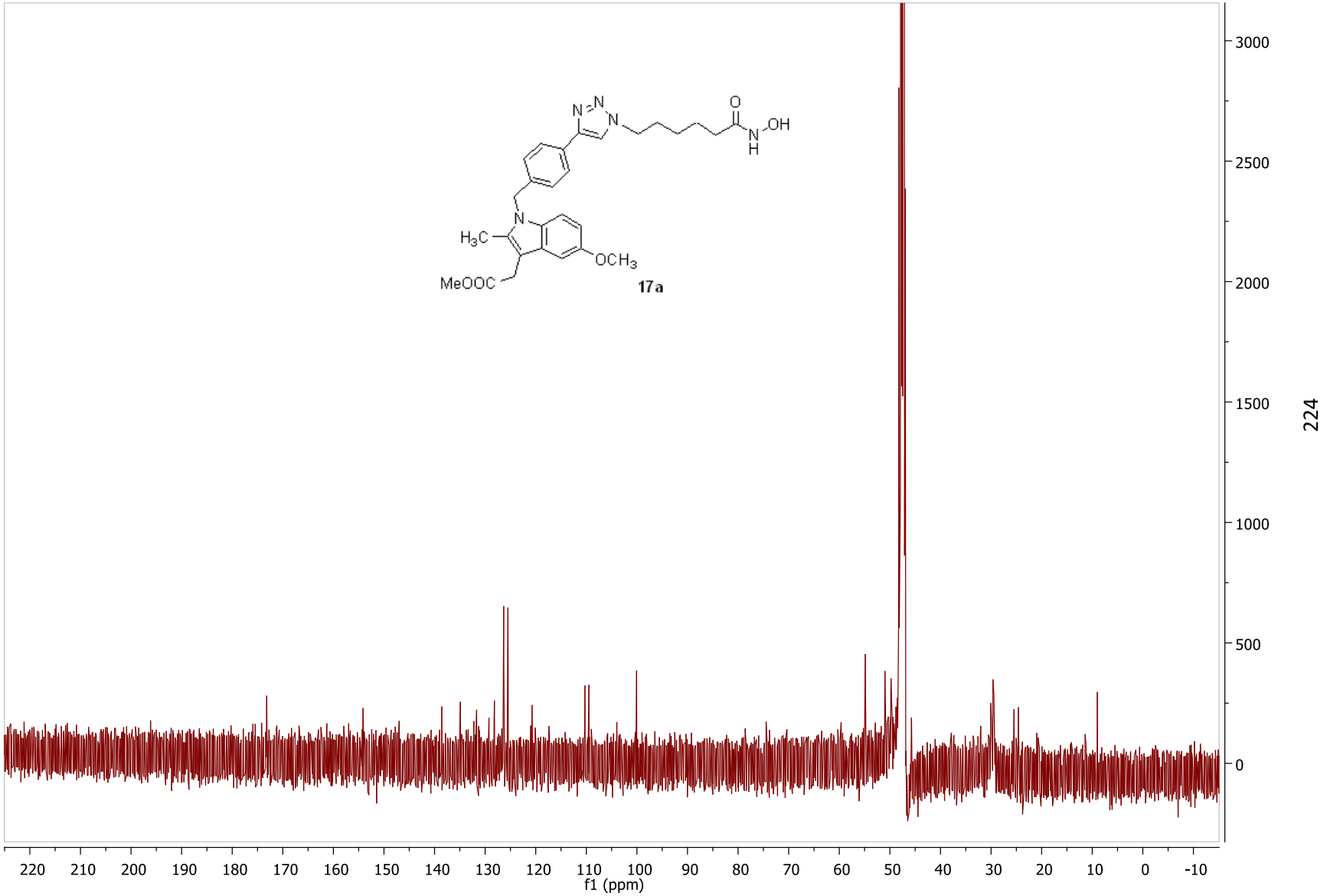
N
N
N
O
N
H
OH
H3C
N
OCH3
MeOOC
17a
3000
2500
2000
1500
1000
500
0
220
210
200
190
180
170
160
150
140
130
120
110
100
90
80
70
60
50
40
30
20
10
0
-10
f1 (ppm)
224

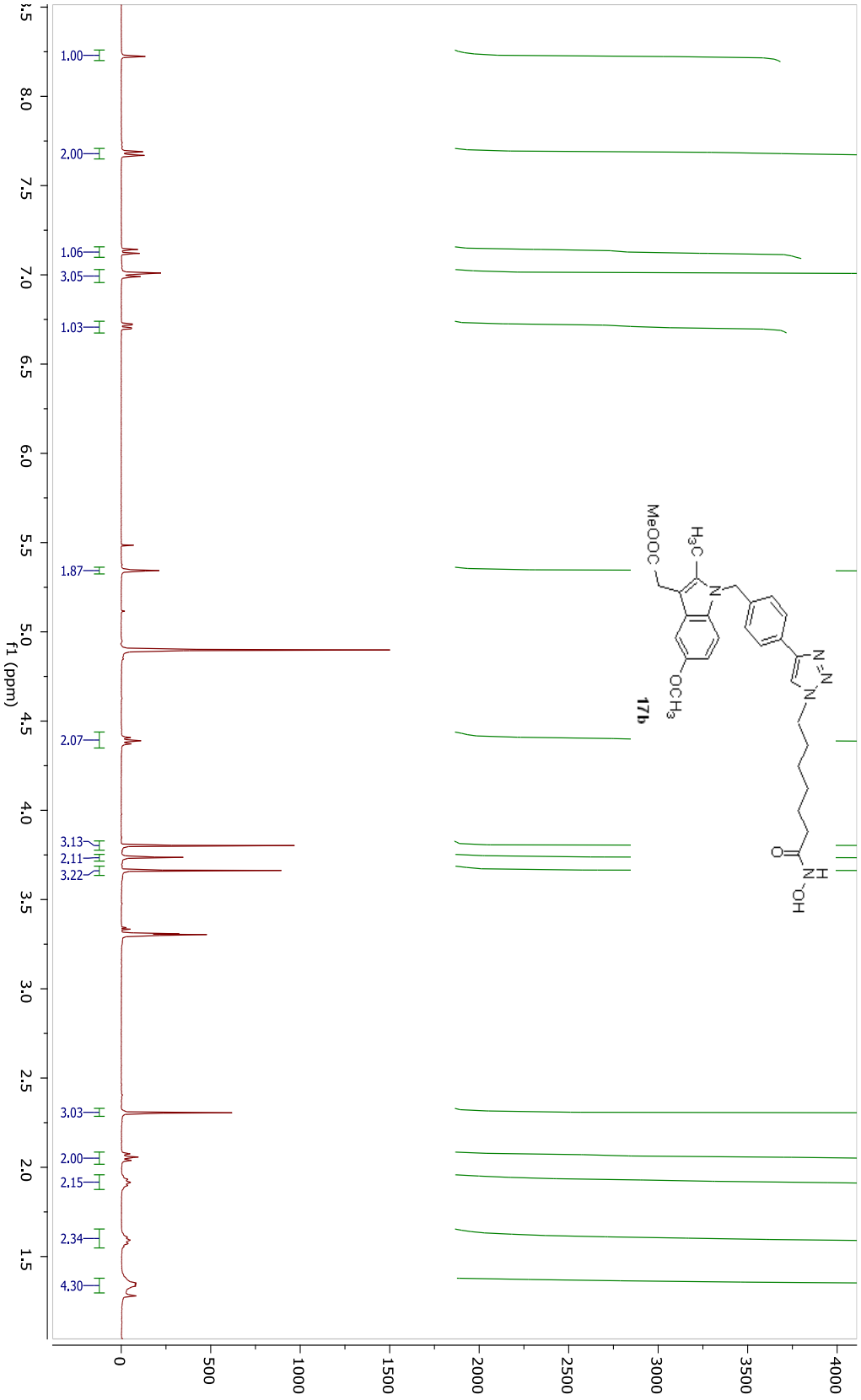
1.00
2.00
1.06
3.05
1.03
1.87
2.07
3.13
2.11
3.22
3.03
2.00
2.15
2.34
4.30
f1 (ppm)
MeOOC
H3C
OCH3
17b
N
N
N
O
H
N
OH

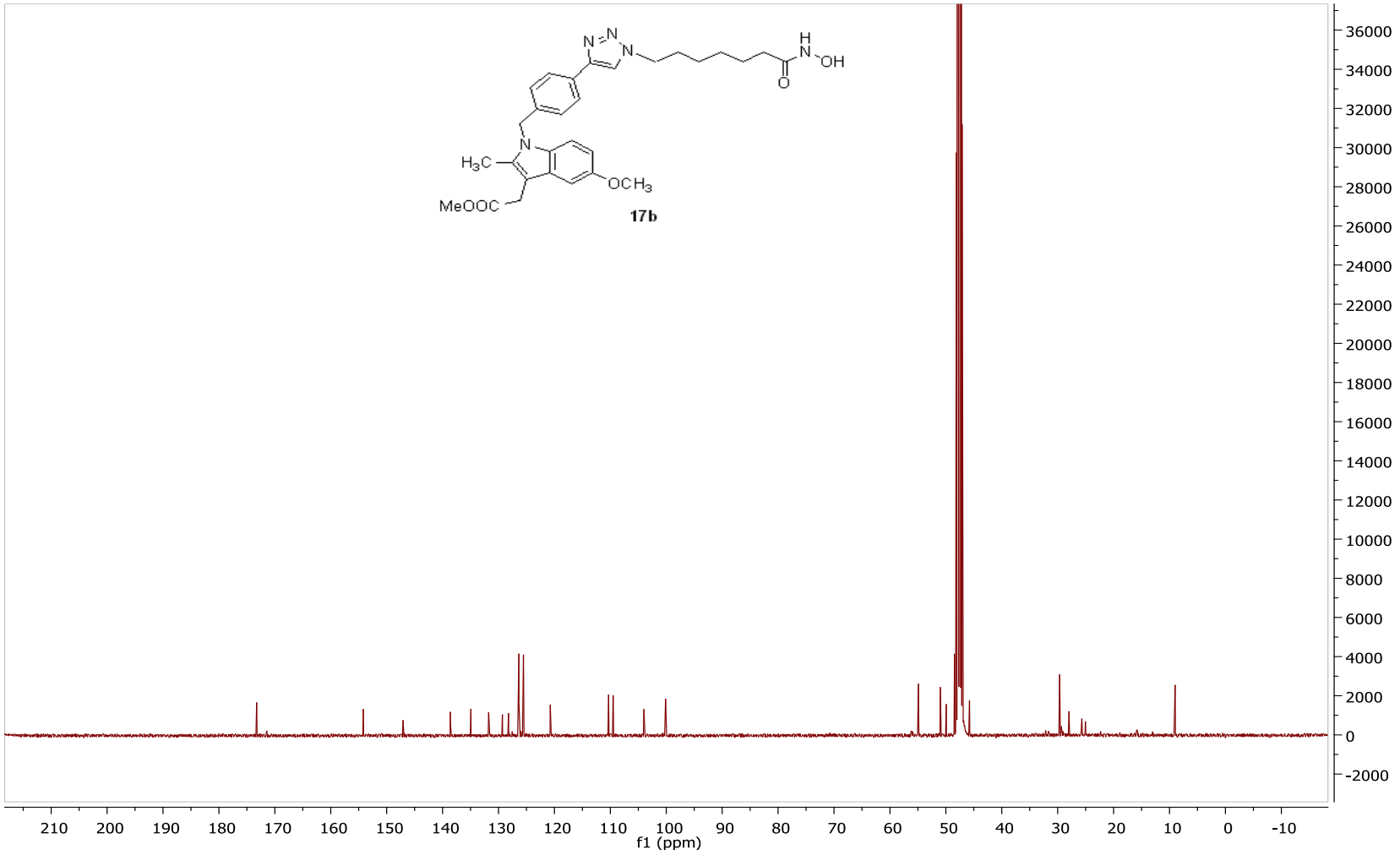
17b
f1 (ppm)

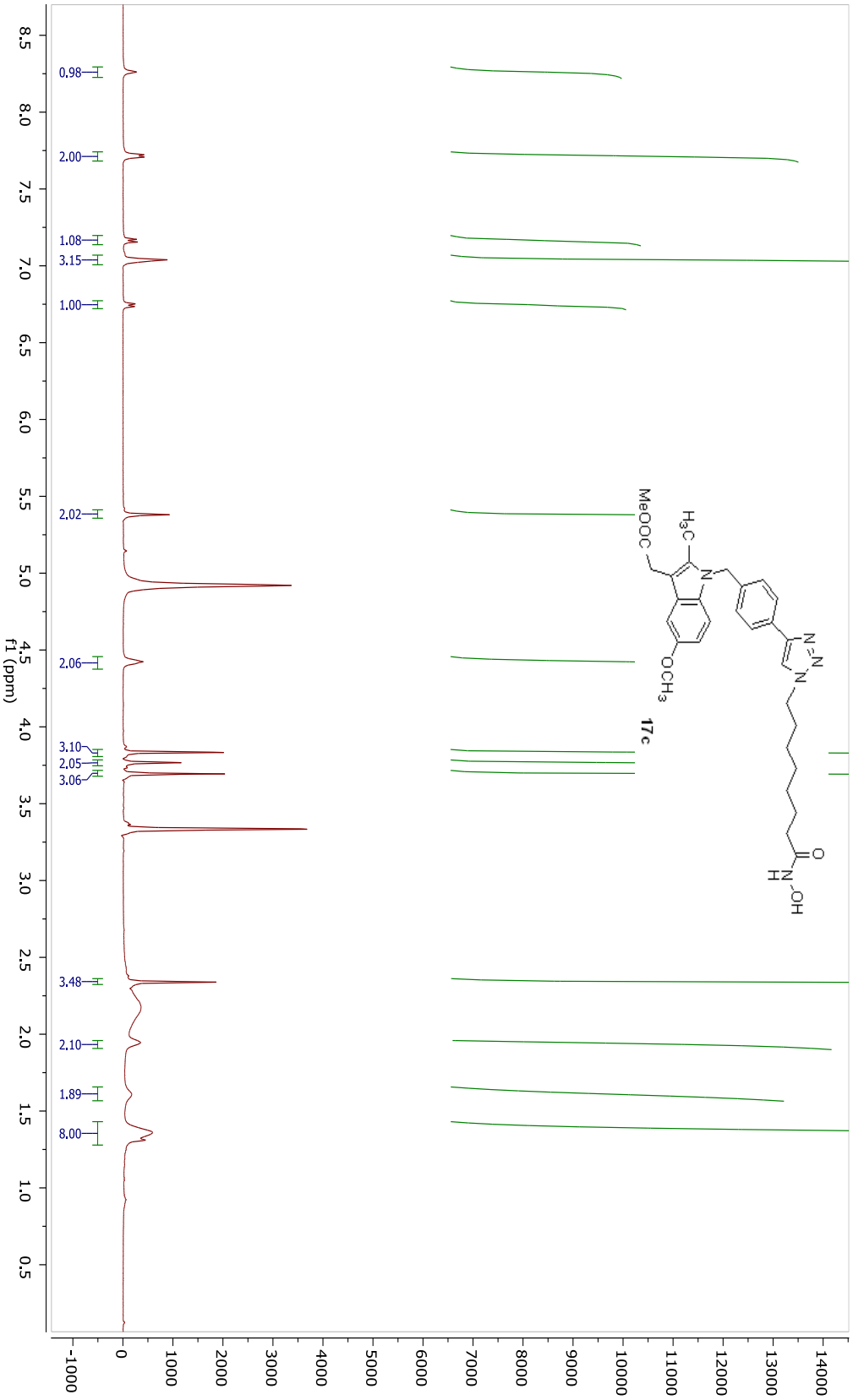
0.98
2.00
1.08
3.15
1.00
2.02
2.06
3.10
2.05
3.06
3.48
2.10
1.89
8.00
f1 (ppm)
MeOOC
H3C
OCH3
17c
N
N
N
O
N
H
OH

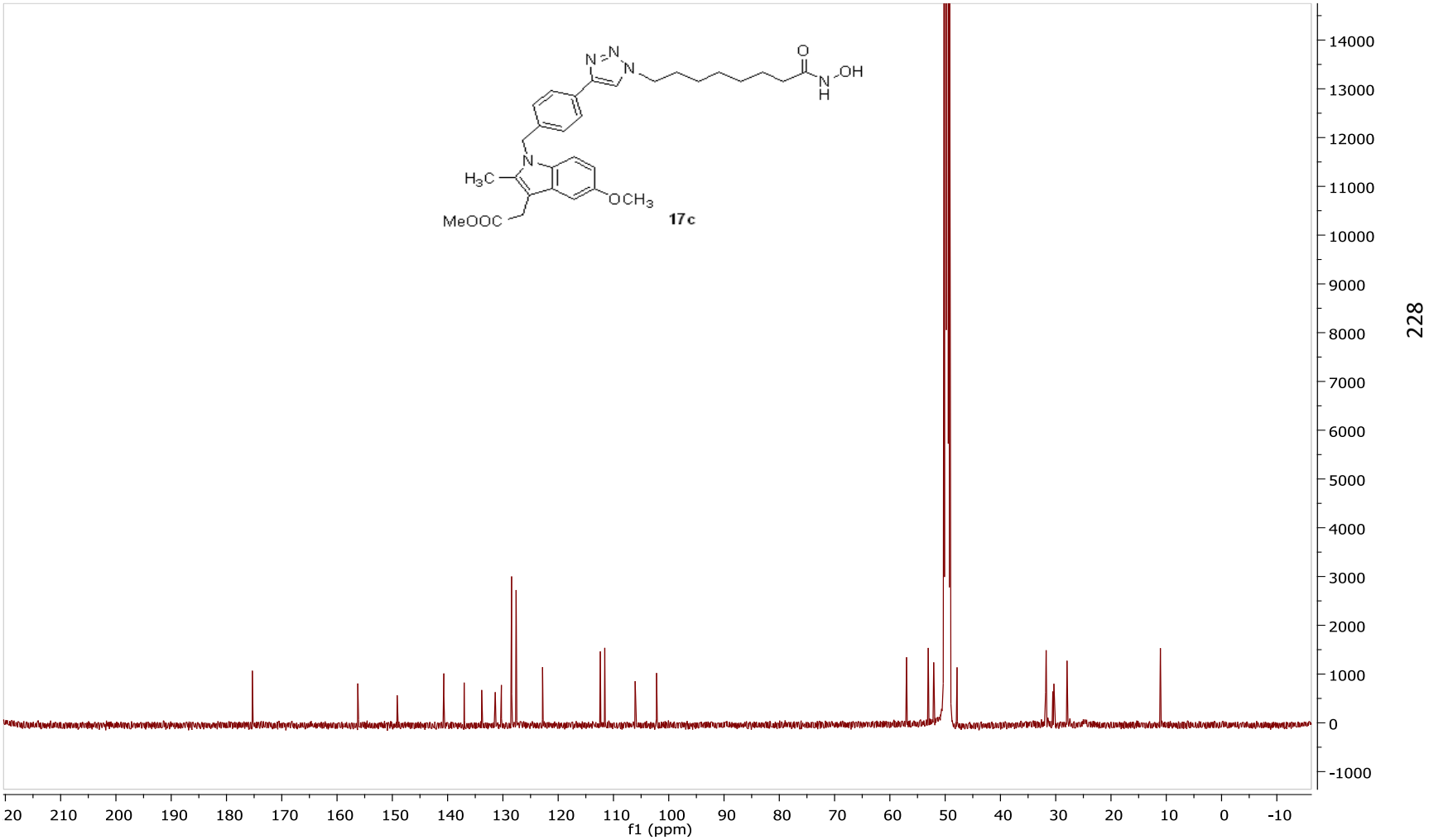
17c
f1 (ppm)

VITA

Idris Raji was born in Lagos, a state in southwestern part of Nigeria. He attended high school in Lagos, then moved to Ondo state (also in southwest Nigeria) to study Chemistry in the university. Upon completion of B. Sc. degree in Chemistry, he was posted to Abia state (southeast Nigeria) to observe a one-year mandatory national service. Afterwards, he returned to Ibadan (a state in southwest Nigeria) to enroll for a master's degree in Chemistry at the country's premier university, University of Ibadan. As soon as he completed the master's degree, he was admitted to Georgia Tech, in 2011, to pursue a PhD in the Department of Chemistry and Biochemistry. For leisure, Idris enjoys playing and watching soccer games.